DTIC FILE COPY

AD_____

AD-A205 334

FIELD MEASUREMENT AND MODEL EVALUATION PROGRAM FOR ASSESSMENT OF THE ENVIRONMENTAL EFFECTS OF MILITARY SMOKES

FIELD STUDY OF FOG-OIL SMOKES

prepared by

J. C. Liljegren, W. E. Dunn, and G. E. DeVault
Department of Mechanical and Industrial Engineering
University of Illinois at Urbana-Champaign
Urbana, IL 61801
217-333-3832

and

A. J. Policastro
Energy and Environmental Systems Division
Argonne National Laboratory
9700 South Cass Avenue
Argonne, IL 60439
312-972-3235

JANUARY 1988

Supported by
U. S. ARMY MEDICAL RESEARCH AND DEVELOPMENT COMMAND
Fort Detrick, Frederick, MD 21701

Contract No. 84PP4822

Project Officer: Major David Parmer
Health Effects Research Division
U. S. ARMY BIOMEDICAL RESEARCH AND DEVELOPMENT LABORATORY
Fort Detrick, Frederick, MD 21701

DTIC
ELECTE
6 MAR 1989
S D
E

Approved for public release;
distribution unlimited

The findings in this report are not to be construed as an offical Department of the Army position unless sc designated by other authorized documents.

REPRODUCED FROM
BEST AVAILABLE COPY

89 3 06 149

NOTICE

Disclaimer

The findings in this report are not to be construed as an official Department of the Army position unless so designated by other authorized documents.

Disposition

Destroy this report when it is no longer needed. Do not return it to the originator.

ADA05 334

SECURITY CLASSIFICATION OF THIS PAGE

REPORT DOCUMENTATION PAGE

Form Approved OMB No. 0704-0188

1a. REPORT SECURITY CLASSIFICATION: Unclassified	1b. RESTRICTIVE MARKINGS
2a. SECURITY CLASSIFICATION AUTHORITY	3. DISTRIBUTION/AVAILABILITY OF REPORT: Approved for public release; distribution unlimited
2b. DECLASSIFICATION/DOWNGRADING SCHEDULE	
4. PERFORMING ORGANIZATION REPORT NUMBER(S)	5. MONITORING ORGANIZATION REPORT NUMBER(S)
6a. NAME OF PERFORMING ORGANIZATION: Argonne National Laboratory; 6b. OFFICE SYMBOL (If applicable)	7a. NAME OF MONITORING ORGANIZATION
6c. ADDRESS (City, State, and ZIP Code): Argonne, Illinois 60439	7b. ADDRESS (City, State, and ZIP Code)
8a. NAME OF FUNDING/SPONSORING ORGANIZATION: U.S. Army Medical Research & Development Comman; 8b. OFFICE SYMBOL (If applicable)	9. PROCUREMENT INSTRUMENT IDENTIFICATION NUMBER: 84PP4822
8c. ADDRESS (City, State, and ZIP Code): Fort Detrick, Frederick, Maryland 21701-5012	10. SOURCE OF FUNDING NUMBERS

PROGRAM ELEMENT NO.	PROJECT NO.	TASK NO.	WORK UNIT ACCESSION NO.
62720A	3E1-62720A835	AA	012

11. TITLE (Include Security Classification): (U) Field Measurement and Model Evaluation Program for Assessment of the Environmental Effects of Military Smokes: Field Study of Fog-Oil Smokes

12. PERSONAL AUTHOR(S): J.C. Liljegren, W.E. Dunn, G.E. DeVaull, and A.J. Policastro

13a. TYPE OF REPORT	13b. TIME COVERED	14. DATE OF REPORT (Year, Month, Day)	15. PAGE COUNT
Final	FROM 1985 TO 1986	1988 January 1	

16. SUPPLEMENTARY NOTATION

17. COSATI CODES		
FIELD	GROUP	SUB-GROUP
04	01	
07	03	

18. SUBJECT TERMS (Continue on reverse if necessary and identify by block number): RA 3, smoke, screening smoke, obscuring smoke, atmospheric boundary layer, atmospheric dispersion, meteorological measurements, aerosol sampling, and particle size; (KF)

19. ABSTRACT (Continue on reverse if necessary and identify by block number)

The atmospheric dispersion of the military obscurant smoke produced from SGF-2 fog oil with the M3A3E3 prototype fog oil smoke generator has been studied in a program of field trials carried out at Dugway Proving Ground. The investigation focused on four areas. Measurements of the mass rate of release, exit velocity and exit temperature were performed to define the smoke source. The smoke aerosol was physically characterized in terms of the particle size distribution. A description of the prevailing meteorology was obtained from measurements of the wind speed, wind direction, temperature and dew point at five levels on each of two 32-m instrument towers located on the test site. Measurements of the average smoke concentration over the period of release were carried out at distances of 25 - 800 m from the release point. At each location measurements of average concentration were performed using adsorbent-filled sampling tubes positioned 1.5 m above ground level. Deposition measurements were also carried out at these locations using glass fiber filters as surrogate-surface collectors. Keywords: Smoke dissemination)

20. DISTRIBUTION/AVAILABILITY OF ABSTRACT	21. ABSTRACT SECURITY CLASSIFICATION
☐ UNCLASSIFIED/UNLIMITED ☑ SAME AS RPT ☐ DTIC USERS	Unclassified

22a. NAME OF RESPONSIBLE INDIVIDUAL	22b. TELEPHONE (Include Area Code)	22c. OFFICE SYMBOL
Mary Frances Bostian	301-663-7325	SGRD-RMI-S

DD Form 1473, JUN 86 — Previous editions are obsolete. — SECURITY CLASSIFICATION OF THIS PAGE

EXECUTIVE SUMMARY

This report summarizes the results of field studies of the dispersion of military smoke conducted at Dugway Proving Ground in March and April, 1985. Fog oil smoke was produced by an M3A3E3 smoke generator over flat terrain and the resulting plume sampled at distances of 25 - 800 m. Measurements made include mean concentration, particle size distribution, deposition on horizontal and vertical surfaces and the chemical composition of the smoke. Mean concentration was determined using aspirated, adsorbent-filled tubes subsequently analyzed by thermal desorption and low resolution gas chromatography. Particle size distribution was measured using cascade impactors of the Mercer design. Deposition was studied using dry, chemically-inert, glass-fiber filter papers serving as surrogate surface collectors. In addition to the plume maps, the source was characterized in terms of mass rate of release, exit temperature and velocity of the smoke, and chemical composition of the raw oil and of the initial smoke. Meteorological data required for model testing and improvement were obtained using two 32-m instrument towers having wind speed, wind direction and temperature sensors at the 2, 4, 8, 16 and 32-m levels and vertical wind angle sensors at the four highest levels. The meteorological data were analyzed in terms of time-averaged vertical profiles from which Monin-Obukhov length and friction velocity were found and in terms of the spectral characteristics of the time-dependent data.

The measurements of mean concentration provide an internally consistent picture of plume behavior, although certain operational difficulties led to suboptimal performance of the concentration sampler. As a result of these difficulties, only three tests yielded useful data, and then only to a distance of 200 m from the smoke generator. Significant improvements in the design of the collector were identified based on the results of these field tests. These improvements can be readily implemented in future field studies to both increase the quantity and improve the detail and reliability of the in-plume data. Only minor difficulties were experienced with the source and meteorological measurements; these systems operated nearly flawlessly.

The major findings of the study are:

1. Concentration levels fall off rapidly with distance and exhibit considerable spatial inhomogeneity at distances beyond a few hundred meters from the source even when hour release times are used. Concentration patterns reflect the combined effects of large-scale variations in wind direction and general plume spreading due to the action of turbulence.

2. The release rate of the generator varies considerably even for ostensibly similar operating conditions and in all cases fell below the nominal level stated for the generator. Exit temperature was found to increase sharply with decreasing release rate. The exit velocity, primarily dependent on the rate of air flow through the generator, was found to be independent of operating conditions for the cases studied.

3. The fog oil smoke was found to exhibit a log-normal distribution of droplet sizes with a mass median diameter of roughly 0.7 microns.

4. For the limited conditions studied, no change in chemical composition was detectable, using low resolution gas chromatography, between the raw oil, the initial smoke and the smoke at the furthest downwind point of sampling.

5. Again, for the conditions studied, no statistically significant levels of deposition were measured on either horizontal or vertical surfaces.

ACKNOWLEDGMENT

The authors wish to thank the members of the Dugway Proving Ground Staff for their assistance in executing these field studies. Especially noteworthy are Mr. Bruce Black and Dr. James Bowers who served as DPG Project Managers. However, numerous other members of the staff participated to varying degrees in the project, and their valuable efforts are gratefully acknowledged.

We also wish to thank our USAMBRDL Project Officer, Major David Parmer, for his important role in shaping this project. His many helpful suggestions and insightful comments added enormously to the success of the effort.

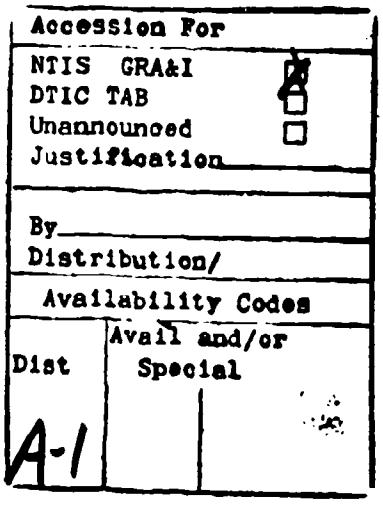

TABLE OF CONTENTS

TABLE OF CONTENTS (CONTINUED)

LIST OF FIGURES

LIST OF FIGURES (continued)

LIST OF FIGURES (continued)

LIST OF FIGURES (continued)

LIST OF FIGURES (continued)

LIST OF TABLES

1.0 INTRODUCTION

1.1 Objectives

This report describes the procedures and results of a field study of the dispersion of military fog-oil smoke carried out at Dugway Proving Ground between March 15 and April 15, 1985. This study was the first in a series of field programs designed to gather data needed to test predictive models currently being used to assess the environmental and civilian health effects of military obscurant smokes such as fog oil and hexachloroethane (HC).

Measurements of mean concentration, deposition, particle size distribution and chemical composition of the smoke produced by an experimental prototype military fog-oil smoke generator were carried out over downwind distances of 25 to 800 m. The use of perfluorocarbon tracers mixed with the fog-oil smoke was also attempted in order to provide a check on the fog oil measurements. Supporting data include comprehensive documentation of source characteristics and prevailing meteorological conditions during the period of release.

An equally important objective of this work was to test the methods and equipment under actual field conditions. Despite extensive laboratory testing and an earlier small-scale field test of the collection procedures, this study represents the first attempt at operating all the equipment simultaneously under actual field test conditions. It was expected that the results of this study would be used to evaluate and refine the experimental methods and equipment as well as the logistical procedures.

1.2 Test Site

This study is restricted to perhaps the simplest possible release scenario: a single fog oil generator on flat terrain with a uniform atmospheric boundary layer, low relative humidity and sparse vegetation. These conditions were chosen in effort to provide an "ideal" set of data for baseline model evaluation. Dugway Proving Ground (DPG) was selected as the site for this pilot study because of (1) a large area of open, flat terrain which provides the desired "ideal" conditions for model testing and (2) a long history of operating and testing smoke generating devices.

The test site was located within the West Vertical Grid test area. A detailed description of the site and surrounding area is included in a meteorological report by Waldron (1977). Figure 1.1, taken from Waldron's report, shows the topology of Dugway and gives the location of West Vertical Grid within the Dugway boundaries. According to Waldron, the variation in the elevation of the desert terrain surrounding West Vertical Grid is less than 40 m. There is a uniform fetch of 5 km in the northwest quadrant and a minimum 9 km fetch in the other quadrants. The primary vegetation on the site is a desert shrub known as Grey Molly having a height of 7 to 30 cm and spaced at one-half to one meter intervals. Waldron also states that the site passes the micrometeorological test of uniform terrain in all directions to a distance of 3 km or greater.

1.3 Overview

In all, eleven releases of fog-oil smoke were carried out under meteorological conditions ranging from near-neutral to very unstable. No tests were conducted under stable atmospheric conditions. Only the last three tests were sufficiently successful to be useful for modeling due to contamination of the concentration sampling tubes, which raised the detection threshold, and the inadequacy of the B/C aspiration units, which resulted in a reduced amount of smoke collected by the tubes. The transitional and unfavorably convective meteorological conditions associated with the late-morning and early-afternoon test periods also proved to be a major problem. Testing was restricted to these periods due to logistical and procedural constraints which prevented the use of the more favorable "dawn" conditions. Additional difficulties with the smoke generators caused the release rates to be much lower than anticipated. These difficulties were attributed, at least in part, to the higher altitude of DPG and added to the complexity of carrying out the field tests.

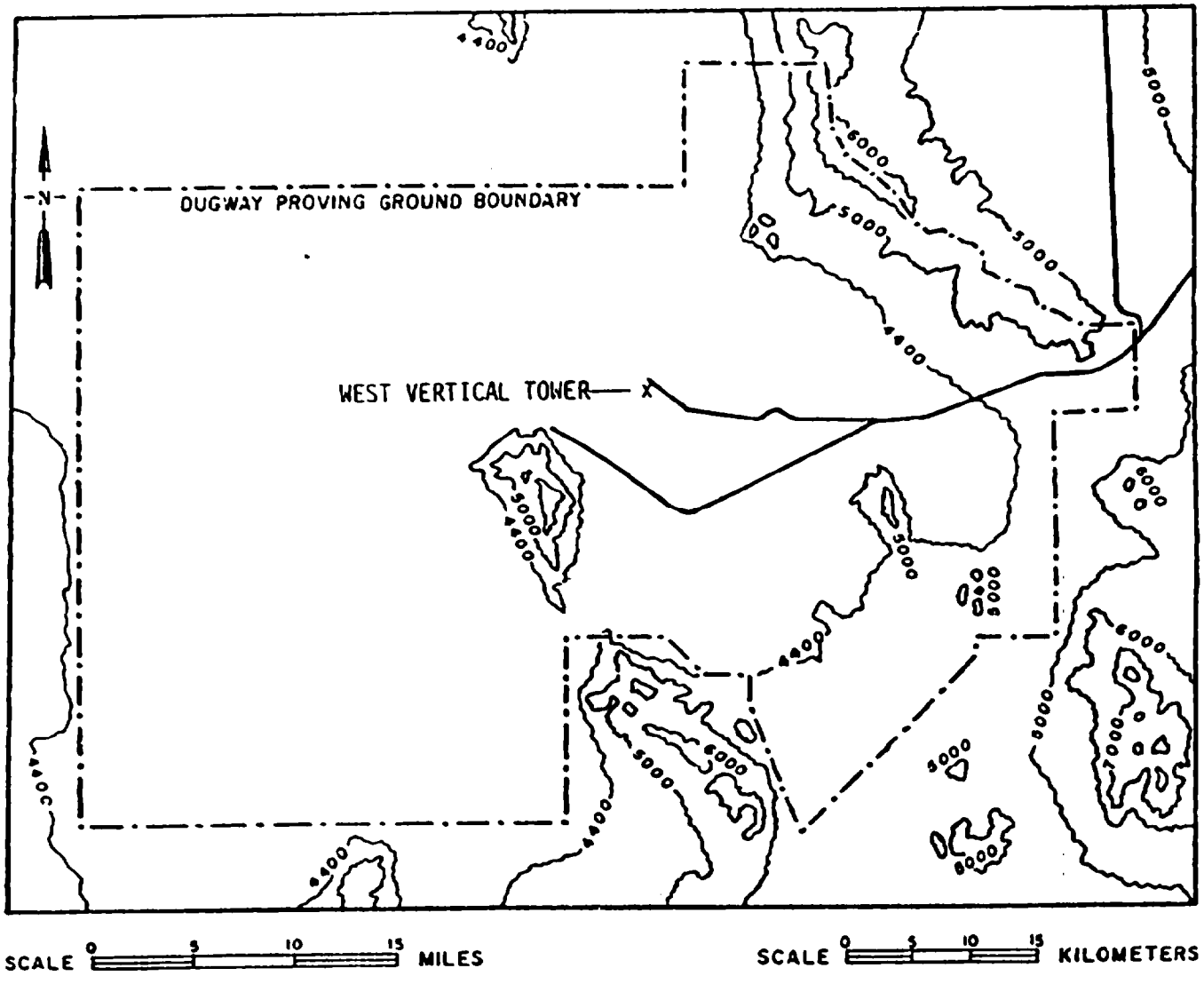

Figure 1.1 Map of Dugway Proving Ground indicating the location of the test site on West Vertical Grid (from Waldron, 1977).

Despite these problems, however, much information on the field characteristics of fog-oil smoke was produced. The concentration data are in agreement with model predictions as well as with the results of other field studies of atmospheric dispersion. Particle size data very nearly replicate the results of a previous laboratory analysis of fog-oil smoke. Time dependent data describing the smoke generator provide a consistent picture of its operation. Meteorological data gathered during this study are in agreement with models derived from extensive investigations of the planetary boundary layer. This information provides baseline data for health effects studies and a platform from which improved field studies of smoke dispersion can be launched.

This report is organized into three sections covering (a) smoke data, (b) source data and (c) meteorological data, respectively. Each of these sections describes in detail the equipment and procedures employed to gather the data and also provides a discussion of the results obtained. Following these components, our overall conclusions and recommendations are presented.

2.0 SMOKE DATA

This section describes the instruments and procedures employed during these dispersion tests in order to acquire the concentration, deposition, particle size and chemical composition data necessary for model evaluation. The measurements are organized into two groups: those which describe the continuum behavior of the smoke plume as a whole (e.g., concentration) and those which describe the features of the fog-oil smoke (e.g., size distribution). This organization parallels the treatment given the dispersion problem by most of the models under study.

Most models of atmospheric dispersion treat the smoke plume or cloud primarily as a continuum and predict its extent or concentration at locations of interest. To evaluate these models, measurements of concentration at a large number of positions are necessary. In the present study, the concentration of fog oil at each location on a network was determined from measurements of concentration carried out at each sampling location. In addition to measuring the concentration of fog oil, we also attempted to measure the concentration of a perfluorocarbon tracer introduced into the fog-oil smoke plume at the generator exit as a check on the fog oil concentrations.

Owing to their potential importance to environmental and civilian health issues and to provide as complete a data set as possible, measurements of the deposition, size distribution, vapor partitioning and chemical aging of the fog-oil smoke were performed during each test.

2.1 Sampling Network

The location of our sampling network within the West Vertical Grid is illustrated by the shaded region in Figure 2.1. Here the circles represent the sampling arcs of the West Vertical Grid, the farthest arc shown (Arc I) having a radius of 2414 m (1.5 miles). As illustrated, the sampling grid consists of a rectanguiar region 1600 m by 800 m, the long axis of which passes through the centers of two existing meteorological instrument towers. These two towers, separated by a distance of 990 m, lie along the approximate direction of the prevailing winds. The towers are logically designated "West Vertical Tower" and "Horizontal Grid Tower", since the former lies near the center of the West Vertical Grid and the latter lies near Horizontal Grid, a somewhat smaller grid within the full extent of West Vertical Grid.

Previous large scale field studies of atmospheric dispersion such as Project Prairie Grass (Barad, 1958) and the Hanford Series (Nickola, 1977; Nickola, *et al.*, 1983) arranged their sampling networks in a series of wide arcs increasing in distance from a fixed source location. With such an arrangement, a large number of samplers had to be deployed in order to cover a sufficiently large angle to accommodate changes in wind direction prior to the test; however, only a small fraction of the samplers were actually exposed. Additionally, the fixed source location restricted testing to those occasions when the wind was in the direction of the sampling arcs.

Owing to a tight field testing schedule which dictated a broad range of acceptable test conditions, we designed a sampling network with a relocatable source; one which would be serviceable for virtually any wind direction. Sampling locations were arranged in a rectangular array with a uniform pitch of 100 m, thus covering the entire 1600 m by 800 m region as illustrated in Figure 2.2. All locations are given in grid coordinates with (0,0) referenced to sampling location J4, as indicated.

During the course of the testing it was observed that under near-neutral atmospheric conditions the smoke plume was confined to a narrow corridor. Because the samplers were spaced 100 m apart, this frequently resulted in very few samplers being exposed to the plume at short range. Conversely, under convective conditions the plume lifted off the ground prior to reaching the first row of samplers (100 m distant), also resulting in very few exposed samplers. Consequently, a more densely spaced network was configured in order to better resolve the smoke plume at short range (25 - 400 m). This high resolution network was laid out in the shaded area in Figure 2.2 between rows 2 and 6 and between columns J and N. As Figure 2.3 illustrates, this network is essentially diamond-shaped. It is comprised of transects at 25 m, 50

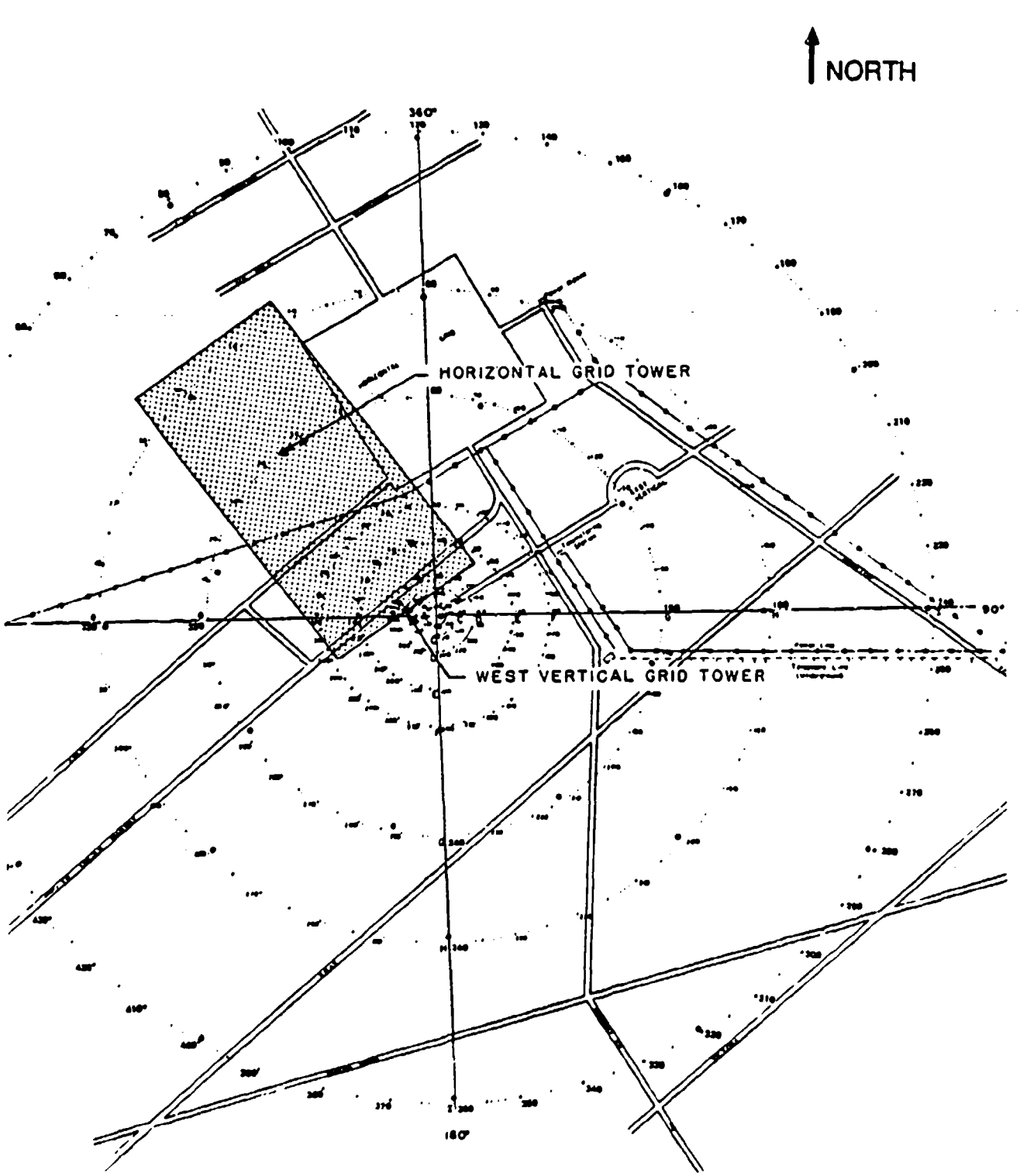

Figure 2.1. Location of test site with respect to Horizontal and West Vertical grids at Dugway Proving Ground. The sampling network is located in the shaded portion of the figure.

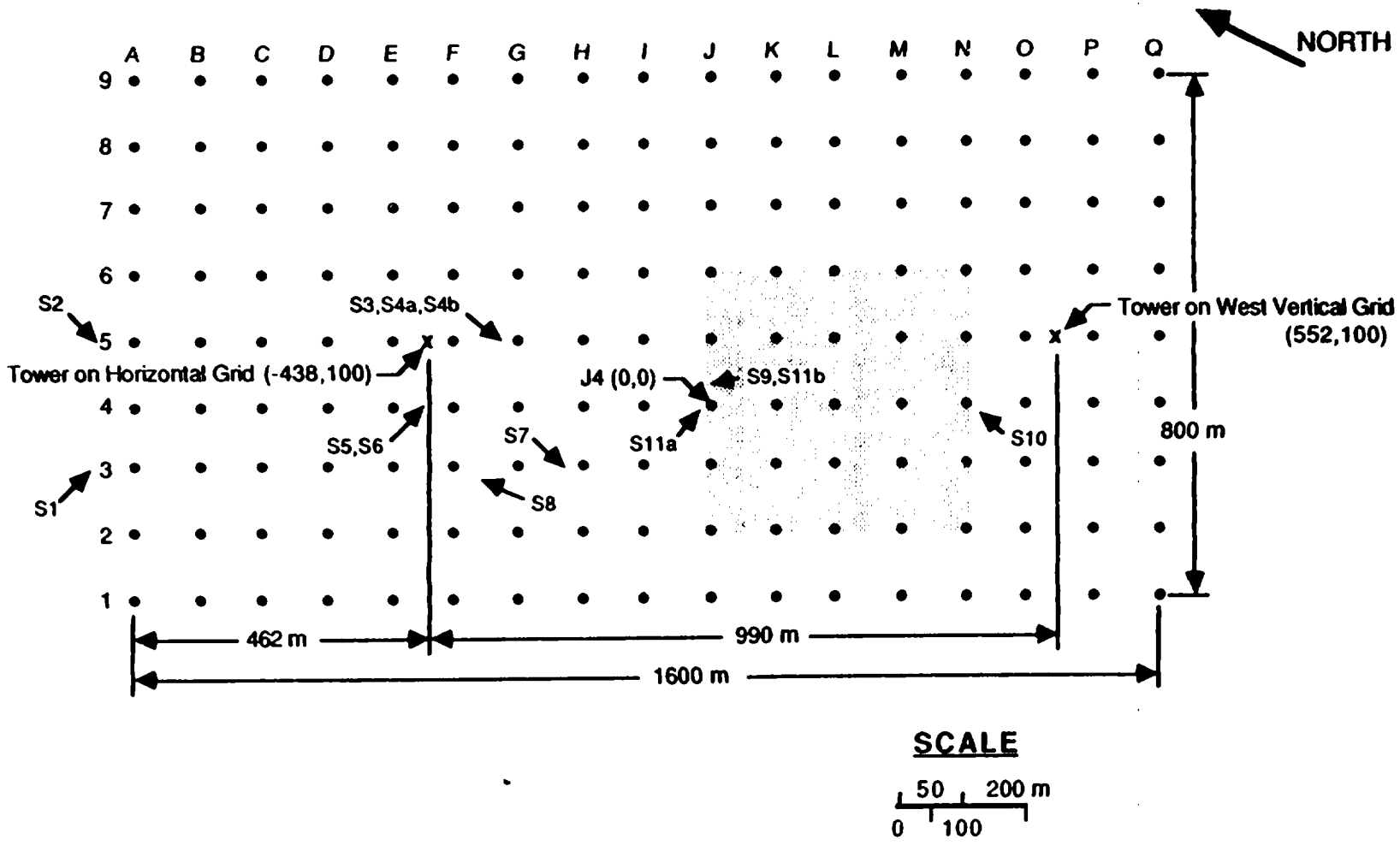

Figure 2.2. Layout of main sampling network and coordinate system. Filled circles indicate sampler locations. Shaded area locates High Resolution Network illustrated in Figure 2.3. Source locations are indicated by test no.

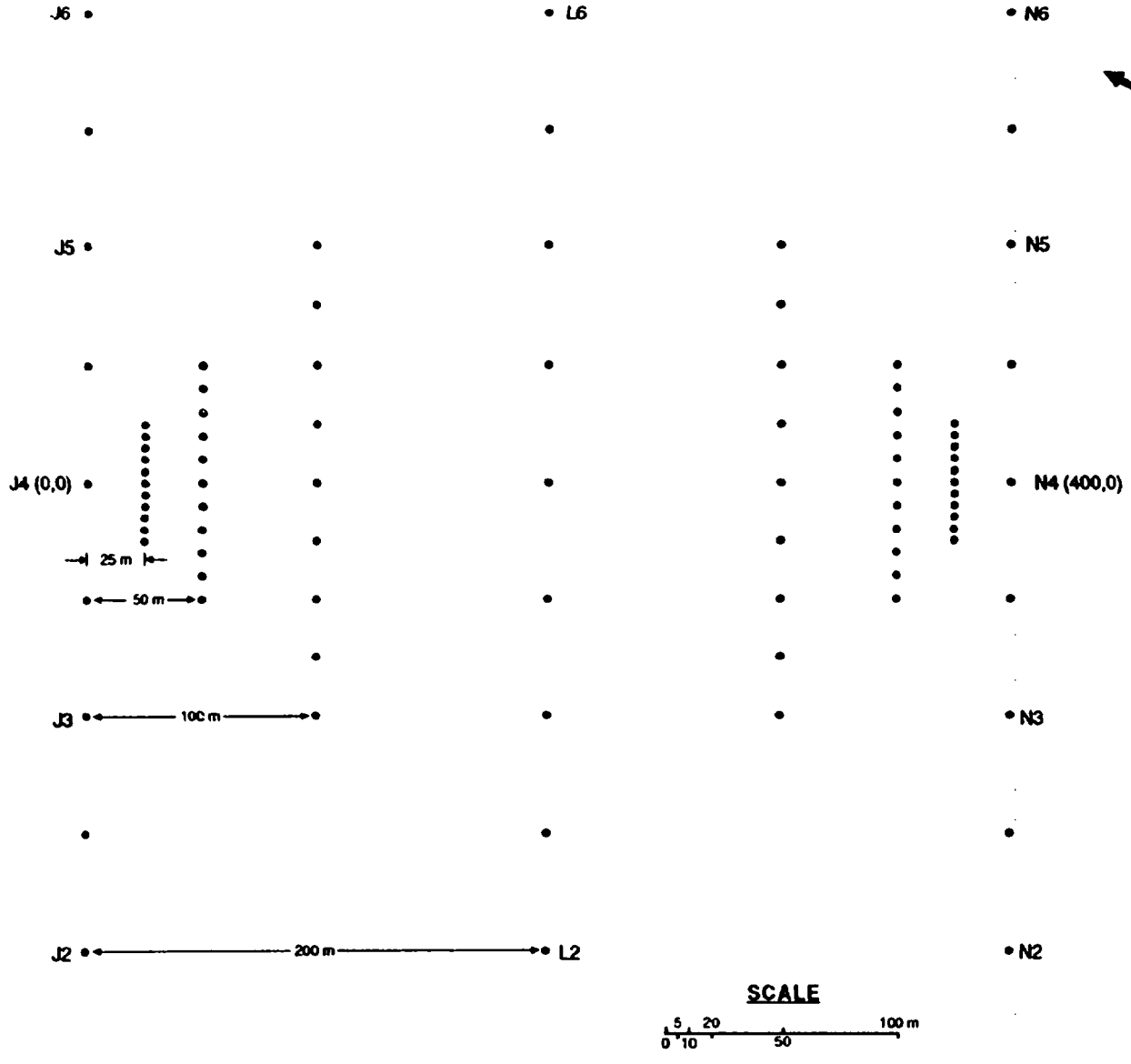

Figure 2.3 High Resolution Sampling Network indicated by the shaded area in Figure 2.2. Filled circles mark the locations of concentration samplers.

m, 100 m, 200 m and 400 m and is symmetric about the 200 m transect. Eleven samplers were located on both the 25 m and 50 m transects at spacings of 5 m and 10 m respectively. Nine samplers were located on the 100 m, 200 m and 400 m transects spaced at 25 m, 50 m and 50 m respectively. The network was designed to minimize the time required to fit the samplers with concentration-measuring tubes and to provide maximum flexibility in coping with shifts in the prevailing wind direction. Thus the smoke source could be located near J4 (0,0) or N4 (400,0) depending on the wind direction.

In order to improve the capability to measure concentrations at large distances (400 - 2000 m), ten B/C samplers with sample tubes or cascade impactors were mounted in the bed of a pickup truck. In this manner they could be quickly relocated to remain in the plume as the wind shifted.

2.2 Sampling Devices and Methods

The sampling equipment located at each position on the network included the following items: (a) a B/C sampler -- a radio-controlled aspiration unit initially fitted with a flow restrictor rated at 1 liter per minute (ℓpm); (b) a sample tube connected to the B/C sampler by means of a vinyl hose and positioned at the 1.5 m level atop the antenna of the B/C sampler; and (c) a deposition tray mounted on a 7/16" steel post at a height of 0.5 m. The 1.5 m sampling height was chosen because it approximates the breathing height of a man. This height was also used for "ground-level" samplers in both the Prairie Grass and Hanford studies.

We had initially planned to aspirate the sample tubes at a rate of 6 ℓpm based on specifications provided to us by DPG personnel. However, during the setup phase of the field testing period, we realized that the B/C sampler could not aspirate our sample tubes at the planned flow rate. To maximize the aspiration rate of the sampler, we ultimately decided to operate the B/C samplers without flow regulation and, as a result, were required to measure the flow rate of each sampler both before and after each test. This significantly increased the time required to deploy and retrieve the concentration samples and contributed substantially to the logistical difficulties which prevented us from testing during stable near-dawn atmospheric conditions. The low flow rate also gave rise to concern over the issue of reduced collection efficiency due to anisokinetic sampling and it significantly reduced the signal-to-noise ratio of our concentration measurements by limiting the total amount of smoke material we could collect during a test.

2.2.1 Concentration Measurements

The concentration sampler used in these field experiments consisted of a stainless steel tube 6 mm in diameter and 89 mm long. The tubes were packed with *Tenax*, a chemical adsorbent which removes hydrocarbons from the air flow drawn through the tube. This approach was used for several reasons. First, whereas a study by Jenkins and Holmberg (1981) indicated that a substantial portion of diesel fuel-based smoke remains in the vapor phase and does not condense into an aerosol, no such information was available for SGF-2 fog-oil smoke prior to this study. The *Tenax*-filled samplers allow both vapor and aerosol to be collected, yielding more correct estimates of exposure. Second, all of the material collected by the sample tube is available for analysis, unlike bubblers (impingers) from which only a small portion of the sample is withdrawn and analyzed. This results in a more accurate concentration measurement. Third, owing to the limited time available for testing and the large number (>100) of sampling locations, ease of deploying and retrieving the samples was critical. The sample tubes are easily deployed, retrieved and packed for shipping. Finally, the analysis of the tubes was readily automated, allowing the results of a test to be determined overnight rather than days or weeks after testing. This was particularly important since it provided rapid feedback on our field techniques and enabled us to quickly change our experimental procedures and improve our results.

Subsequent to each test, the sample tubes were collected, capped and shipped to the University of Illinois for analysis. Analysis of the concentration samples by thermal desorption/gas chromatography provided the total mass and chemical composition of the fog-oil smoke collected over the period of aspiration. In order to reduce the amount of time required to analyze the data collected (130-210 samples per test), a packed column chromatographic method was employed. This method produced the correct total

mass but could not resolve the mass of any particular constituent. From these data, average concentrations were determined by dividing the mass collected by the total volume of air drawn through the tube during the period of aspiration. Details of the chemical analysis procedure are provided in a companion report (DeVault, *et al.*, 1988).

2.2.2 Aerosol Measurements

Deposition was measured via surrogate surfaces: dry, chemically inert, circular glass-fiber filter papers 125 mm in diameter. Although a variety of techniques have been utilized to measure dry deposition (that is, deposition by processes other than precipitation) no one method has gained acceptance. In 1980, a group of scientists critiqued various monitoring methods and concluded that surrogate surfaces are inadequate because they do not simulate natural surfaces (Hicks, *et al.*, 1980). However, the dissenting view at the same meeting held that surrogate surfaces, despite their limitations, represent the only method available for large field studies of deposition, due to their simplicity and low cost. In their dissenting discussion, Davidson and Lindberg point out several field studies in which dry deposition measurements, carried out with surrogate surfaces, showed both internal consistency and fair agreement with theoretical predictions.

Additionally, Lindberg and Lovett (1982), found that deposition measurements made with rimmed polycarbonate filters (9.4 cm diameter) were slightly higher than data gathered from foliar leaf washing. They attributed the difference to variations in leaf orientation and leaching. Sickles, *et al.* (1982) compared foliar washings of *Ligustrum* having smooth, oval leaves of about 1 cm^2 with data from polycarbonate buckets, petri dishes and cellulose filter papers. The filter paper had the highest collection efficiency of the surrogate surfaces; the surrogates all had higher collection efficiencies than the natural leaf surface. All surfaces exhibited the same trends, however, which indicates that while the surrogates do not replicate the natural surfaces, their degree of variability is no greater than the variability found among natural surfaces. The authors concluded that surrogate surfaces are, in fact, reliable and useful for measuring dry deposition.

Dasch (1982) compared several types of surrogate surfaces, including nylon, teflon, quartz fiber and glass fiber filters, to determine their collection efficiencies. In these tests, the filters exhibited consistently higher efficiencies with the glass fiber having the greatest. For this reason, glass fiber filters were selected for use in the present study. The filters were affixed to steel support plates by means of steel clips. Both horizontal and vertical orientations of the plate/filter assembly were employed in order to assess both deposition and impaction as removal mechanisms. After a test was completed, the collected filter papers were sealed in glass vials and shipped to the University of Illinois along with the sample tubes. In the laboratory, these vials were filled with a solvent (hexane). The mixture was then concentrated and injected onto a sample tube packed with glass wool for a chromatographic analysis similar to that carried out for the sample tubes. As a check on this analysis method, some of the filters were cut in half. One half was then analyzed by the above method and the other half was inserted into an empty sample tube for direct thermal desorption/gas chromatographic analysis. Both methods yielded very similar results.

In addition to these instruments, twelve seven-stage Mercer-style cascade impactors manufactured by Intox Products (model no. 02-100) were utilized to measure the particle size distribution of the fog-oil smoke between 0.33 and 4.5 µm. Due to the limited time available to recover the samples from one test and to prepare for the next, no more than six cascade impactors were employed per test. These six were widely spaced to assure that at least one would be exposed to the plume. Their location on the sampling network was selected based on the prevailing wind direction just prior to each test in order to maximize the likelihood of their exposure to the plume.

The cascade impactors were aspirated at nominally 1 $\mathcal{L}$pm via a B/C sampler. The actual aspiration was measured and recorded because the 50% cutoff (D_{p50}) for each stage depends on the flow rate according to the ratio

$$\frac{(D_{p50})_{actual}}{(D_{p50})_{1\ Lpm}} = \sqrt{\frac{1\ Lpm}{actual\ flow\ rate\ (Lpm)}}$$

The D_{p50} sizes for cascade impactor stages aspirated at 1 Lpm are given in Table 2.1.

Table 2.1 Cascade Impactor Stages at 1 Lpm Flow Rate

Stage	D_{p50} (μm)
1	4.5
2	3.0
3	2.15
4	1.6
5	1.06
6	0.72
7	0.33

It proved very difficult to gauge how long to aspirate an impactor, since the time at which overloading occurred depended on several factors including the rate of release, the distance from the point of release, and the prevailing meteorology (wind speed, direction fluctuations, etc.) Although through experience we were eventually able to determine proper aspiration times, we frequently underexposed or overexposed the impactors during the first tests. In addition, the fine jets in the impactors which effect the particle sizing were easily clogged by the dusty conditions prevalent at the site.

After exposure, the impactors were sealed. Later, the seven 22-mm glass cover slips (one for each stage) and the backup glass-fiber filter were removed and sealed in glass vials and shipped to the University of Illinois for analysis. There they were washed twice with solvent (hexane) and the mixture was concentrated. The concentrate was then injected on glass wool inside a stainless steel tube of the same design as that used for the concentration samplers. The mass of fog oil was determined by thermal desorption and gas chromatography following the same procedure used for the sample tubes.

2.2.3 Anisokinetic Sampling

Due to the low aspiration rate possible with the B/C samplers, anisokinetic sampling (the deviation of particle paths from the streamlines of the air) posed a potentially serious problem (Watson,1954). Sehmel (1967) describes the corrections necessary for horizontally oriented filter cassettes at an angle to the wind, such as those used at Hanford. In order to minimize the effects of anisokinesis as well as the sample bias due to fluctuations in wind direction, both the sample tubes and the cascade impactors were mounted vertically with their sampling inlets facing upward. The bubbler inlets in the Prairie Grass study were also oriented vertically for the same reason.

In order to assess the effects of anisokinetic sampling on the data, an empirical correlation due to Laktionov (1973) for oil droplets sampled at 90° to the mean flow was utilized to produce the curves given in Figure 2.4 for 0.5 μm droplets:

$$A = 1 - 3\,(Stk)^{\alpha}\ ;\ \alpha = \left(\frac{U_{tube}}{U_{wind}}\right)^{1/2} \qquad (2.1)$$

Here the aspiration coefficient A, defined as the ratio of the measured concentration to the actual concentration, is shown to be a function of the mean horizontal wind speed u_{wind} and the aspiration rate of

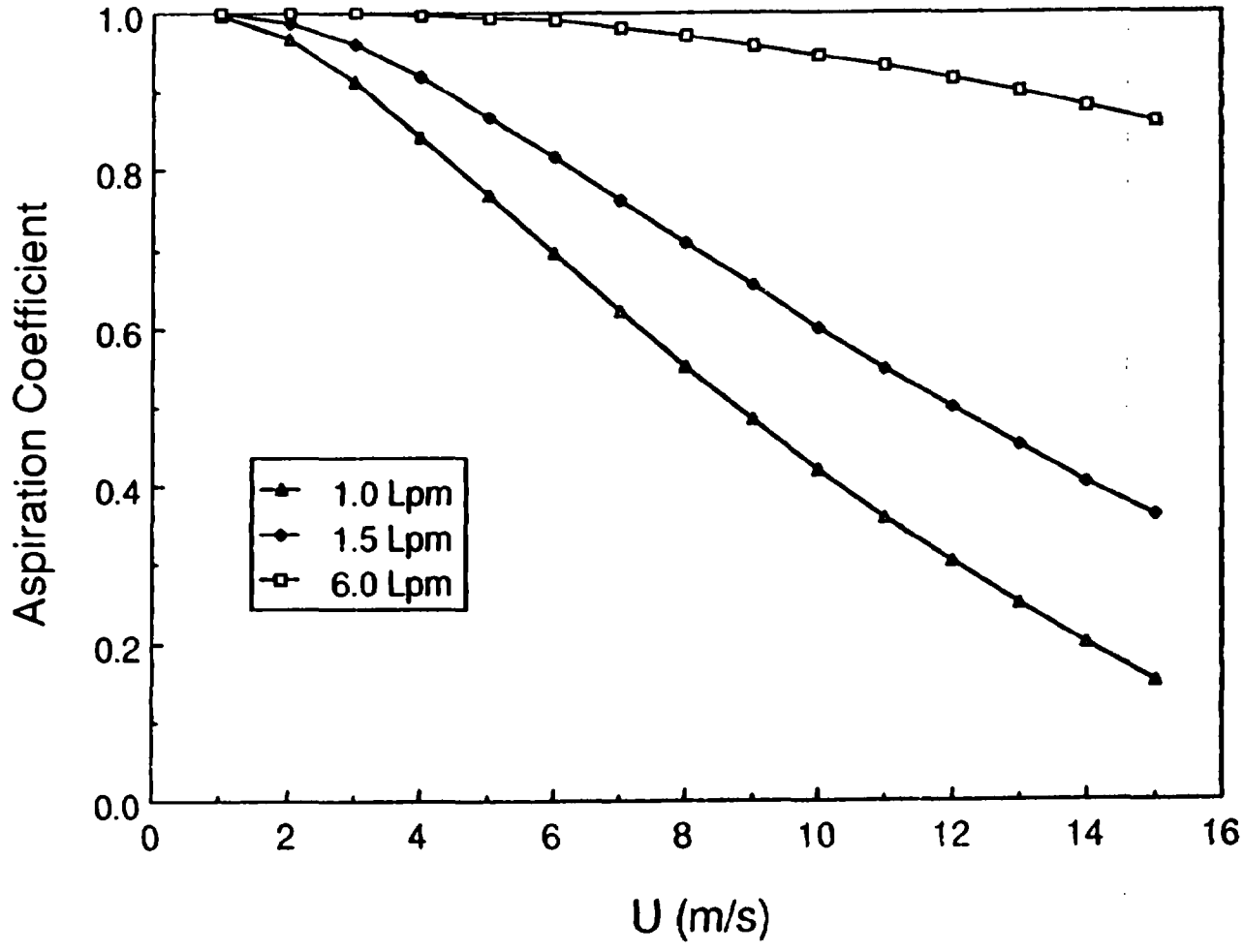

Figure 2.4. Aspiration coefficient of 0.5 micron oil droplets into a vertical tube in a cross flow as a function of mean wind speed for several aspiration rates computed using Laktionov's (1973) empirical correlation.

the sampler (u_{tube} is the velocity of air in the sample tube). The Stokes number is defined in terms of the particle response time τ:

$$Stk = \tau\left(\frac{U}{D}\right); \tau = \frac{d_p^2 \rho_p}{18 \mu} \qquad (2.2)$$

Here $U = u_{wind}$ and D is the tube diameter; d_p and ρ_p are the diameter and density of the particle, respectively, and μ is the viscosity of the air. It is clear from Figure 2.4 that as the mean wind speed increases, the error in the measured concentrations will also increase. It is also apparent that this may be overcome with a sufficiently high aspiration rate. In order to achieve the maximum aspiration rate possible with the B/C samplers, the 1 Lpm flow restrictors were removed. Although this only increased the aspiration rate to about 1.5 Lpm, a substantial improvement in the aspiration efficiency of the concentration sampler appears to have been realized.

The experimental work of Durham and Lundgren (1980) and Tufto and Willeke (1982) both show close agreement with equation (2.1). However, all three of these studies were carried out for Stokes numbers in the range $0.003 \leq Stk \leq 3.0$, whereas the Stokes numbers encountered in our field study were much smaller ($0.0001 \leq Stk \leq 0.001$). Thus the applicability of the results of these studies to our data is questionable. Because of this, no correction for anisokinetic sampling has been applied to our data.

2.2.4 Perfluorocarbon Tracer

Because the *Tenax* removes all hydrocarbons from the air (including, for example, automobile exhaust emissions) the background "noise" level of the sample tubes was much higher than that of a simple filter which would have collected only the aerosol portion. In order to provide a check on the fog oil concentrations as well as to extend our detection range to 2000 m, we released small amounts of perfluorocarbon tracers with the fog-oil smoke. The appeal of perfluorocarbon tracers, described by Lovelock and Ferber (1982) is threefold: 1) they are readily detectable well below the part-per-trillion level and the total atmospheric perfluorocarbon burden is very low, thus making very long range measurements possible; 2) they are non-toxic and resistant to environmental and thermal degradation unlike the more familiar halocarbons; 3) they are relatively inexpensive.

Perfluorocarbon tracer deployment and analysis techniques were developed and demonstrated by the Air Resources Laboratory (ARL) of the National Oceanic and Atmospheric Administration (NOAA) and by Brookhaven National Laboratory (BNL) as described by Ferber, *et al.* (1981) for perfluoromonomethylcyclohexane (PMCH) and perfluorodimethylcyclohexane (PDCH). These two compounds were successfully employed as gaseous tracers in the CAPTEX 83 Cross-Appalachian Tracer Experiments (Ferber and Heffter, 1983). Dietz and Dabberdt (1983) have compiled an extensive report describing both PMCH and PDCH as well as the preferred methods of release, sampling and chemical analysis for atmospheric dispersion experiments.

Because we were interested in measuring both the vapor and aerosol phases of the fog-oil smoke, we investigated perfluorocarbon compounds having much lower vapor pressures than PMCH and PDCH, such as the Fluorinert series manufactured by the 3M Company. We also considered decachlorobiphenyl (DCBP) which was used as a tracer by Jenkins, *et al.* (1983) in their studies of the inhalation toxicity of fog-oil smoke in rats. We chose to use Fluorinert FC-72 and FC-70; FC-72 was expected to remain in the vapor phase while FC-70 was expected to recondense after vaporization.

Prior to each test, a 10 ml syringe was filled with an equal mixture of FC-72 and FC-70 and loaded into a syringe pump. The tracer was dispensed at a rate of 3 ml/hr or 6.2 g/hr into the hot exhaust stream of the fog-oil smoke generator where it was vaporized. The tracers were not mixed directly into the fog oil for several reasons. Ensuring a homogeneous mixture of tracer and fog oil would have been difficult. It would also have been impossible to determine exactly how much tracer had been released. Most importantly, we

were concerned that subjecting the tracers to the high temperatures experienced inside the M3A3E3 generator might cause them to breakdown.

To avoid the potential thermal decomposition of the tracer (and to make sure that this study did not contribute significantly to the atmospheric background concentration of perfluorocarbons), we released the minimum amount of tracer material which we estimated would be detectable at 2000 m. This minimum was determined assuming the minimum amount detectable by the electron capture detector (ECD) on the gas chromatograph to be the rated 10^{-6} mg and the aspiration rate of the samplers to be 1 Lpm for 1 hour. Thus the minimum detectable concentration was determined to be

$$\chi_{min} = \frac{10^{-6}\ mg}{(1\ L pm)\ (10^{-3}\ m^3/L)\ (60\ min)} = 1.67 \times 10^{-5}\ mg/m^3 \qquad (2.3)$$

With the minimum dilution factor χ (= concentration / release rate) computed from a simple gaussian plume model to be 1×10^{-5} s/m^3 at 2000 m for a 5 m/s wind speed, the minimum release rate was computed to be

$$\dot{m}_{min} = \frac{1.67 \times 10^{-5}\ (mg/m^3)}{1 \times 10^{-5}\ (s/m^3)} = 1.67\ mg/s \rightarrow 6.0\ g/hr \qquad (2.4)$$

It should be noted, however, that a higher priority was assigned to the sampling and analysis of the fog-oil smoke over the tracers. This priority is reflected in many aspects of the experimental design; for example, the separation column and temperature programming of the gas chromatograph were optimized for fog oil, not perfluorocarbons, and the sample tubes were filled with *Tenax* rather than *Ambersorb* (the adsorbent recommended by Dietz and Dabberdt). Because of the many compromises favoring fog-oil smoke measurements we considered deleting the tracers altogether from the experiments. However, since this was a pilot study to investigate various measurement approaches, we attempted their use but de-emphasized their role in favor of directly measuring ambient fog-oil smoke concentrations.

2.3 DISCUSSION OF FIELD DATA

Eleven trials in all were carried out but only the last three were sufficiently successful to be useful for modelling purposes. Although many factors contributed to this outcome, three were particularly problematic. Firstly, because of Dugway's extremely tight schedule, we were compelled to conduct at least one test each day despite the fact that a minimal chemical analysis of the samples acquired during any given test required nearly 48 hours to complete, including shipping by Federal Express. This meant that we could not implement any changes in test procedure suggested by the results of the data analysis until several more tests had already been conducted.

Secondly, our original sampling network (Figure 2.2) was designed to accommodate a wide range of wind directions and so the samplers were laid out in such a manner as to cover a large area (1600 m by 800 m at 100 m intervals). This resulted in insufficient spatial resolution: during tests with high winds, the plume was less than 100 m wide until it was more than 400 m down range, thus fewer than a half dozen samplers were actually exposed to the plume at less than 400 m; during convective, low wind speed tests the initial upward momentum of the plume was augmented by strong insolation which caused the bulk of the plume to rise above the height of the samplers (1.5 m) by the time it had traveled to the first row. This problem was overcome by implementing the high resolution network (Figure 2.3); however, because of the tight test schedule, eight tests had been conducted before this problem could be identified and corrected.

Finally, the distance from the point of release at which the smoke could be detected was limited to about 200 m due to the high background "noise" level caused by contamination of the sample tubes. The reason for this high background level centers on the basic design of the concentration sampler itself. Since the

Tenax readily adsorbs hydrocarbons from the atmosphere, each sample tube had to be thermally conditioned prior to use to remove any hydrocarbons already present. Subsequent to this conditioning procedure, the tubes were allowed to cool and were then sealed with plastic endcaps. Laboratory tests indicated that this produced adequately conditioned tubes; however, tubes which were transported to Dugway, but not used, showed an average contamination of 0.37 µl per tube. This contamination was eventually traced to the apparent outgassing of the plastic endcaps. As a result, smoke concentrations less than about 1 mg/m^3 (which resulted in substantially less than 0.37 µl of oil collected) were not discernible from the noise; such concentration levels occurred at roughly 200 m for these tests.

2.3.2 Concentration Data

The results of tests T0009, T0010 and T0011, conducted on the high resolution grid, are given in Appendix D. Isopleths of these data are plotted in Figures 2.5 through 2.7. In these figures the sampler locations are indicated by small open circles. The position of the source is also indicated along with an arrow which shows the mean wind direction during the testing period. The shaded area on each side of the arrow is proportional to the standard deviation of the wind direction. During the course of each of these tests the M3A3E3 smoke generator unit failed. This is the reason for the STOP and RESTART times indicated in the figures. During T0011 (11 April 1985) the wind direction changed while the generators were being field-repaired. To accommodate this wind shift, the generator was relocated prior to restarting the test; both locations are indicated in Figure 2.7.

These figures give a somewhat distorted impression of the plume. This is largely due to the difficulty encountered in contouring irregularly gridded data such as these. The extent of this difficulty is best revealed by comparing these figures to the predictions of a simple gaussian plume model (Pasquill and Smith, 1983, p. 320)

$$\chi(x,y,0) = \frac{Q}{\pi U \sigma_y \sigma_z} \exp\left(-\frac{y^2}{2\sigma_y^2}\right) \qquad (2.5)$$

where $\chi(x,y,0)$ is the mean concentration at ground level, Q is the release rate, U is the mean wind speed and σ_y and σ_z are the plume parameters defined by

$$\sigma_y = \sigma_\theta \times f_1(x)$$
$$\sigma_z = \sigma_\phi \times f_2(x) \qquad (2.6)$$

Here σ_θ and σ_ϕ are the measured standard deviations of the wind direction and inclination, respectively; x is the distance downwind of the source and the f(x) are empirical functions of downwind distance. We have used Draxler's (1976) form for the f(x)

$$f_1(x) = f_2(x) = \frac{1}{1 + 0.90\sqrt{x/(UT_i)}} \qquad (2.7)$$

Draxler defines T_i as the travel time (=x/U) for f(x) to fall to one half of its initial value. Based on diffusion data from several field studies, Draxler suggests T_i = 300 s for diffusion from a near surface level source.

Isopleths of the predictions of the model for tests T0009, T0010 and T0011 are presented in Figures 2.8 through 2.10, respectively. These contours were determined from predictions for a rectangular grid (7 x11) and do not appear to be in especially close agreement with the field data. However, Figures 2.11 through 2.13 present isopleths of the same model predictions determined at the sampler locations used to

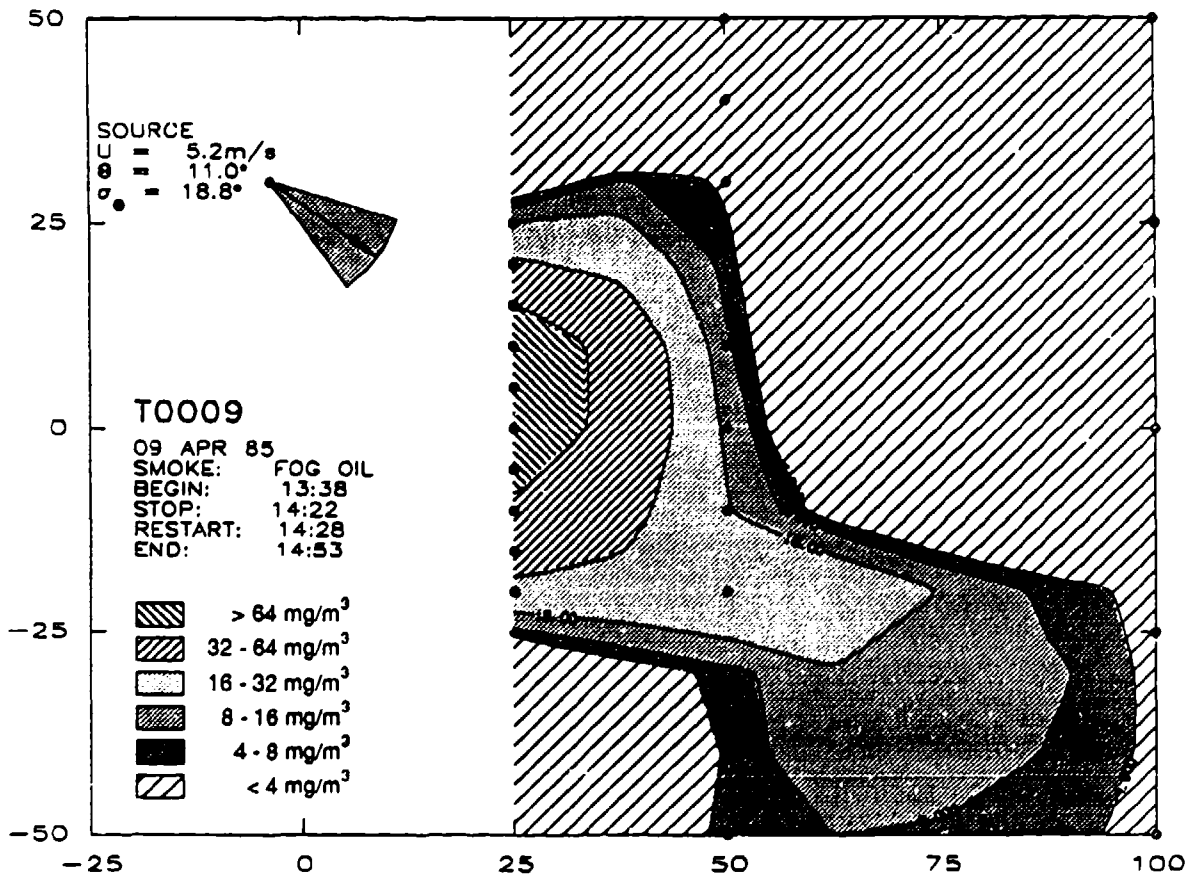

Figure 2.5 Isopleths of average concentration for test T0009. Sampler locations are indicated by small filled circles. the arrow at the source location indicates the mean wind direction; its length is proportional to the mean wind speed. The shaded sector around the arrow indicates the standard deviation of the wind direction.

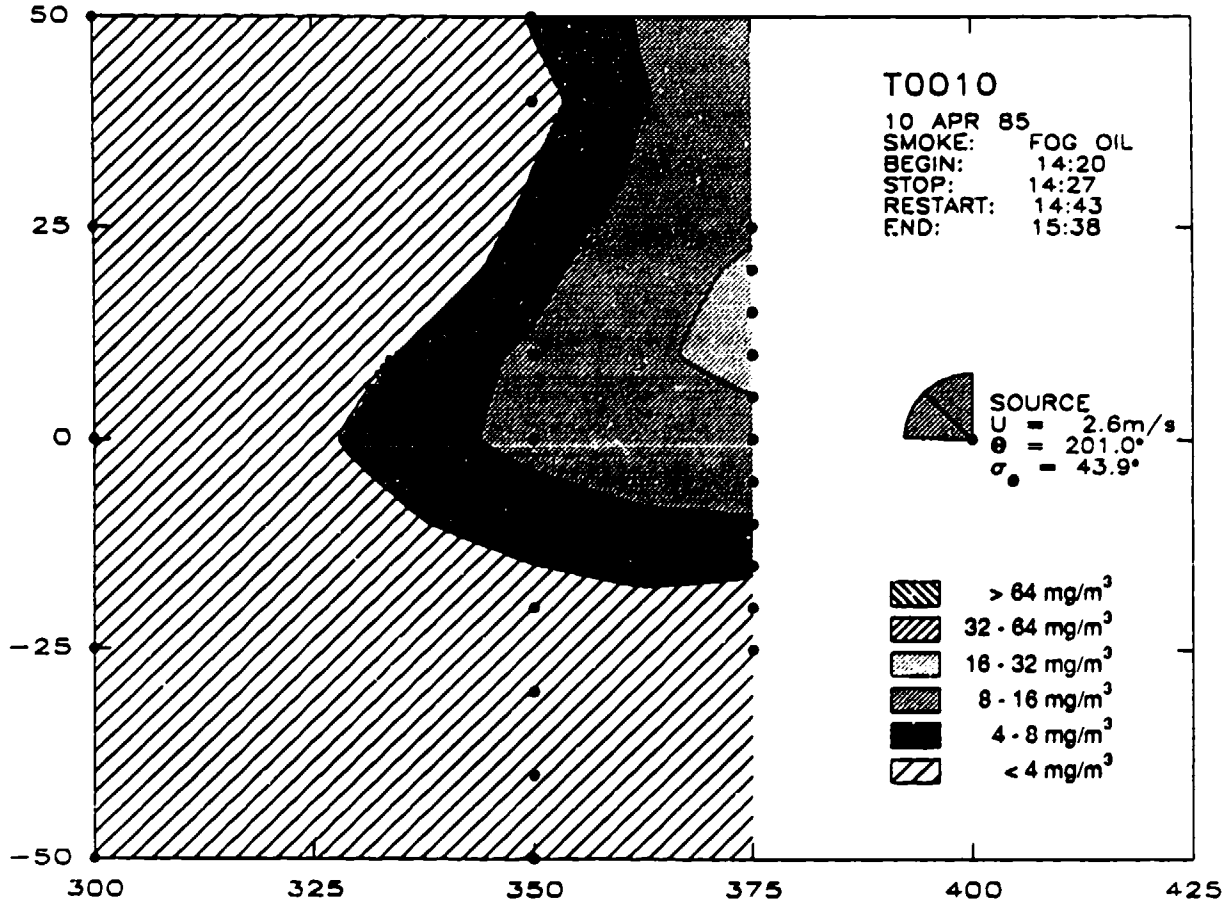

Figure 2.6 Isopleths of average concentration for test T0010. Sampler locations are indicated by small filled circles. The arrow at the source location indicates the mean wind direction; its length is proportional to the mean wind speed. The shaded sector around the arrow indicates the standard deviation of the wind direction.

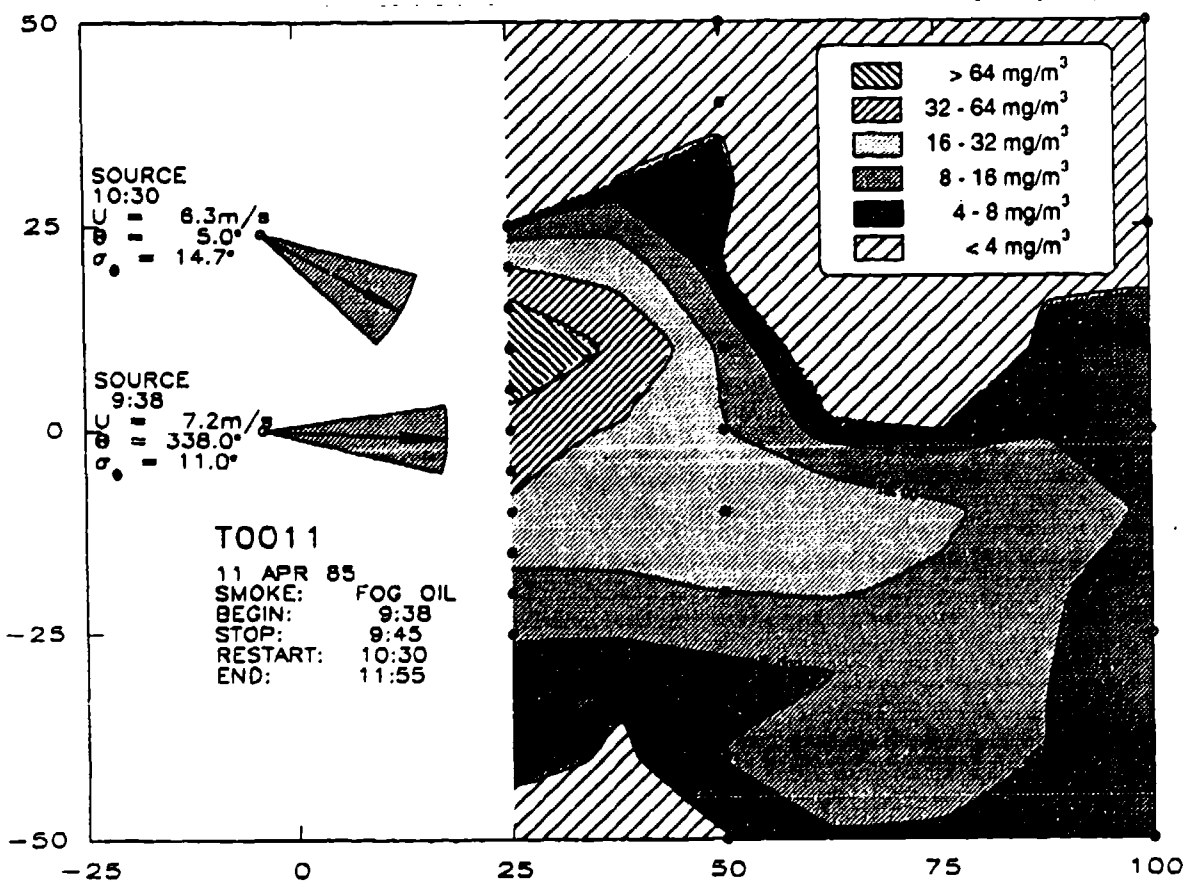

Figure 2.7 Isopleths of average concentration for test T0011. Sampler locations are indicated by small filled circles. The arrow at the source location indicates the mean wind direction; its length is proportional to the mean wind speed. The shaded sector around the arrow indicates the standard deviation of the wind direction.

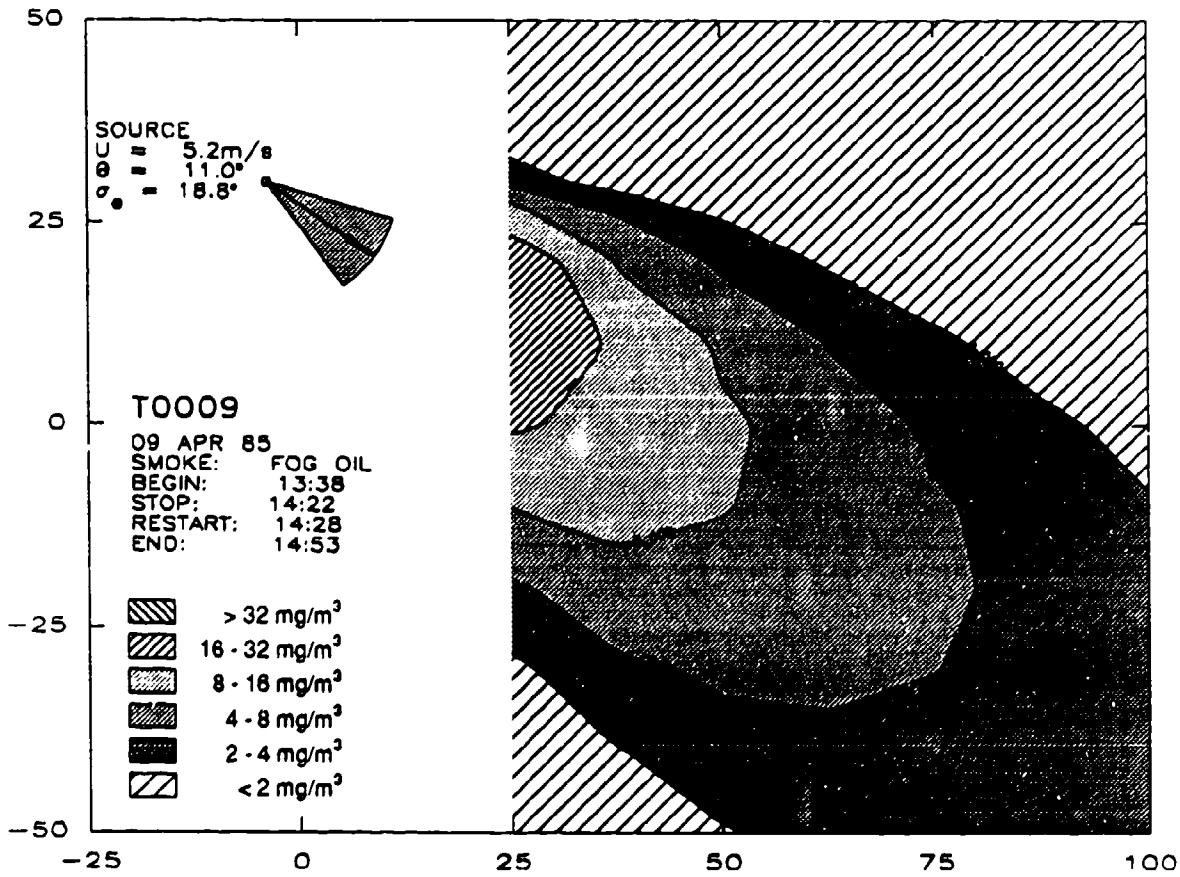

Figure 2.8 Isopleths of average concentration computed on a rectangular grid (7 x 11) using Draxler's (1976) model for test T0009.

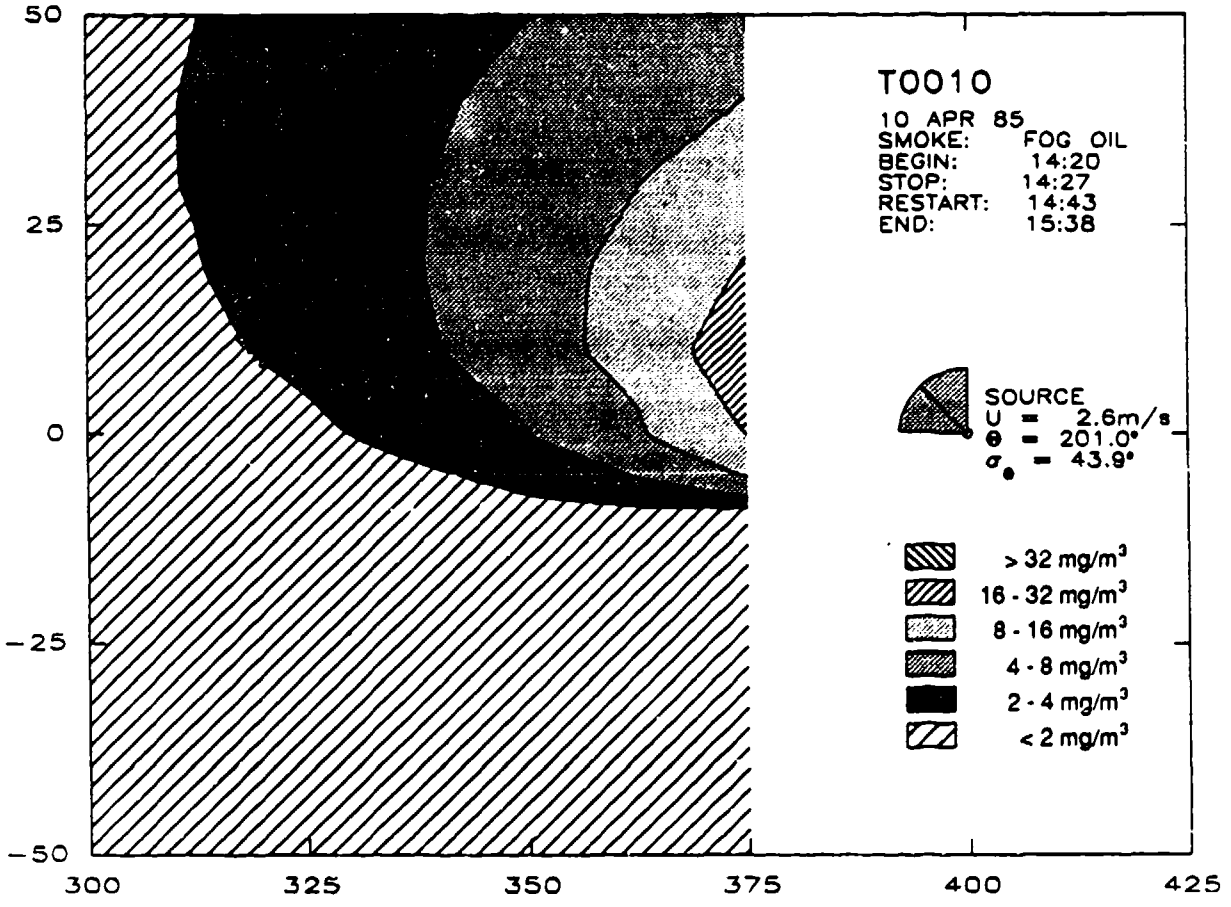

Figure 2.9 Isopleths of average concentration computed on a rectangular grid (7 x 11) using Draxler's (1976) model for test T0010.

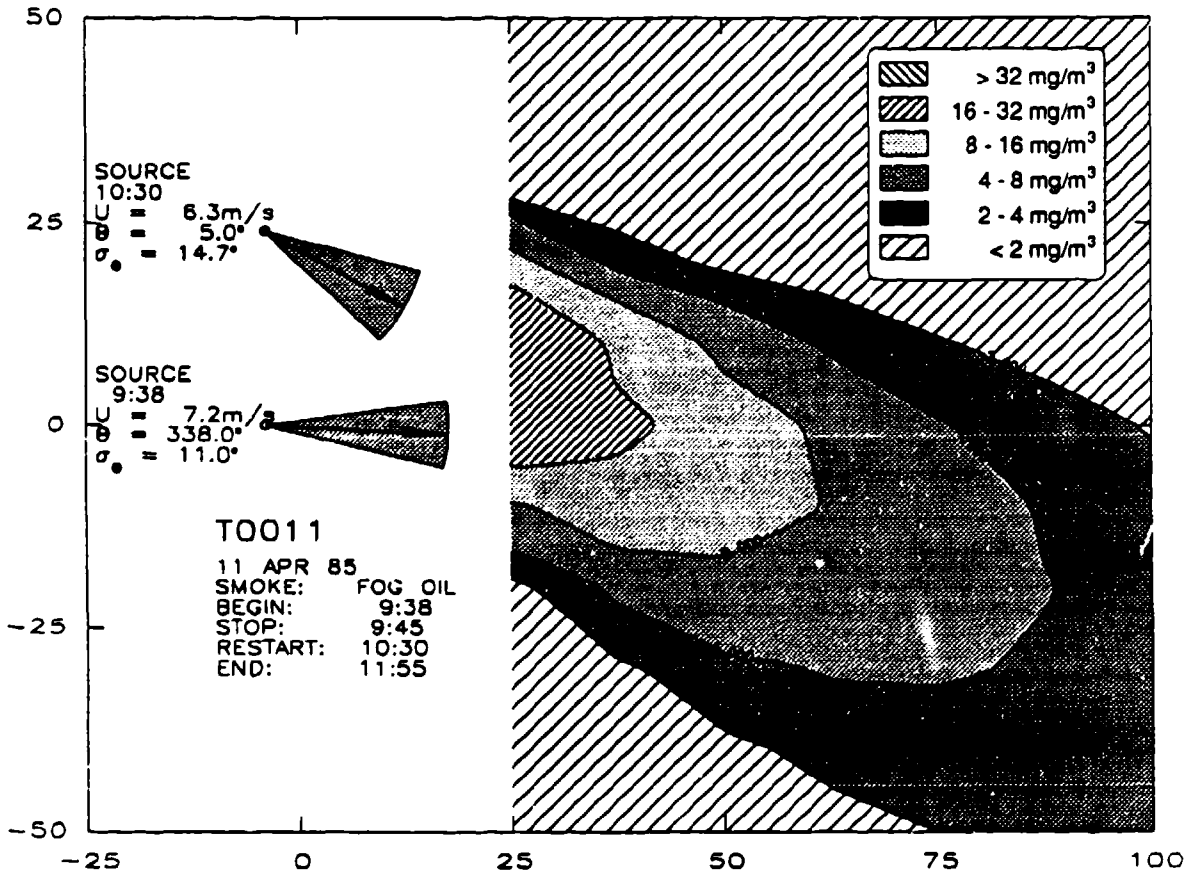

Figure 2.10 Isopleths of average concentration computed on a rectangular grid (7 x 11) using Draxler's (1976) model for test T0011.

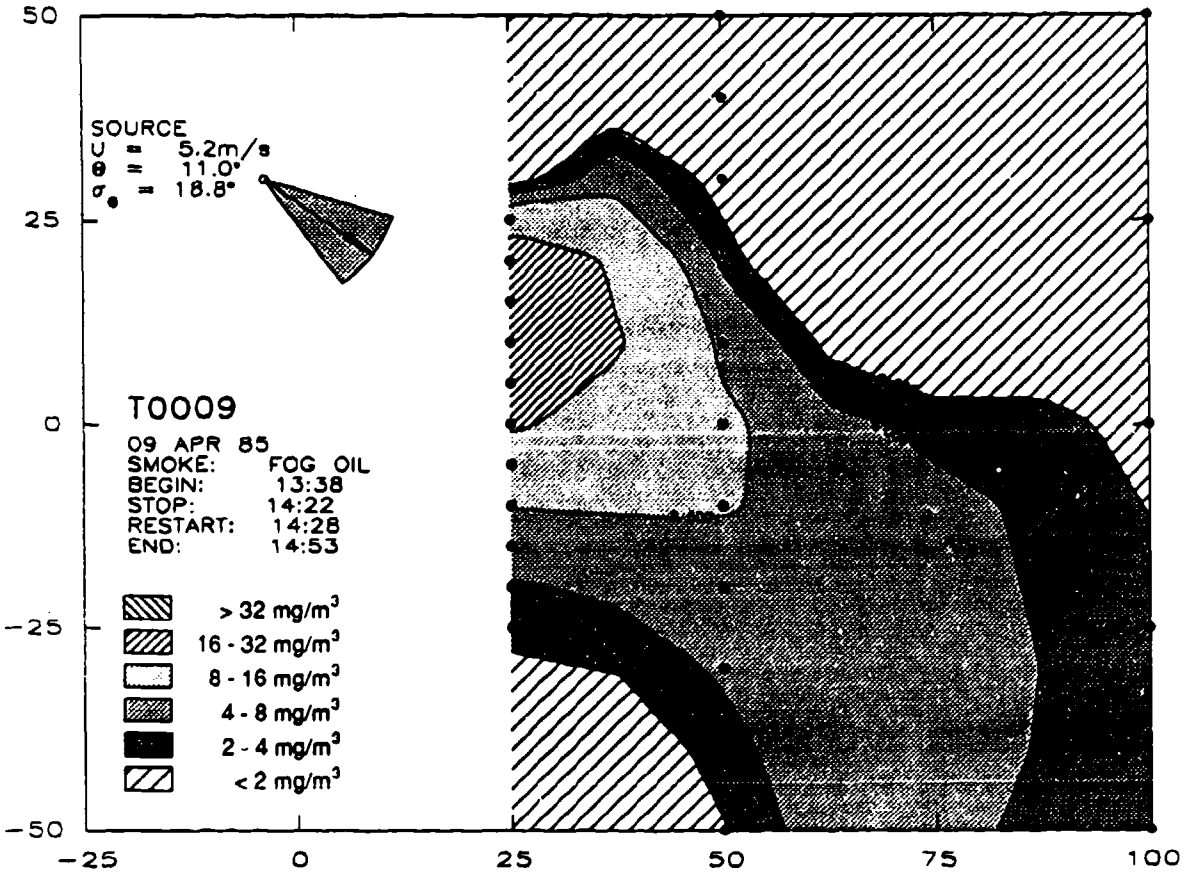

Figure 2.11 Isopleths of average concentration based on values computed at the sampler locations using Draxler's (1976) gaussian plume model for test T0009.

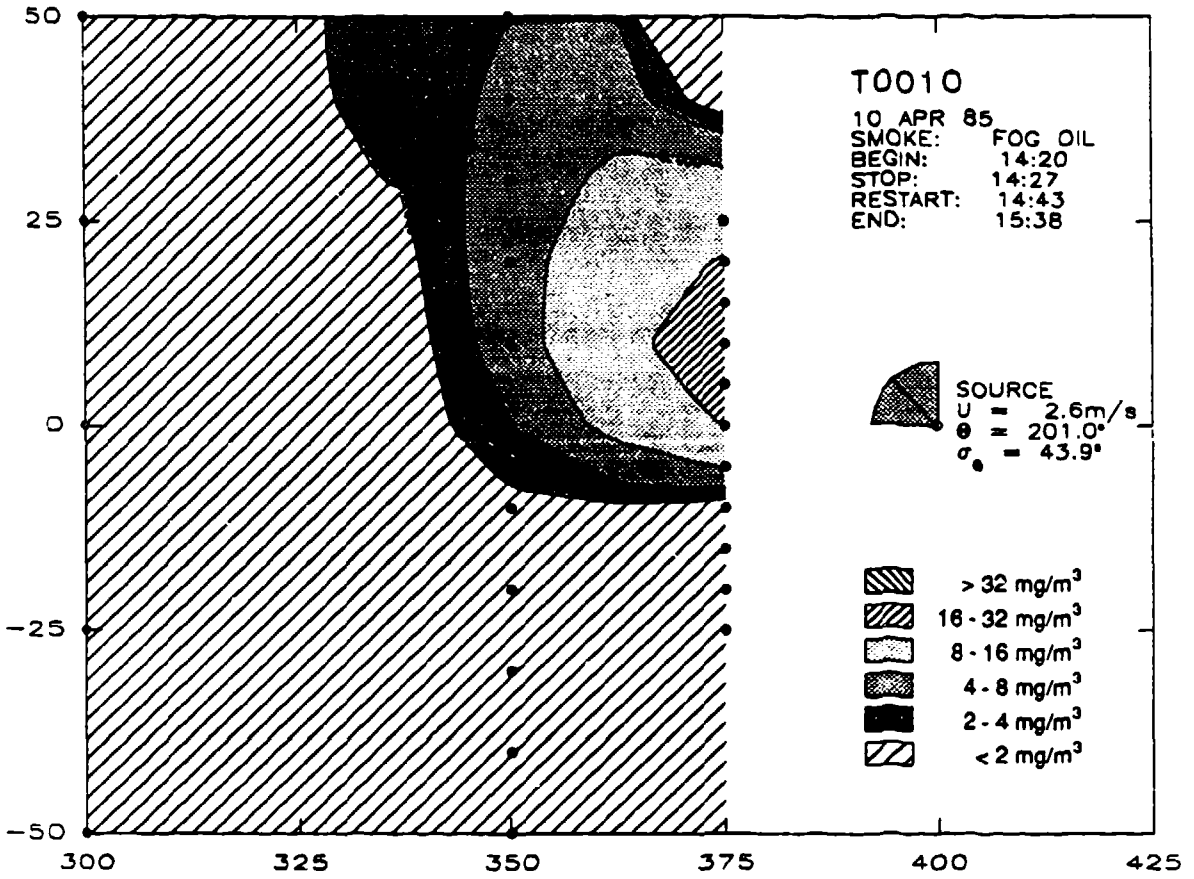

Figure 2.12 Isopleths of average concentration based on values computed at the sampler locations using Draxler's (1976) gaussian plume model for test T0010.

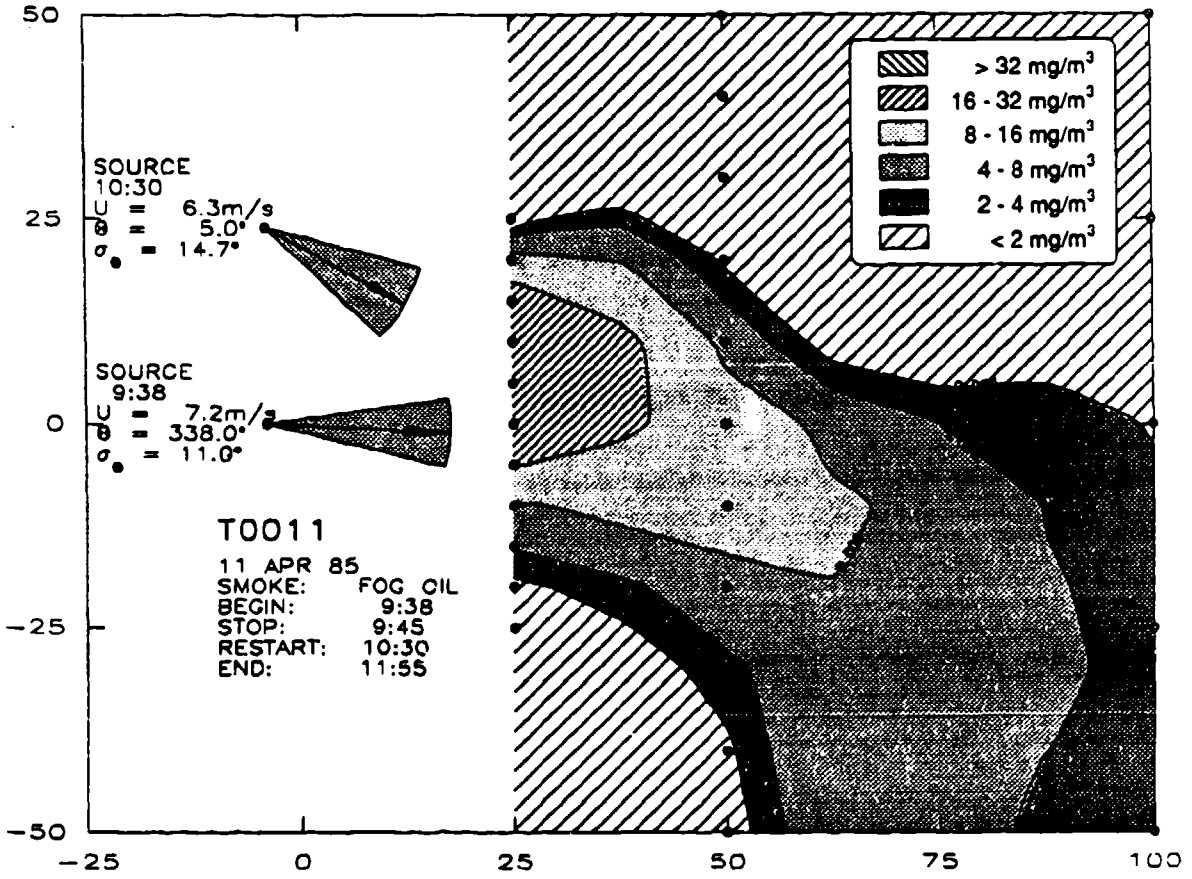

Figure 2.13 Isopleths of average concentration based on values computed at the sampler locations using Draxler's (1976) gaussian plume model for test T0011.

collect the data. These figures appear much more like those representing the field data; the distortion is thus seen to be largely due to interpolation ambiguities and not a fault in the data.

It should be noted that for T0009, the source was initially located at J4 (0,0) rather than (-4,30) as indicated in the figures. However, because the bulk of the plume missed the sampling grid to the west (toward the bottom of the figure) from this release point, the source was relocated to (-4,30) within the first 15 minutes of the test. Because the dissemination of smoke continued during the relocation, the data closest to the release point appear to suggest a release point between (0,0) and (-4,30).

Another apparent discrepancy between the data and model predictions occurs for test T0010 where the field data appear to be at odds with the wind direction. As Figure 2.17 indicates, the wind direction frequency distribution for T0010 was actually bimodal and thus not well represented by the mean value of 201°. As a result, the model prediction for T0010, which assumes a normal wind direction frequency distribution, is not in as close agreement with the field data as those for T0009 and T0011 when the wind direction frequency distributions were both nearly normal. Furthermore, a careful examination of the frequency distribution and the contour plots for T0010 shows that the data do indeed reflect the observed wind pattern.

Comparison of Figures 2.11 - 2.13 with Figures 2.5 - 2.7 indicates that the model and data are in reasonably good qualitative agreement. More quantitative comparisons may be made by examining Figures 2.14 - 2.16 where model predictions and data are plotted for each transect. These comparisons indicate that the maxima are in virtually the same locations on each transect, the lateral spreading is roughly equal and the concentrations decline with distance in a similar manner. However, the magnitude of the data is larger than the model predictions by about a factor of three. This difference is most likely an indication of the shortcomings of this simple model rather than of problems with the data. Comparisons of more sophisticated dispersion models with these data, carried out by Policastro, *et al.* (1986), reveal much closer agreement between the field data and the model predictions.

Data from other field studies also support the field data. Table 2.2 presents a comparison of data from the present study with selected tests from Project CONDORS (Kaimal, *et al.*, 1986) and Project Prairie Grass. All of these tests were comprised of near-surface releases into unstable atmospheric conditions. Project CONDORS involved the measurement by lidar and doppler radar of fog-oil smoke concentrations at elevations above 50 m resulting from both surface and elevated releases. Estimates of ground level concentration were obtained by extrapolating downward from the 50 m elevation assuming a zero concentration gradient. Gaseous sulphur dioxide was released during the Prairie Grass study. In the table, U/w_*, the ratio of the mean velocity to the convective velocity scale, provides an indication of the strength of the convection; a value near or less than unity indicates strong convection. The dilution factor, χ/Q, is the average concentration along the centerline of the plume divided by the release rate; it will be used to compare the results of the different studies.

The tabulated values reveal that the dilution factors computed from the Prairie Grass data are two to three times greater than the corresponding values from our data on both the 50 m and 200 m transects. This may be due to the differences in release conditions: the SO_2 was released close to the ground and with an exit velocity and temperature near ambient whereas we generated fog-oil smoke with a high exit temperature and velocity directed upward at a 45° angle to the ground. This probably caused the fog-oil smoke plume to develop farther from the ground and thus to yield lower concentrations near the ground than would have ocurred had a release scheme more similar to the Prairie Grass method been adopted. Conversely, the values from the CONDORS data are somewhat lower than ours, probably due to a combination of the 3 m release height and the assumed zero gradient between the ground and the 50 m measurement height.

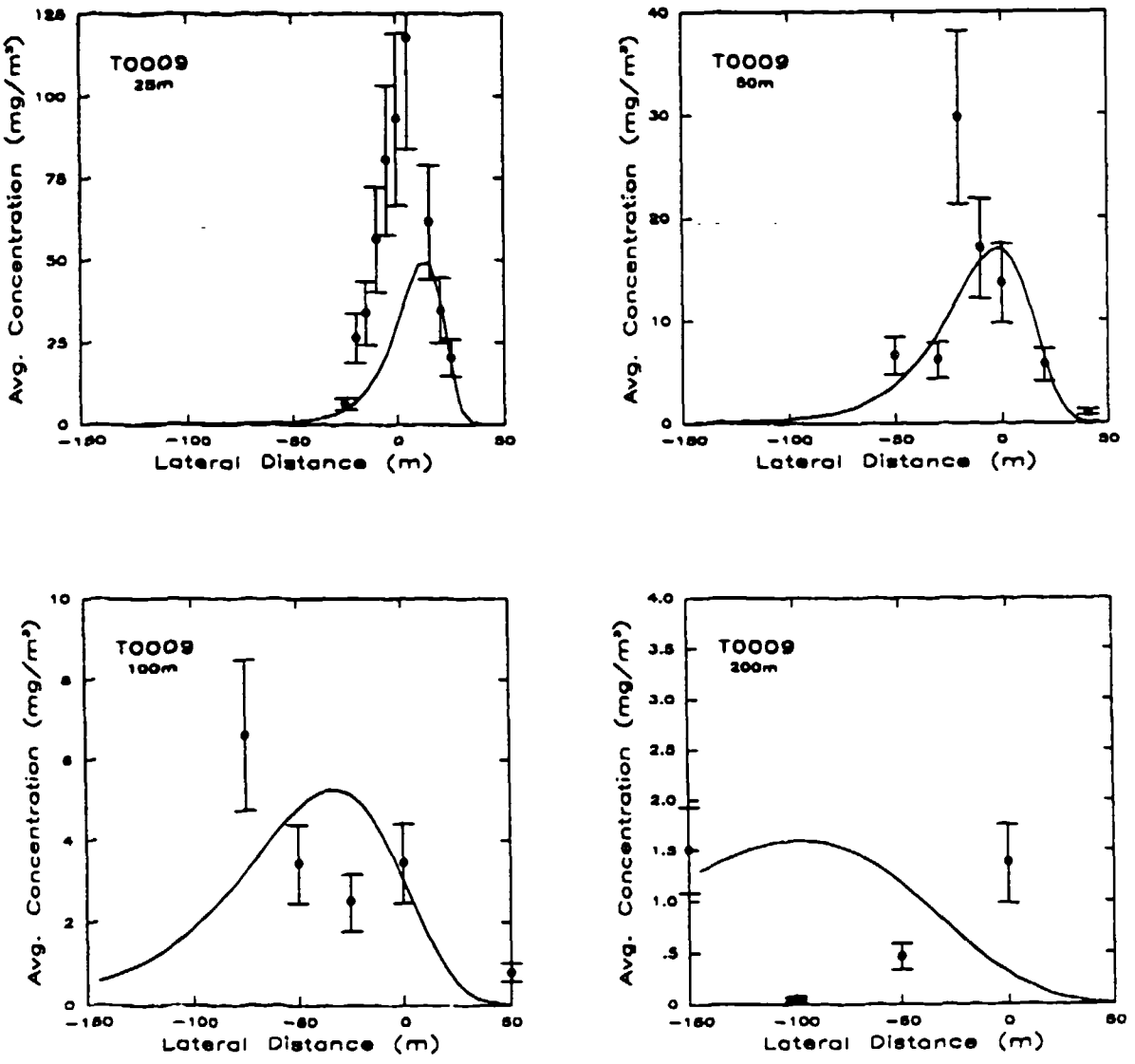

Figure 2.14 Concentration data (•) from test T0009 compared with Draxler's gaussian plume model (—) along the 25 m (upper left), 50 m (upper right), 100 m (lower left) and 200 m (lower right) transects. The error bars indicate the 90% confidence limits.

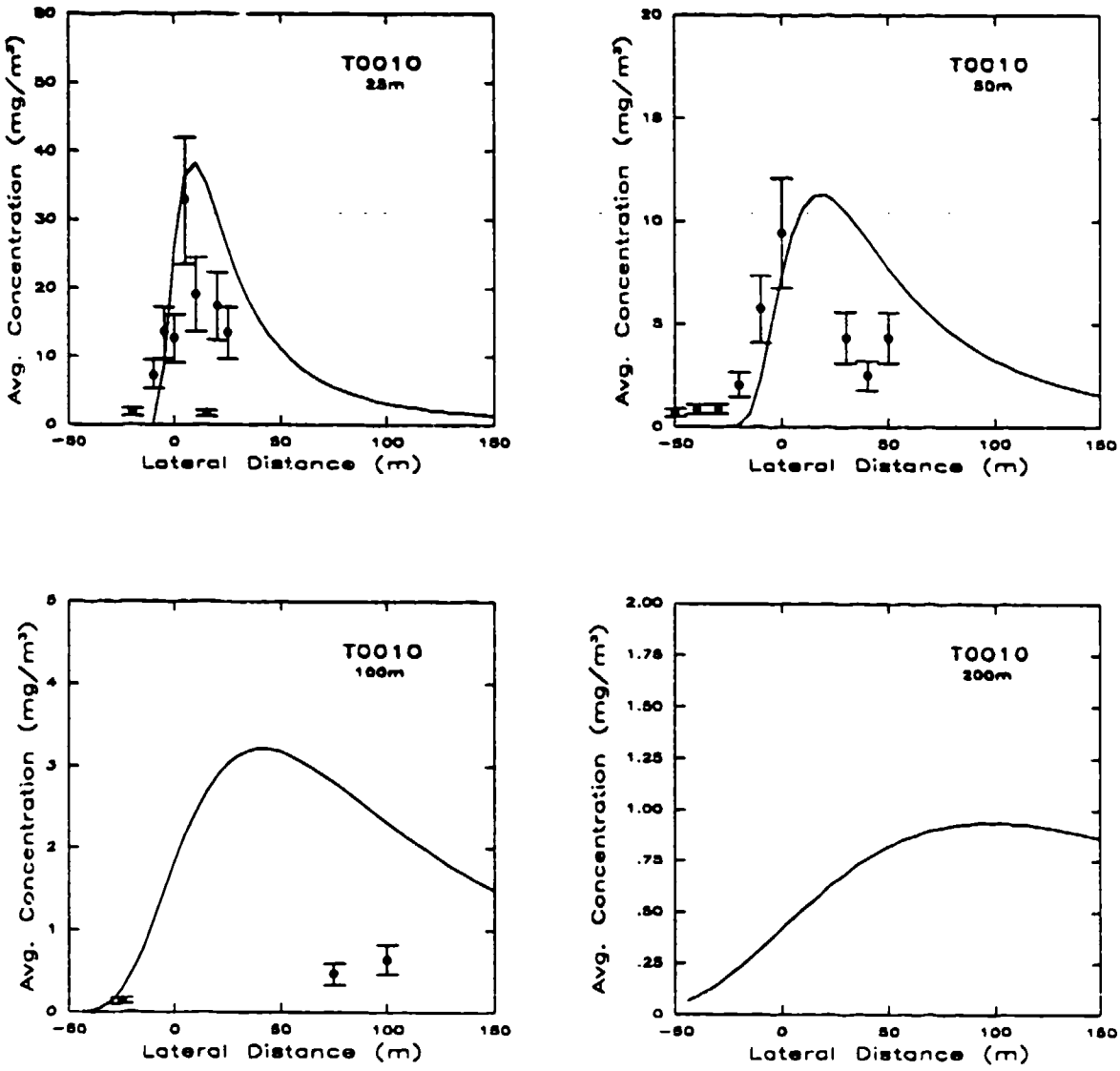

Figure 2.15 Concentration data (•) from test T0010 compared with Draxler's gaussian plume model (—) along the 25 m (upper left), 50 m (upper right), 100 m (lower left) and 200 m (lower right) transects. The error bars indicate the 90% confidence limits.

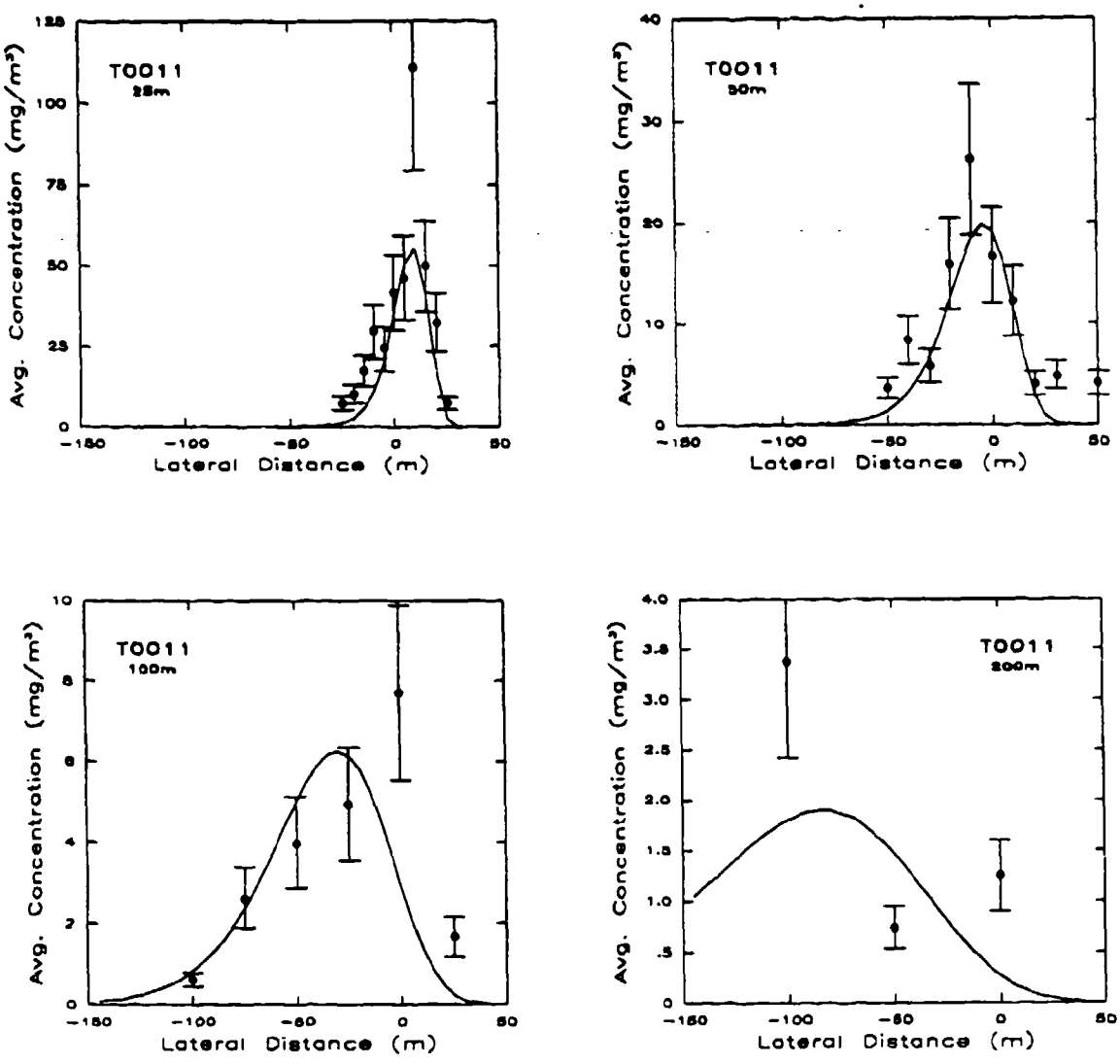

Figure 2.16 Concentration data (•) from test T0011 compared with Draxler's gaussian plume model (—) along the 25 m (upper left), 50 m (upper right), 100 m (lower left) and 200 m (lower right) transects. The error bars indicate the 90% confidence limits.

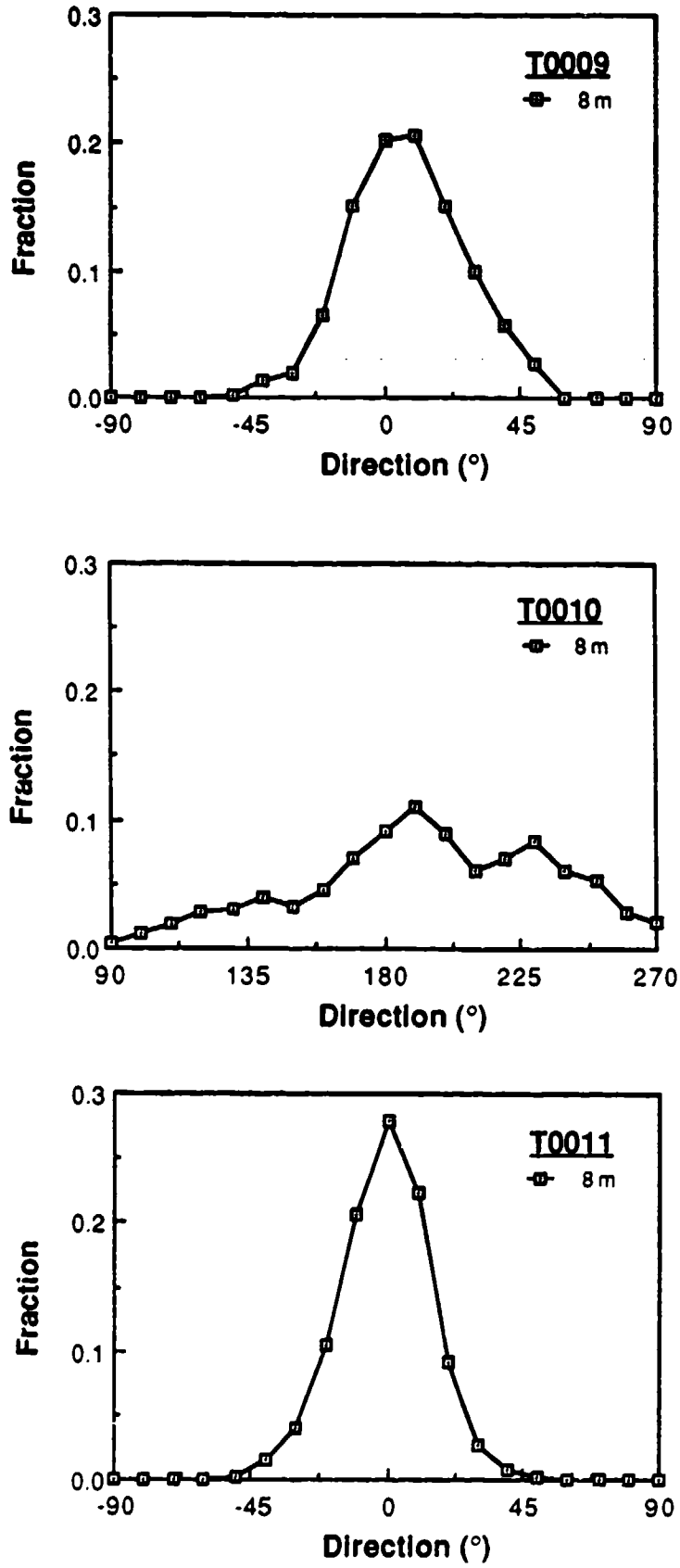

Figure 2.17 Frequency distributions of 8 m wind direction for T0009 (top), T0010 (center), T0011 (bottom).

Table 2.2 Comparison of Concentration Data from Several Field Studies

	Test	U/w_*	χ/Q (s-m^{-3})	
			50 m	200 m
Present Study	T0009	3.0	6.88×10^{-4}	3.17×10^{-5}
	T0010	0.9	2.26×10^{-4}	8.61×10^{-5}
	T0011	3.2	6.94×10^{-4}	8.97×10^{-5}
Prairie Grass	7	2.8	10.3×10^{-4}	4.70×10^{-5}
	10	2.6	18.5×10^{-4}	11.4×10^{-5}
	16	1.4	42.7×10^{-4}	21.9×10^{-5}
	25	2.7	28.3×10^{-4}	7.55×10^{-5}
CONDORS	4-82	1.3	—	1.29×10^{-5}
	5-82	0.9	—	3.96×10^{-5}
	1-83	1.6	—	2.93×10^{-5}
	2-83	0.9	—	4.85×10^{-5}
	3-83	1.3	—	2.31×10^{-5}
	4-83	1.0	—	2.03×10^{-5}

2.3.3 Particle Size Data

Particle size data were successfully acquired during tests T0009, T0010 and T0011. The data from these trials is summarized in Table 2.3 along with the results of a measurement using our laboratory fog-oil smoke generator.

Table 2.3 Summary of Particle Size Data

	Impactor No.	Flow Rate (Lpm)	Location (x,y)	d_M (μm)	MMAD (μm)	σ_g
T0009	6	1.4	(25,0)	0.61	0.34	2.06
	7	1.2	(50,0)	1.27	0.79	1.86
T0010	1	0.7	(375,0)	1.18	0.88	2.82
	6	0.6	(350,0)	1.35	1.31	4.44
	3	1.4	(300,-50)	0.86	0.85	3.81
	4	1.1	(300,-50)	1.06	0.51	3.04
T0011	7	1.3	(25,0)	0.71	0.35	3.19
	8	1.0	(50,0)	1.32	0.89	3.34
	5	1.4	(400,0)	0.63	0.71	7.04
Lab Smoke	-	1.0	—	0.70	0.42	2.18

In the table, the flow rate through the impactor is listed as well as its position on the sample grid during the test. The mass mean diameter d_M, mass median aerodynamic diameter (MMAD) and geometric standard deviation σ_g are also given. These are used to characterize the size distribution of the fog-oil smoke and to provide a basis for comparison with the results of a previous examination of fog-oil smoke by IITRI (Katz, *et al.*,

1980). The mass mean diameter is computed by summing the products of the mass fractions per stage x_i, and the 50% cutoff sizes D_{p50} (Table 2.1) after adjustment for the measured flow rate (Hinds, 1982; page 79):

$$\overline{d_M} = \sum_{i=1}^{7} x_i D_{p50,i} \; ; \; x_i = m_i / \sum_{i=1}^{8} m_i \qquad (2.8)$$

Here m_i is the mass collected on an individual stage of the impactor. Note that the first summation, to compute the mean, is over the seven stages of the impactor only whereas the mass fraction computation must also include the mass collected on the backup filter. IITRI computed the mass mean diameter somewhat differently: instead of using the D_{p50} value for each stage, they used an average comprised of the D_{p50} for a given stage and the previous stage. That is, the D_{p50} for stage 2 would be an average of the values for stage 1 and 2.

The mass median aerodynamic diameter (MMAD) indicates the particle size at which 50% of the cumulative mass occurs. The aerodynamic diameter is the diameter of a spherical particle exhibiting the same aerodynamic behavior as the particle in question. However, since the fog-oil smoke droplets are essentially spherical, the droplet diameter and the aerodynamic diameter are equivalent. Together with the geometric standard deviation σ_g, the MMAD describes a log-normal distribution (Hinds,1982; page 85):

$$df = \frac{1}{\sqrt{2\pi}\; d_p \ln \sigma_g} \exp\left(-\frac{(\ln d_p - \ln MMAD)^2}{2 (\ln d_p)^2} \right) d\, d_p \qquad (2.9)$$

Here df is the fraction of particles having diameters between d_p and $d_p + d\, d_p$.

Plots of the data collected from each impactor listed in Table 2.3 are presented in Figures 2.18 through 2.27. These figures represent the percentage of the total mass collected that was contributed by particles less than or equal to a given aerodynamic diameter. The D_{p50} sizes for each impactor have been corrected for the actual, measured flow rate. The straight line in these figures represents a log-normal distribution having the same MMAD and geometric standard deviation σ_g as the data.

The smoke generated in the laboratory is shown in Figure 2.18 to be well characterized by a log-normal distribution; the data all lie close to the straight line. Most of the field data are also well represented by a log-normal distribution, as the figures demonstrate. Several, however, deviate significantly from log-normal. Figure 2.19, for example, is essentially monodisperse (most of the mass collected on stage 6) at 0.62 μm. Figures 2.24 and 2.26 also deviate from log-normal but in a manner which suggests clogged jets.

The average mass mean and mass median diameters for the data are 1.0 and 0.74 μm respectively. This is slightly smaller than IITRI's results (1.16 and 0.9 μm for mass mean and mass median diameters, respectively) which probably reflects our smaller D_{p50} values. (Recall that we did not average successive D_{p50} sizes as IITRI did.) IITRI also observed that the aerosol agglomerated with time in their test chamber. No similar trend of increased particle size with distance is discernible from our data. Although this may be due to a rather large amount of scatter in the present data, it might also be true that agglomeration is not as significant in an unconfined aerosol.

2.3.4 Deposition Data

No significant amounts of fog-oil smoke were detected on the deposition filters for any test whether they were oriented horizontally or vertically. Since both analysis procedures outlined earlier produced consistent results for laboratory-prepared standard samples (filters on which a known amount of oil had been deposited), it may be concluded that within the resolution of our method of analysis, deposition and

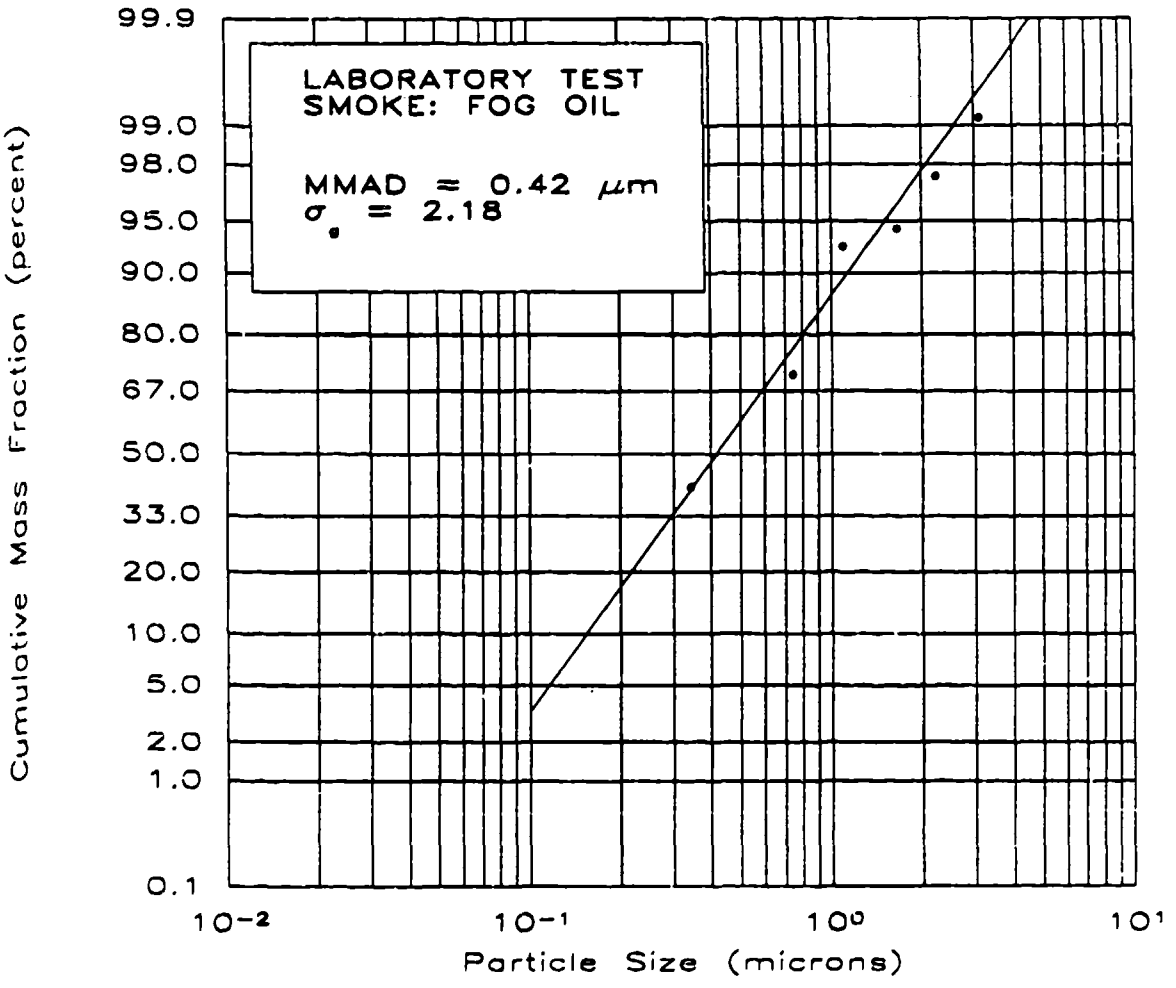

Figure 2.18 Log-probability plot of the cumulative size distribution of a laboratory-generated oil fog aerosol. Aspiration Rate: 1.0 Lpm; Mass Median Aerodynamic Diameter (MMAD): 0.42 microns; Geometric Standard Deviation: 2.18.

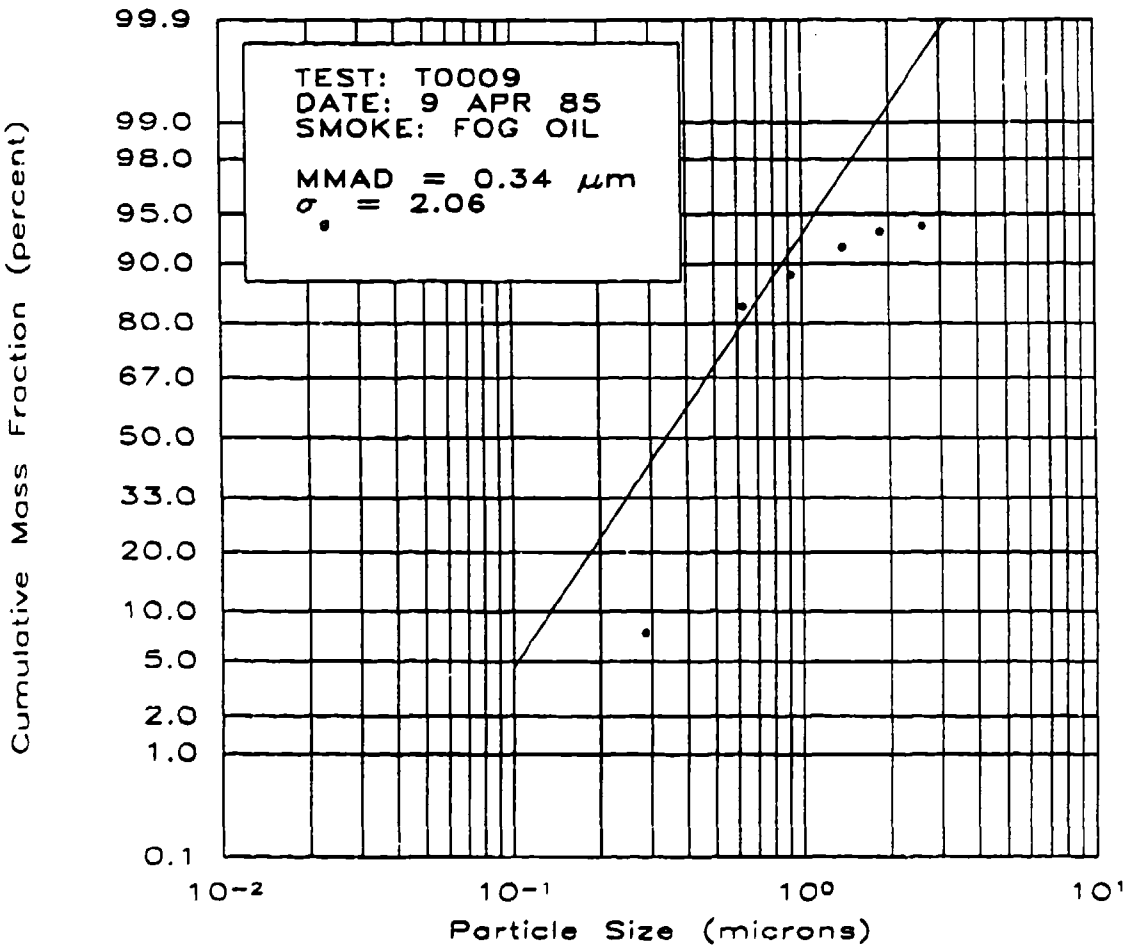

Figure 2.19 Log-probability plot of the cumulative size distribution of oil fog aerosol for test T0009. Cascade Impactor no. 6 located at (25,0), about 40 m downwind of the smoke source. Aspiration Rate: 1.42 Lpm; Mass Median Aerodynamic Diameter (MMAD): 0.34 microns Geometric Standard Deviation: 2.06.

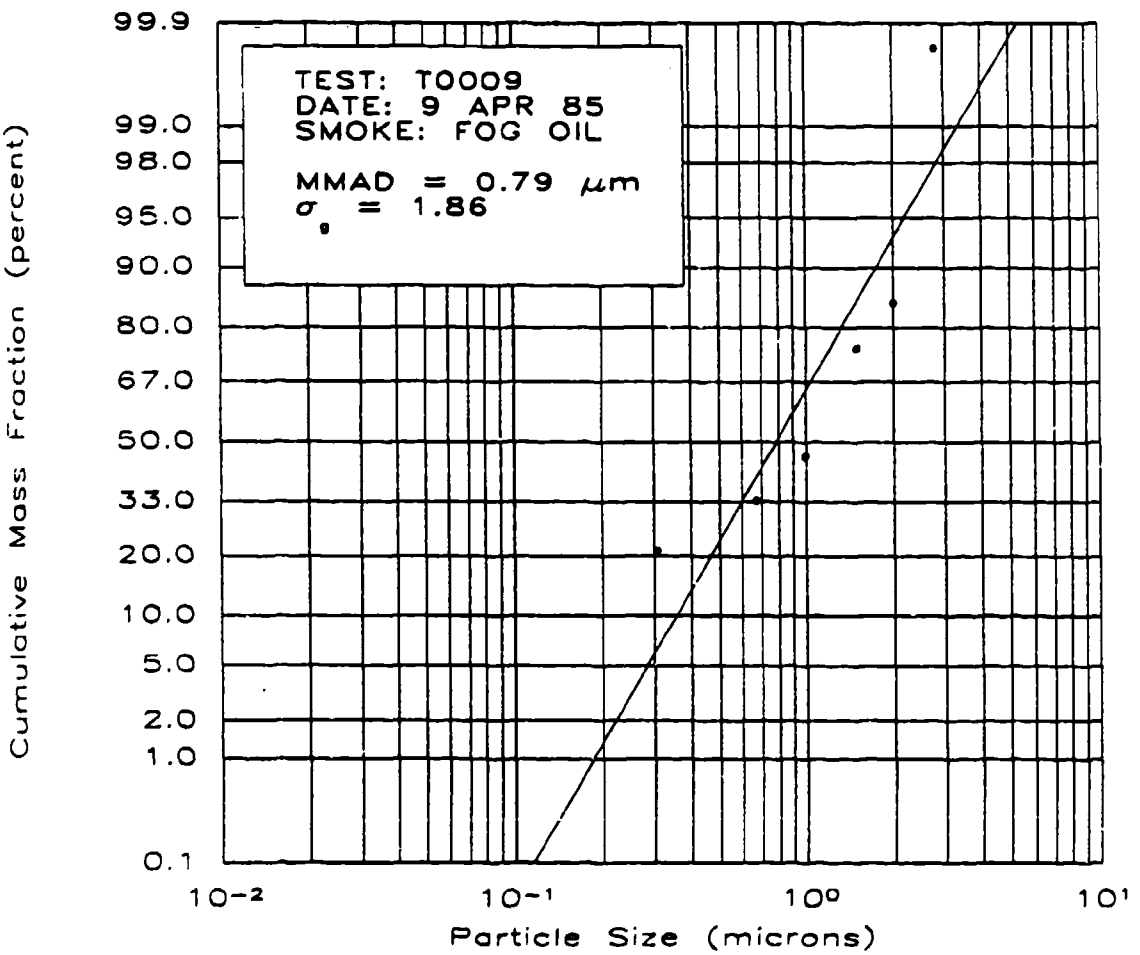

Figure 2.20 Log-probability plot of the cumulative size distribution of oil fog aerosol for test T0009. Cascade Impactor no. 7 located at (50,0), about 60 m downwind of the smoke source. Aspiration Rate: 1.23 Lpm; Mass Median Aerodynamic Diameter (MMAD): 0.79 microns Geometric Standard Deviation: 1.86.

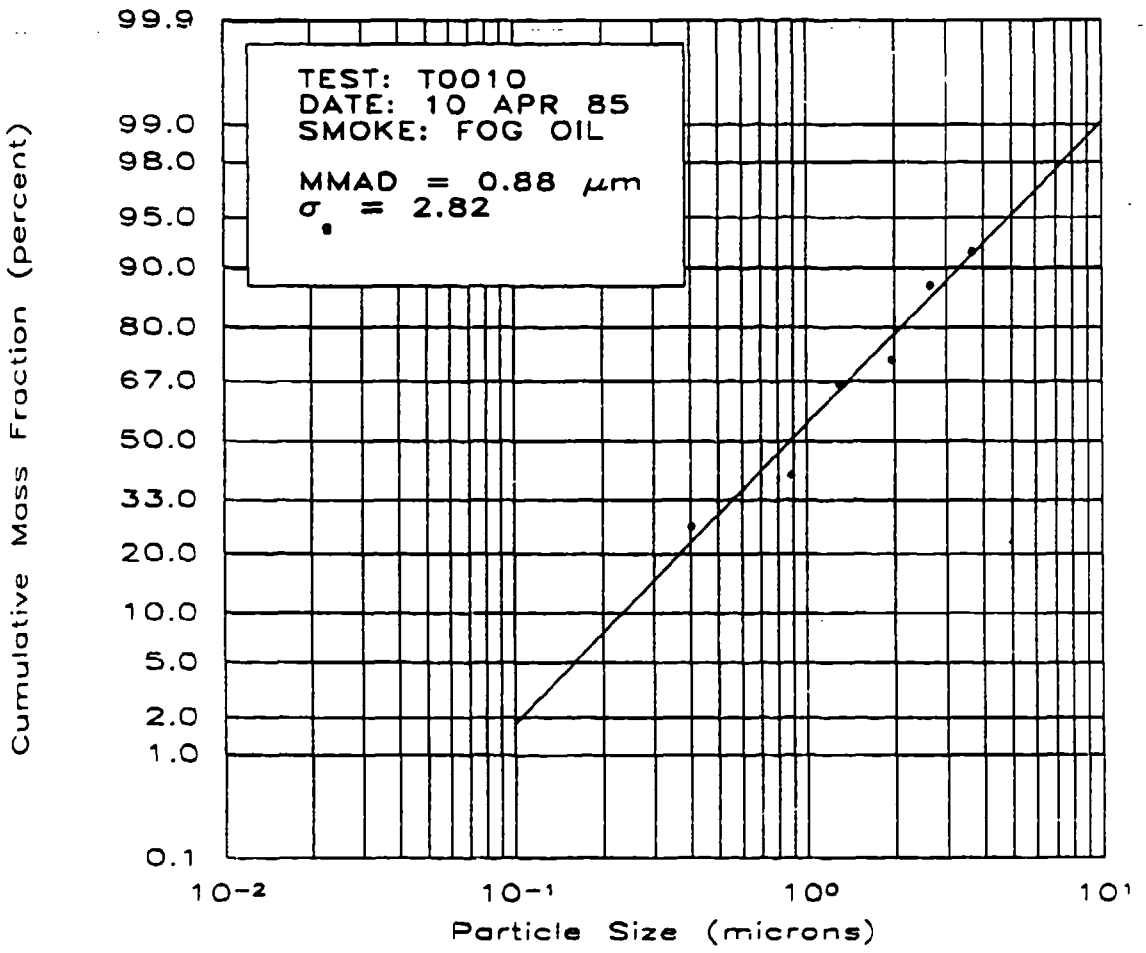

Figure 2.21 Log-probability plot of the cumulative size distribution of oil fog aerosol for test T0010. Cascade Impactor no. 1 located at (375,0), about 25 m downwind of the smoke source. Aspiration Rate: 0.71 Lpm; Mass Median Aerodynamic Diameter (MMAD): 0.88 microns Geometric Standard Deviation: 2.82.

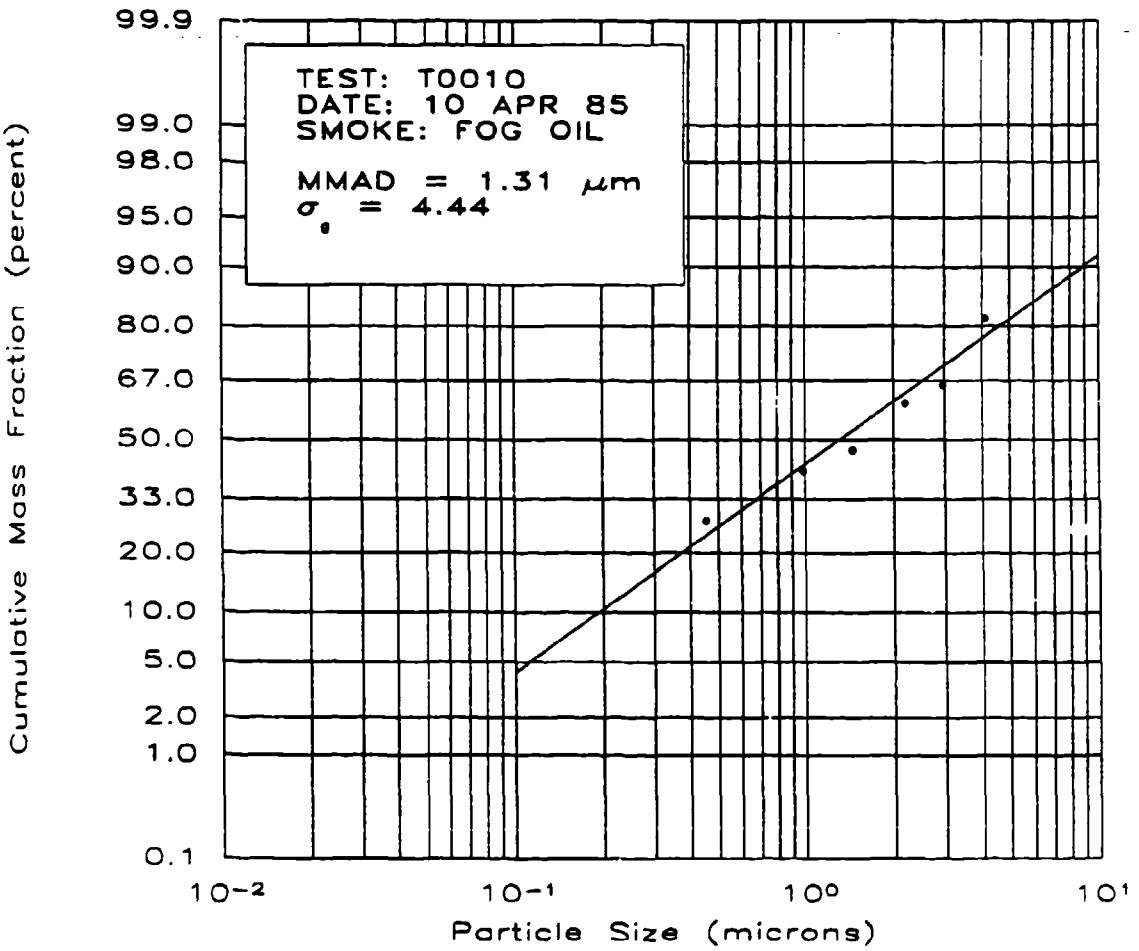

Figure 2.22 Log-probability plot of the cumulative size distribution of oil fog aerosol for test T0010. Cascade Impactor no. 6 located at (350,0), about 50 m downwind of the smoke source. Aspiration Rate: 0.57 Lpm; Mass Median Aerodynamic Diameter (MMAD): 1.31 microns Geometric Standard Deviation: 4.44.

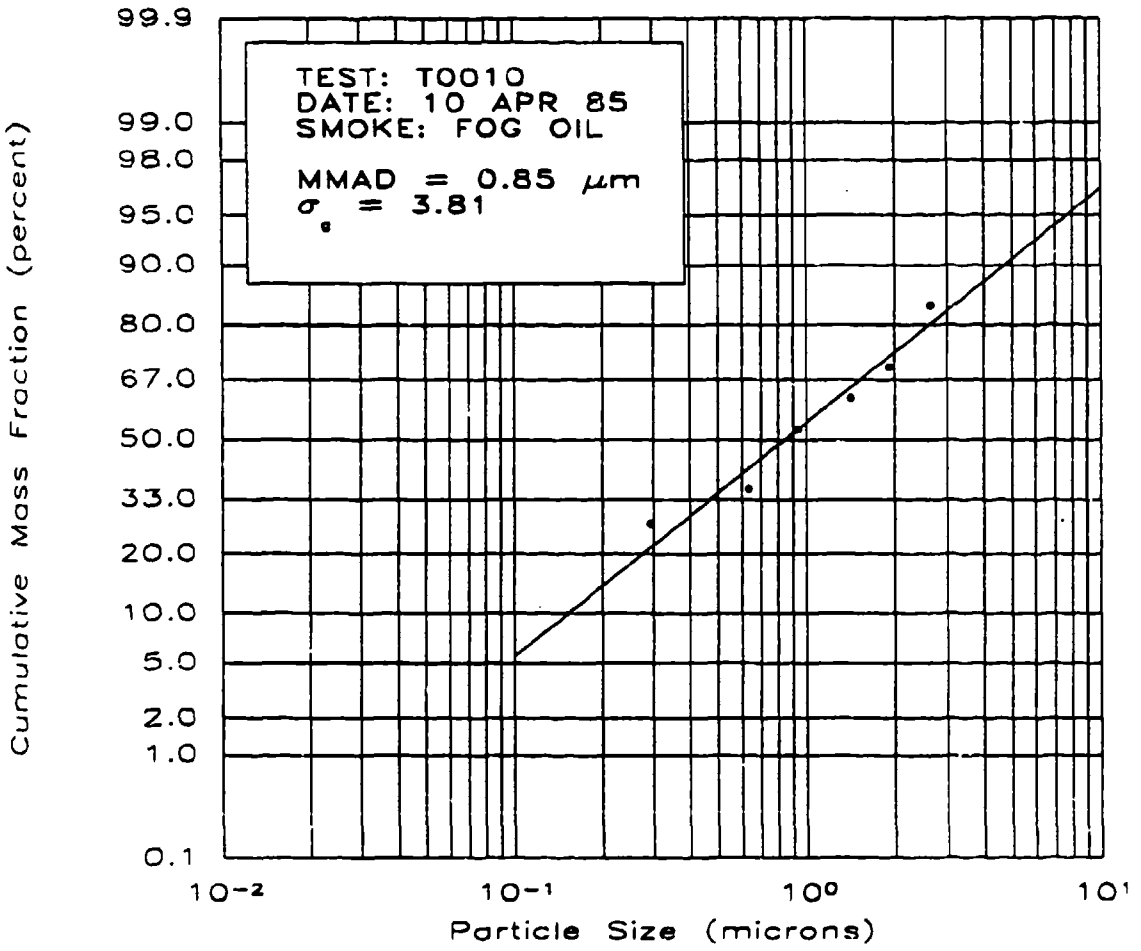

Figure 2.23 Log-probability plot of the cumulative size distribution of oil fog aerosol for test T0010. Cascade Impactor no. 3 located at (300,-50), about 110 m downwind of the smoke source. Aspiration Rate: 1.37 Lpm; Mass Median Aerodynamic Diameter (MMAD): 0.85 microns Geometric Standard Deviation: 3.81.

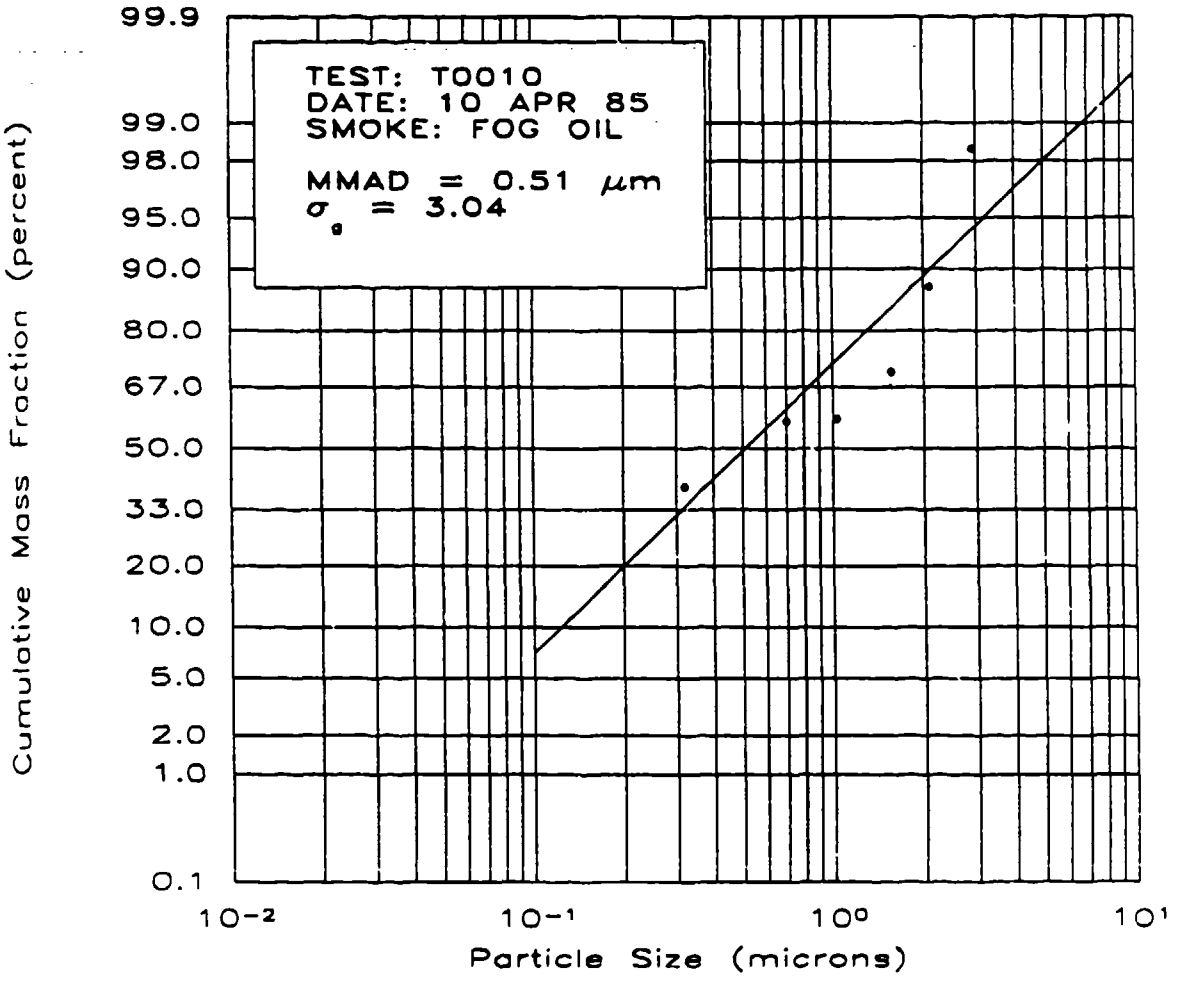

Figure 2.24 Log-probability plot of the cumulative size distribution of oil fog aerosol for test T0010. Cascade Impactor no. 4 located at (300,-50), about 110 m downwind of the smoke source. Aspiration Rate: 1.13 Lpm; Mass Median Aerodynamic Diameter (MMAD): 0.51 microns Geometric Standard Deviation: 3.04.

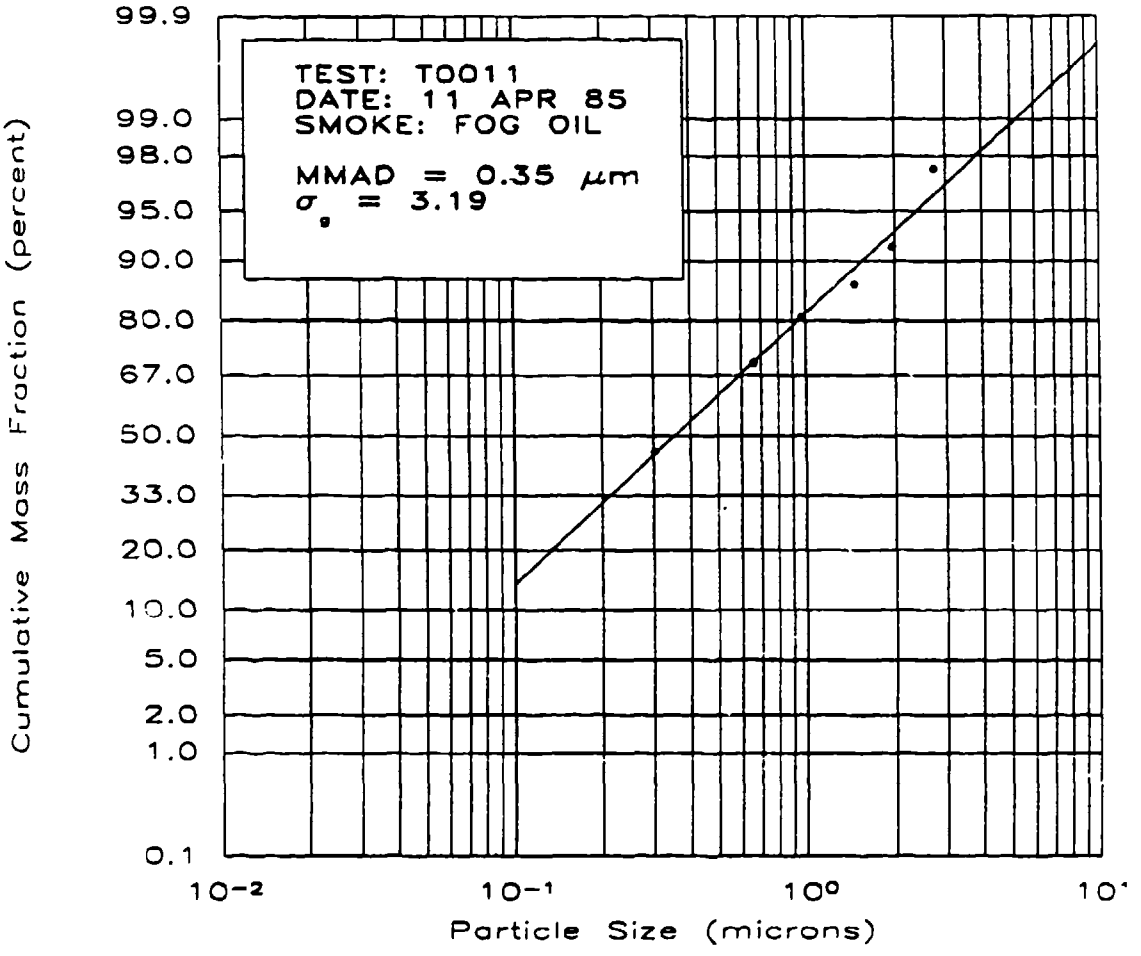

Figure 2.25 Log-probability plot of the cumulative size distribution of oil fog aerosol for test T0011. Cascade Impactor no. 7 located at (25,0), about 35 m downwind of the smoke source. Aspiration Rate: 1.27 Lpm; Mass Median Aerodynamic Diameter (MMAD): 0.35 microns Geometric Standard Deviation: 3.19.

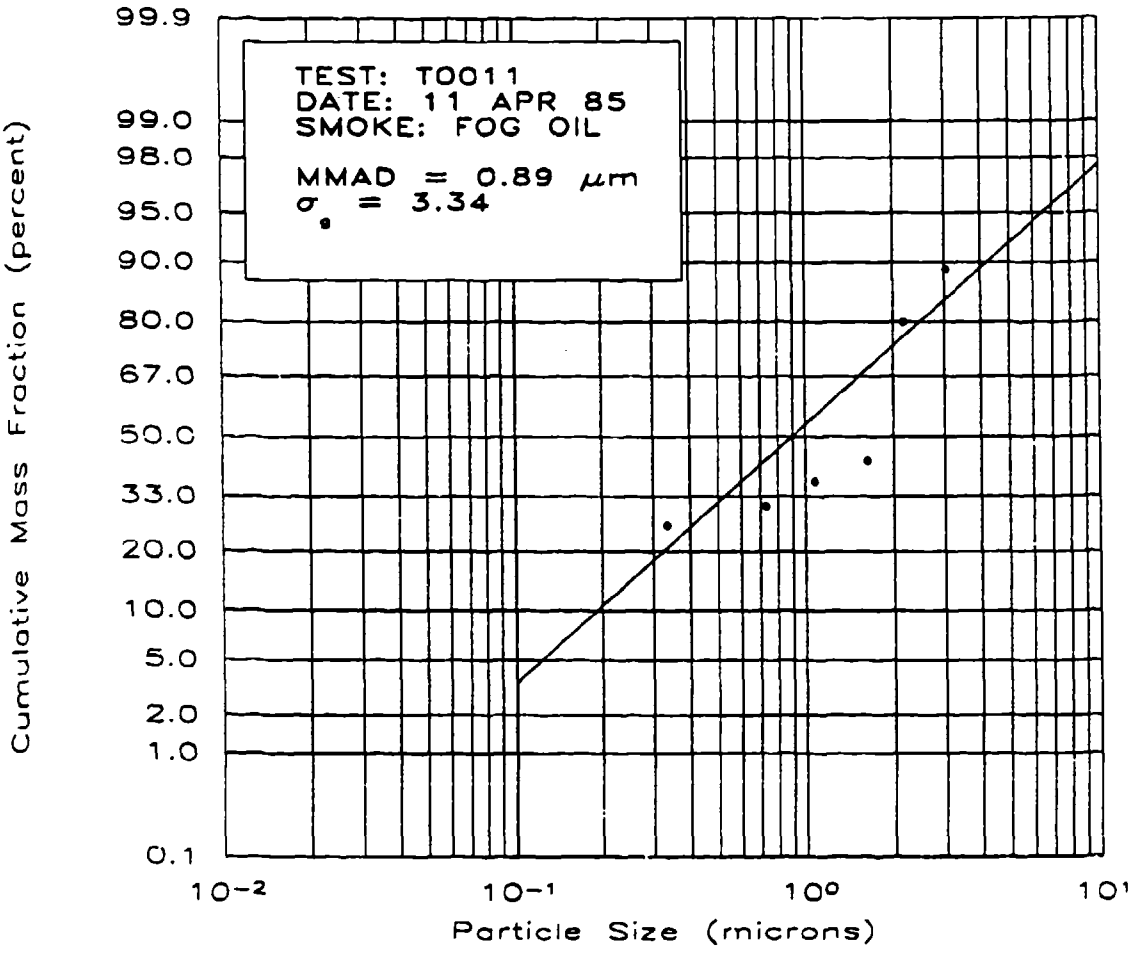

Figure 2.26 Log-probability plot of the cumulative size distribution of oil fog aerosol for test T0011. Cascade Impactor no. 8 located at (50,0), about 55 m downwind of the smoke source. Aspiration Rate: 1.04 Lpm; Mass Median Aerodynamic Diameter (MMAD): 0.89 microns Geometric Standard Deviation: 3.34.

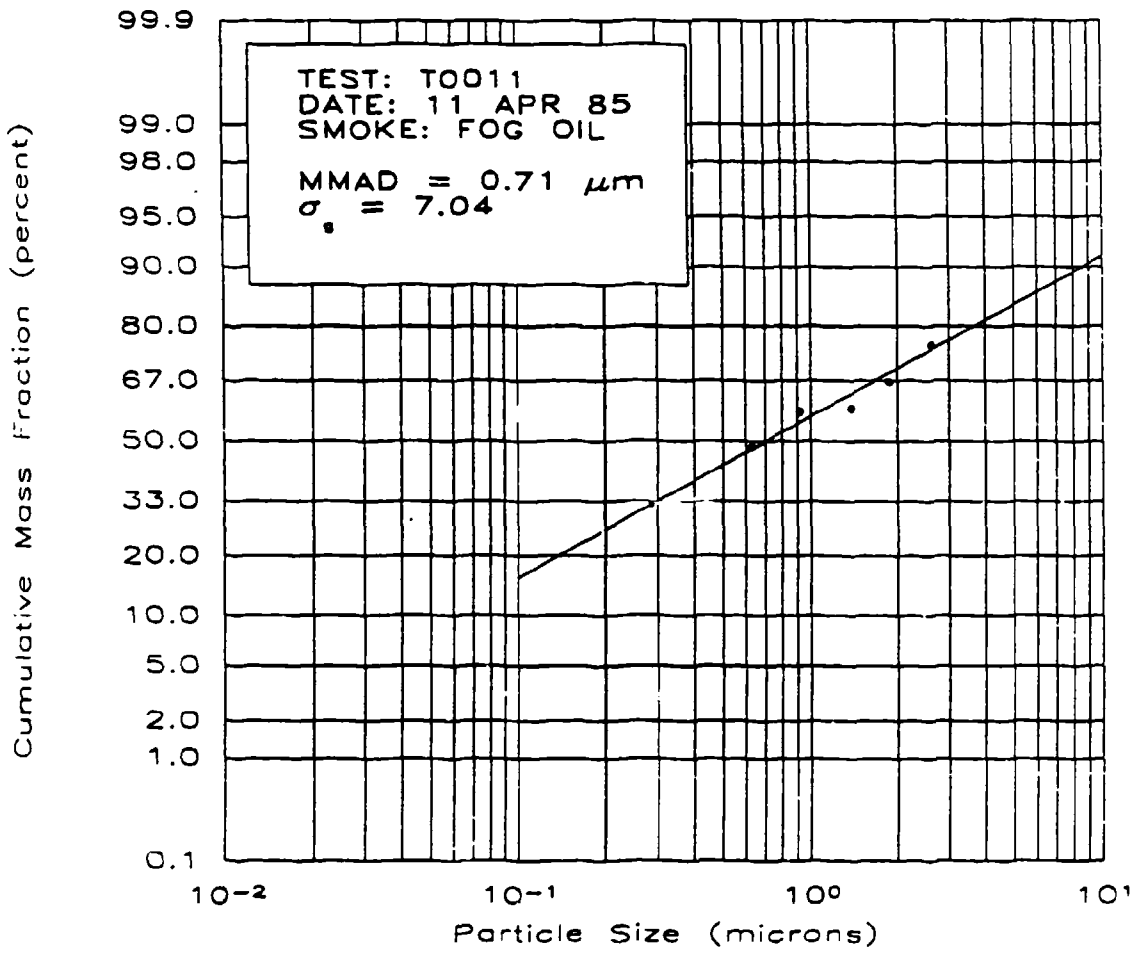

Figure 2.27 Log-probability plot of the cumulative size distribution of oil fog aerosol for test T0011. Cascade Impactor no. 5 located about 440 m downwind of the smoke source. Aspiration Rate: 1.42 Lpm; Mass Median Aerodynamic Diameter (MMAD): 0.71 microns Geometric Standard Deviation: 7.04.

impaction are not significant removal mechanisms for fog-oil smoke produced by an M3A3E3 unit. This is consistent with the size distribution data gathered from the cascade impactors: for micron-sized particles having a density of 0.9 g/cm^3, deposition is not expected to be significant. This can be seen by examining the dimensionless parameter h_*

$$h_* = \frac{w_s\, h}{\sigma_w^2\, T_L} = \frac{\tau\, g\, h}{\sigma_w^2\, T_L} \qquad (2.10)$$

Here w_s is the settling velocity and is equal to the product of the response time (equation (2.2)) and the acceleration due to gravity; h is the release height of the particle, σ_w^2 is the variance of the vertical velocity fluctuations and T_L is the Lagrangian integral time. Together, $(\sigma_w^2\, T_L)$ is a measure of the local turbulence. Boughton (1983) has shown that this parameter indicates the relative significance of settling and turbulent dispersion. If w_s or τ is very small, then $h_* << 1$ and settling is not significant compared with turbulence. This is the case for the fog-oil smoke since $\tau = 10^{-6}$ s, g = 9.8 m/s, h = 1.2 m and $\sigma_w^2\, T_L = 100$ m^2/s leads to $h_* \sim 10^{-7}$. (However, if we were to consider a hailstone having $\tau \sim 10^1$ s and h = 10^3 m then $h_* \sim 10^2$ and turbulence would not be significant compared to settling.)

This finding is also in agreement with the experimental work of Clough (1973). Clough measured the rate of deposition of solid particles to smooth extended surfaces and horizontal filter paper in a large wind tunnel. His results supported the theoretical work of Sehmel (1973) who predicted that deposition was exceedingly small for particles in the range 0.1 - 1.0 μm. In this range, the particles are too large for diffusion to significantly influence deposition but too small to have an appreciable settling velocity, as the analysis in the previous paragraph demonstrates. Clough presents data from a study of deposition to grass by Chamberlain which shows that although the settling velocity has a minimum in the range 0.1 - 1.0 μm, it is larger (by as much as ten times) than that indicated by Sehmel or Clough. This is probably due to impaction on the upright blades of grass. Garland (1982) discusses more recent field studies having the same results. Since we were unable to detect measurable levels of fog-oil smoke on either horizontal or vertical surfaces, the deposition of fog-oil smoke, whether by settling, diffusion or impaction, is probably insignificant at distances greater than 25 m from the source.

2.3.5 Aerosol Phase Partitioning

In order to assess the degree to which the fog-oil smoke is partitioned into vapor and droplet phases, concentration sampling tubes were placed in series with cascade impactors. All of the droplet phase was collected on the seven stages of the impactor or on its backup filter. Any vapor would pass through the impactor and be adsorbed by the Tenax in the concentration sampler. The results of all of these measurements were that no amount of fog-oil smoke significantly above the background level was detected on the concentration samplers whereas oil droplets were clearly visible and present in significant quantities on the stages of the impactors. Subsequent laboratory tests were carried out due to concern over the high detection threshold of the sample tubes used in the field. These tests confirmed our finding that, unlike diesel fuel based smokes, 99% of the fog-oil smoke exists in the droplet phase.

2.3.6 Chemical Aging

Chemical analysis of the fog-oil smoke samples by packed column gas chromatography revealed no discernible differences between the composition of the raw fog oil and either the smoke immediately downwind of the M3A3E3 or at large distances from the generator. However, analysis by a higher resolution method is necessary to confirm this finding. Details of the chemical analysis are presented in DeVault, *et al.* (1988).

3.0 SOURCE MEASUREMENTS

Detailed, time-dependent data concerning the behavior of the smoke source are necessary for the accurate prediction of downwind dosages as well as for the evaluation of models which predict such dosages. In the present study of fog-oil smoke, data describing the behavior of the M3A3E3 oil fog generators were collected during the release periods. This section describes the instruments and procedures employed to acquire and reduce these source data in addition to providing a summary and discussion of the data obtained.

3.1 The M3A3E3 Generator

The M3A3E3 fog-oil smoke generator, illustrated in Figure 3.1, produces smoke by vaporizing fog oil and ejecting it into the atmosphere at a nominal rate of 48 gallons of SGF-2 fog oil per hour (U. S. Army). A fog oil pump assembly, driven by a small, one-cylinder reciprocating engine, draws fog oil from a reservoir and pumps it into the engine tube of a pulse jet engine. The high temperature of the combustion gases causes the fog oil to vaporize. The vaporized fog oil is forced through three outlet nozzles at high velocity into the atmosphere where it condenses forming a dense, white smoke. The resulting aerosol is a two phase mixture of micron sized droplets and vapor.

Two M3A3E3 generators, prototypes of a design to replace the Korean War vintage M3A3 units, were secured for use in the present study. Both units were considered to be in new condition: one had never been operated and the other had only been test fired briefly prior to shipment. During a preliminary test of the generators and sampling system at Argonne National Laboratory in January 1985, both units were operated without incident.

Upon arriving at DPG, the generators and their associated instrumentation were mounted on a flatbed trailer. This was done to enable siting decisions to be based on the prevailing wind direction immediately prior to the testing period. As a result, the exit nozzles were located at an elevation of 1.2 m (4 ft) above the ground. The two generators were never operated simultaneously but rather were used to provide redundant capability and thus minimize the time lost in the event of equipment failure. No difference in either operating or smoke characteristics was detected between the two M3A3E3 units.

This redundant capability proved to be necessary as failure of the generators occurred frequently despite the presence of trained M3A3 operator/technicians supplied by DPG. The most trouble-prone aspects of the M3A3E3 were the gasoline engine and the rubber air hoses. The gasoline engine on each M3A3E3 unit was difficult to start and idled roughly. This was eventually diagnosed by Dugway Proving Ground personnel as the effects of altitude. To overcome this problem, the float level in the carburetor was adjusted and the fuel metering jets resized on both units. The spark plug and ignition points were also replaced. The rubber air hoses repeatedly ruptured. This resulted from the embrittlement and melting caused by their close proximity to the red hot body of the pulse jet engine assembly (17 in Figure 3.1). This problem was overcome by replacing the rubber hoses with thick-walled copper tubing.

In addition to these failure modes, many of the M3A3E3 oil lines leaked excessively. This might explain why the actual release rate was always less than the nominal rate of 48 gallons per hour. In fact, during our next to last test, the fog oil pump on one M3A3E3 unit failed completely. Upon returning to Illinois we discovered that the pump's impeller had become friction welded to the casing, probably as a result of an insufficient oil flow rate. These problems with the M3A3E3 caused many delays and occasional cancellations of testing. Several tests were cut short by a failure of one of the M3A3E3s while the other was being repaired.

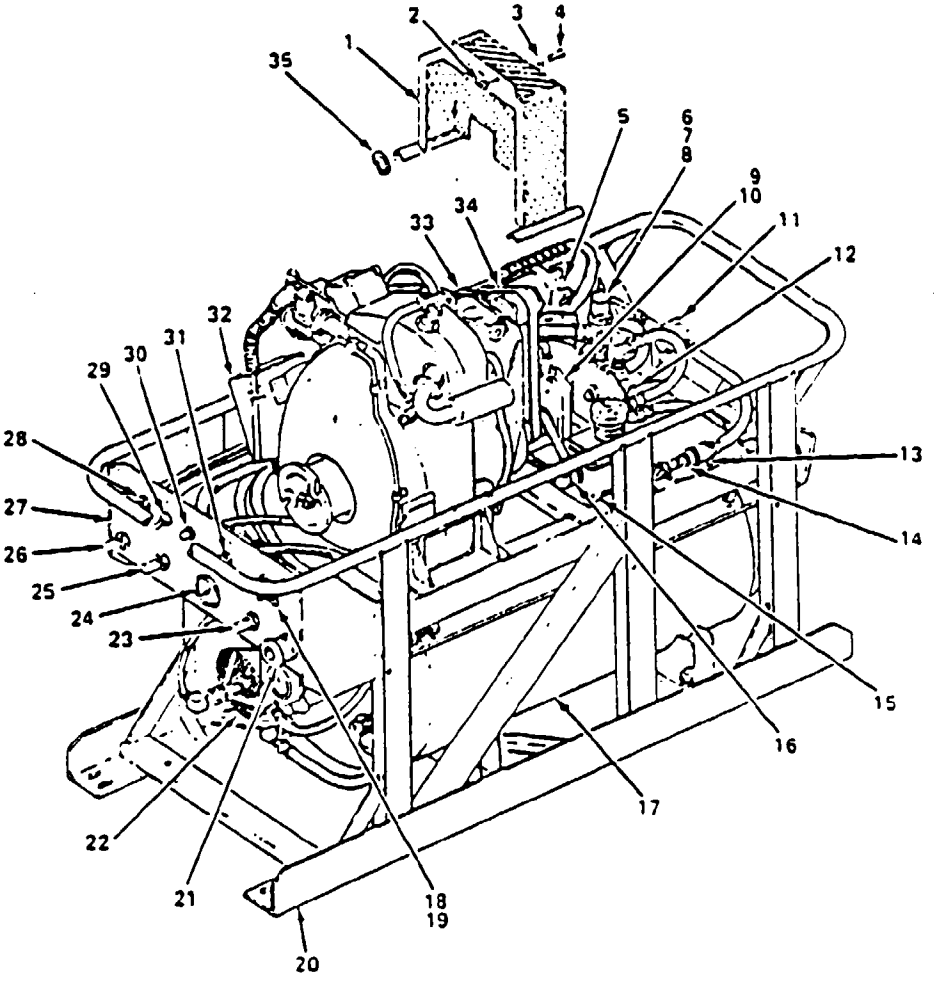

1	BELT GUARD ASSEMBLY	13	LOOP CLAMP	25	QUICK DISCONNECT
2	NUT	14	PRESSURE SWITCH	26	QUICK DISCONNECT
3	WASHER	15	AIR COMPRESSOR ASSY	27	CONTROL PANEL
4	SCREW	16	BELT	28	TOGGLE VALVE
5	FOG OIL PUMP ASSY	17	PULSE JET ENGINE ASSY	29	SWITCH
6	FOG OIL CONTROL VALVE	18	GLOBE VALVE	30	PURGE AIR SWITCH
7	SWIVEL NUT TEE ASSY	19	MALE ELBOW	31	START AIR SWITCH
8	MALE ELBOW	20	FRAME ASSY	32	ENGINE ASSY
9	COMBUSTION IGNITION MAGNETO	21	QUICK DISCONNECT	33	FUEL PUMP ASSY
10	MAGNETO PULLEY	22	NOZZLE ASSEMBLY	34	BELT
11	HOT GAS ISOLATOR	23	QUICK DISCONNECT	35	HOSE CLAMP
12	UNLOADER VALVE ASSY	24	AIR PRESSURE GAGE		

4A150-001

Figure 3.1. M3A3E3 Smoke Generator Assemblies and Major Components (from M3A3E3 Operation's Manual).

3.2 The Ideal Data Set

Policastro and Dunn (1985) have described the ideal data set for evaluation of smoke hazard models. For the purposes of source definition, this data set includes:

(a) the location(s) and elevation(s) and exit diameter(s) of the smoke release point(s) and the direction of smoke plume release when a smoke generator or vehicle exhaust is utilized,

(b) the mass release rate (kg/s) of smoke material as a function of time over the entire period of smoke generation,

(c) the particle size distribution and composition of material as it leaves the generating device, and

(d) the exit temperature and velocity of the smoke plume, also as a function of time.

In the present study, all of these characteristics were measured.

3.3 Data Acquisition and Reduction

In order to effect time-dependent measurements of the exit temperature, all three exhaust ports on each generator were instrumented with chromel/alumel (type K) thermocouples. During a test, the output of these thermocouples was scanned at 20-second intervals with a model CR7 datalogger manufactured by Campbell Scientific, Inc. (Logan, Utah) and stored on cassette tape. Since the measured exit temperatures varied by only a degree or less between adjacent ports, the instantaneous exit temperature was determined by averaging the three measured values. Additionally, the instantaneous exit temperature fluctuated due to the action of the pulse jet engine. The effect of these fluctuations upon the data were reduced by averaging the instantaneous values over 1-minute periods.

Fog oil was drawn from a 55-gallon drum located on the flatbed trailer. Since the M3A3E3 also uses the fog oil as a coolant, both a supply and return line must be connected to the 55-gallon drum. For this reason, direct measurements of the rate of fog oil release were impractical. Instead, the 55-gallon drum was placed on a 500 kg capacity digital scale manufactured by Circuits and Systems (Rockaway, New York) which had been mounted on the flatbed trailer. The analog voltage output of the scale was recorded at 20-second intervals with the CR7 datalogger. In this manner the instantaneous mass of the drum was obtained. By differentiating these data, the instantaneous rate of release could be determined. Due to the vibration of the generator, the instantaneous mass values exhibited fluctuations. These were overcome by averaging the data over 1-minute periods and smoothing the results using a 5-point moving average technique. The data were then numerically differentiated to obtain the instantaneous rate of release.

Estimates of the exit velocity of the smoke were obtained periodically during a test by measuring the difference between the static and stagnation pressures at the nozzles with a pitot probe and a Magnehelic differential pressure gauge. The calculation of the exit velocity took into account the high temperature of the exhaust stream as well as the increased density of the exhaust stream due to the fog oil. The calculation proceeded in an iterative fashion as follows: with the well known relation

$$\Delta p = 1/2\, \rho\, u_e^2 \qquad (3.1)$$

where $\Delta p = p_{stagnation} - p_{static}$ and ρ is the density of the flow stream, a first estimate of the exit velocity u_e was made using the measured value of Δp and taking ρ equal to the density of air at atmospheric pressure and the average exit temperature. Next, the mass rate of release was estimated:

$$\dot{m} = \rho\, u_e\, A \qquad (3.2)$$

where ρ is the density and u_e is the exit velocity computed previously. A is the area of the three exhaust

ports ($A = 3 \times 1/4\ \pi d_e^2$) where d_e is the port diameter. Note that this is really the mass flow rate of the air alone. To estimate the total mass flow rate, the mass rate of release of the oil, which was computed directly from the instantaneous weight of the oil drum was added:

$$\dot{m}_{total} = \dot{m}_{air} + \dot{m}_{oil} \tag{3.3}$$

With this result, a new estimate of the density of the flow stream could be made:

$$\rho = \frac{\dot{m}_{total}}{u_e A} \tag{3.4}$$

Using this estimate of ρ in equation (3.1), u_e was recomputed and the procedure repeated until it converged.

Periodically, samples of the fog-oil smoke 1 m downwind of the M3A3E3 were obtained in order to compare its chemical composition both with raw fog oil from the supply drum and with samples obtained at greater downwind distances. This was accomplished by placing a large-mouth glass jar in the plume for 1-minute. The jar was then sealed and labeled according to test and time of day for subsequent analysis.

A Mercer-style cascade impactor, Intox Products, Inc. (Albuquerque, New Mexico) model 02-100, was located 1 m downstream of the M3A3E3 in order to measure the initial size distribution of the smoke. The impactor was aspirated at a rate of 1 liter per minute (Lpm). Due to the proximity of the impactor to the generator, it was very difficult to obtain an adequate sample of the fog-oil smoke without overloading the impactor.

3.4 Results

Plots of the time-dependent exit temperature and rate of release for nine of the eleven tests conducted are given in Figures 3.2 through 3.8. Test-averaged values for the duration of release, release rate and exit velocity are presented in Table 3.1. No real-time source data were gathered during the tests on March 21 and 25. During the test on April 4, the recording tape jammed 34 minutes into the test. This was not detected until 73 minutes into the test and resulted in a loss of source data during that interval. Failure of the recording equipment on April 10, 1985 prevented the acquisition of time-dependent data from the tests on April 10 and 11. For these tests, the mass of oil released was determined from the initial and final weights of the fog oil drum, independently recorded.

Careful examination of the results presented in Figures 3.2-3.8 leads to several conclusions. First, the exit temperature is strongly dependent on the rate of release. This is especially evident in Figure 3.8 where significant changes in release rate lead to precipitous changes in exit temperature. The reverse is not necessarily true, however. Figure 3.7 shows a dramatic decline in the exit temperature due to the failure of an air line. The release rate is seen to be unaffected.

Secondly, it is apparent that both the release rates and exit temperatures varied significantly both from test to test and during a given test. This highlights the need for time-dependent data. This also demonstrates the difficulty encountered in operating the fog-oil smoke generators. The generators had to be constantly monitored and the flow rate continuously adjusted in order to maintain successful operation.

Finally, it should be noted that the release rate rarely approached the nominal value of 45 g/s (48 gallons/hour) stated in the operator's manual. Although the generator was operated with the flow control valve in the fully open position as often as possible, the release rates were in the range 18 g/s to 43 g/s with an average of 30 g/s.

The exit velocity was computed from the measured difference in the static and stagnation pressures at the nozzle exit plane. The computation was corrected for the average exit temperature and average release rate. The small variation in the computed values of the exit velocity is largely due to the test to test variations

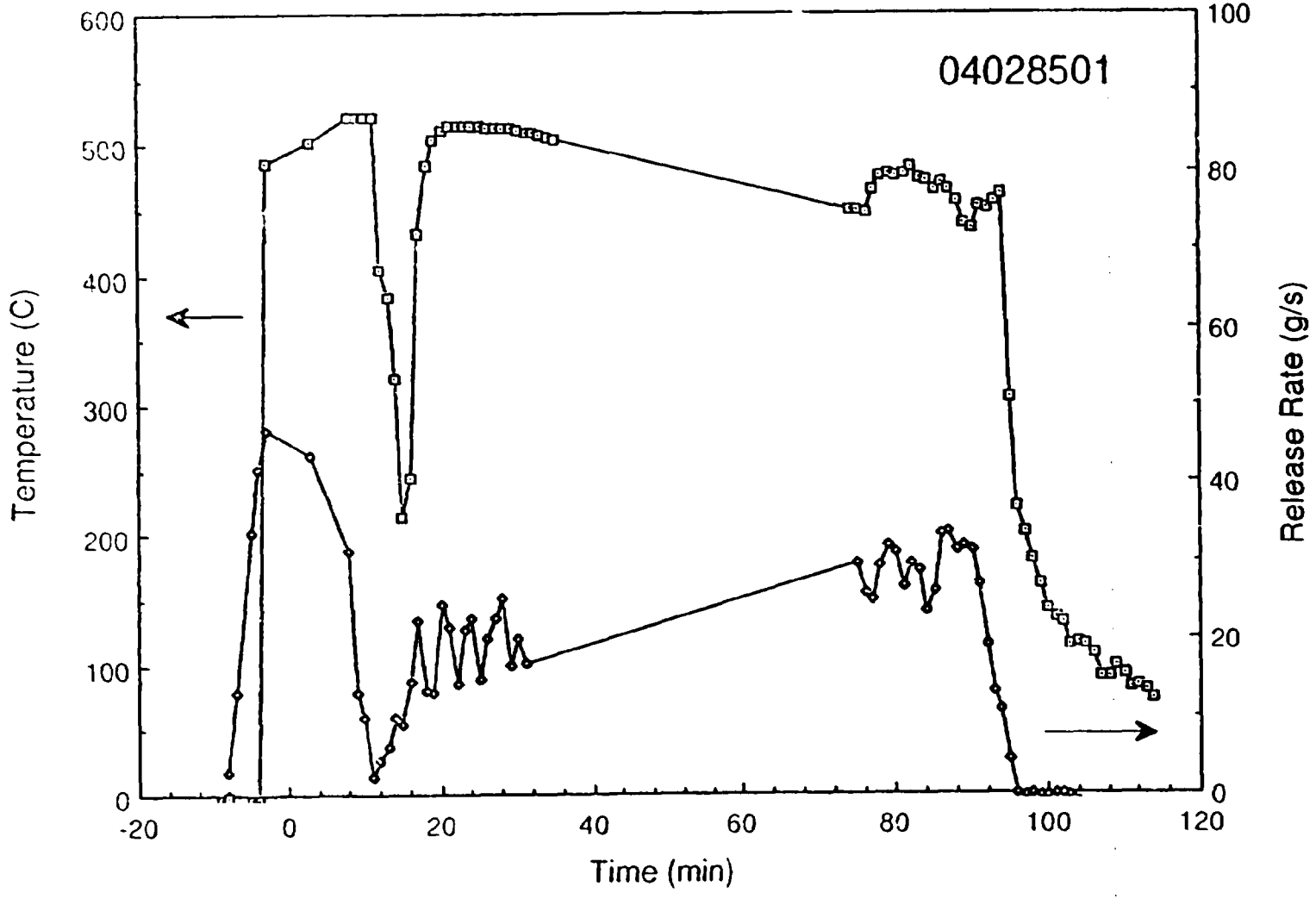

Figure 3.2. Exit Temperature (°C) and Release Rate (g/s) as a function of time for test T0003 (2 April 85). Missing data due to equipment failure (tape jam).

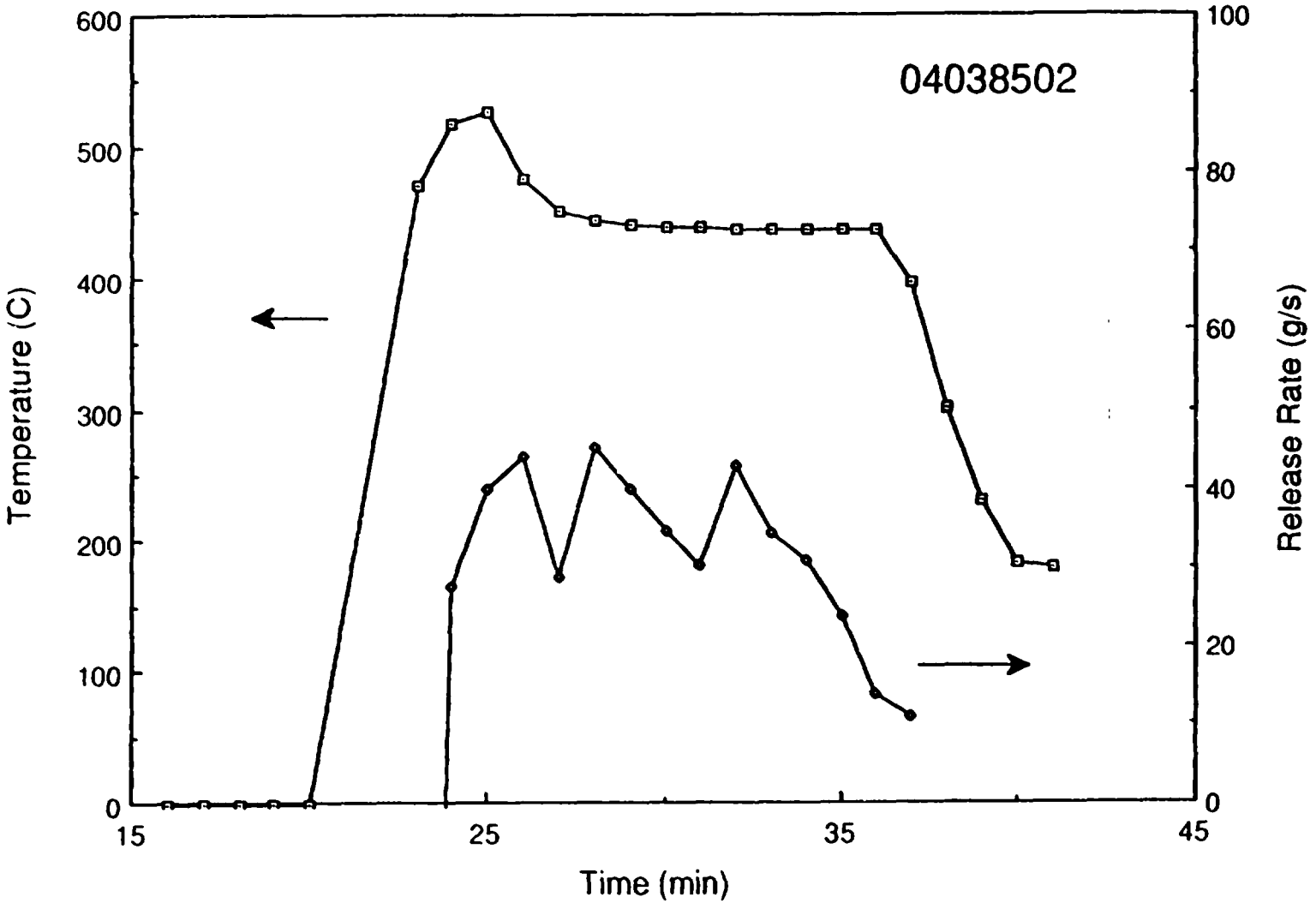

Figure 3.3. Exit Temperature (°C) and Release Rate (g/s) as a function of time for test T0004 (3 April 1985).

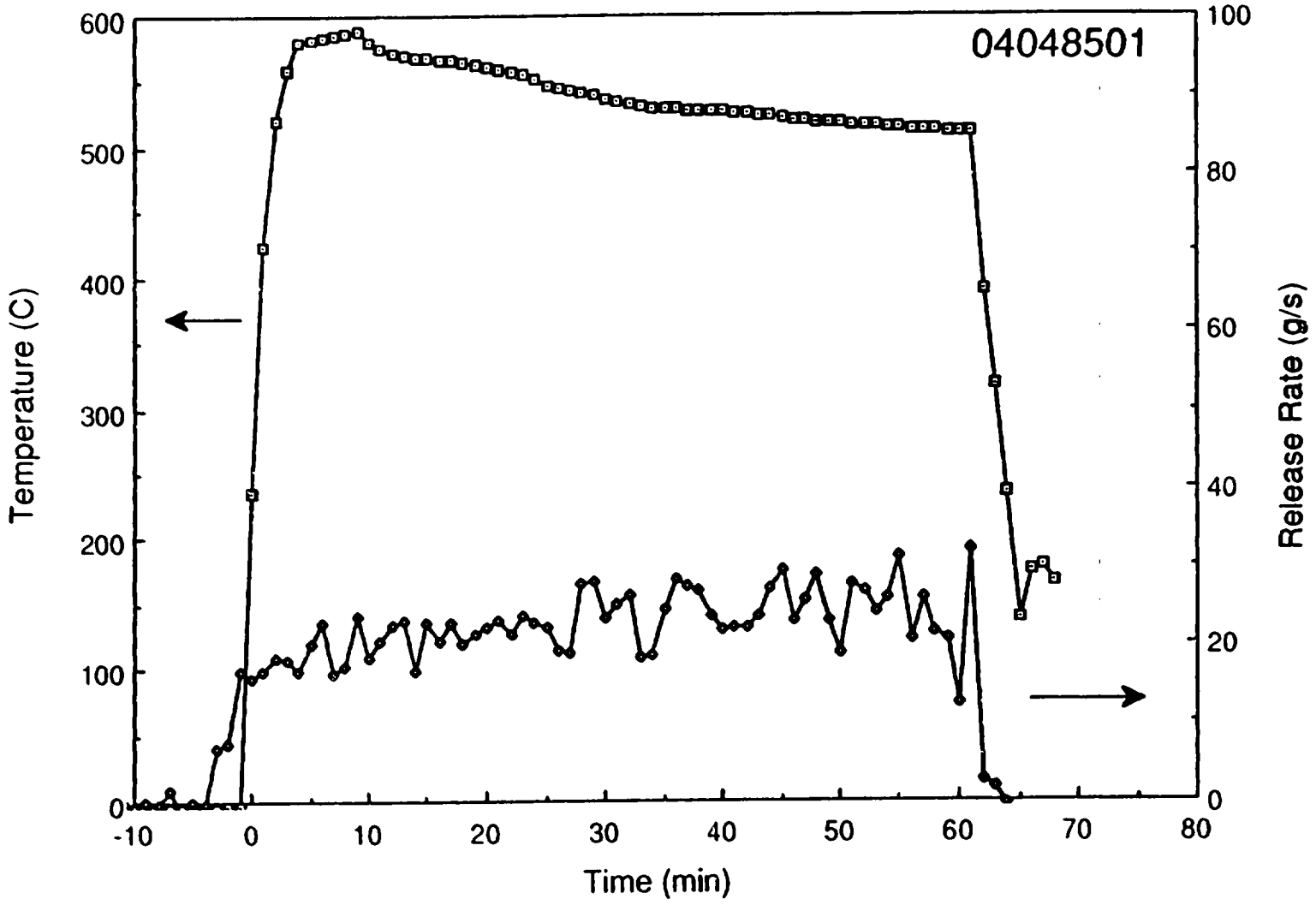

Figure 3.4. Exit Temperature (°C) and Release Rate (g/s) as a function of time for test T0005 (4 April 1985).

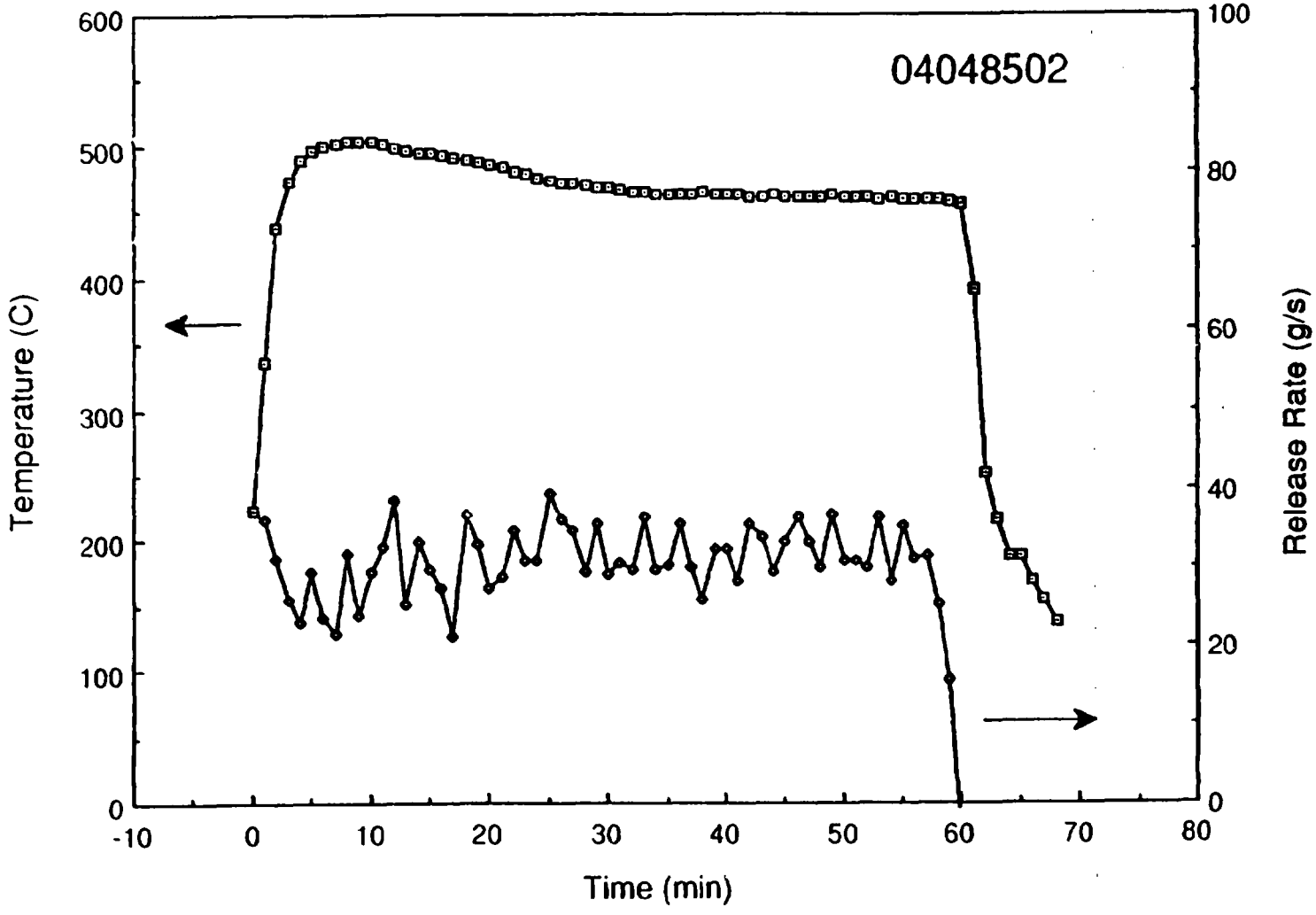

Figure 3.5. Exit Temperature (°C) and Release Rate (g/s) as a function of time for test T0006 (4 April 1985).

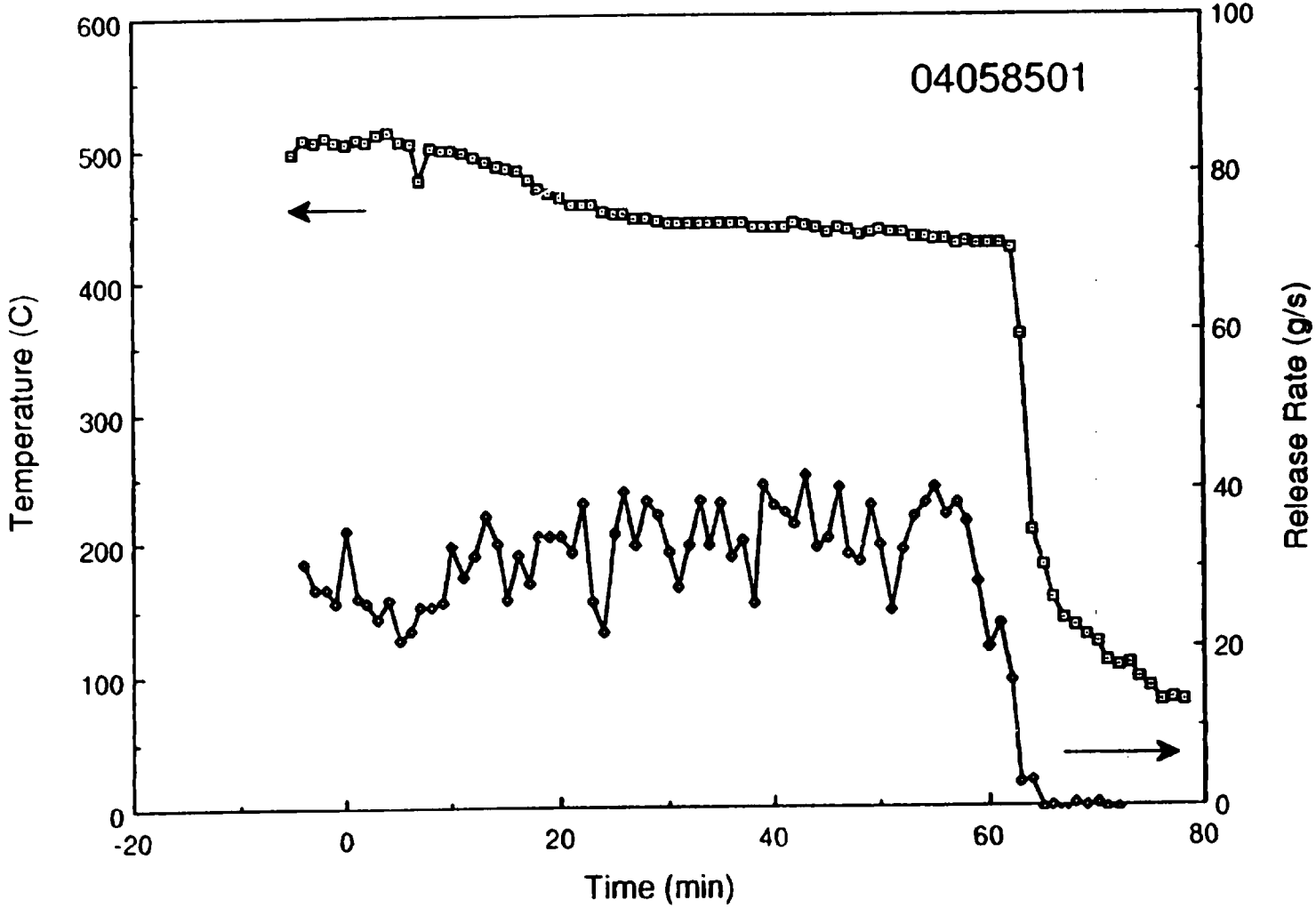

Figure 3.6. Exit Temperature (°C) and Release Rate (g/s) as a function of time for test T0007 (5 April 1985).

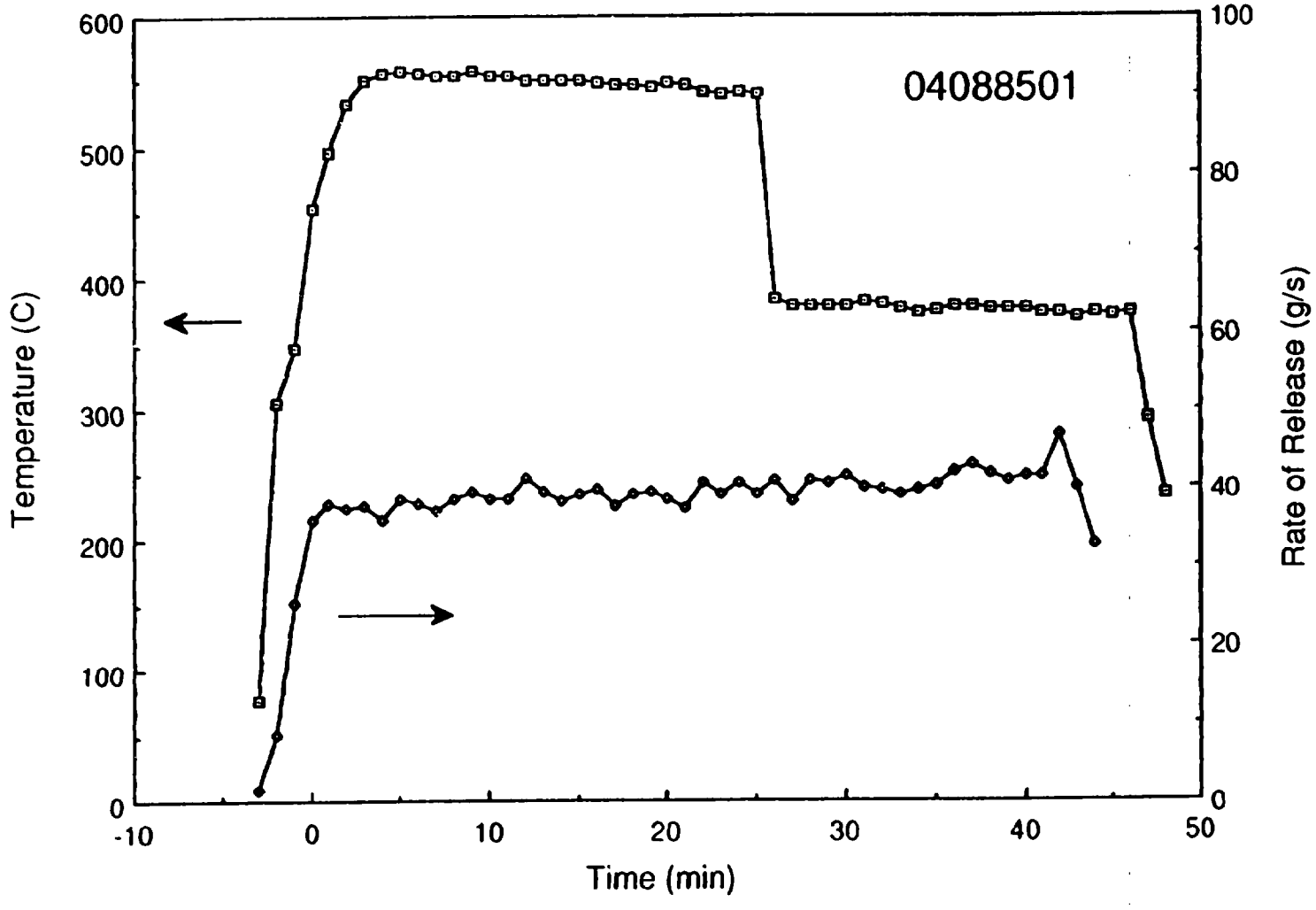

Figure 3.7. Exit Temperature (°C) and Release Rate (g/s) as a function of time for test T0008 (8 April 1985).

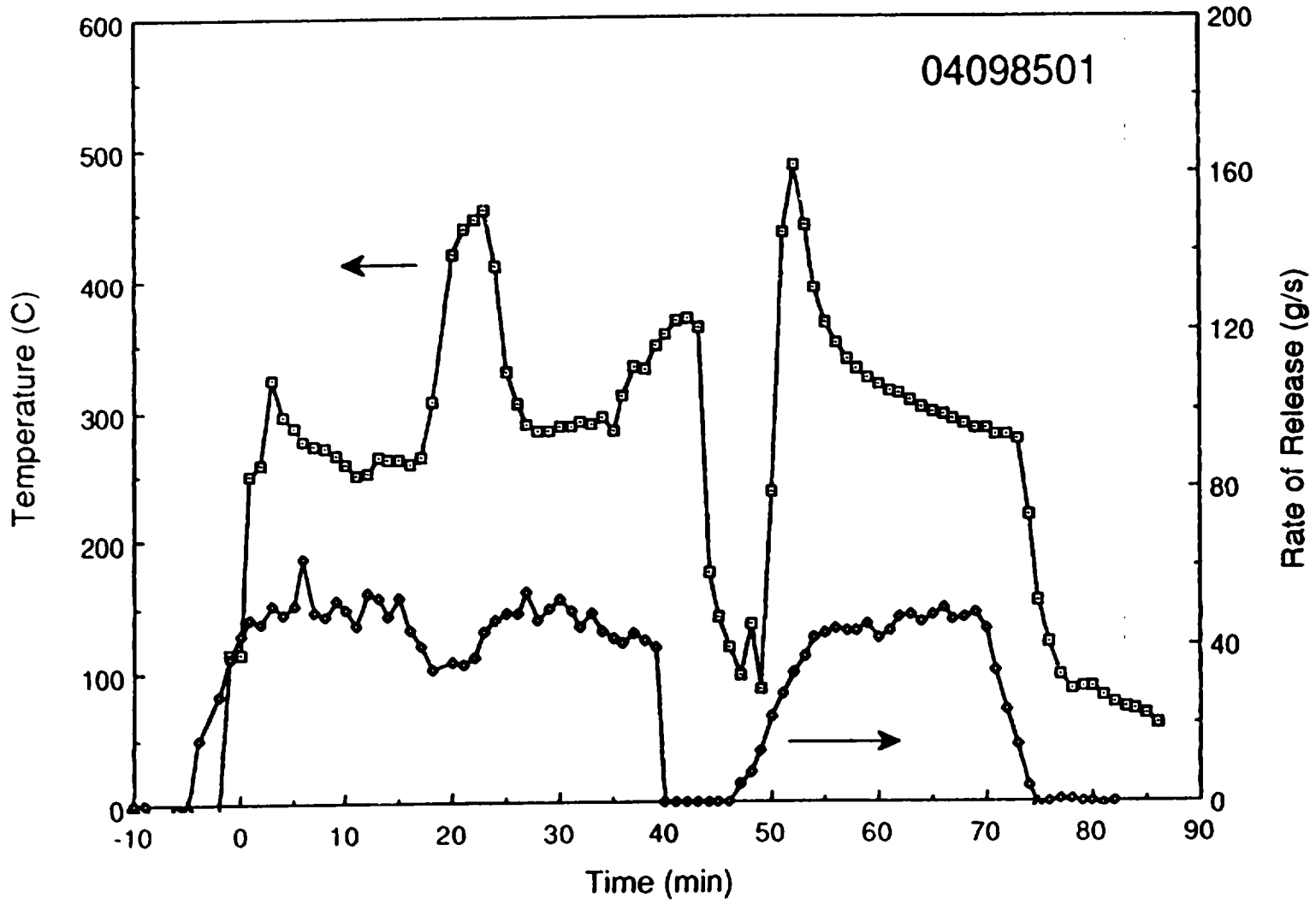

Figure 3.8. Exit Temperature (°C) and Release Rate (g/s) as a function of time for test T0009 (9 April 1985).

Table 3.1. Summary of Source Data.

Test	Date/Time	Source Coordinates (m)	Generator Run Time (s)	Emission Mass (kg)	Emission Rate (g/s)	Emission Rate (gal/hr)	Exit Velocity (m/s)
T0001	21-Mar-85 10:34-11:27	-950,-100,1.2	3180	58.8	18.5	19.6	82.8
T0002	25-Mar-85 9:54-11:07	-950, 100,1.2	2760	52.3	18.9	20.1	82.6
T0003	2-Apr-85 10:20-11:56	-325, 100,1.2	5400	131.4	24.3	25.8	80.1
T0004a	3-Apr-85 9:42-10:20	-325, 100,1.2	2280	50.9	22.3	23.7	83.1
T0004b	3-Apr-85 10:20-10:33	-325, 100,1.2	780	17.7	22.7	24.1	78.6
T0005	4-Apr-85 10:24-11:27	-450, 0,1.2	3780	84.6	22.4	23.7	82.8
T0006	4-Apr-85 13:46-14:48	-450, 0,1.2	3660	105.0	28.7	30.4	78.1
T0007	5-Apr-85 13:10-14:14	-225,-100,1.2	4380	134.6	30.7	32.6	75.2
T0008	8-Apr-85 14:29-15:17	-370,-110,1.2	2880	104.6	36.3	38.5	77.1
T0009	9-Apr-85 13:38-14:53	-3.7, 30,1.2	4140	179.0	43.2	45.8	66.6
T0010	10-Apr-85 14:20-15:38	400, 0,1.2	3720	155.0	41.7	44.2	73.2
T0011a	11-Apr-85 9:38-9:45	-4.0, 0,1.2	420	16.0	38.1	40.4	74.6
T0011b	11-Apr-85 10:30-11:55	-4.0, 24,1.2	5100	192.0	37.6	39.9	74.6

Notes:
1. Tests marked "a" and "b" have been divided in two to account for changes in the wind direction.
2. For tests T0001, T0002, T0010 and T0011, the mass released was determined from the initial and final weight of the oil drum.
3. Run times may be less than the difference between the start and end times due to failures of the M3A3E3.

in average exit temperature and release rate; the exit plane pressure differences are more uniform. This suggests that the average exit velocity of 78 m/s is probably sufficiently accurate to characterize these tests.

Chemical analysis of the fog-oil smoke samples by low-resolution gas chromatography revealed no discernible differences between the composition of the raw fog oil and either the smoke immediately downwind of the M3A3E3 or at large distances from the generator. Analysis of the cascade impactor data revealed that the size distribution of the fog-oil smoke is nearly log-normal with a mass median diameter of about 0.74 μm. Details of the chemical and size distribution analyses are described by DeVaull, *et al.* (1988).

4.0 METEOROLOGICAL DATA

Meteorological data are available for eleven trial releases of oil fog smoke. Five trials were conducted under Pasquill stability class D (near-neutral) conditions, three under class C (slightly unstable) conditions, two under class B (moderately unstable) conditions and one under class A (very unstable) conditions.

Data were collected from two 32 m towers located at the test site (see Figure 2.2) in order to provide an accurate description of the ambient meteorology during fog-oil smoke releases. These data were gathered in order to determine those quantities required by predictive models of short-range atmospheric dispersion and thus, in conjunction with the measured values of dosage, provide a comprehensive data set for modeling and hazard evaluation purposes.

Time dependent measurements of wind speed, wind direction, angle of inclination and temperature were carried out at five levels. From these data, averages over periods of 30 seconds, ten minutes and the duration of the test were computed. Parameters indicating the state of the planetary boundary layer such as the friction velocity, Monin-Obukhov length and other scales used by the models were also determined from the data.

The data were examined for internal consistency and for agreement between the two instrument towers. For example, the computed variance of each measurement was compared with the value of its auto-correlation at zero time and with the integral of its power spectrum. The computed values of the Monin-Obukhov length were compared with the Pasquill stability classification and with the exponent of the power law fit to the vertical profile of the wind speed. Time histories from each tower were examined for correlated large scale phenomena and their separation in time compared with travel times estimated from measurements of wind speed and direction. This analysis showed that the data were, in fact, self-consistent and that the data from the two towers were in close agreement.

In order to assess the quality of the meteorological data in more of an absolute sense, selected trials representing extreme cases of atmospheric stability were compared to a model of atmospheric turbulence developed by Højstrup (1982). The model describes the spectral distribution of turbulent energy in the three components of velocity. The model can also be used to predict velocity variance and integral scales. It was selected because it covers a broad range of stability conditions, as do the data. It was developed from, and agrees very closely with, data gathered in two extensive studies of turbulence in the planetary boundary layer over Kansas and Minnesota (Kaimal *et al.*, 1972, 1976, 1978). In this way, our data may be indirectly compared with data from those studies.

4.1 Meteorological Instrumentation

The instrumentation necessary for measuring wind speeds and directions was provided for both towers by Dugway Proving Ground. The instruments had been checked for proper operation and calibrated in January 1985.

Wind speeds were measured with Climet cup anemometers, model number 014-102 mounted at 2, 4, 8, 16 and 32 m. Fluctuations in the horizontal and vertical wind angles were measured with Climet model 014-47 or 014-48 bivanes mounted at 4, 8, 16 and 32 m. Horizontal wind fluctuations at the 2-m level were measured with a Climet 014-6 direction vane. A careful analysis of the dynamic response of the wind instruments was performed and is presented in Appendix A. This analysis indicates that, within the frequency range of interest to the present study, no correction for instrument response need be applied to the data.

The temperature values obtained with the RTDs on the Horizontal Grid Tower agreed very closely with those obtained from the thermistors on the West Vertical Grid Tower. The values obtained from the thermocouples on Horizontal Grid Tower were often as much as three degrees lower than those obtained with the RTDs or thermistors. Thus, no analysis of the thermocouple readings was attempted.

On the West Vertical Grid tower, temperature was measured at the 2, 4, 8, 16 and 32 m levels with aspirated Climet 015-3 thermistors having a rated accuracy of ±0.15 C°. On the Horizontal Grid tower, temperature was measured with individually calibrated CGS type 21A-10 platinum RTDs accurate to ±0.25 C°. Differential temperatures were measured with copper-constantan (type T) thermocouple pairs. Both the RTDs and the thermocouples were housed in aspirated radiation shields.

Both instrument towers were 32 m in height with a 1.2 m by 1.8 m cross section; the long dimension was located along a north-south line. The instrument booms on the West Vertical Grid tower projected east 2.1 m from the south side of the tower ; whereas, those on the Horizontal Grid tower projected west 2.1 m from the north side. The wind speed cups were mounted at the outer end of the boom; the wind vanes were mounted 0.61 m from the outer end. Aspirator tubes for the thermistors were mounted on the northeast corner of West Vertical tower facing north; whereas, those for the RTDs and thermocouples were mounted on the west side of Horizontal Grid tower facing south. Additionally, measurements of solar radiance and dew point were made at the 2-m level on the West Vertical Grid tower. A cup anemometer and direction vane mounted atop a two meter high mast provided wind speed and direction information at the generator location.

The data from the West Vertical Grid tower and the two meter mast was digitized and recorded on-site with an HP 2250L computer and telemetered to Data Central located in the Ditto Technical Center of Dugway Proving Ground for processing. The data from the Horizontal Grid tower was digitized and recorded on-site with a Fluke 2280A Datalogger and transferred from magnetic tape to an IBM PC/AT for first-pass processing. Subsequent processing was performed at the University of Illinois.

All instruments on the West Vertical Grid tower were sampled at 1-second intervals. On the Horizontal Grid tower all wind instruments (e.g., cups, vanes) were sampled at 5-second intervals while the temperature instruments (e.g., RTDs and thermocouples) were sampled at 1-minute intervals. The recording of meteorological data was initiated prior to the commencement of smoke generation and lasted until after generation had ceased. This resulted in data record lengths of 40 to 90 minutes. From these data, estimates of the mean and variance of the wind speed, direction, inclination and temperature were computed for periods of 30 seconds as as well as for the duration of the data recording period. The 30-second averages were plotted to provide a time history of test meteorology for visual inspection and comparison.

4.2 Data Reduction and Analysis

The two major factors complicating the analysis of atmospheric turbulence are the extreme range in scale and the non-stationary character of the flow. Whereas laboratory flows are limited in scale to the physical dimensions of the apparatus, atmospheric scales can extend to several km in the vertical and tens or hundreds of km in the horizontal. As a result, the statistics of the flow are very sensitive to the duration of the sampling period. Worse yet, due to variations in terrain, diurnal variations in ground heating and changes in the macroscopic weather system, atmospheric flows are generally non-stationary. (A stationary flow is one whose statistics are invariant with time, therefore the statistics of a non-stationary flow are functions of time.) This renders most statistical methods of analysis including correlations and spectra theoretically invalid.

However, it is possible to transform a non-stationary signal into a stationary one by filtering out the non-stationary components. This is the purpose of "trend removal" (Bendat and Piersol, 1977, page 288). Low frequency components with a period less than the period of interest are approximated by a mean value or linear trend and subtracted from the signal prior to analysis. In our analysis, the data were high-pass filtered to limit the range of scales to those relevant to short-range dispersion. The data were subsequently low-pass filtered to estimate the magnitude of the non-stationary components which were then removed.

4.2.1 Means and Variances

Estimates of the means and variances of the meteorological data were computed as time averages over the period of interest. According to ergodic theory, if the turbulence is homogeneous and stationary along a given spatial coordinate, then such a time average is equal to the ensemble average encountered in turbulence theory. The inhomogeneous and non-stationary nature of atmospheric turbulence, discussed earlier in this report, implies that estimates derived from time averages may be substantially in error. The importance of this issue is discussed and illustrated with several examples by Chatwin and Allen (1985). It therefore seems worthwhile to examine the averages and the averaging process to discover the nature and magnitude of the errors introduced.

Pasquill and Smith (1983) provide an extensive discussion of the effects of finite sampling and averaging times. They state that since finite sampling times partially exclude slow variations and since instrument response affects fast fluctuations (essentially averaging them over some short but finite period), "the mean velocity is thus recognized as a purely arbitrary quantity..." Clearly, this is true not only for velocity but for all time-varying quantities. For this reason, the 30-second averages (which have a statistical error of 18.25%) are provided only for qualitative visual reference purposes.

Figures 4.1 and 4.2 present the time traces of 30-second averaged wind speeds for a case of near-neutral stability (T0005) conducted under overcast skies in the late morning of April 4, 1985 and an unstable case (T0010) conducted under clear skies in the early afternoon of April 10, 1985. It is apparent from these data that the turbulence intensity σ_U/U for the near-neutral test is small (≈10%) while it is much greater for the unstable case (≈50%). Figures 4.3 and 4.4 indicate that although the wind direction was very steady for test T0005, it was highly variable during T0010, which made the latter test very difficult to carry out.

The behavior of the vertical velocities may be inferred from the behavior of the vertical angle plotted in Figures 4.5 and 4.6 for T0005 and T0010, respectively. (A positive angle corresponds to an upward velocity.) These data reveal large differences in the intensity of the vertical velocity fluctuations. Clearly there is much more vertical transport during the unstable test. It should be noted that the mean values of the vertical angles indicated on Figures 4.5 and 4.6 are uncorrected. After correction for systematic errors due to the fact that the bivanes were not mounted exactly parallel to the ground, the mean vertical velocities were within the 99% confidence interval of zero.

Since estimates of the variance are of greater interest in predicting the diffusion of scalars in the atmosphere, Pasquill and Smith's discussion focuses more quantitatively on them. They demonstrate that the effect of finite sampling and averaging times is to apply low-pass and high-pass filters to the data. As the neutral limit is approached, the peak of the spectra shifts toward higher frequencies and so more energy is at frequencies greater than 0.5 Hz (the Nyquist frequency for a 1-second sampling interval). As conditions become more unstable, the spectral peaks shift toward lower frequencies and thus more energy is at frequencies lower than 0.0003 Hz (corresponding to a record length of one hour). A graph presented by Olesen, *et al.* (1984) has been used to estimate these losses. The correction factors have been tabulated in Table 4.1.

For the near-neutral case, the variances of the horizontal components shown in Figures 4.7 and 4.8 agree quite well with the model predictions while the model seems to slightly underpredict the vertical values as shown in Figure 4.9. For the unstable case, the opposite is true: for the vertical component there is good agreement between the model and data as Figure 4.12 indicates while the model slightly overpredicts the horizontal values presented in Figures 4.10 and 4.11. The discrepancy in the horizontal components is most likely due to the sensitivity of the model to the value of the inversion height z_i. The inversion height was not measured in these experiments but only crudely estimated. Another factor which should be borne in mind is that these data reflect only one realization of the turbulence. The model is based on an ensemble of realizations and cannot be expected to predict the outcome of an individual experiment exactly.

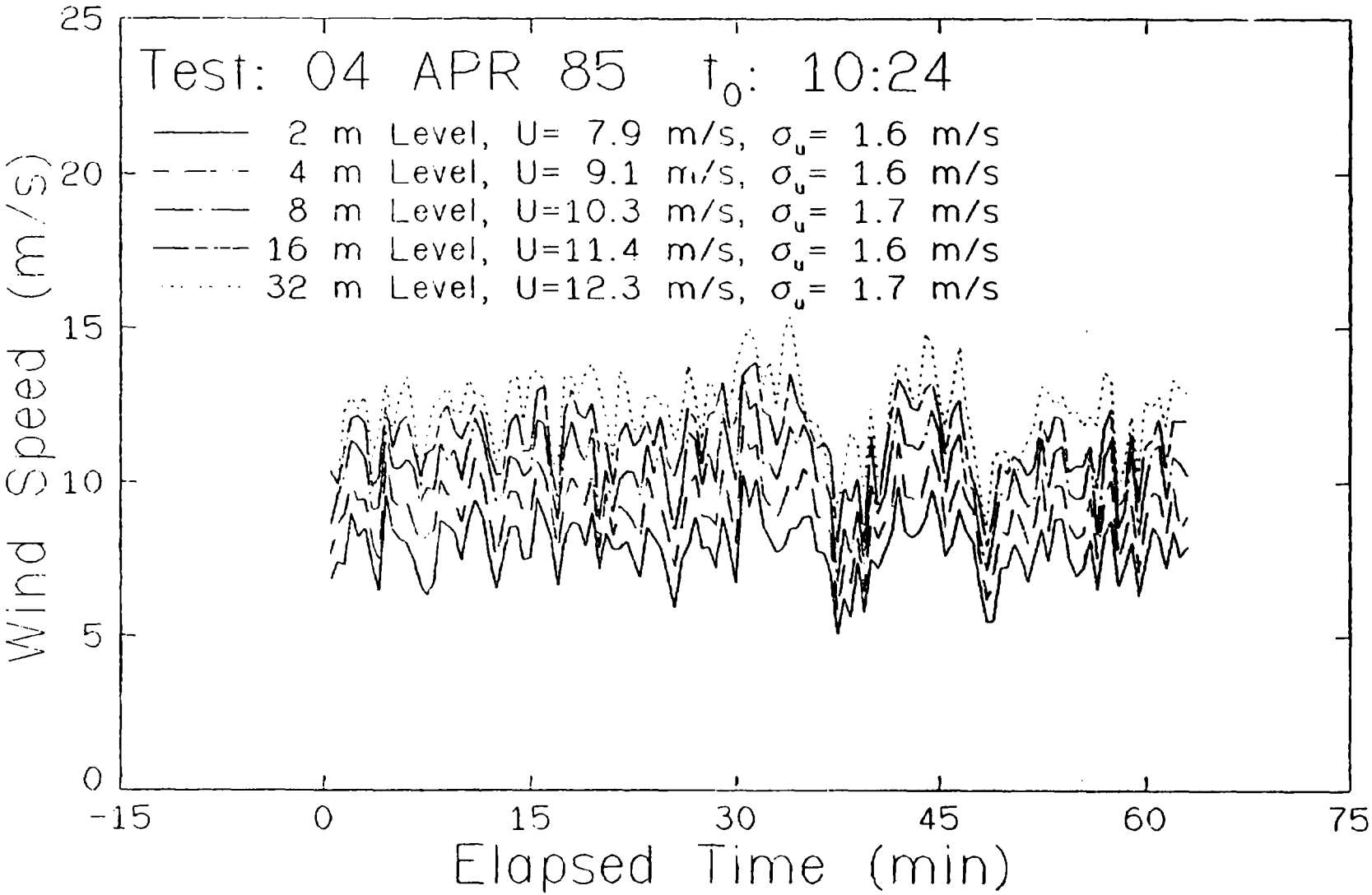

Figure 4.1. Trace of 30-second averaged wind speeds for near-neutral atmospheric conditions.

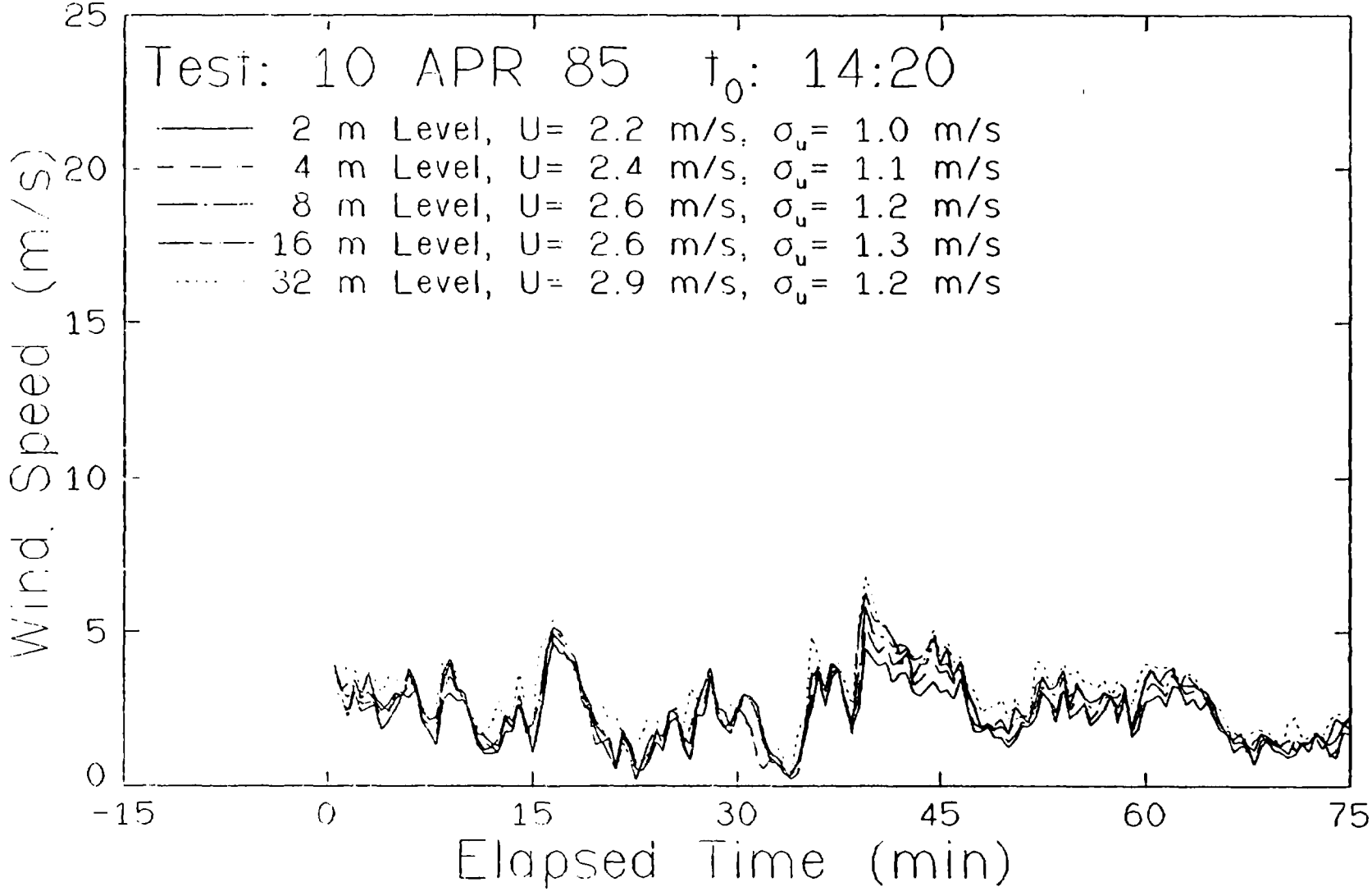

Figure 4.2. Trace of 30-second averaged wind speeds for unstable atmospheric conditions.

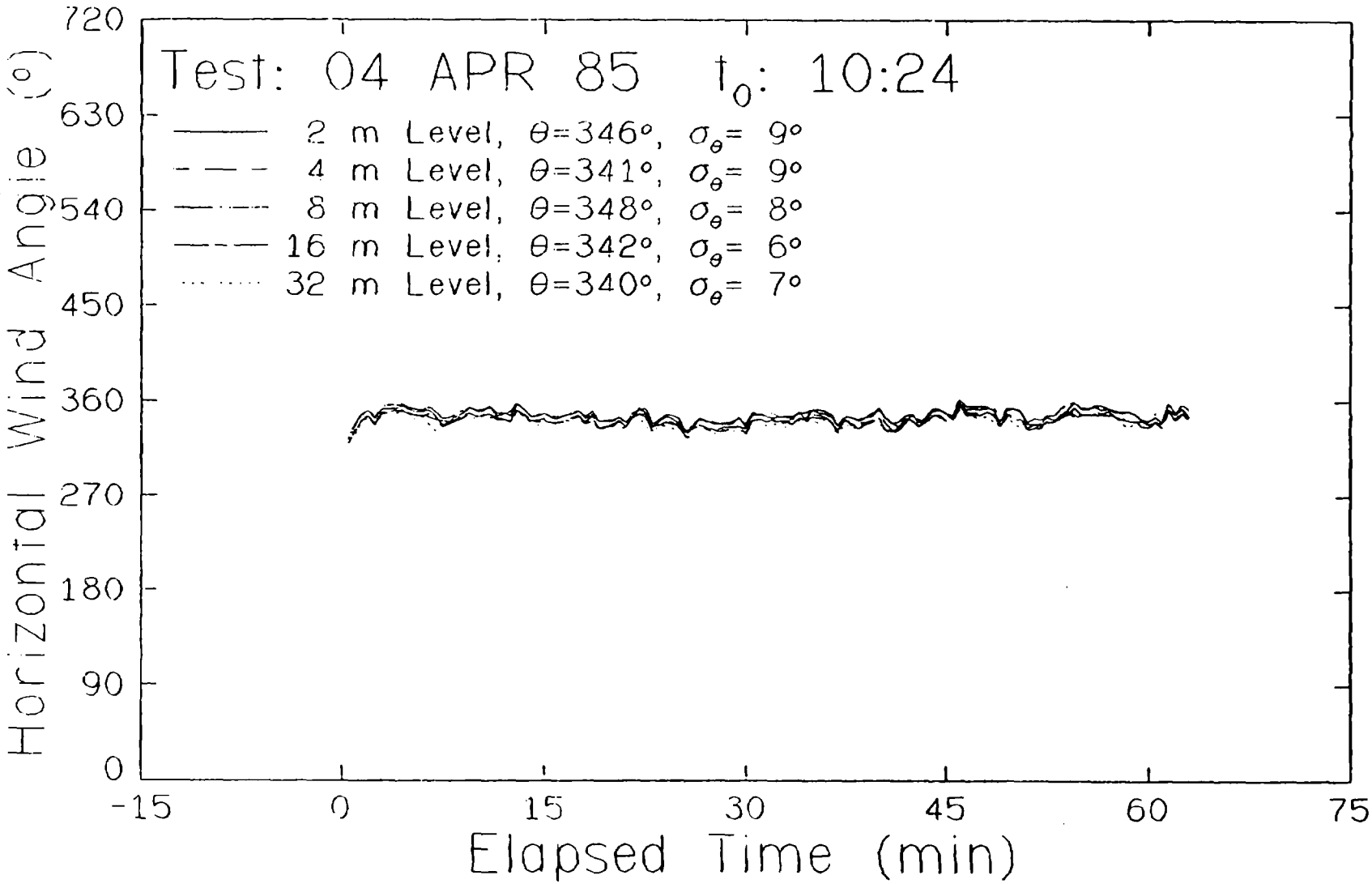

Figure 4.3. Trace of 30-second averaged wind direction for near-neutral atmospheric conditions.

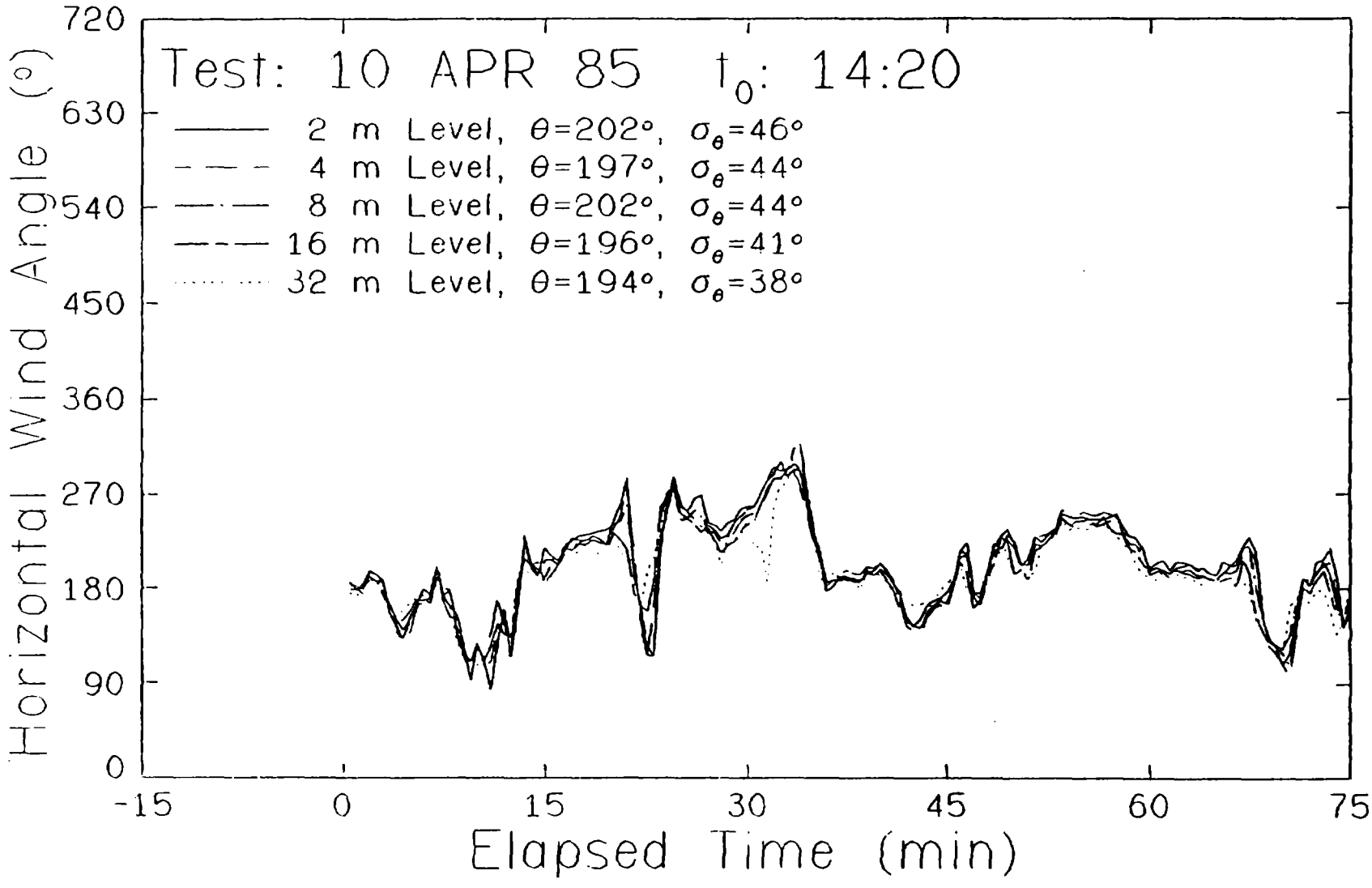

Figure 4.4. Trace of 30-second averaged wind direction for unstable atmospheric conditions.

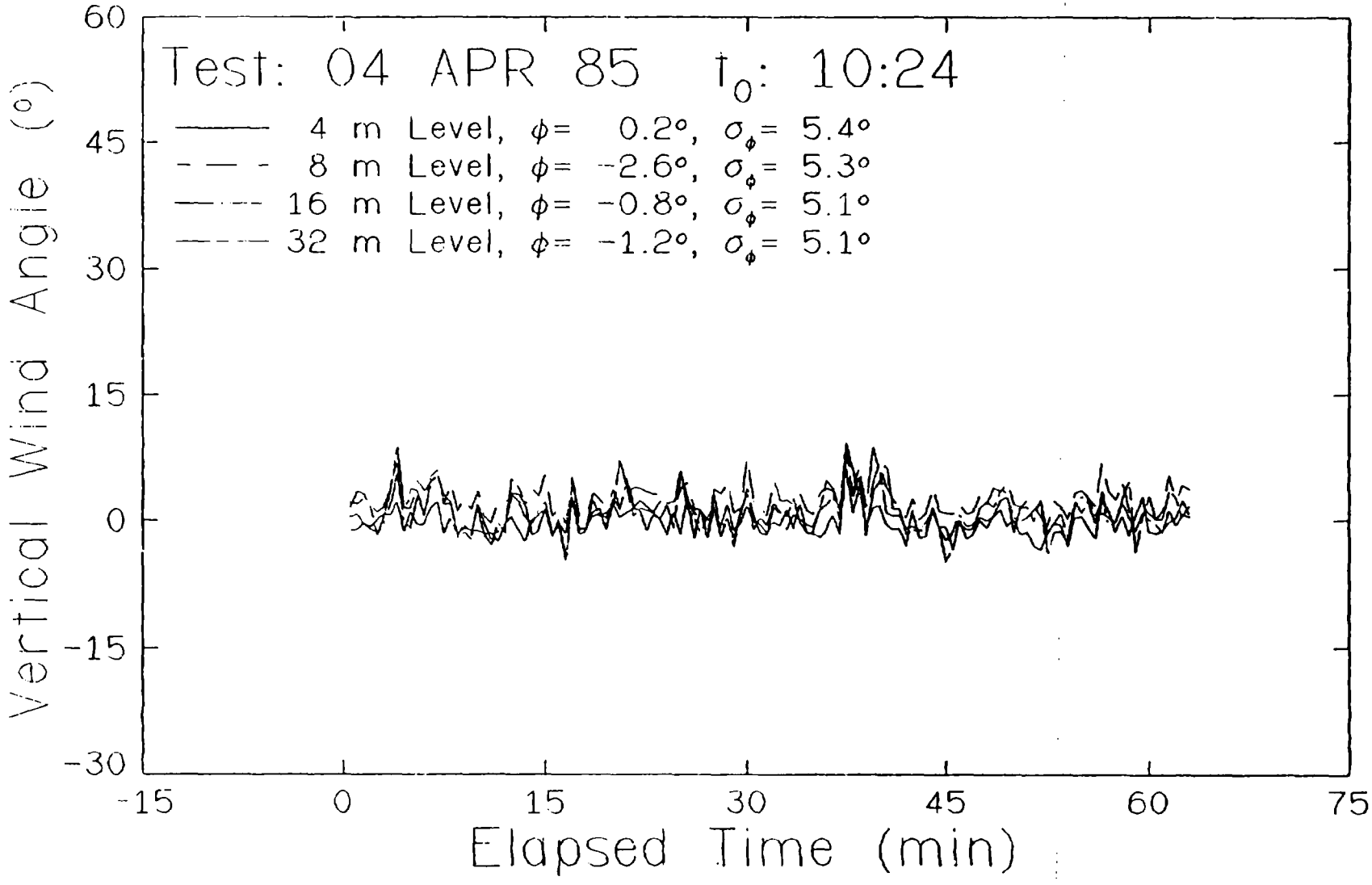

Figure 4.5. Trace of 30-second averaged vertical wind angle for near- neutral atmospheric conditions.

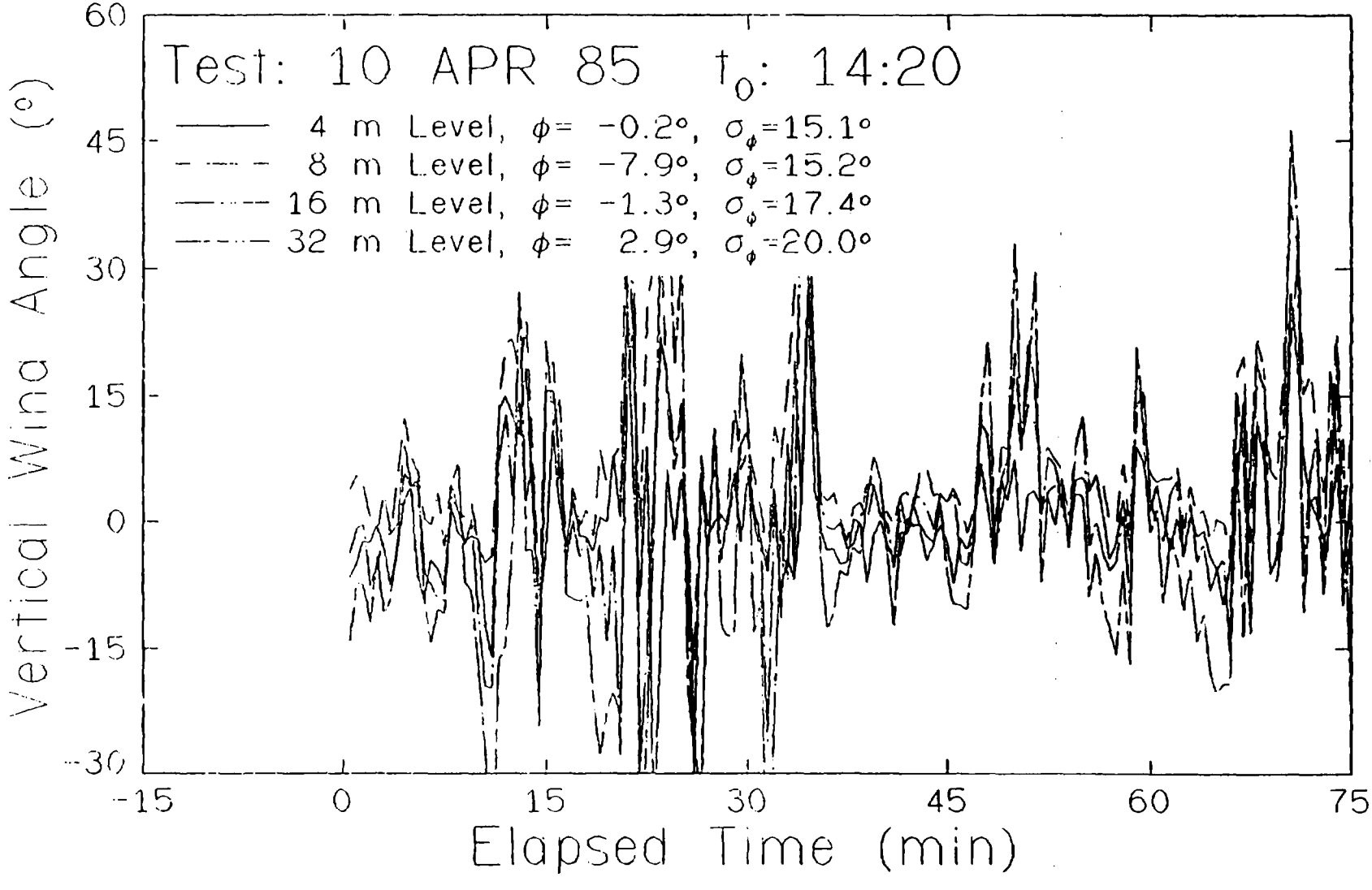

Figure 4.6. Trace of 30-second averaged vertical wind angle for unstable atmospheric conditions.

Table 4.1 Energy Losses Due to Limited Sampling (%)

	T0005				
	2m	4m	8m	16m	32m
U-Component					
High Frequency	11	8	6	5	3
Low Frequency	1	1	2	3	4
Total Lost	12	9	8	8	7
V-Component					
High Frequency	16	8	6	5	4
Low Frequency	0	1	2	3	3
Total Lost	16	9	8	8	7
W-Component					
High Frequency	-	29	29	20	15
Low Frequency	-	0	0	0	0
Total Lost	-	29	29	20	15

	T0010				
	2m	4m	8m	16m	32m
U-Component					
High Frequency	2	2	2	2	23
Low Frequency	5	5	5	5	5
Total Lost	7	7	7	7	7
V-Component					
High Frequency	1	1	1	1	1
Low Frequency	9	9	9	9	9
Total Lost	10	10	10	10	10
W-Component					
High Frequency	-	10	5	5	4
Low Frequency	-	1	3	2	3
Total Lost	-	11	8	7	7

4.2.2 Scaling Parameters

Atmospheric turbulence is generated by mechanical forces (momentum flux or shear) and convective forces (heat flux). The friction velocity u_* is a measure of the shear stress τ at the surface:

$$u_*^2 = \tau/\rho = \overline{u'w'} \qquad (4.1)$$

where ρ is the air density, and the kinematic heat flux Q describes the convection:

$$Q = \frac{H}{\rho c_p} = \overline{T'w'} \qquad (4.2)$$

and H is the sensible heat flux at the surface: $H = -k\, dT/dz$, where k is the thermal conductivity of the air and dT/dz is the temperature gradient at the surface. Thus a negative temperature gradient at the surface implies a positive heat flux; that is, heat is moving upward, away from the warmer surface. The Monin-Obukhov length L is a measure of the relative contributions of shear and convection to the turbulent energy:

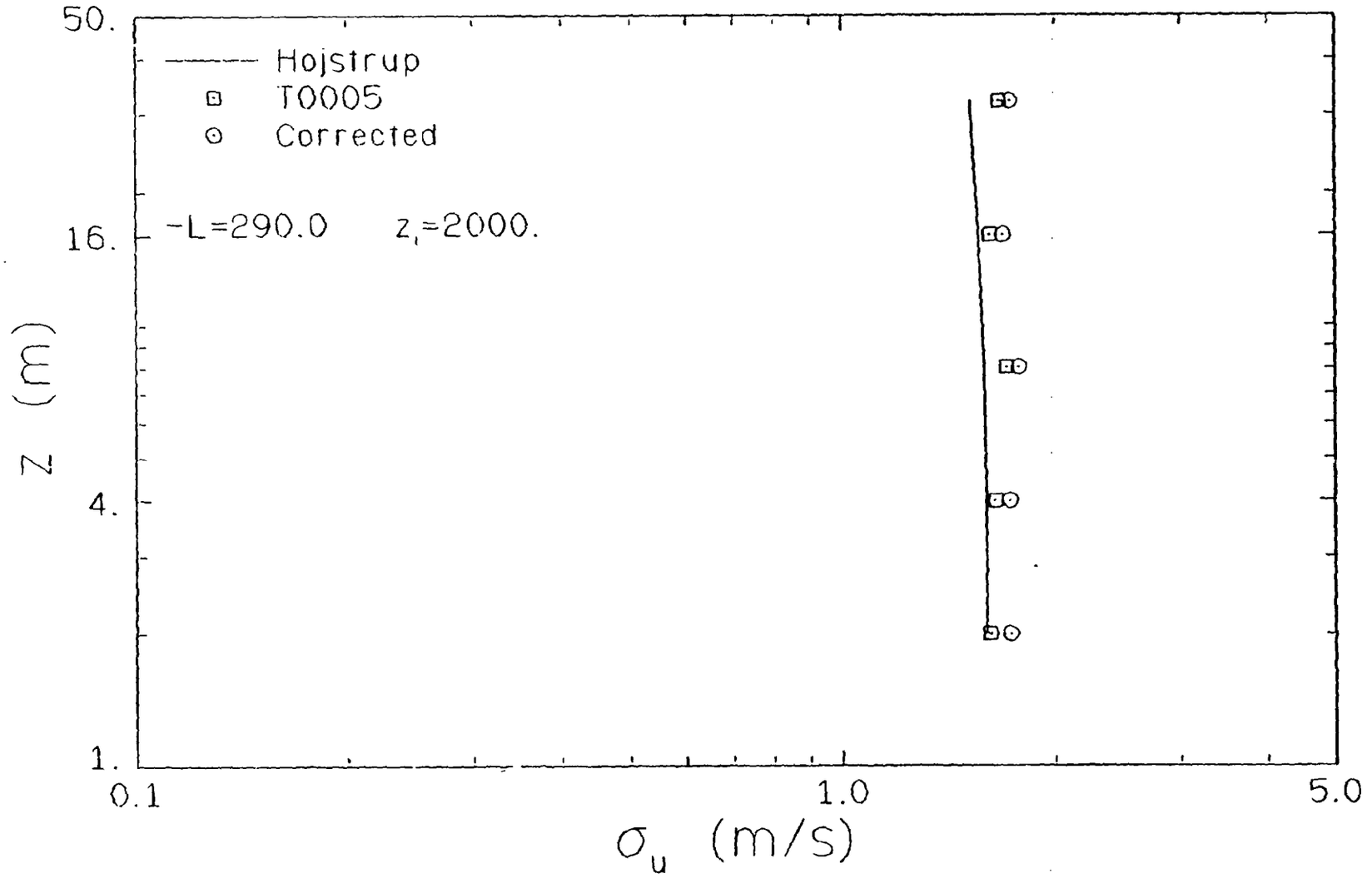

Figure 4.7. Variances of U-velocity fluctuations before and after correction for sampling frequency limitations compared with model variance predictions for near-neutral stability.

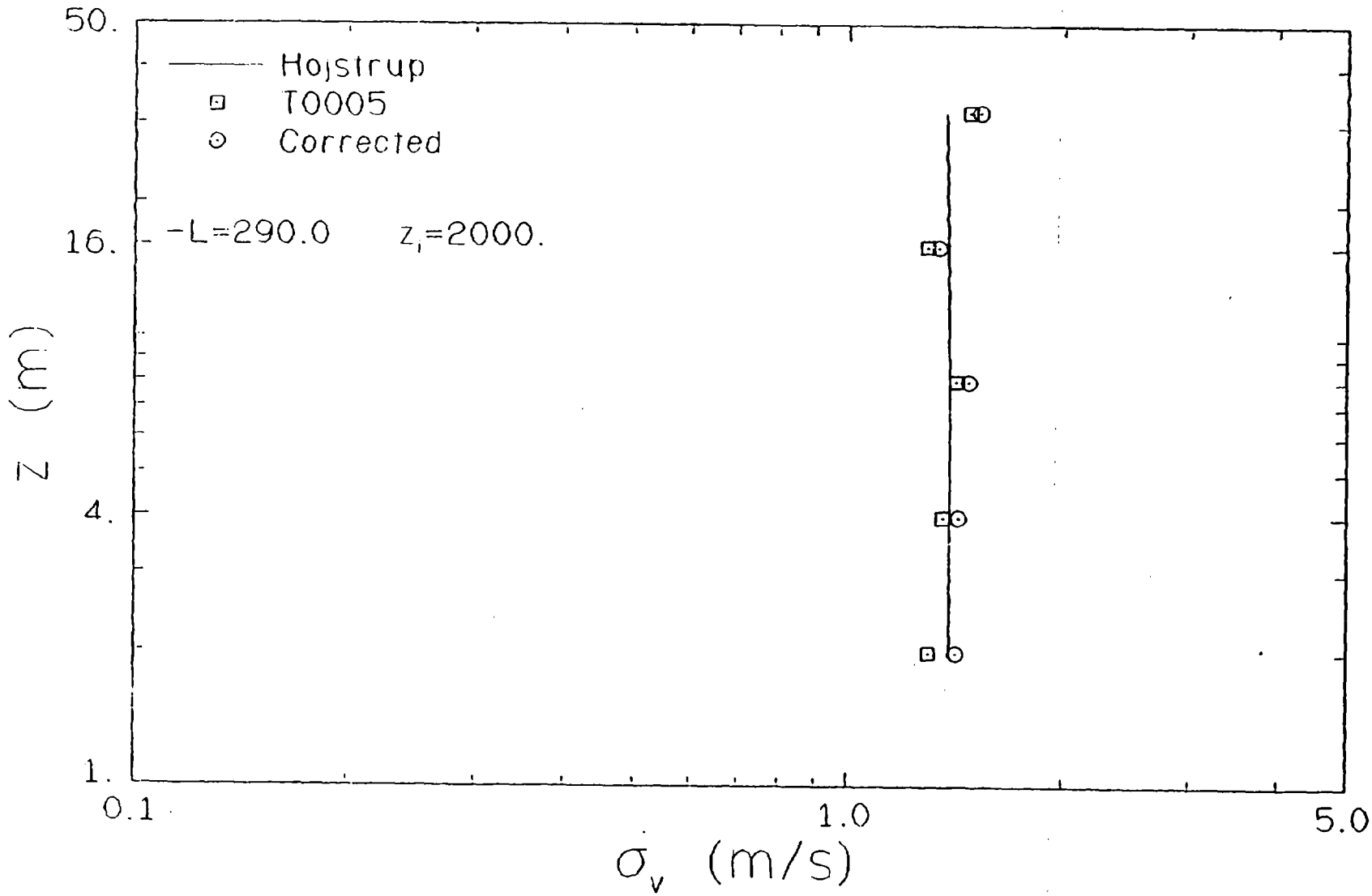

Figure 4.8. Variances of V-velocity fluctuations before and after correction for sampling frequency limitations compared with model predictions for near-neutral stability.

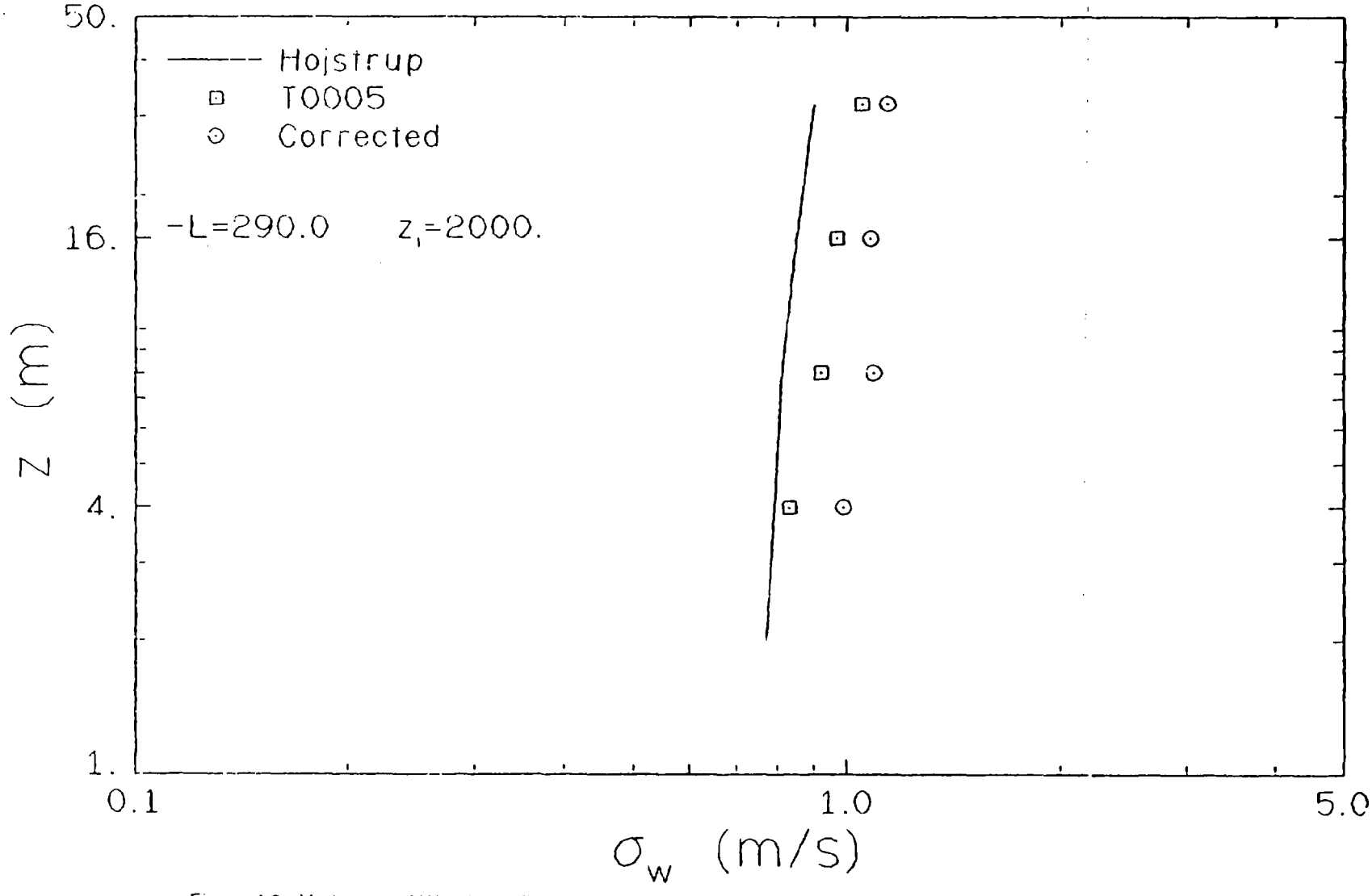

Figure 4.9. Variances of W-velocity fluctuations before and after correction for sampling frequency limitations compared with model predictions for near-neutral stability.

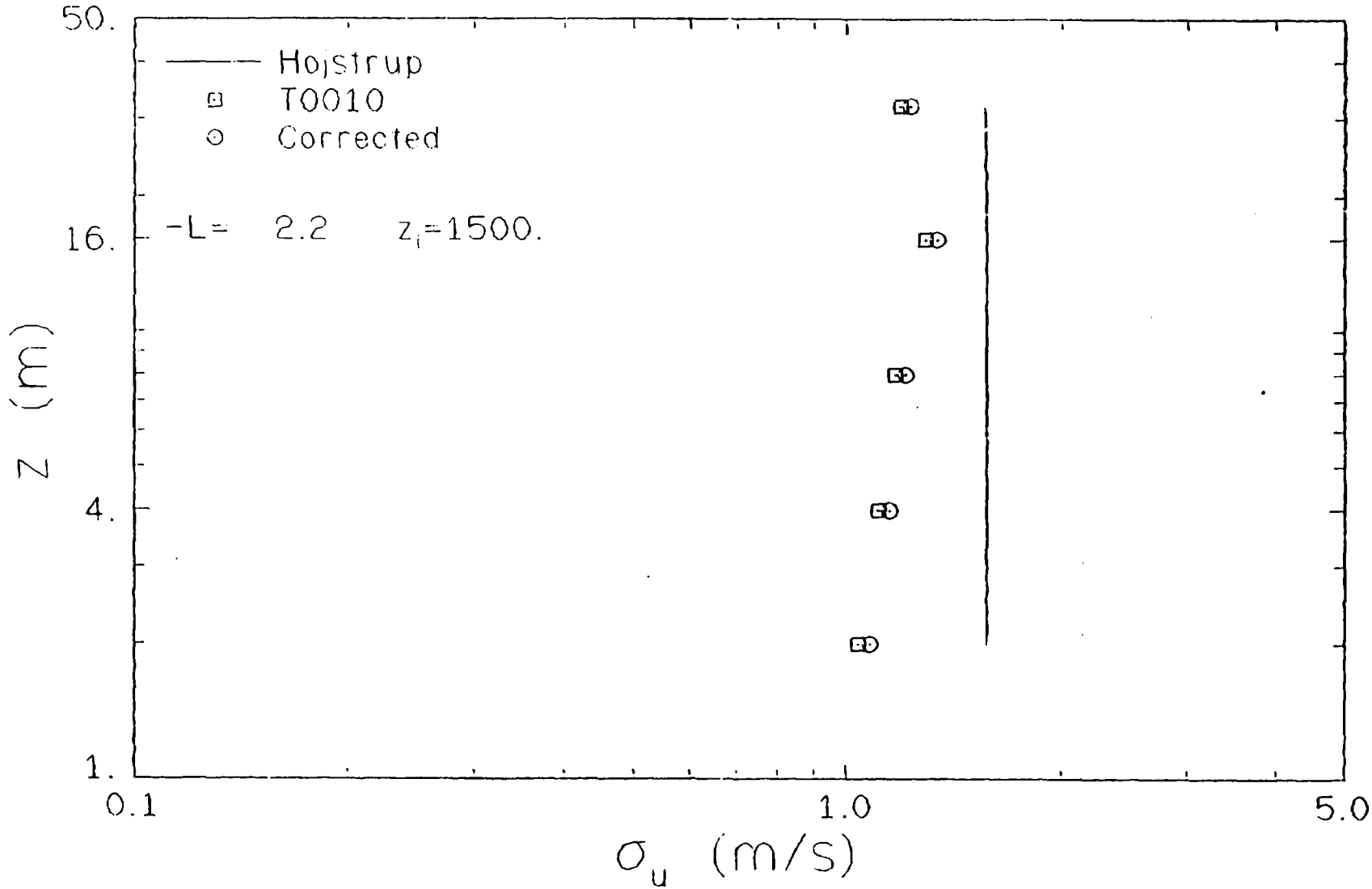

Figure 4.10. Variances of U-velocity fluctuations before and after correction for sampling frequency limitations compared with model predictions for unstable conditions.

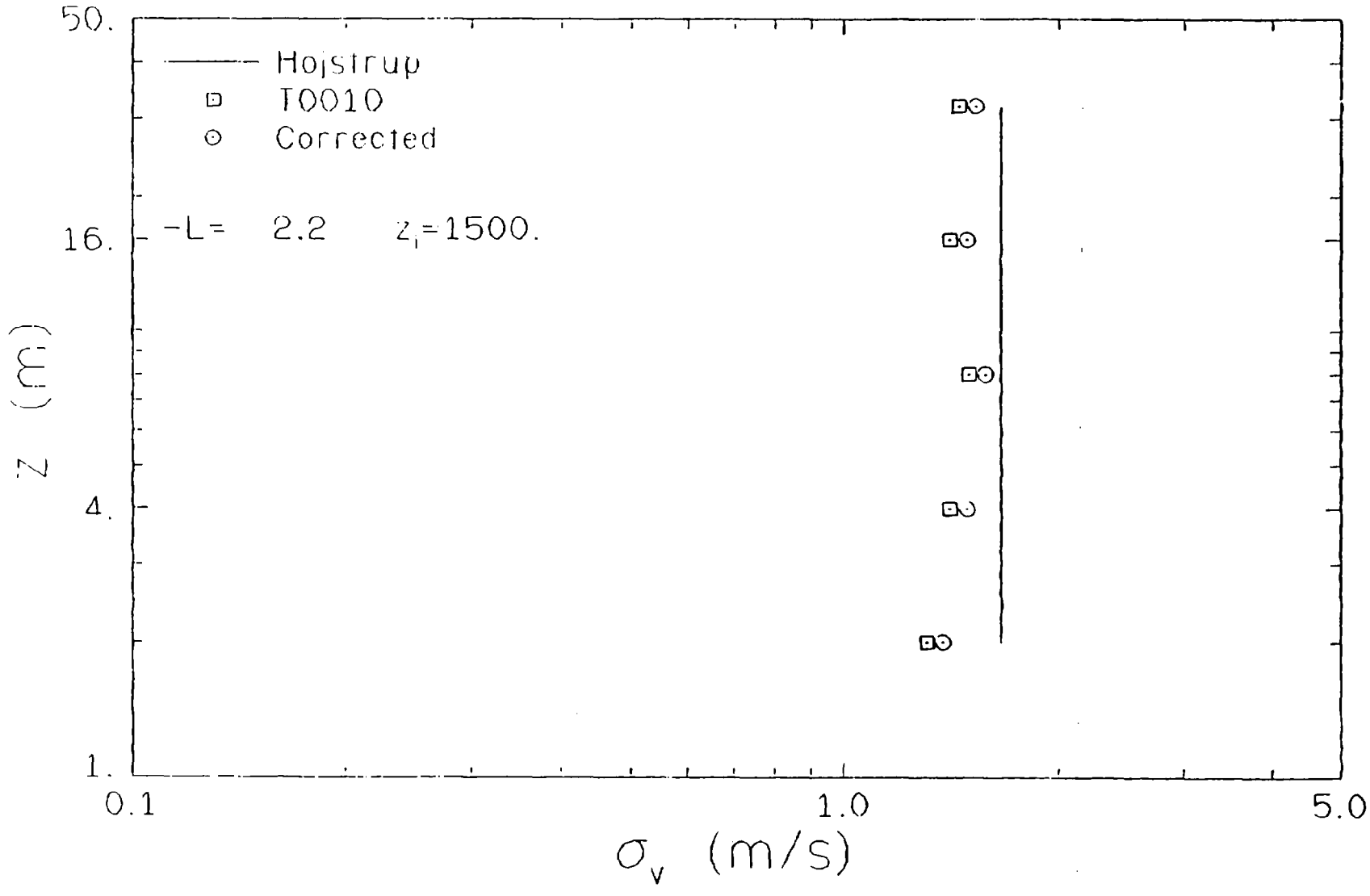

Figure 4.11. Variances of V-velocity fluctuations before and after correction for sampling frequency limitations compared with model predictions for unstable conditions.

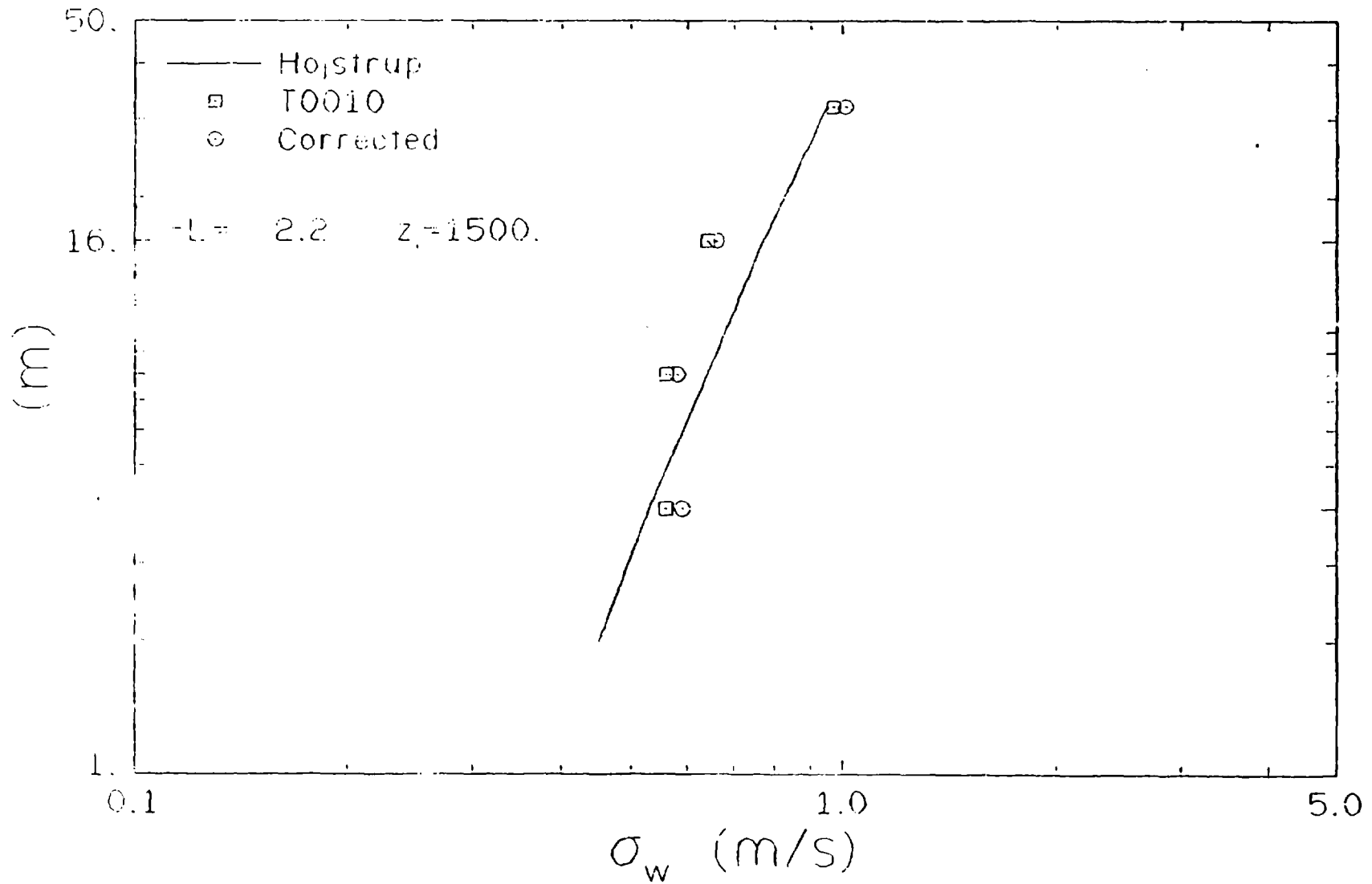

Figure 4.12. Variances of W-velocity fluctuations before and after correction for sampling frequency limitations compared with model predictions for unstable conditions.

$$L = -\frac{u_*^3}{(g/T)\,Q} \qquad (4.3)$$

where g is the acceleration due to gravity and T is the average (absolute) temperature in the surface layer. L is defined so that it has the same sign as the temperature gradient at the surface. That is, if the temperature gradient is positive (the surface is cooler than the overlaying fluid) then $L > 0$ and the fluid is stably stratified. If, on the other hand, the gradient is negative (the surface is warmer than the overlaying fluid) then $L < 0$ and the fluid is unstably stratified. At heights less than L shear is the dominant mechanism for the production of turbulent energy; above this height convection dominates. On windy, overcast days there is very little solar heat flux: as $|Q| \rightarrow 0$, $|L| \rightarrow \infty$ and shear dominates the entire boundary layer. Conversely, during calm, sunny days there is a strong positive heat flux: as $Q \rightarrow \infty$, $-L \rightarrow 0$ and shear is confined to a very shallow layer near the surface while convection (evident by the presence of updrafts and downdrafts) dominates. Thus knowlege of these scaling parameters is necessary for determining the state of the planetary boundary layer turbulence which, in turn, is responsible for the transport and dispersion of airborne material such as smoke. A detailed discussion of turbulence scaling in the planetary boundary layer is provided by Tennekes (1982).

The friction velocity, u_*, the Monin-Obukhov length, L, and the temperature scales θ_* and θ_0 were determined at 5-minute intervals from running 10-minute averages of the wind speed and temperature profiles by fitting the following scaling relations to the profiles:

$$\frac{\kappa z}{u_*}\frac{dU}{dz} = \phi_m(z/L) \qquad (4.4)$$

$$\frac{\kappa z}{\theta_*}\frac{dT}{dz} = \phi_h(z/L) \qquad (4.5)$$

Here κ is Von Kármán's constant, U and T are mean wind speed and temperature and ϕ_m and ϕ_h are the ostensibly universal functions for momentum and heat flux, respectively, which have been empirically determined by Businger, *et al.* (1971), Dyer and Hicks (1970) and Hansen (1980).

This method, suggested by Nieuwstadt (1977), minimizes the combined mean square error in fitting the velocity and temperature profiles simultaneously. An estimate of the roughness height z_0 is required to fit the data to the profiles in this way. A value of $z_0 = 0.02$ m was found to yield the best fit for all cases. This agrees with Biltoft's (1982) findings that $0.02 < z_0 \leq 0.04$ and with Waldron's (1977) average value of $z_0 = 0.039$ for the same general area.

Figures 4.13 and 4.14 show 10-minute averaged wind speed data for a case of near-neutral stability (T0005) and an unstable case (T0010) along with profiles fitted to the data using the relationships due to Businger *et al.* Profiles of the potential temperature and the fits for the same trials are given in Figures 4.15 and 4.16, respectively. It is apparent from these figures that the data are well represented by the Businger forms. In fact all three forms for the profiles (Businger *et al.*, Dyer and Hicks as well as Hansen) fit the data well. This is not surprising since in this stability range all three forms were very similar. (Hansen's formulation is identical to Dyer and Hicks' for $L<0$.) Because of this agreement, the values for u_*, L, θ_* and 0_0 derived from fitting the profile data to these forms are believed to be accurate. Additionally, all comparisons between the data and the Højstrup model requiring the Monin-Obukhov length as a parameter were in good agreement. In all cases the stability class determined from the computed value of L using the work of Golder (1972) was in agreement with the Pasquill stability classification provided by Dugway Proving Ground meteorologists.

Means and standard deviations of the wind speed, horizontal and vertical wind angles as well as the vertical and transverse velocity were computed over the period of each test and interpolated to the10-m level. These data are tabulated in Table 4.2. Also tabulated are values of the Obukhov length, Pasquill stability class, friction velocity, exponent of the power law fit of the wind profile, ambient temperature, temperature lapse rate and relative humidity.

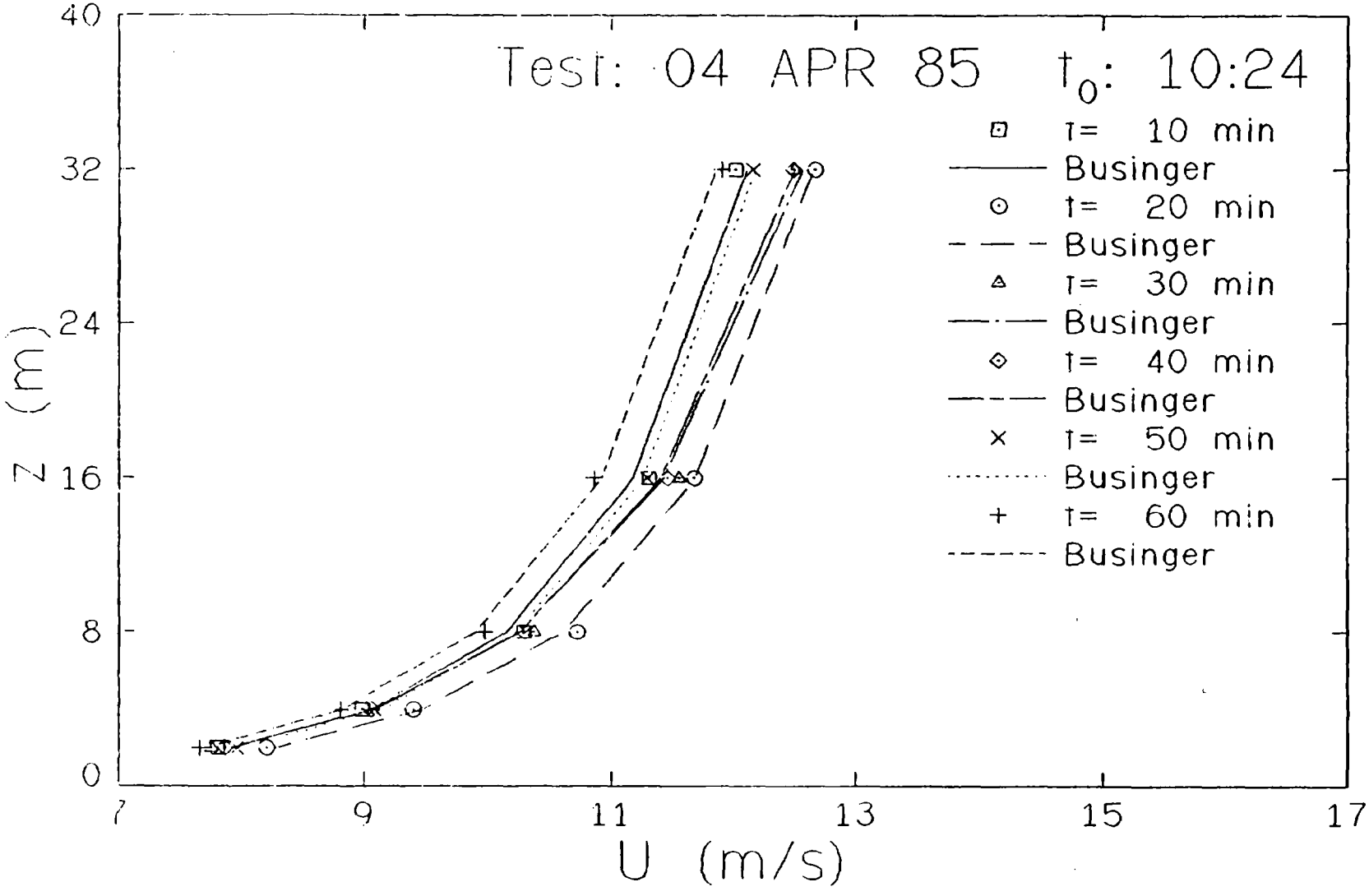

Figure 4.13. Profiles of 10-minute averaged wind speed along with fits due to Businger, et. al. for near-neutral stability.

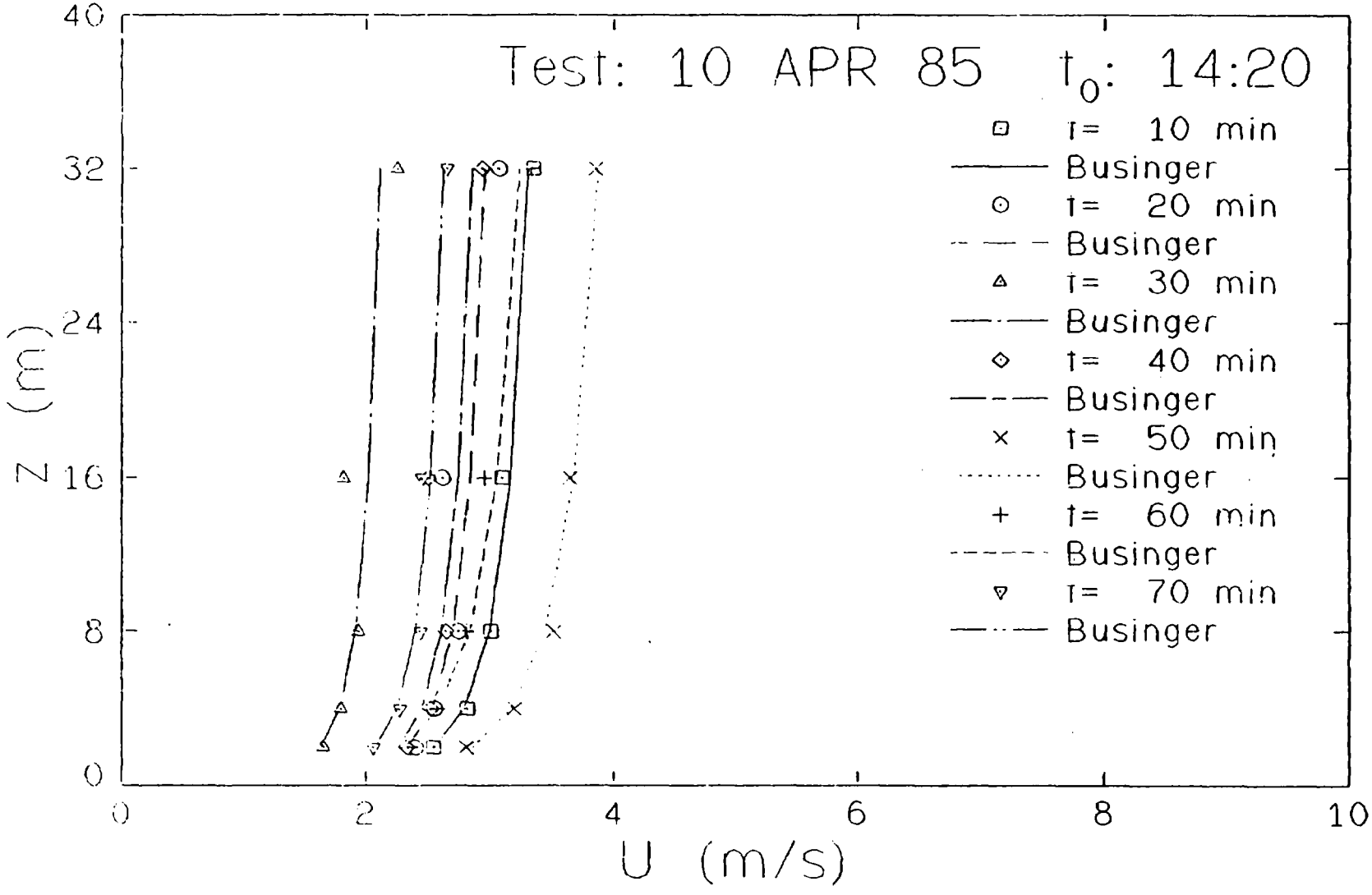

Figure 4.14. Profiles of 10-minute averaged wind speed along with fits due to Businger, et. al. for unstable conditions.

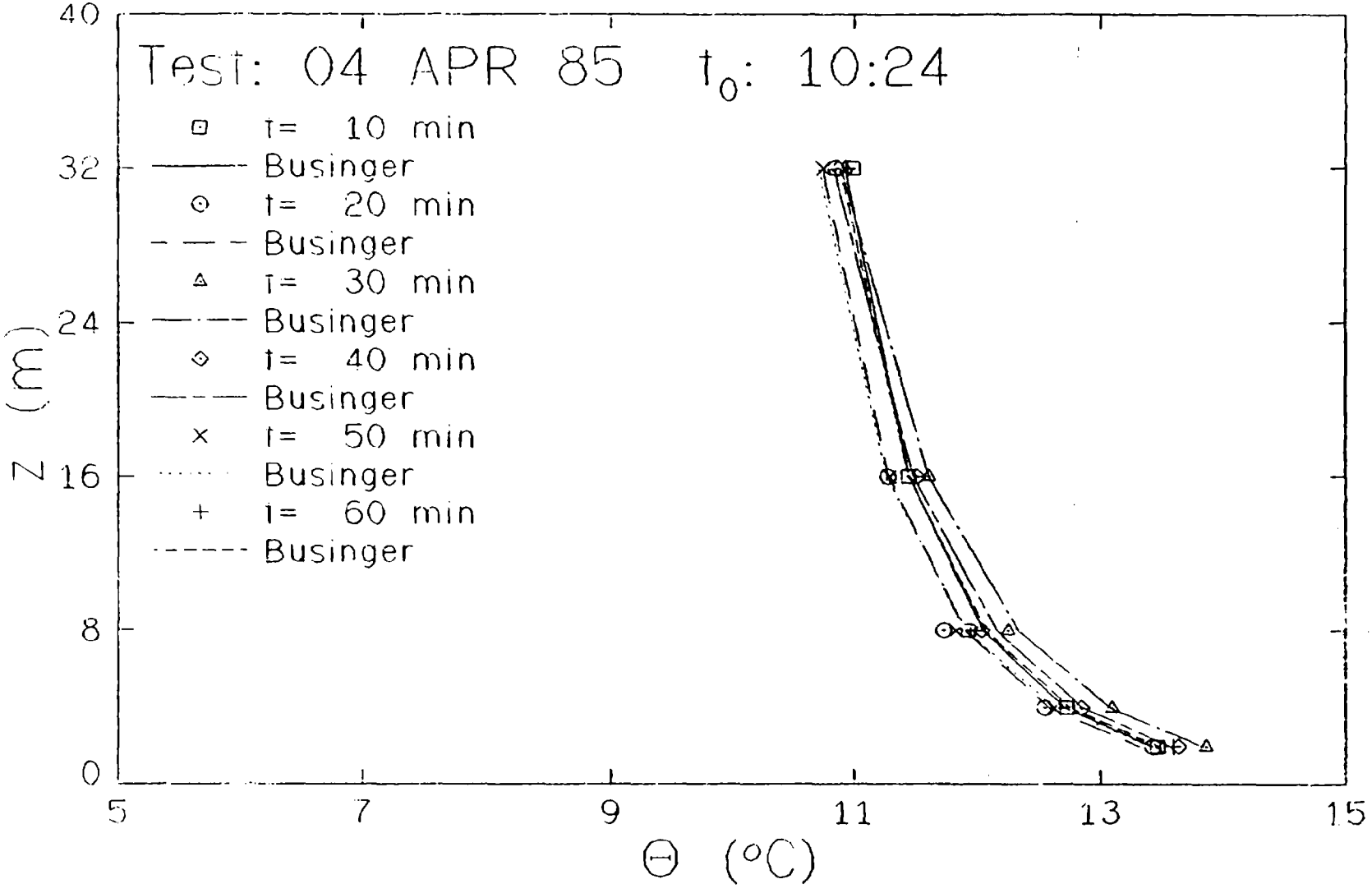

Figure 4.15. Profiles of 10-minute averaged potential temperature and fits due to Businger, et. al. for near-neutral conditions.

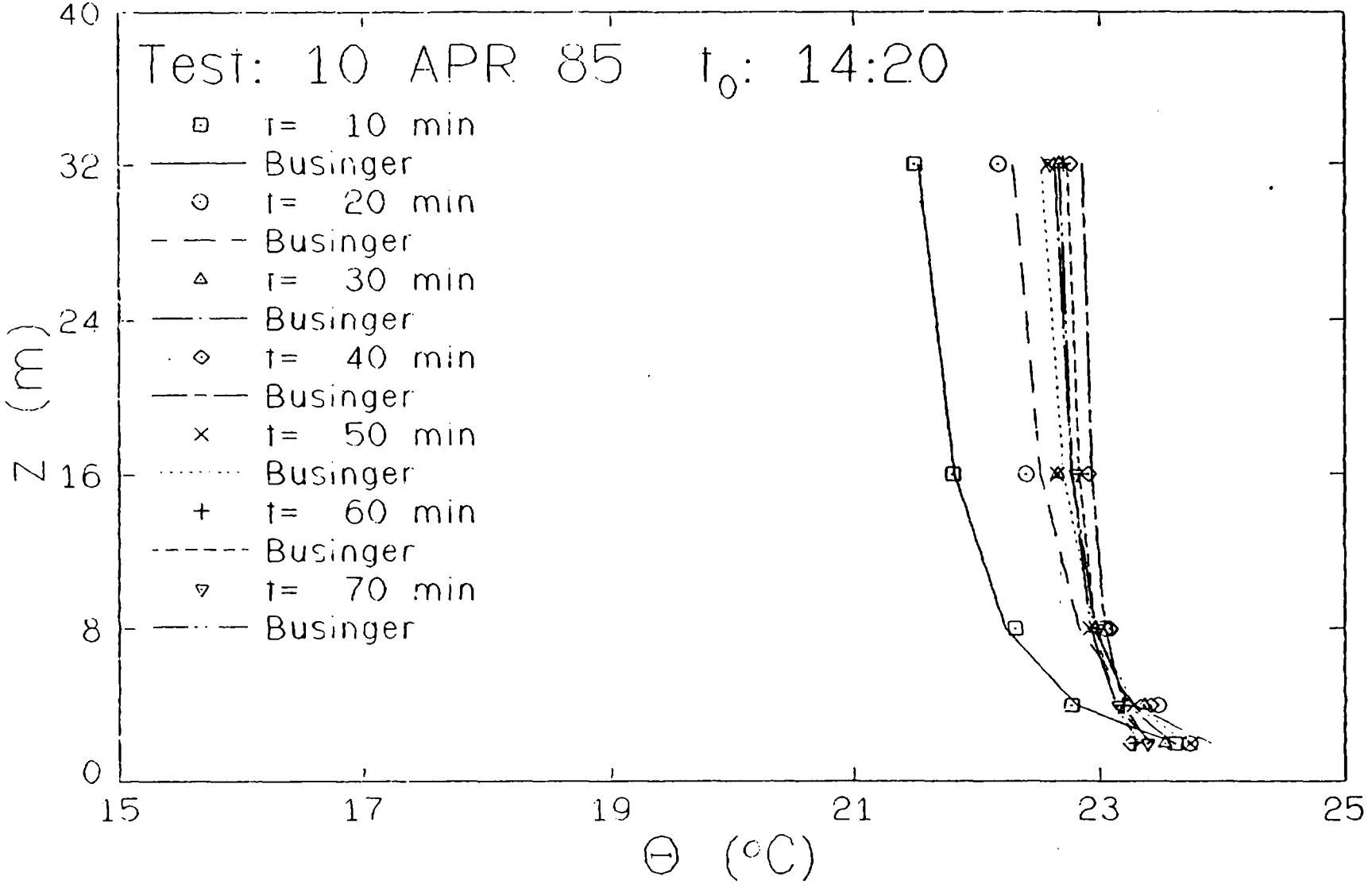

Figure 4.16. Profiles of 10-minute averaged potential temperature and fits due to Businger, et. al. for unstable conditions.

Table 4.2. Summary of Meteorological Data

Test Designation	T0001	T0002	T0003	T0004	T0004	T0005	T0006
Date	21-Mar-85	25-Mar-85	2-Apr-85	3-Apr-85	3-Apr-85	4-Apr-85	4-Apr-85
Begin Release (MDT)	10:34	9:54	10:20	9:42	10:20	10:24	13:46
End Release (MDT)	11:27	11:07	11:56	10:20	10:33	11:27	14:48
Wind Speed (m/s)	9.8	6.1	3.8	3.6	2.0	10.6	9.6
Wind Direction (°E of N)	300	334	184	182	274	347	4
Sigma-u (m/s)	2.3	1.2	1.1	1.0	1.0	1.7	1.7
Sigma-theta (°)	9.0	12.3	25.1	19.3	45.8	8.0	13.9
Sigma-phi (°)	4.9	5.6	11.2	9.9	18.8	5.3	5.5
Sigma-v (m/s)	1.7	1.3	1.5	1.1	1.4	1.4	2.2
Sigma-w (m/s)	0.8	0.6	0.7	0.6	0.6	0.9	0.9
Ambient Temp (°C)	10.9	7.3	15.5	17.1	17.9	11.7	12.7
Lapse Rate (°C/m)	-0.0187	-0.0236	-0.0622	-0.0584	-0.0493	-0.0437	-0.0427
Rel. Humidity (%)	47	58	36	48	32	34	27
Stability Class	D	D	B	B	A	D	D
Monin-Obukhov Length (m)	-INF	-136	-5.4	-6.7	-1.4	-290	-75
Wind Power Exponent	0.163	0.140	0.101	0.105	0.096	0.156	0.138
Friction Velocity (m/s)	0.56	0.35	0.28	0.26	0.18	0.61	0.57
Roughness Height (cm)	2	2	2	2	2	2	2

Test Designation	T0007	T0008	T0009	T0010	T0011	T0011
Date	5-Apr-85	8-Apr-85	9-Apr-85	10-Apr-85	11-Apr-85	11-Apr-85
Begin Release (MDT)	13:10	14:29	13:38	14:20	9:38	10:30
End Release (MDT)	14:14	15:17	14:53	15:38	9:45	11:55
Wind Speed (m/s)	4.7	8.5	5.2	2.6	7.2	6.3
Wind Direction (°E of N)	347	236	11	201	338	5
Sigma-u (m/s)	1.8	2.1	1.7	1.2	1.3	1.7
Sigma-theta (°)	25.4	16.2	18.7	43.9	11.0	14.7
Sigma-phi (°)	9.7	4.9	8.8	15.7	4.8	7.1
Sigma-v (m/s)	1.9	2.4	1.6	1.5	1.4	1.5
Sigma-w (m/s)	0.7	0.7	0.7	0.6	0.6	0.7
Ambient Temp (°C)	15.3	22.0	18.5	22.7	16.0	18.2
Lapse Rate (°C/m)	-0.035	-0.0428	-0.0403	-0.0196	-0.0438	-0.0517
Rel. Humidity (%)	28	23	23	21	36	31
Stability Class	C	D	C	B	D	C
Monin-Obukhov Length (m)	-29	-100	-19	-2.2	-107	-22
Wind Power Exponent	0.125	0.140	0.114	0.093	0.150	0.120
Friction Velocity (m/s)	0.30	0.51	0.34	0.22	0.42	0.41
Roughness Height (cm)	2	2	2	2	2	2

Notes:
1. All values are averages over the period of the test.
2. All values are for the 10 m level except for the relative humidity which is reported for the 4 m level.

4.2.3 Power Spectra and Auto-Correlations

Estimates of the single-sided power spectra S(n) of the wind speed, direction and inclination were computed using the Fast Fourier Transform (FFT) as implemented by Rabiner (1979). The data record was first divided into overlapping segments of 512 points (for the data from the West Vertical Grid tower, sampled at 1-second intervals) or 128 points (for the data collected from the Horizontal Grid tower, sampled at 5-second intervals.) This was done to accommodate the requirement of the FFT routine that the length of the input data record be a power of 2 while maintaining a segment length near 10 minutes: (512 points) x (1 s) = 512 s or 8.5 min; (128 points) x (5 s) = 640 s or 10.7 min. The 10-minute segment length was selected to limit the range of scales to those relevant to the problem under study as well as to reduce the non-stationarity of the wind statistics. Values for the mean and variance are then computed for each segment and the mean subtracted from the data comprising that segment. Pasquill and Smith show that overlapping the data segments in this manner reduces aliasing and the accompanying distortion of the high-frequency end of the spectrum thus providing a better estimate of the spectrum and the variance in the frequency range of interest.

A Hanning weighting function was applied to each segment prior to the Fast Fourier Transformation in order to reduce "leakage" from one spectral band into adjoining bands. The ensemble average of the FFT of these segments provides a raw estimate of the power spectrum. This estimate is inverse transformed to yield the estimate of the auto-correlation. The resulting auto-correlation is normalized by its value at zero lag time to conform with the required physical limit that the correlation must be unity at zero lag. The raw spectral estimate is then normalized by the ensemble average of the segment variances. The ensemble average of the segment variances is used in order to account for the filtering effects of limiting the sample size.

The resulting estimate is subsequently smoothed in the frequency domain. Smoothing is accomplished by averaging over a frequency range Δn centered on the frequency of interest. The range Δn varies with frequency such that $\Delta n/n$ remains approximately constant. Bendat and Piersol have shown that frequency smoothing is essential to reduce the substantial random error and to make the estimate consistent, that is, to make the estimate convergent in the limit of an infinite sampling period. A more detailed discussion of the errors ocurring in estimates of power spectra and quantities derived from power spectra such as correlations and integral scales is presented in Appendix B.

A check on the accuracy of the FFT was provided by comparing the ensemble averaged 10-minute variance with the value of the auto-correlation at zero lag and with the integral of the power spectrum. In most cases these agreed to within 2% and in no case did they differ by more than 10%. It was in the most unstable cases that the 10-minute variance differed more than 2% with R(0) and the integral of the auto-correlation. This is a direct consequence of the deviation of the turbulence from its assumed stationarity.

The 10-minute variance ranged from 90% of the 1-hour variance in the near-neutral cases down to 50% of the 1-hour variance in the most unstable case. This is due to the high-pass filtering effect of limiting the record length to 10 minutes. This increases the low frequency limit by a factor of 10 from 0.0003 Hz to 0.003 Hz. Of course, this has its greatest effect on the unstable cases for which the energy containing range of the spectrum is at much lower frequencies than for near-neutral cases.

Comparison of the spectra of wind speed and direction for unstable (class B) and near-neutral (class D) tests reveal that in the frequency range of the data, the unstable cases followed the inertial subrange scaling (-2/3 slope) reasonably well while the near-neutral cases did not. (Compare Figures 4.17 and 4.18.) The explanation for this is provided by Højstrup who argues that the spectrum results from the superposition of a buoyancy-produced, stability-dependent spectrum and a shear-produced spectrum which is independent of stability. For unstable atmospheric conditions, the buoyancy-produced spectrum dominates and the inertial subrange covers much of the frequency range of the data, whereas the shear-produced spectrum is equally important for the near-neutral tests and so the data do not exhibit inertial subrange behavior. For a thorough discussion of the spectral dynamics of turbulence, see Tennekes and Lumley (1972).

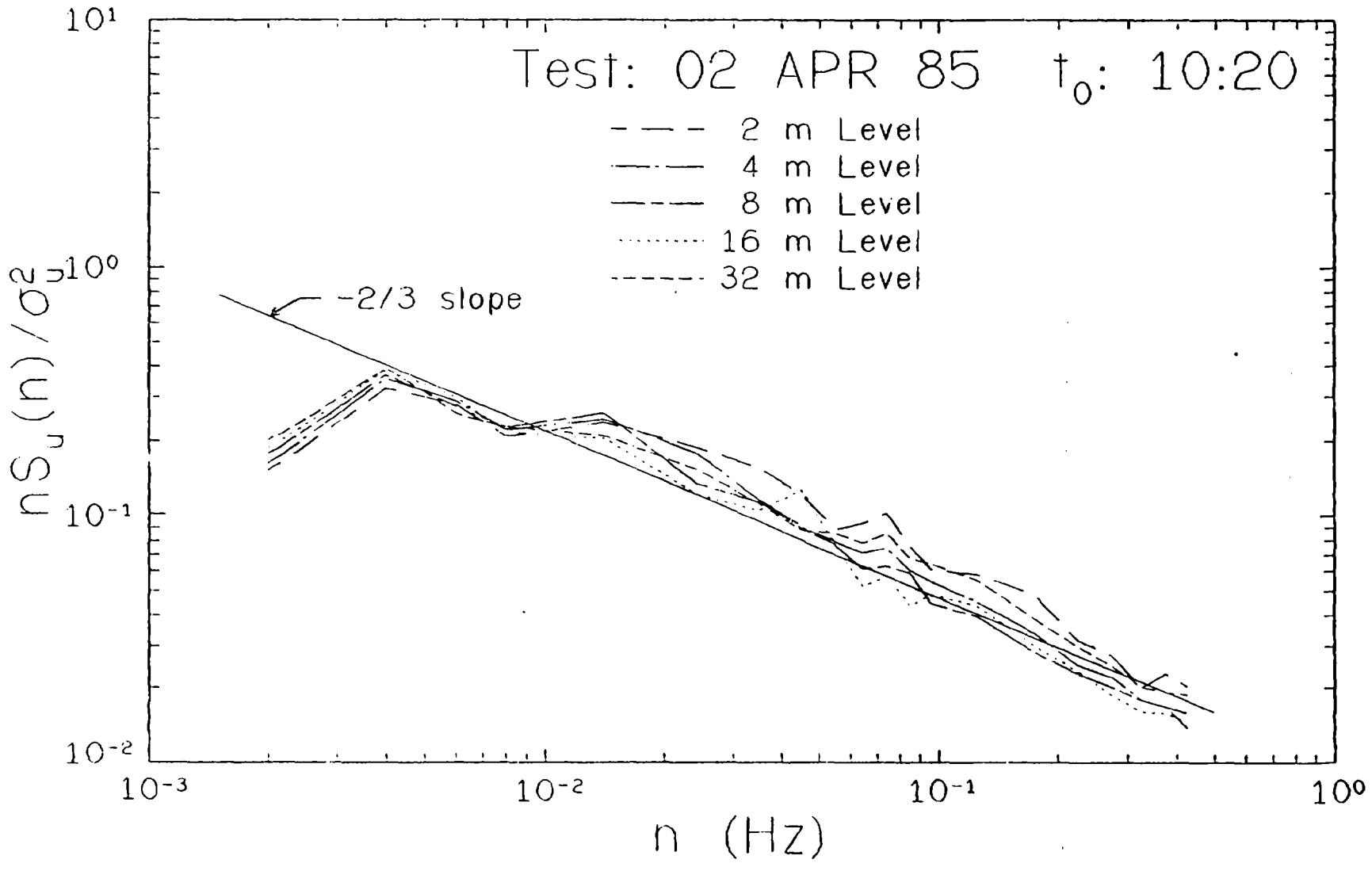

Figure 4.17. Uncorrected power spectrum for U ≈ 3.5 m/s (class B stability).

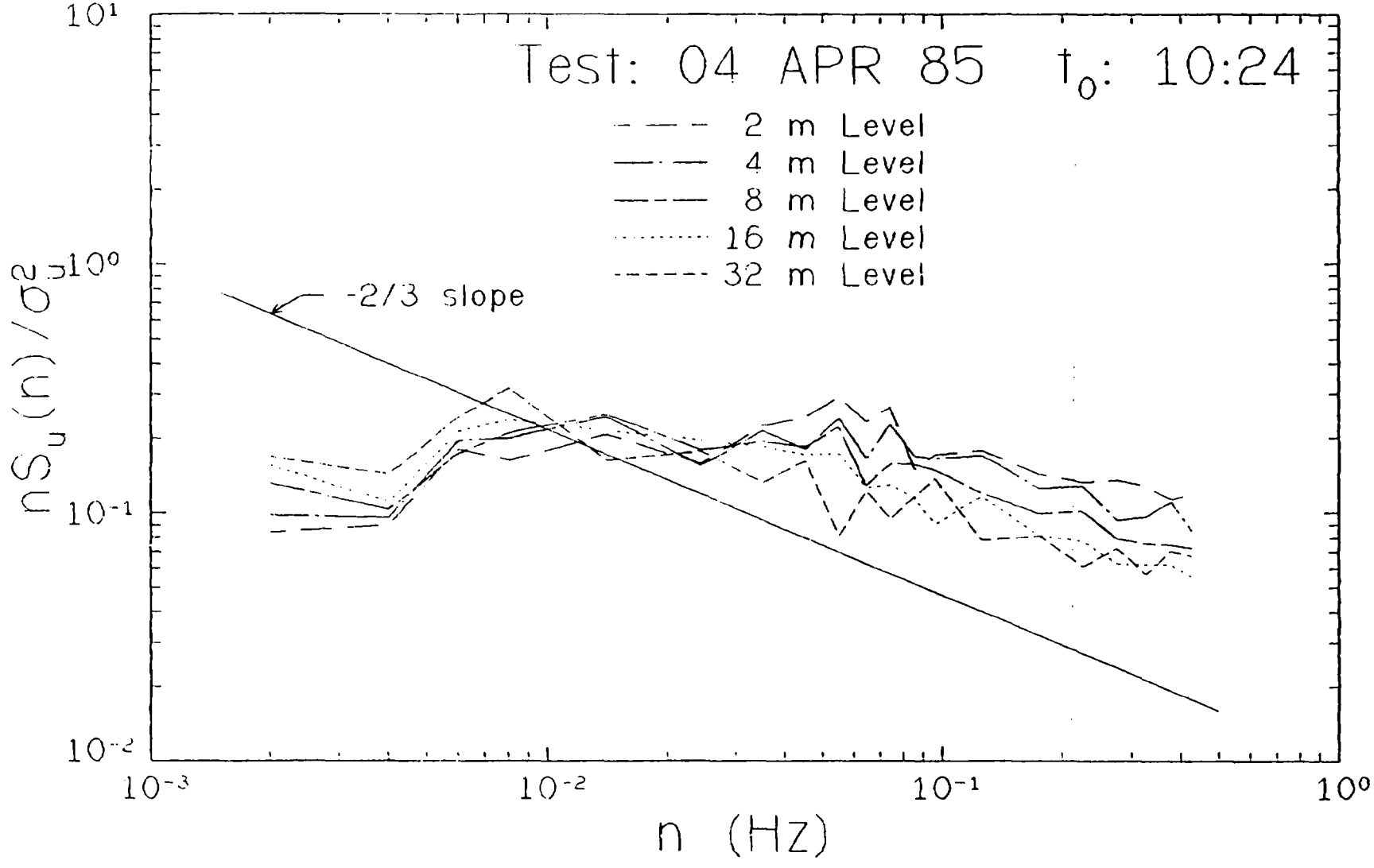

Figure 4.18. Uncorrected Power Spectrum for Near-Neutral (Class D) Stability.

In order to investigate this stability dependence further, as well as to check on the quality of our data, selected tests representing the most unstable and most nearly neutral conditions were compared with Højstrup's model spectra. An important parameter in the model, the height of the lowest inversion, z_i was not measured during our tests. Based on the data provided by Waldron and summarized in Table 4.3, z_i was estimated to be 2000 m for the near-neutral case and 1500 m for the unstable case.

Table 4.3 Estimated Inversion Height

Date	Time	Stability Class	L (m)	Estimated z_i (m)
2/25/77	9:00	D	-71	290
2/25/77	12:00	D	-27	1200
2/25/77	15:00	D	-32	1867
2/28/77	11:00	D	-12	529
2/28/77	14:00	D	-27	600
3/1/77	11:00	D	—	9
3/1/77	14:00	C	-5	518
3/2/77	11:00	D	-36	695
3/2/77	14:00	D	-333	914
3/8/77	12:00	C	-3	287
3/8/77	14:00	B	-9	1227
3/14/77	12:00	C	-11	758
3/14/77	14:00	B	-5	1372
3/30/77	12:00	A	-1	1278

Figures 4.19 and 4.20 compare the normalized wind speed spectra derived from the data from tests T0005 and T0010 with the model u-spectra for L= -200 and -2.2; these spectra have been corrected for the effects of the cup anemometer response. T0005 was conducted on the morning of April 4 with wind speeds about 10 m/s. T0010 took place on the afternoon of April 10 under low wind speed conditions (≈ 2 m/s). The error analysis presented in Appendix B indicates that the rms error in the unsmoothed power spectral density estimates is roughly 30%. Frequency smoothing reduces this error, more for higher frequencies than lower frequencies since the averaging "width" is chosen to maintain $\Delta n/n$ approximately constant. Frequency smoothing, however, has the disadvantage of reducing the resolution of the spectrum estimate. With this in mind, the wind speed spectra computed from the data may be judged to agree well, both qualitatively and quantitatively, with the model u-spectra.

As Figures 4.21 and 4.22 indicate, the θ-spectra show good qualitative agreement with the model v-spectra, each having roughly the same shape. Quantitatively, the θ-spectra appear to be somewhat low. This is partially due to real differences between the θ-spectra and the v-spectra and partially due to the substantial rms error in the estimate. Recall also that the θ-spectra result from only one realization of the turbulence and that some deviation from the model must be accepted.

This explanation gains credibility from a comparison of the φ-spectra with the model w-spectra given in Figures 4.23 and 4.24. Here again good qualitative agreement exists for the most part with quantitative disagreement at low frequencies in the near-neutral case and at high frequencies in the unstable case. These deviations do not show any apparent relationship to those of the θ-spectra. For the most part, the spectra computed from the data agree with the model spectra.

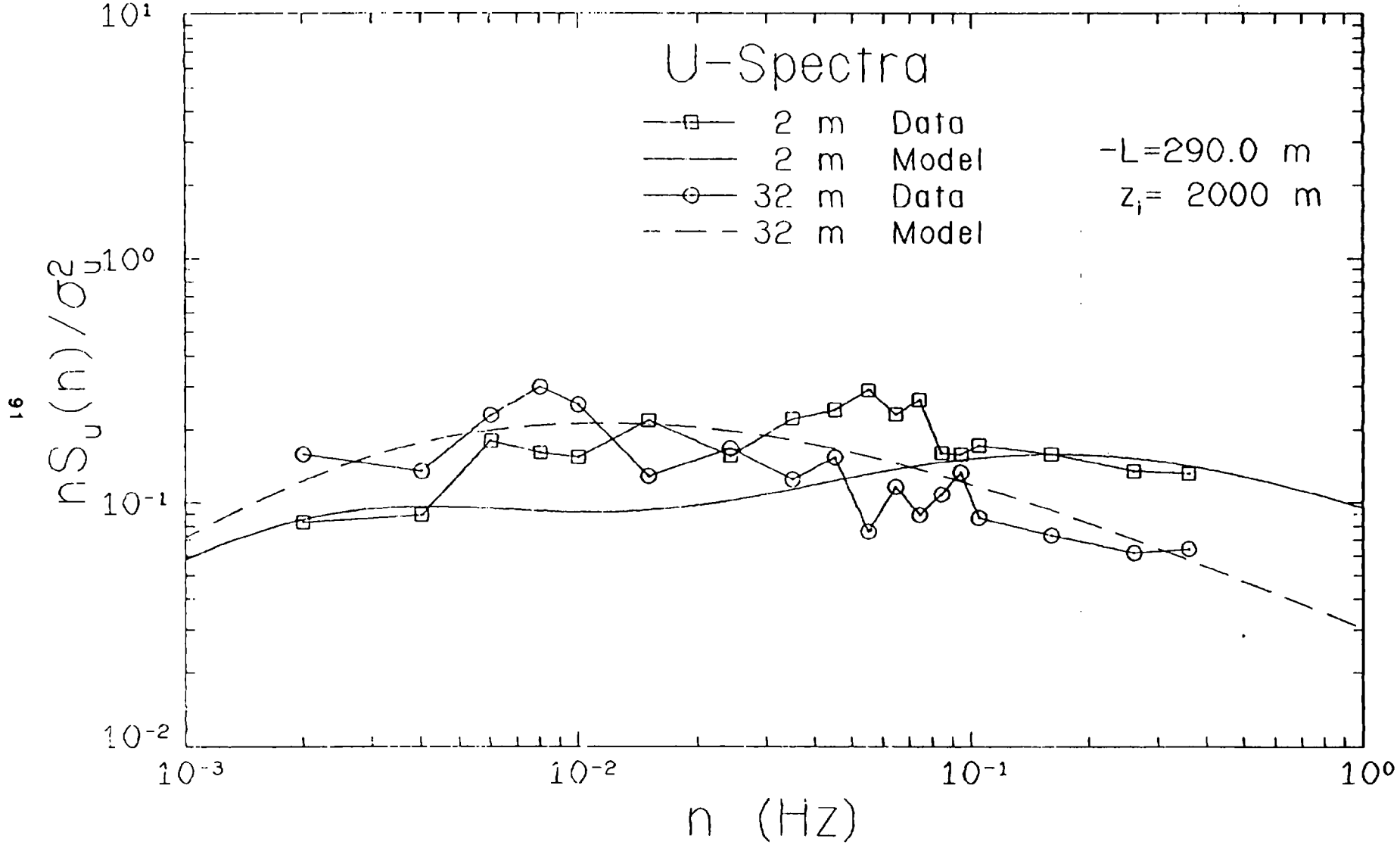

Figure 4.19. Normalized wind speed spectra and model U-spectra for near- neutrai stability.

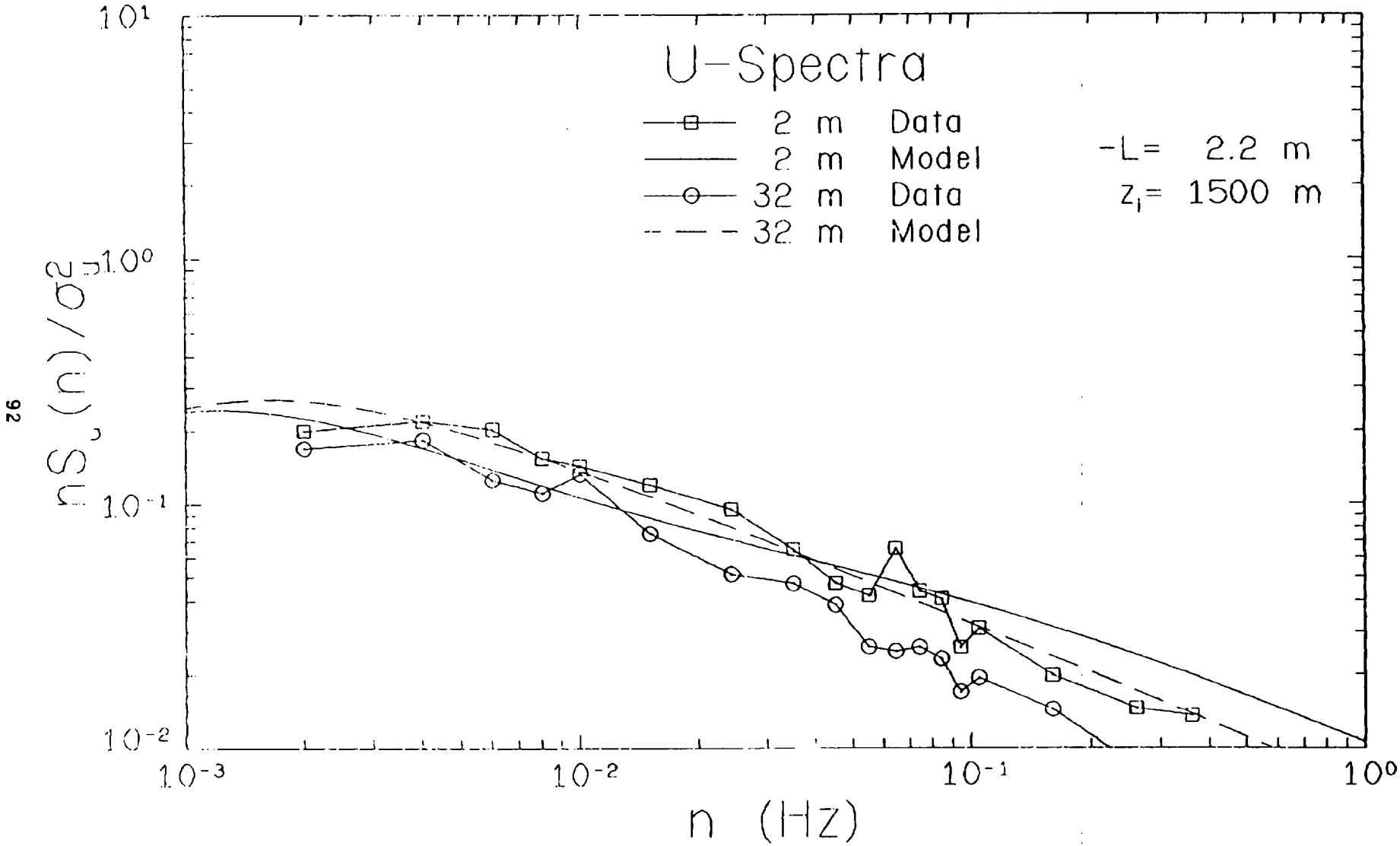

Figure 4.20. Normalized wind speed spectra and model U-spectra for unstable conditions.

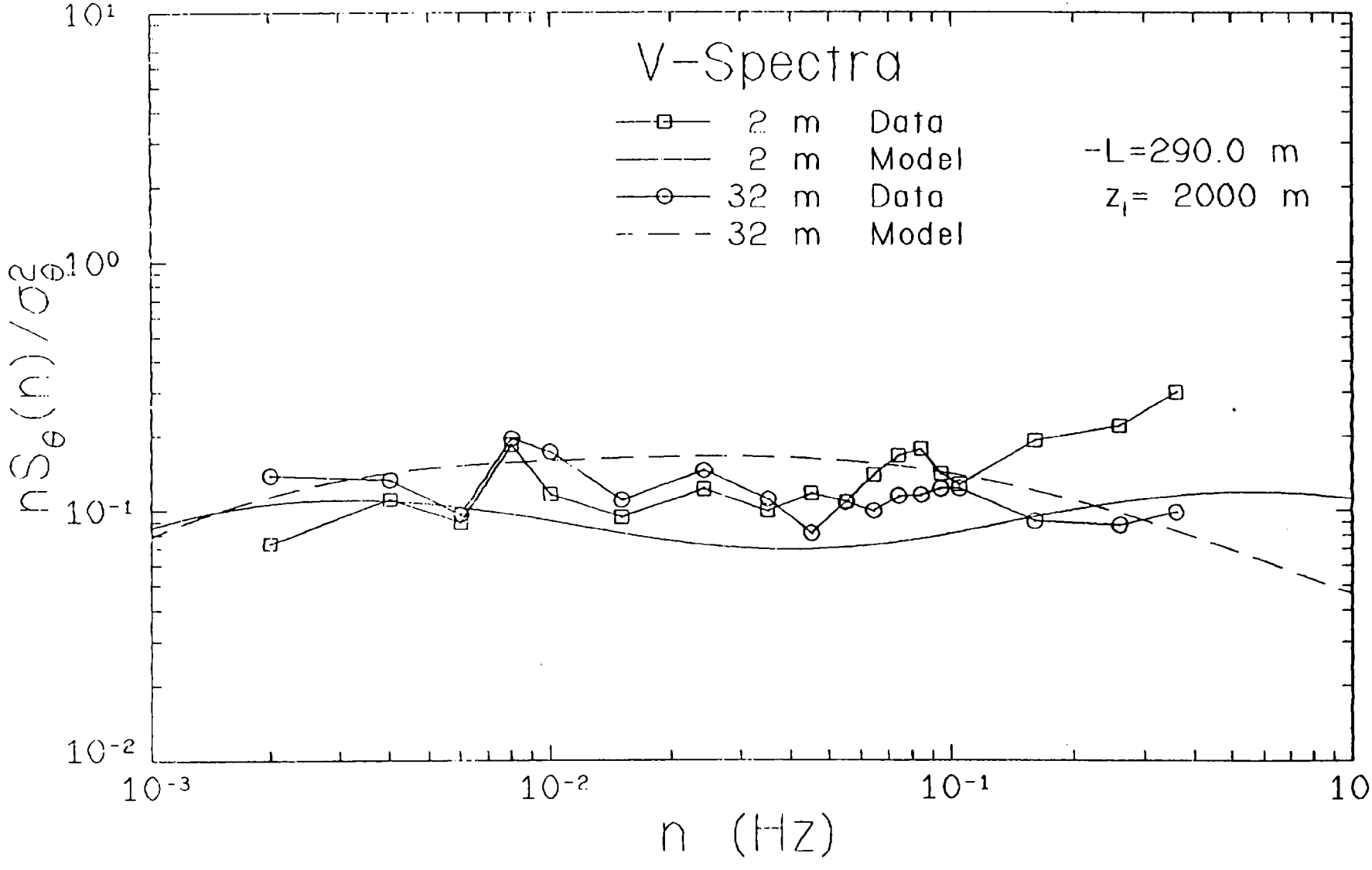

Figure 4.21. Normalized wind direction spectra and model V-spectra for near-neutral conditions.

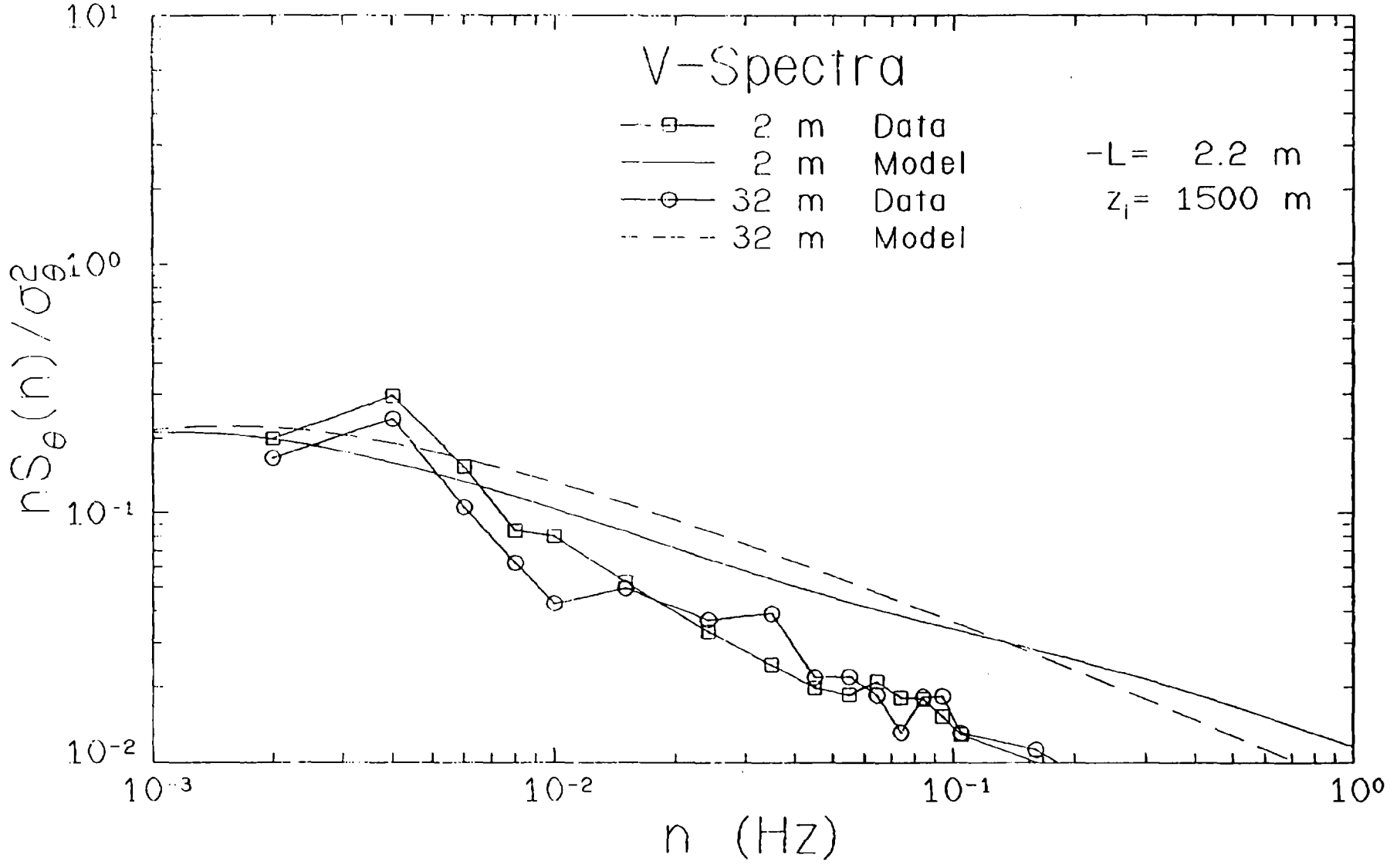

Figure 4.22. Normalized wind direction spectra and model V-spectra for unstable conditions.

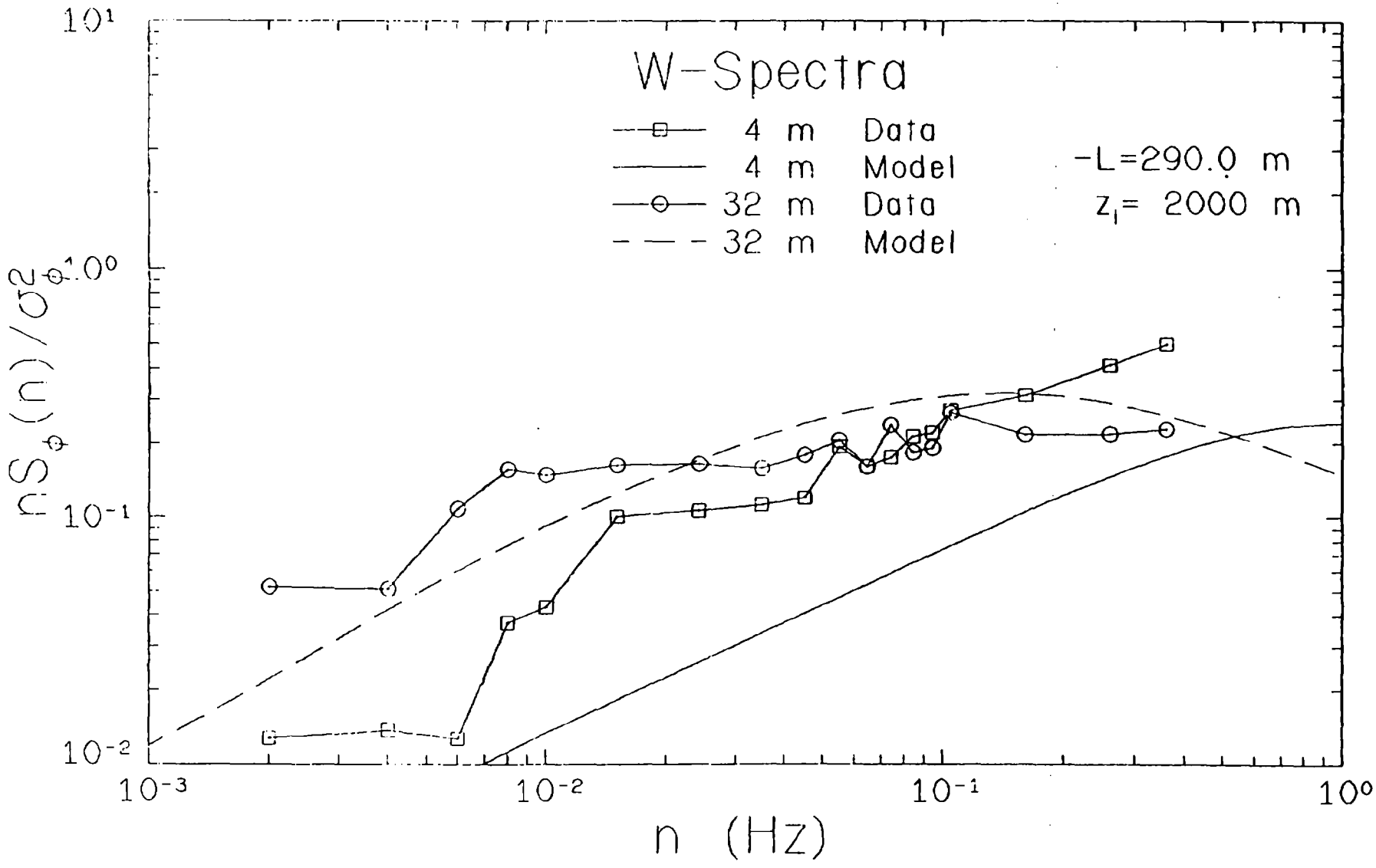

Figure 4.23. Normalized wind inclination spectra and model W-spectra for near-neutral conditions.

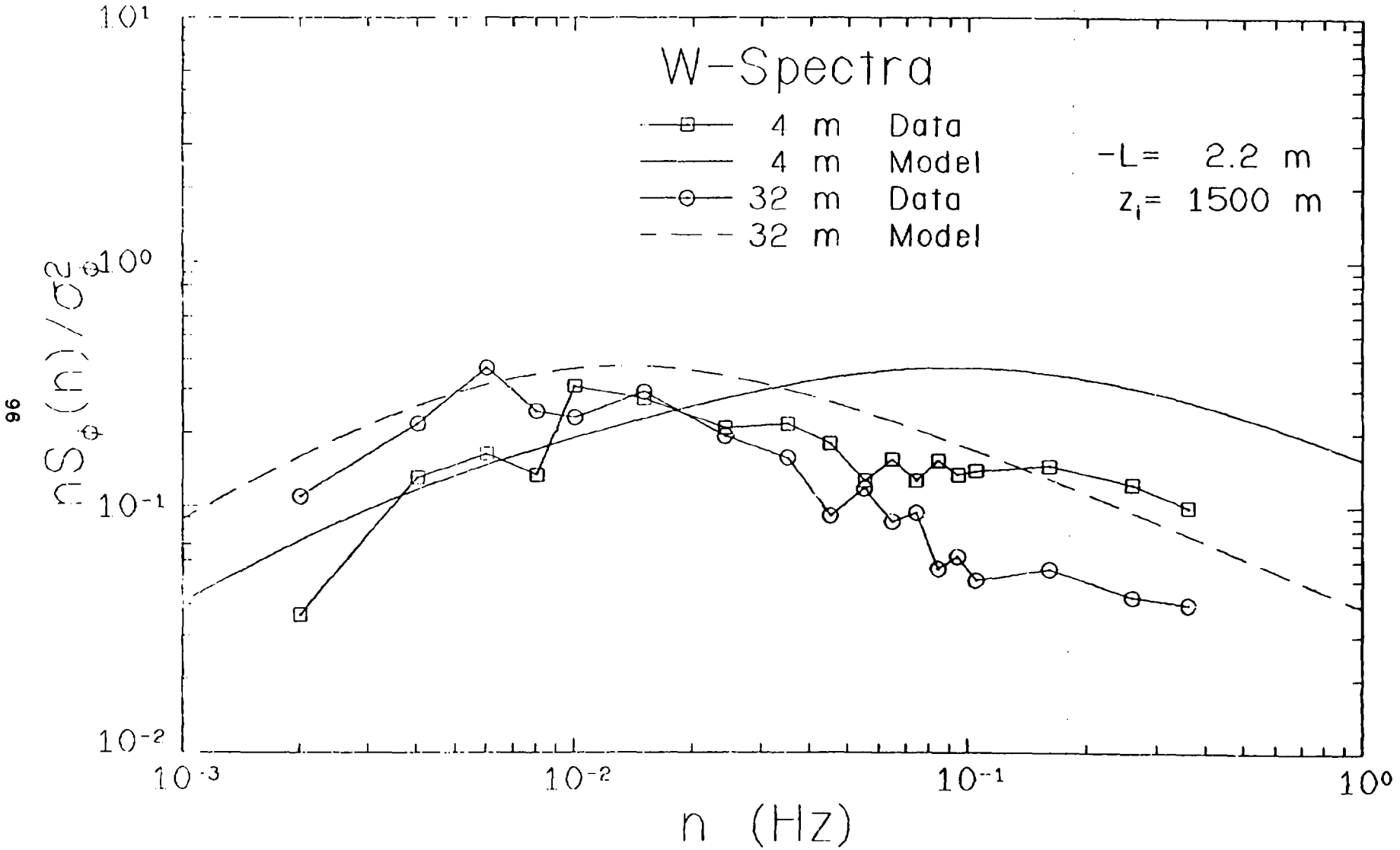

Figure 4.24. Normalized wind inclination spectra and model W-spectra for unstable conditions.

As previously discussed, the auto-correlations were computed as the inverse FFT of the spectra. The Højstrup model does not directly predict auto-correlations and so no direct comparisons between computed and model correlations were performed.

Comparisons of the measured correlations and those derived under similar atmospheric conditions over similar terrain have been undertaken. Teunissen (1980) measured the three components of velocity at a height of 11 m from five towers in a neutrally stable atmosphere over "typical rural terrain" with a roughness length of "a few centimeters." His results appear very similar to those presented in Figures 4.25 through 4.27 which represent, respectively, the auto-correlations of the wind speed, direction and inclination under nearly neutral conditions. The correlations appear to be exponential in shape with some oscillation about zero. Moore, *et al.* (1985) computed auto-correlations from vertical velocity data gathered for the Electric Power Research Institute's Plume Model Validation study at Kincaid, Illinois. They reported that under unstable conditions the spectrum "exhibits a generally exponential shape with a tail which oscillates near zero." This also agrees with our results. Figures 4.28 through 4.30 present the auto-correlations for unstable conditions. They appear to be very similar in shape to those of the neutral case with the exception that the integral time scale is greater.

4.2.4 Integral Scales

Integral time scales may be computed from the value of the integral of the auto-correlation or from the value of the power spectrum at zero frequency. However, since much of the energy in atmospheric flows is at low frequencies, both of these values are extremely sensitive to the manner in which the high frequency and low frequency components are separated (i.e., the duration of the sampling period and the period over which the mean is computed). As a result, the integral scales may be greatly in error. In fact, Panofsky and Dutton (1984) recommend against using integral scales for this reason.

Hanna (1981) has suggested two alternative methods of determining the integral scales. Both of these methods require the assumption that the auto-correlation is an exponential function, $R(t) = \sigma_v^2 \exp(-t/\tau_L)$ where τ_L is the Lagrangian integral time scale. Neumann (1978) and Tennekes (1979) argue that this is a valid and reasonable assumption. They show that expressions for the mean square lateral dispersion of infinitesimal particles from a point source in stationary, homogeneous turbulence obtained assuming an exponential form for the auto-correlation are consistent both with theoretical and experimental results.

The power spectrum corresponding to the exponential correlation is of the form $1/(1+\omega^2\tau^2)$, where ω is angular frequency $2\pi n$; this form exhibits the correct inertial subrange behavior ($\propto \omega^{-2}$ for $\omega\tau \ll 1$). At small time intervals, the exponential correlation can be approximated by a linear function of the time difference. This behavior is in agreement with the expression for the Lagrangian structure function $D(t) = 2\sigma_v^2 - R(t)$ in the inertial subrange. One disadvantage of the exponential correlation function is that its slope is infinite at the origin, which limits its application to large Reynolds number flows such as are found in the atmosphere.

The first method is based on the relationship between the frequency at which the maximum of the frequency-weighted spectrum, nS(n) occurs and the integral scale, namely $\tau = 1/(2\pi n_{max})$. The derivation of this relationship is presented in Appendix C. The second method is to find t for which $R(t) = R(0)e^{-1}$ and use this value for τ. Hanna found agreement (±10%) between these methods for both Eulerian data collected from a tower and Lagrangian data collected from pilot balloons and tetroons. Teunissen (1980) and Moore, Liu and Shi (1985) have also computed integral scales using these methods in addition to a straightforward integration of the auto-correlation. Their results are similar to Hanna's. In the present study, integral scales have been computed by integrating the auto-correlation and by both of the methods just described.

In Figures 4.31-4.36 the results of these different methods are presented for tests T0005 and T0010 which represent the most nearly neutral and most unstable cases. For the purpose of comparison, the near-neutral and unstable limiting forms of the Højstrup model predictions for the integral times are also plotted. The results are in fair qualitative agreement with the model predictions, although the comparison is sensitive to the value chosen for z_i. The near-neutral case ($-z_i/L=0$) shows the correct trend of increasing

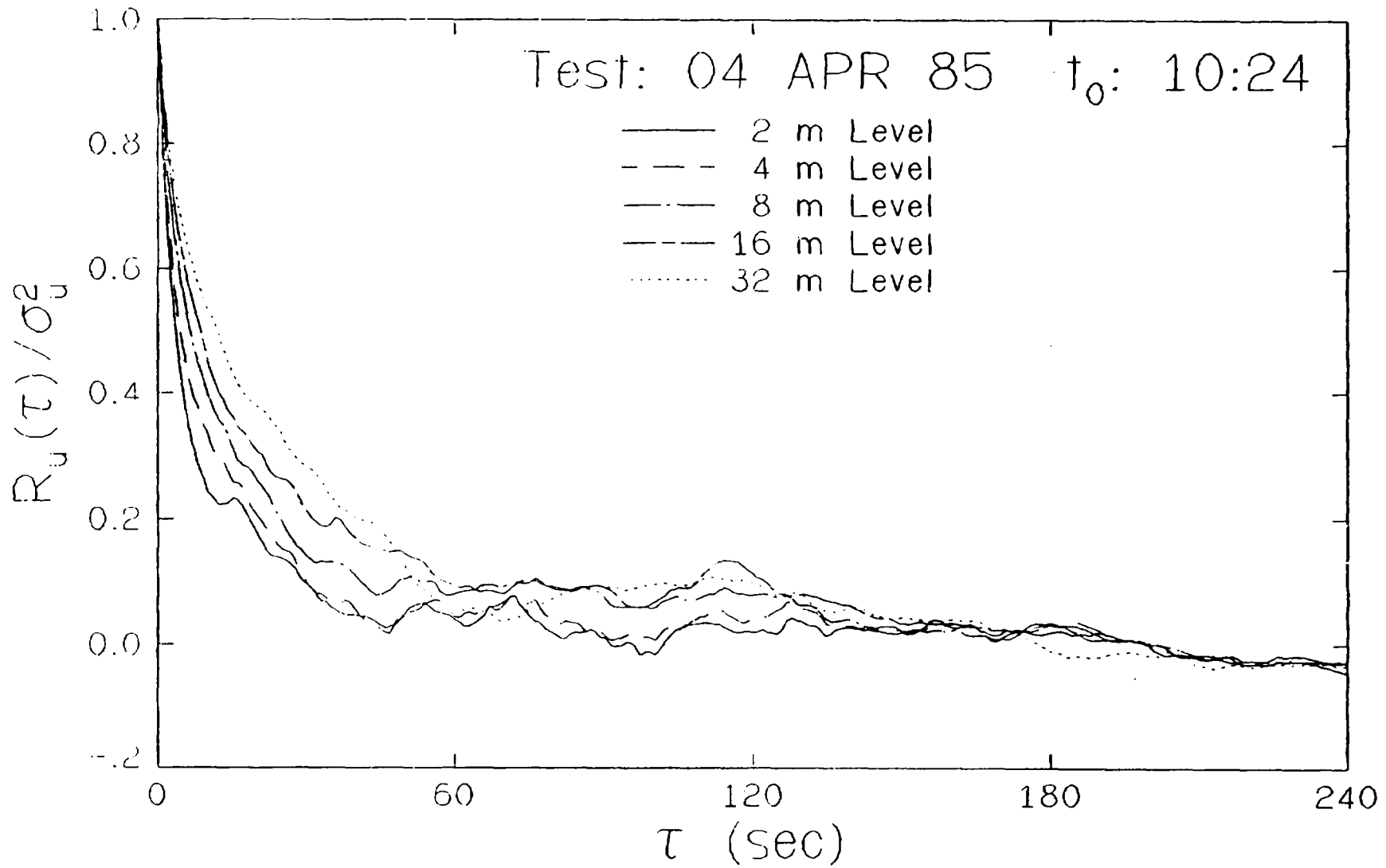

Figure 4.25. Normalized wind speed auto-correlations for near-neutral conditions.

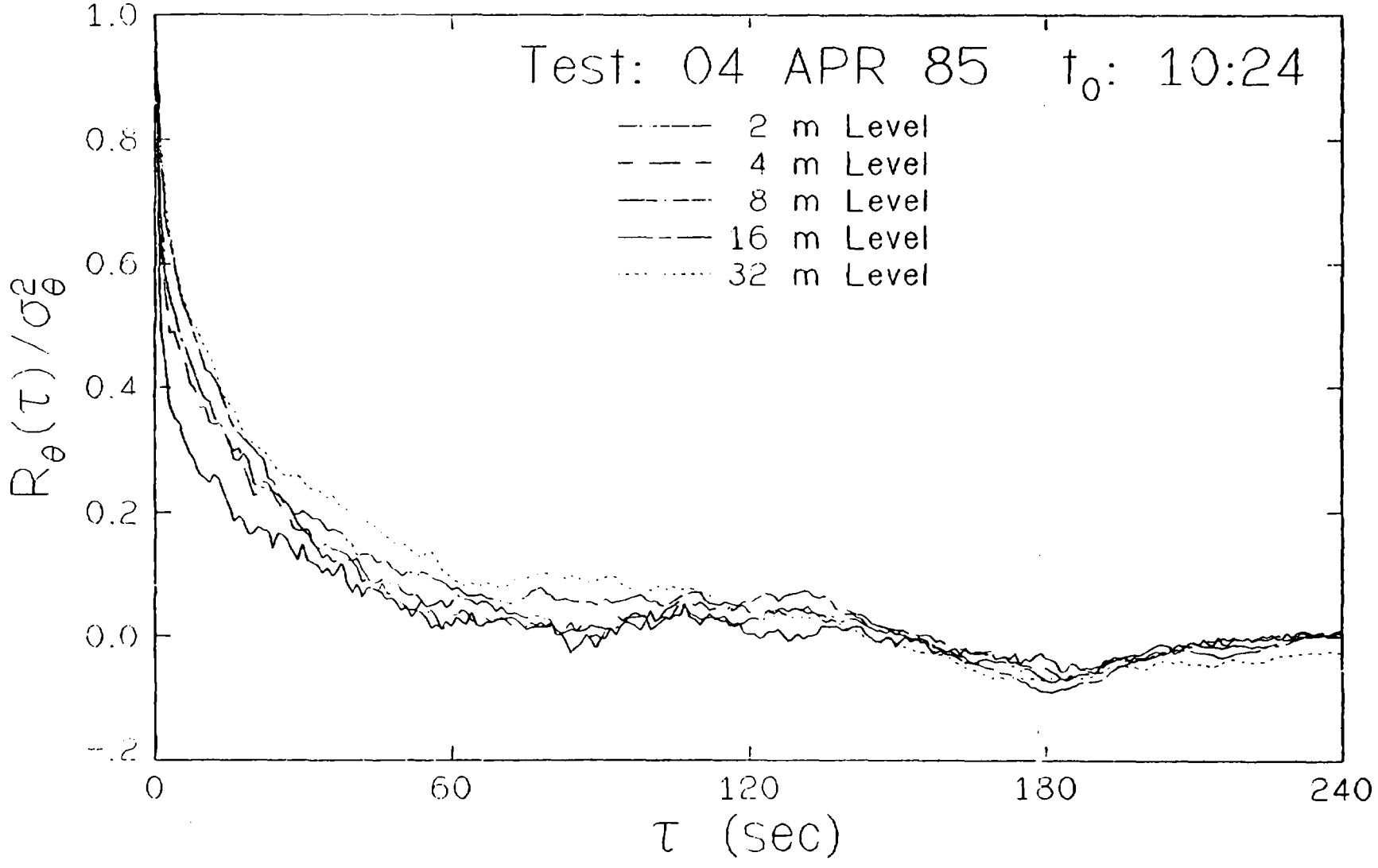

Figure 4.26. Normalized auto-correlations for the horizontal wind angle under near-neutral conditions.

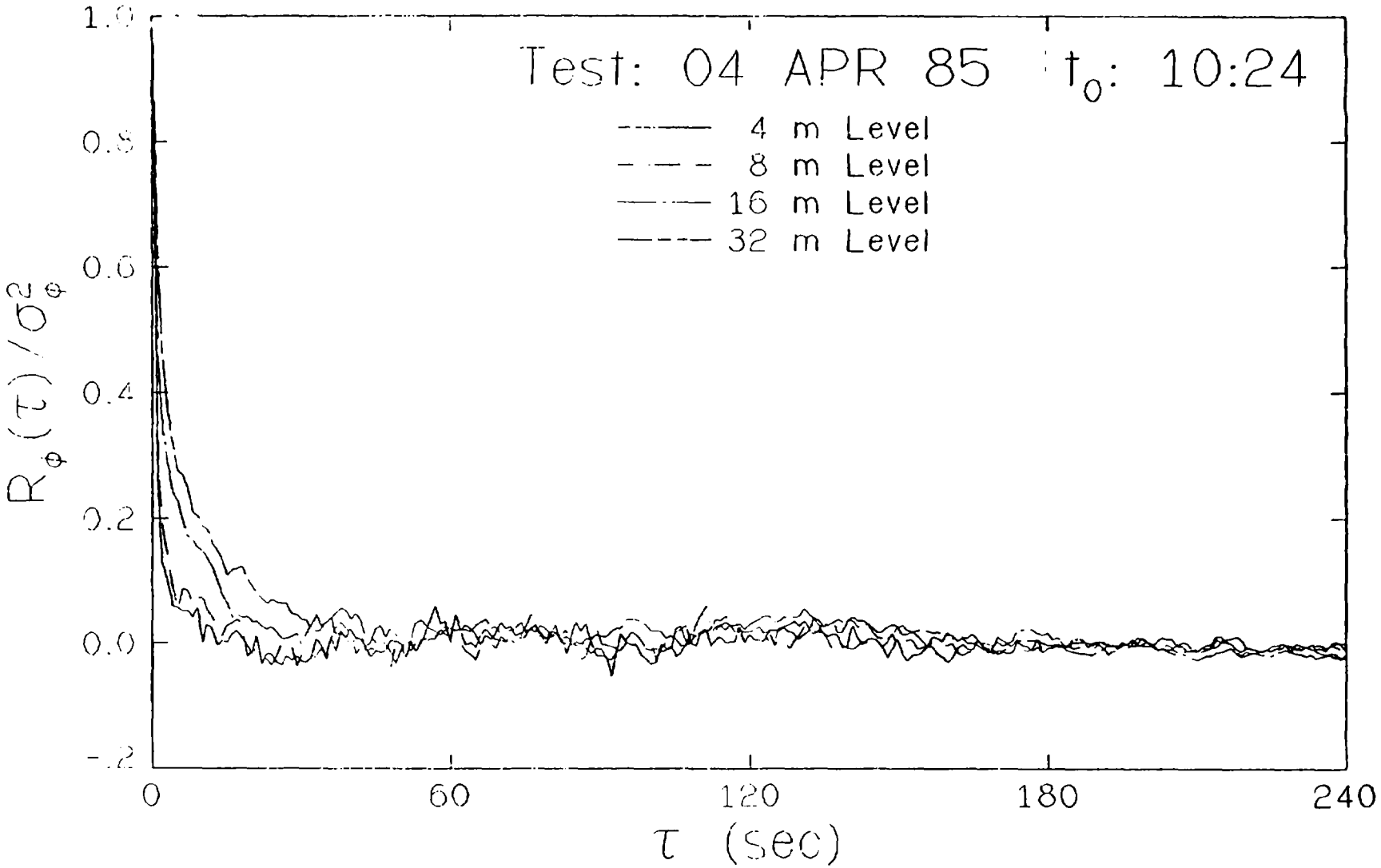

Figure 4.27. Normalized auto-correlations for the vertical wind angle under near-neutral conditions.

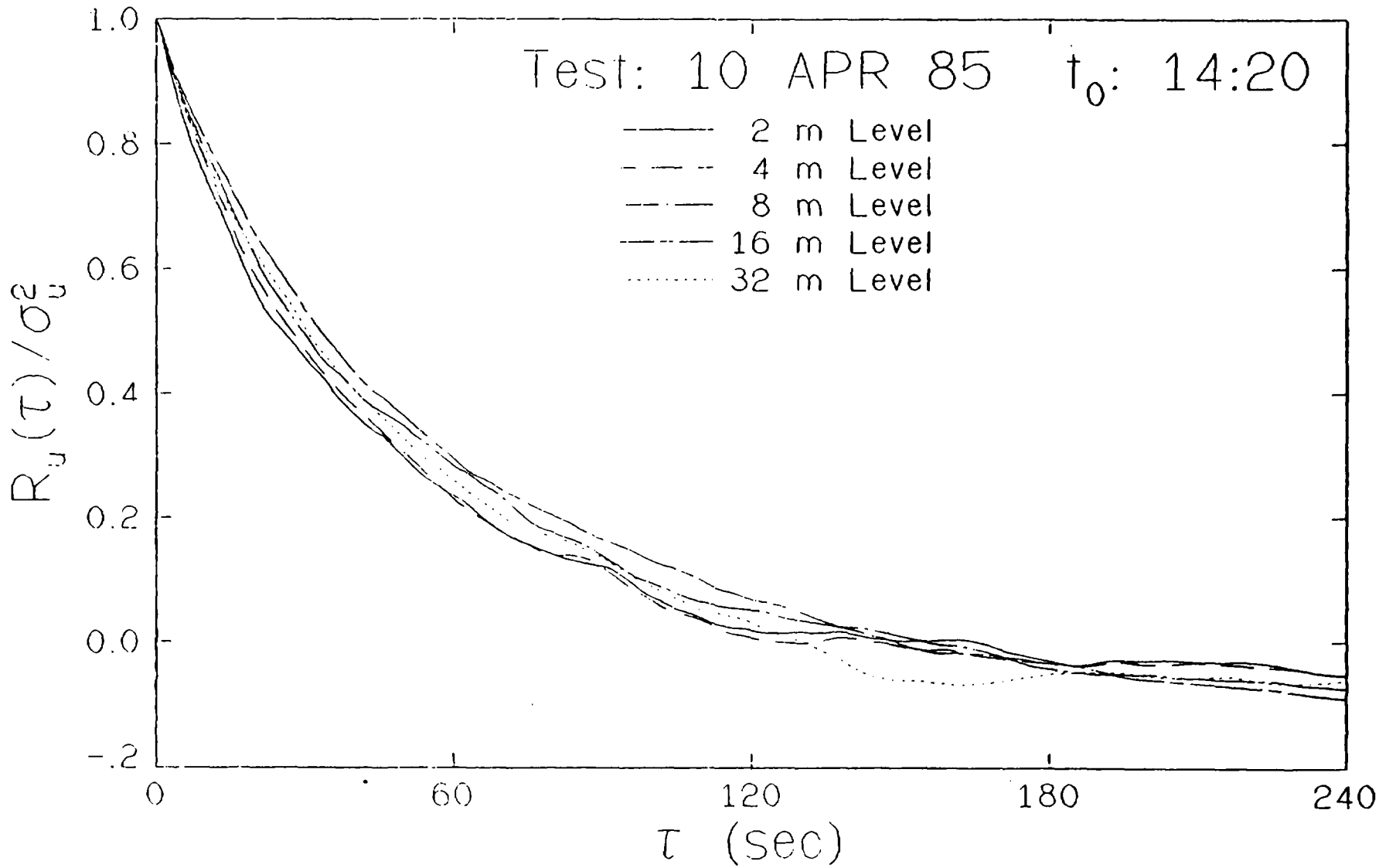

Figure 4.28. Normalized wind speed auto-correlations for unstable conditions.

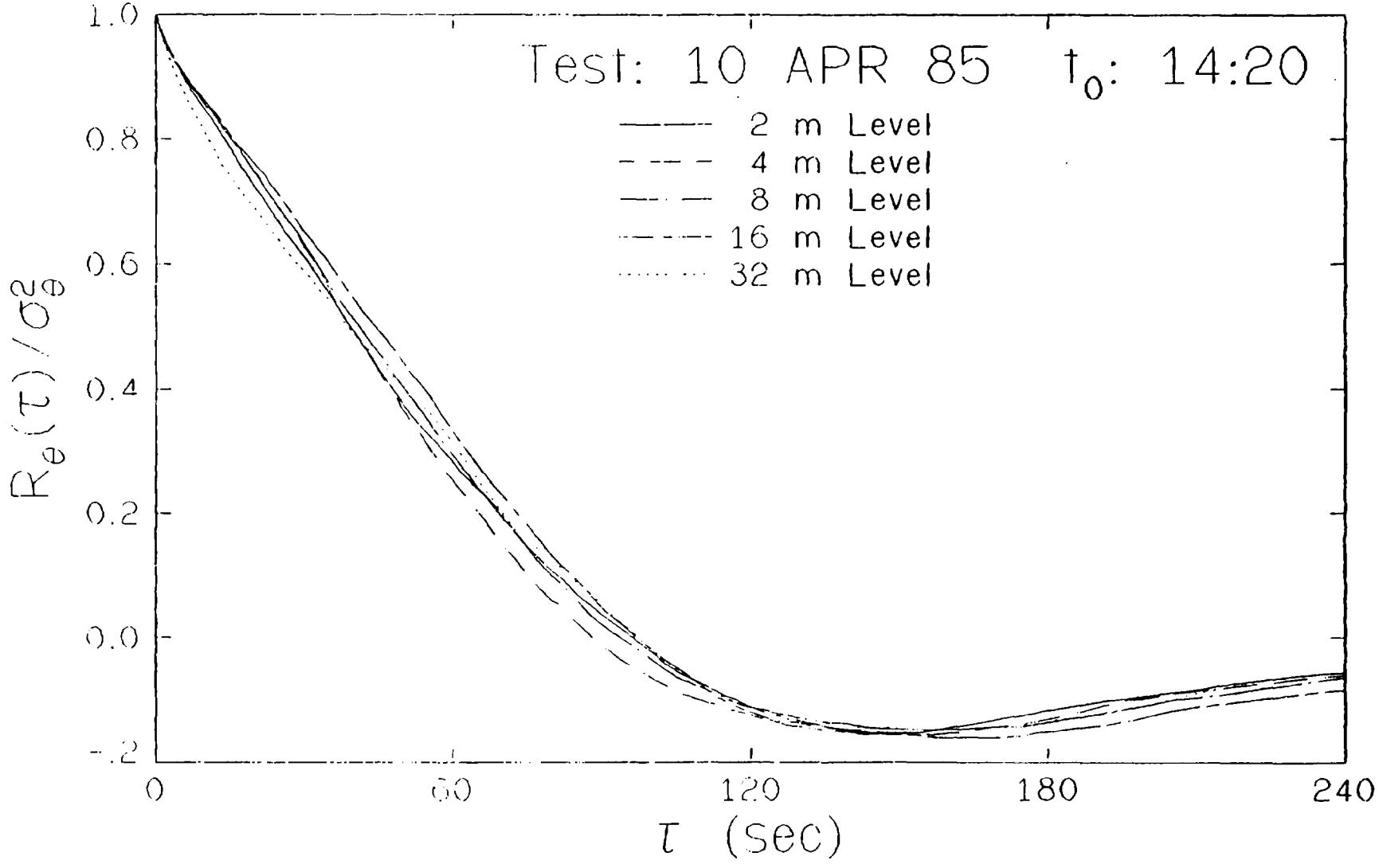

Figure 4.29. Normalized auto-correlations for the horizontal wind angle under unstable conditions.

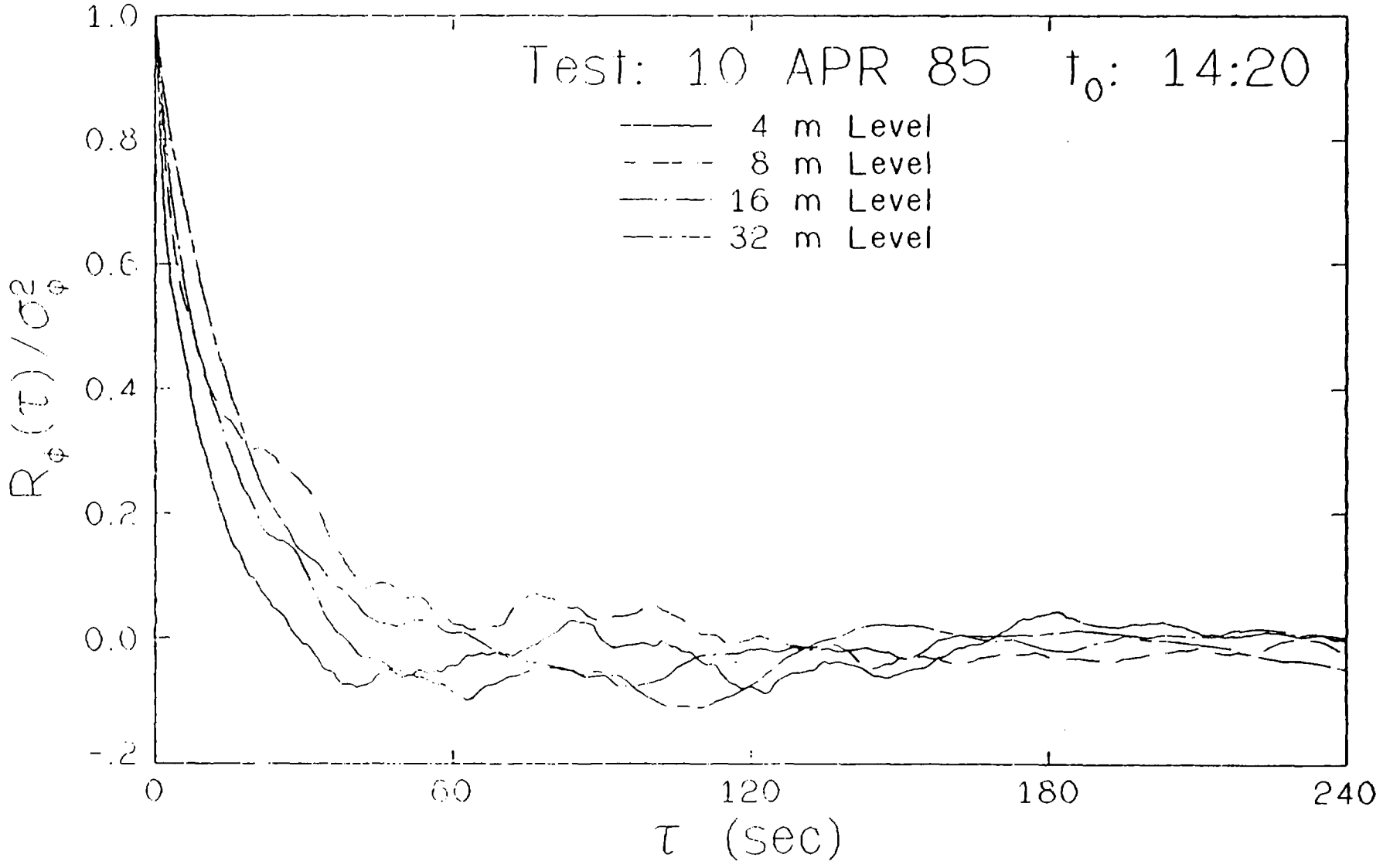

Figure 4.30. Normalized auto-correlations for the vertical wind angle under unstable conditions.

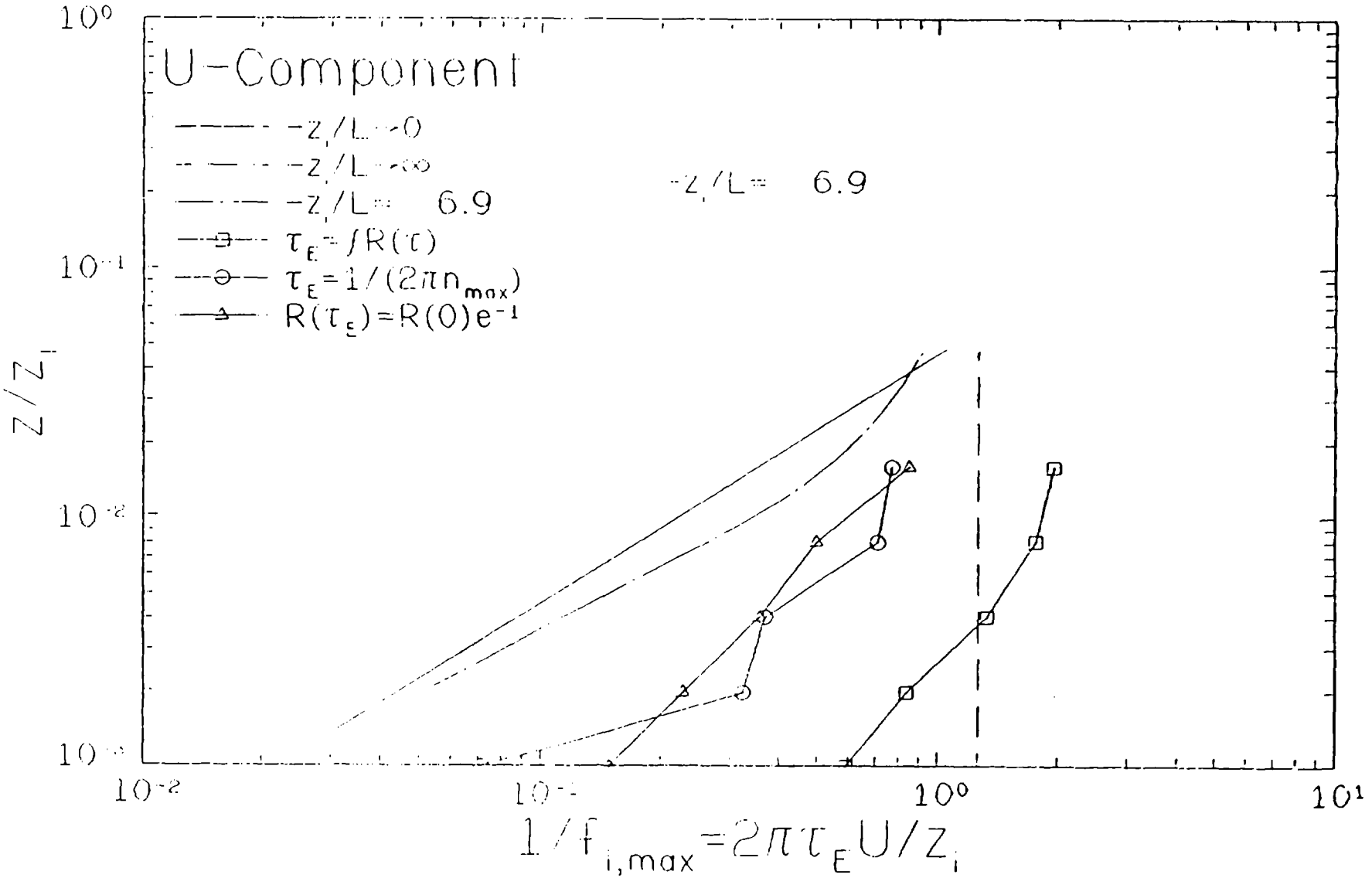

Figure 4.31. Integral scales of along-wind velocity for near-neutral conditions computed via three different methods compared with Højstrup model predictions.

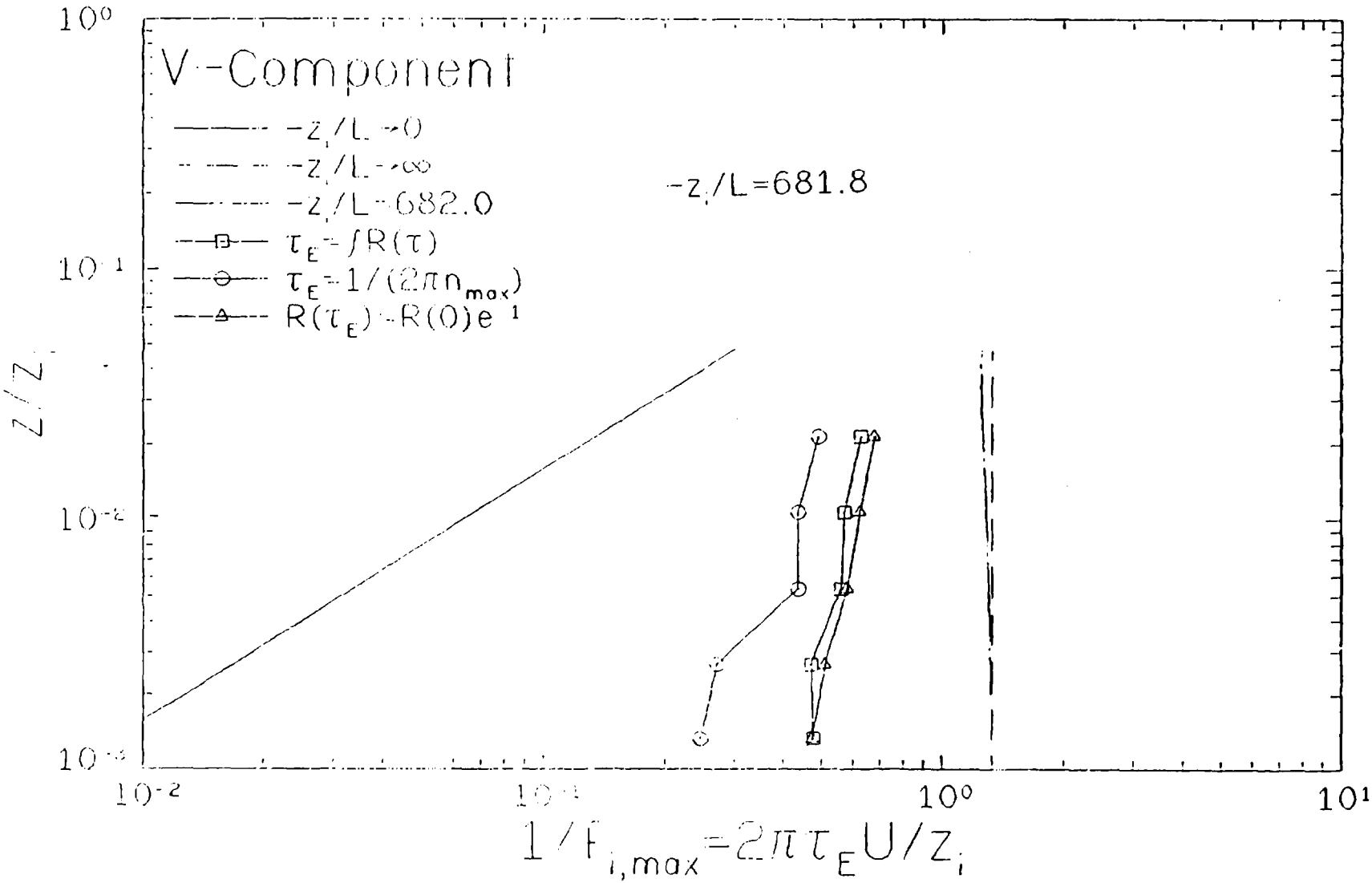

Figure 4.32. Integral scales of horizontal wind angle for near-neutral conditions computed via three different methods compared with Højstrup model predictions.

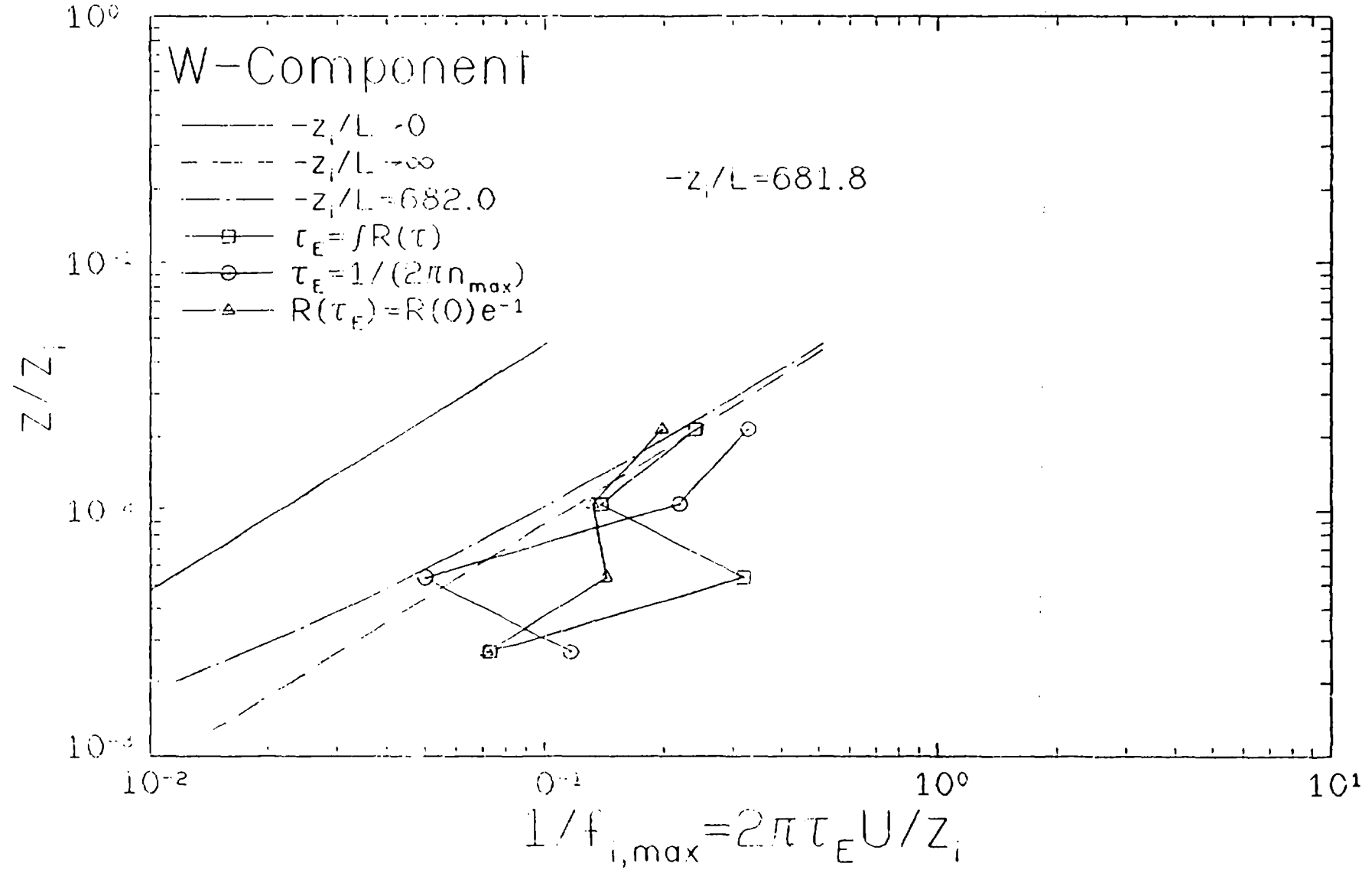

Figure 4.33. Integral scales of vertical wind angle for near-neutral conditions computed via three different methods compared with Højstrup model predictions.

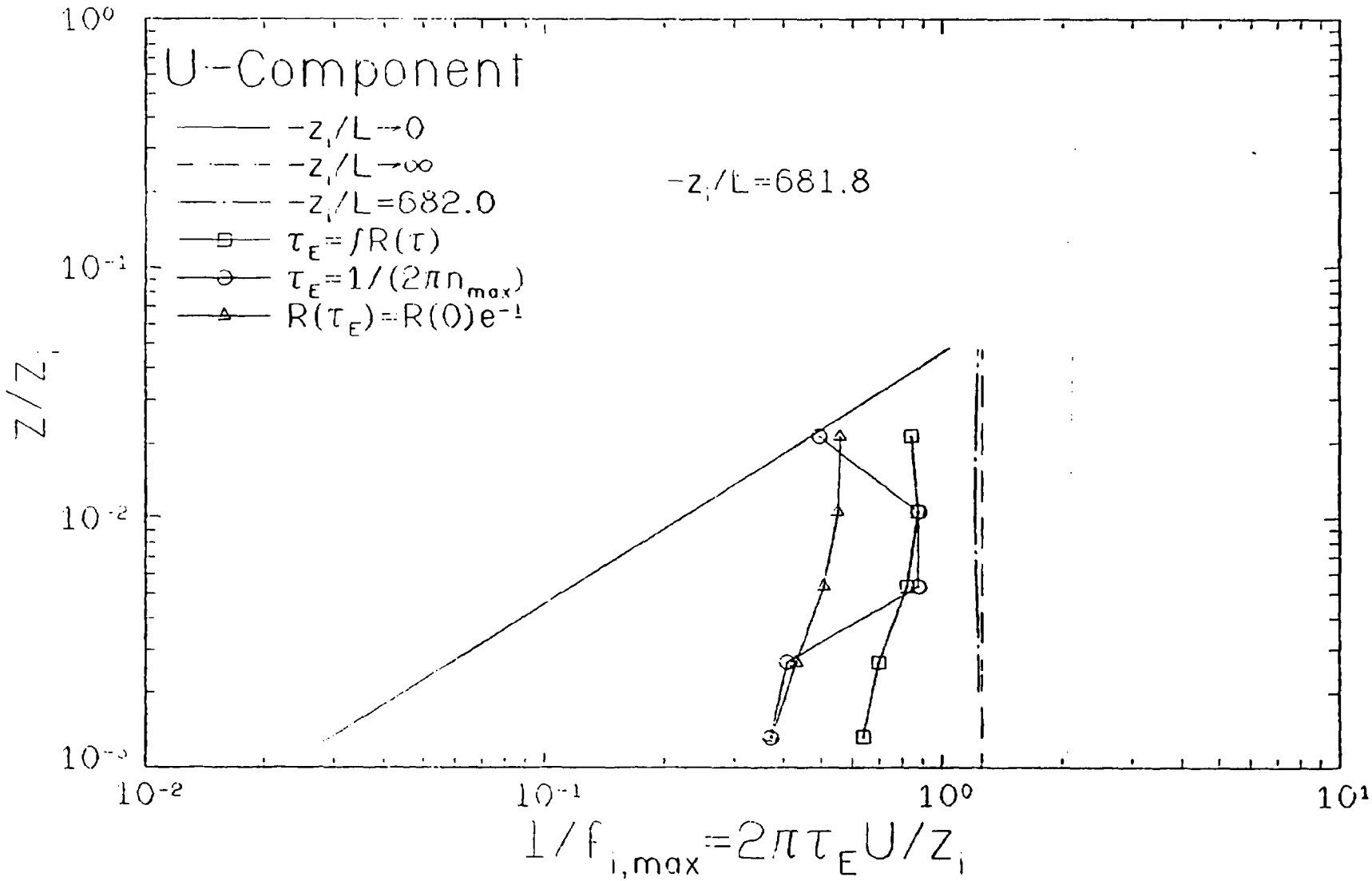

Figure 4.34. Integral scales of along-wind velocity for unstable conditions computed via three different methods compared with Højstrup model predictions.

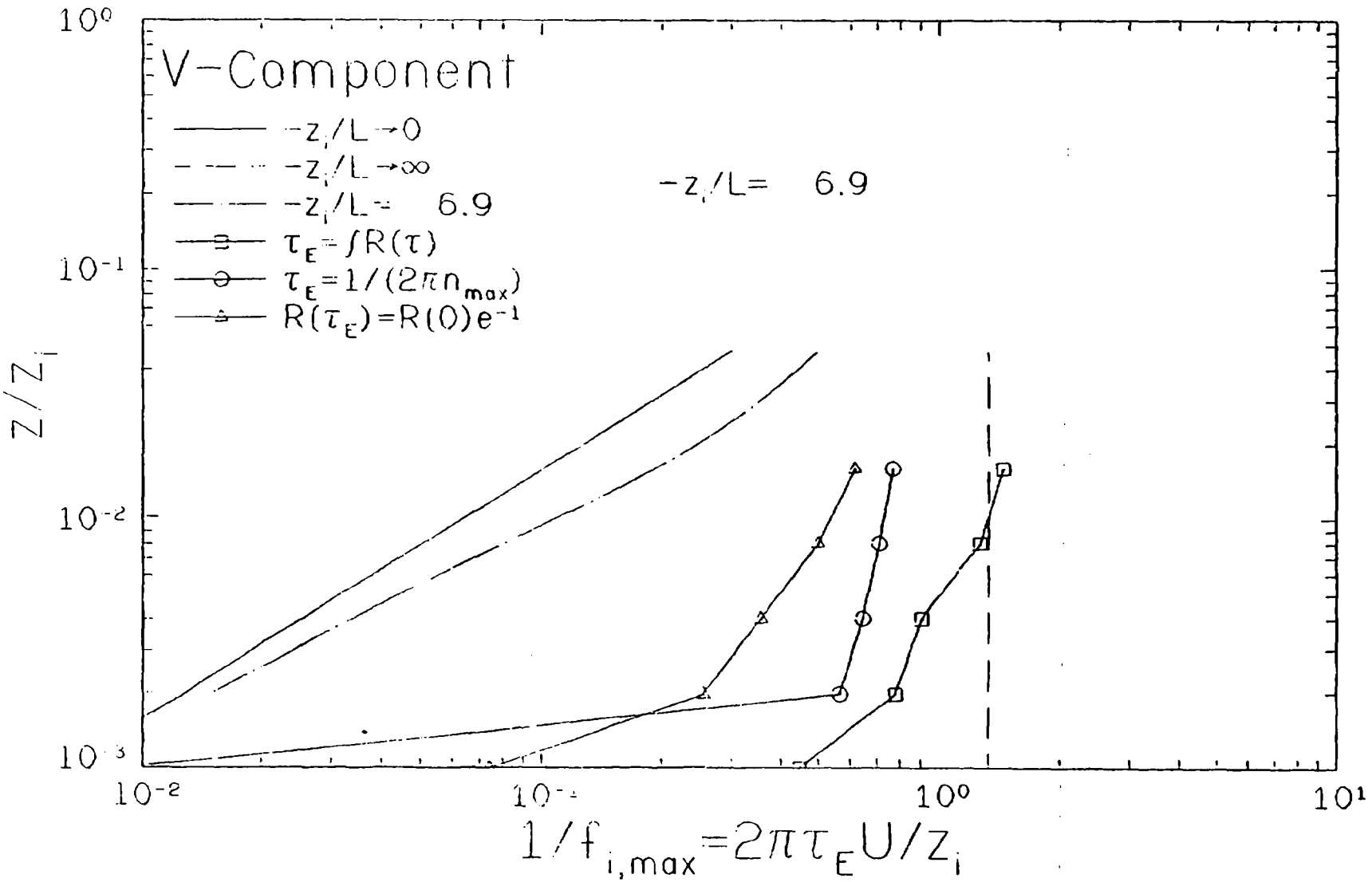

Figure 4.35. Integral scales of horizontal wind angle for unstable conditions computed via three different methods compared with Højstrup model predictions.

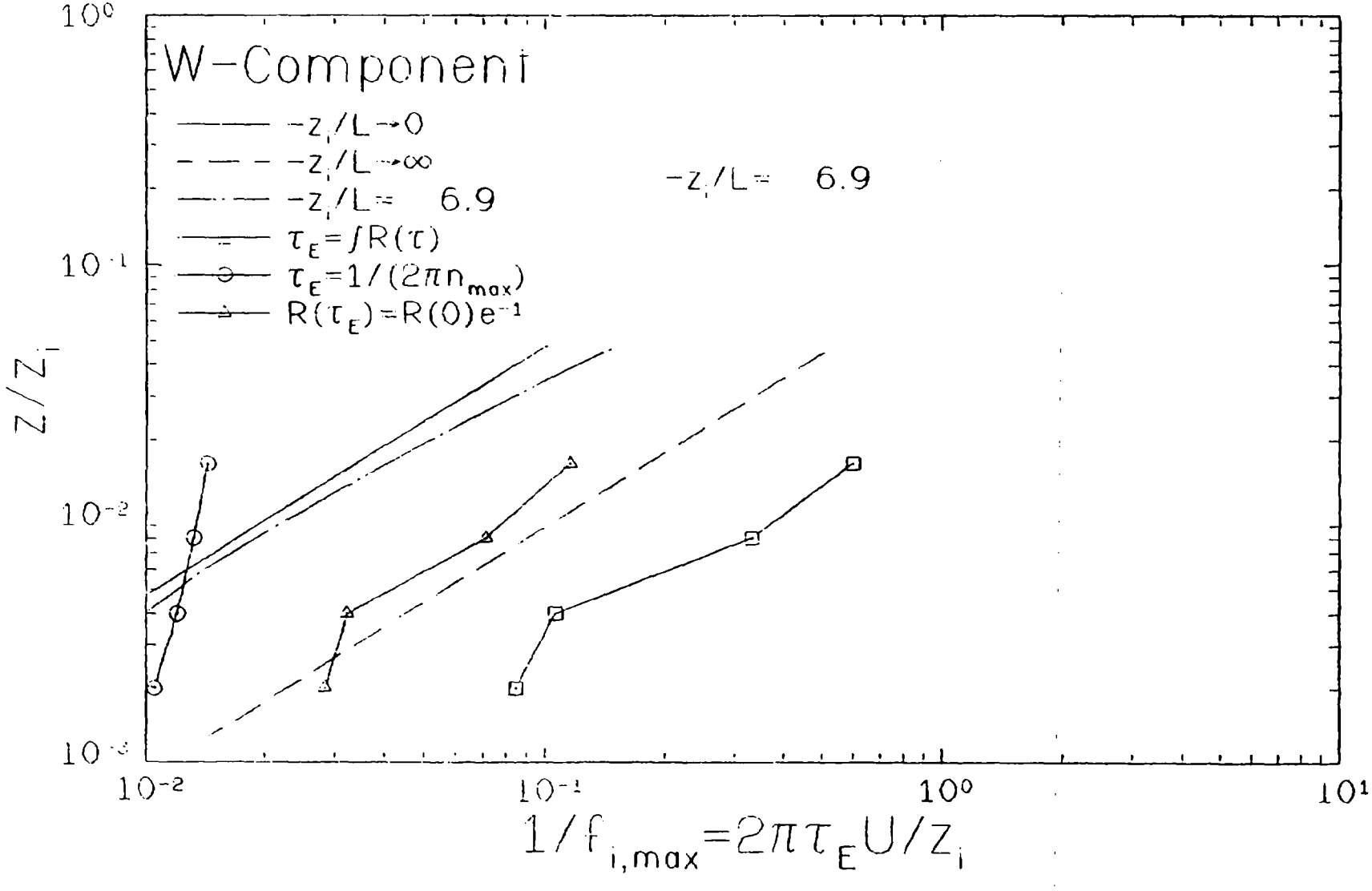

Figure 4.36. Integral scales of vertical wind angle for unstable conditions computed via three different methods compared with Højstrup model predictions.

integral time with height while clearly the quantitative agreement is only fair. Integral scales for an unstable case ($-z_i/L = \infty$) similarly display the correct trend: a small increase with height; however quantitative agreement is again only fair. This is probably due in large part to the estimated value of the inversion height as well as to the large variability in the measured scales due to the substantial rms error in the estimates of the power spectra. The rms error in the estimate of the spectra results in auto-correlations with similar error. This means that integral scales computed by direct integration of the auto-correlation will be subject to large errors.

Accurately determining the frequency at which the peak of the spectrum occurs is also difficult. If the maximum is determined prior to frequency smoothing then the substantial rms error can lead to a false peak being selected. If, on the other hand, the maximum is identified after smoothing, then the resolution is degraded sufficiently to lead to an incorrect positioning of the peak. This is most serious when the peak is at low frequencies which is the case for the horizontal components and for the vertical component in unstable conditions.

The most successful method should be the one whereby τ_E is chosen as the time at which the correlation falls to e^{-1} of its initial value. This is due to the fact that the small lag times correspond to high frequencies. The higher frequencies benefit most from frequency smoothing and are less subject to the effects of non-stationarity. This is borne out by the figures. Table 4.4 presents a comparison of integral length scales from the present study with those reported by Teunissen. The length scales were computed from time scales by using Taylor's frozen field hypothesis.

Table 4.4 Average Integral Length Scales, m (after Teunissen)

Method	Component	Present Results z_o=2 cm	Teunissen (1980) z_o=3 cm	Flay (1978) z_o=3 cm
Direct	U	240	130	144
Integration	V	279	52	66
of R(t)	W	30	18	19
Location	U	140	62	83
of Spectral	V	218	11	15
Maximum	W	4	5	6
Exponential	U	97	124	97
Decay of	V	146	39	51
R(t)	W	16	11	19

Teunissen's data indicate that direct integration of the auto-correlation produces the largest estimate of the integral scale. His results further show that fitting the data to a spectral model in order to determine the frequency at which the peak occurs yields the smallest value for the integral scale. Our results indicate that indeed the largest estimate is produced by direct integration. We did not fit the computed power spectrum to a model, but rather used the frequency at which the data spectrum reached a maximum to estimate the integral scale. The relatively poor resolution of our spectral estimate at low frequencies resulted in overly large estimates of the integral scale in the horizontal directions. Integral scales determined as the point at which the auto-correlation fell to e^{-1} of its initial value gave results which agreed reasonably well with Teunissen's in the along-wind and vertical directions. For all three methods, the cross-wind estimate is greater than the along-wind estimate which is in disagreement with Teunissen. This bears out Panofsky and Dutton's admonition concerning the extreme difficulty of accurately determining integral scales.

5.0 SUMMARY AND CONCLUSIONS

This section summarizes the results of field studies of the dispersion of military smokes conducted at Dugway Proving Ground in March and April, 1985. In this study, one of two candidate M3A3E3 military fog-oil smoke generators was operated for a period of roughly an hour and the resulting plume measured at downwind distances of 25 to 800 m from the source. A total of eleven runs were made using both generators although only the last three were sufficiently successful to be useful for modeling purposes.

The plume was characterized in terms of the average concentration over the period of operation, the particle size distribution of the smoke, the rate of deposition of fog-oil smoke on horizontal and vertical surfaces exposed to the smoke and the chemical composition of the smoke as determined by low resolution gas chromatography. Average concentration was determined by collecting smoke material in an adsorbent-filled tube aspirated by a battery-powered unit at 1 - 2 liters per minute (Lpm). The collected mass was subsequently determined by thermally desorbing the sample and analyzing the vapor by low resolution gas chromatography. The time-averaged concentration was then calculated as the total mass collected divided by the product of the release time and the measured aspiration rate. The particle size distribution was measured using seven-stage cascade impactors of the Mercer design with the mass collected on each stage also determined by gas chromatography. Deposition was measured using dry, chemically inert glass-fiber filter papers as surrogate surface collectors. Both horizontal and vertical orientations of the deposition surfaces were investigated.

Source characteristics were documented in terms of the mass rate of fog-oil smoke release, the exit temperature of the generator exhaust, the exit velocity of the generator exhaust and the chemical composition of the raw oil and of the fog-oil smoke just after formation.

Meteorological data were acquired using two 32-m instrument towers with sensors positioned at the 2, 4, 8, 16 and 32-m levels. Wind speed, horizontal wind angle and temperature were measured at all levels and vertical wind angle was measured at the four highest levels. The resulting mean vertical wind speed and temperature profiles were analyzed to obtain Monin-Obukhov length and friction velocity. The time-dependent data were also analyzed to obtain power spectra and integral time scales.

Detailed presentations and discussions of the source, meteorological and sampling data are given in the preceding sections of this report. The major findings and results are summarized below.

Some difficulty with the operation of the prototype M3A3E3 fog-oil smoke generators was encountered. The rubber air hoses used on the generator failed on several occasions due to embrittlement and melting caused by their close proximity to the hot outer shell of the pulsed jet engine. Also, the gasoline engine used on the M3A3E3 operated poorly at the higher altitude of Dugway Proving Ground. Other difficulties encountered in operating the generators include failure of the seals on the fog oil pump and on the air compressor.

Source data were acquired for nine of the eleven tests. Only average values are available for the last two tests because the cassette recorder used to acquire the time-dependent source data failed due to the excessive dust and vibration associated with field operation at Dugway Proving Ground. The source data reveal that the release rate varies over a wide range even for ostensibly similar operating conditions. The exit temperature was found to follow the expected pattern of increasing as the flow rate of fog oil decreased and decreasing as the flow rate of fog oil increased. Thus, the exit temperature exhibited changes directly opposite to those shown by the release rate, varying from about 300 °C to about 550 °C. In one case, the exit temperature was observed to increase rapidly even though the release rate remained constant. This behavior was attributed to the failure of an air line and thus a sharp drop in air flow rate through the pulsed jet engine. The release rate varied from 18 to 43 g/s over the full set of eleven trials with an average value of about 30 g/s. In no case did the release rate reach the value of 45 g/s stated in the specifications for the generator.

The exit velocity of the generators varied only slightly over the course of the tests with a mean value of about 78 m/s. Also, samples of the raw oil and of the fog-oil smoke taken just after formation showed identical chemical compositions using low resolution gas chromatography. The source data provide a valuable insight into the operation of a fog oil generator, illustrating firstly that mass release rate can vary significantly with time and secondly that nominal release rates are poor estimates of actual release rates.

The meteorological data reveal that both the "mean" and "turbulent" components of the wind and temperature fields change over the course of an hour test period, especially in light of the transitional conditions characteristic of most of the tests. Using ten-minute averaging times to treat the non-stationarity of the atmospheric conditions gave vertical profiles of wind speed and potential temperature that are well represented by the forms of Businger et al., Dyer and Hicks, and Hansen. The values of friction velocity and Monin-Obukhov length computed by fitting the profile data to these forms are consistent with their Pasquill stability classification. The meteorological data have also been shown to be in close agreement with an accepted model of atmospheric turbulence. Since the model is based on the data from the Minnesota and Kansas boundary layer experiments, carried out for flat terrain, the data from the present study are thus shown indirectly to agree with those experiments. This fact, coupled with the overall internal consistency of the data themselves, provides confidence in the accuracy of the measurements.

The measurements made of the smoke plume provide an internally consistent picture of plume behavior, although several significant operational difficulties were encountered. As a result, useful data were acquired only during the last three tests. Three factors, in combination, led to this suboptimal performance. First, our original sampling network provided insufficient spatial resolution. This was remedied by changing the layout of the sampling network to a denser, more compact design. However, eight of our eleven tests were conducted before this change was identified and implemented. All three tests carried out on the "high resolution network" were successful.

Secondly, the performance and reliability of the aspiration units supplied by Dugway (B/C samplers) was less than we had expected. The low flow rate of the B/C sampler (1.5 liters per minute) both limited the amount of smoke material collected and raised the issue of aerodynamic sampler efficiency (isokinesis).

Finally, contamination of the adsorbent-filled sampling tubes caused their detection threshold to be much higher than anticipated. This severely limited the range of our concentration measurements to about 200 m down wind of the release point. Beyond 200 m, the fog oil concentration was below the detection threshold and thus on the same order as the sampler noise level.

Although the adsorbent-filled sampler performed well in laboratory tests, the combination of high detection threshold levels and low aspiration rates in the field yielded fewer successful tests than was hoped. On the other hand, we fully expected to uncover problems in a full scale field study which could not be foreseen from the isolated evaluation of the individual components in the laboratory. Considering the results of the field tests in aggregate, the sampler data do provide valuable information about the smoke plume.

The concentration data collected during this study are shown to be in good qualitative and quantitative agreement with a simple gaussian plume model as well as with data collected during the Project Prairie Grass and Project CONDORS field studies of atmospheric dispersion. Our data indicate that fog-oil smoke deposition is negligible, at least at distances greater than 25 m from the smoke generator. Particle size measurements carried out during the study show the fog-oil smoke to have a log-normal distribution with a mass mean diameter of 1.0 microns and a mass median diameter of 0.74 microns. These findings are in agreement with particle size measurements carried out in laboratory tests of fog-oil smoke by the IIT Research Institute.

No significant vapor fraction in excess of the background levels was detected; this finding was confirmed in laboratory tests. Thus fog-oil smoke is shown to exist 99% in the droplet phase. This result

contrasts with studies of diesel oil which indicate that a significant fraction of that smoke exists in vapor form. This difference perhaps explains, in part, why fog oil is widely regarded as a far superior obscurant.

Since our tests showed that the fog-oil smoke exists almost exclusively in the droplet phase, or at least, that the level of vapor phase is below the general background level of similar hydrocarbon vapors even in areas of high smoke concentration, this detection threshold can be lowered by using a filter sampler which passes the vapor phase and collects only droplets and particulates larger than say 0.1 microns. Had we chosen to ignore the vapor phase and instead sample only the droplet phase, the threshold of detection would have been much lower, and it is probable that many more statistically significant values would have been obtained.

Finally, we observed that the composition of the fog-oil smoke appeared to be the same as that of the raw oil, as determined by low-resolution gas chromatography.

RECOMMENDATIONS

Based on the results of this initial field test of the dispersion of fog-oil smoke in flat terrain, we make the following recommendations for improving the methodology and procedures of future field studies.

(1) Future tests should focus on near-dawn (stable atmospheric) conditions during which the smoke plume remains close to the ground and extends to far downwind distances. Transitional and unstable meteorological conditions not only present major difficulties to execution of the field tests, but also produce uncharacteristically low exposure levels.

(2) A vertical array of samplers extending to a height of about 8 m should be used in place of the single sampler at 1.5 m. This modification will provide additional information on the vertical distribution of the smoke cloud which is extremely valuable for model testing and improvement.

(3) The maximum possible aspiration rate should be increased to at least 20 liters per minute. This will increase the amount of material collected thus improving the signal-to-noise ratio of the sampling method and extending the distance to which measurements are possible. An increased flow rate can be accomplished using an air-pump/generator combination.

(4) Filter samplers which collect only the droplet phase of the smoke should be used for fog oil; the observation that fog-oil smoke exists almost exclusively in the droplet phase should continue to be studied at selected locations using filter samplers in combination with adsorbent-filled or liquid-filled collectors. The combined effect of items 1 - 4 should greatly increase the number of statistically significant dosage levels measured and allow many more data sets to be obtained.

(5) The findings of the current study concerning changes in the composition of the fog oil material as it passes through the generator and as it is dispersed in the atmosphere should be tested under different atmospheric conditions.

(6) The effect of multiple generators should be studied in any future tests involving unstable atmospheric conditions. A large-scale smoke screen can dramatically reduce ground heating, thereby changing the local meteorological conditions and, in turn, the smoke plume itself.

(7) A real-time detection method for the smoke should be added to provide time-dependent data to supplement the dosage levels measured using the aspirated samplers. This information not only is valuable for model testing and improvement but also documents the ratio of the maximum exposure to the average exposure, a parameter of interest in toxicology studies. Developing a successful real-time detection method is a significant undertaking and will involve an effort similar to that required to develop a technique for measuring mean concentrations.

(8) Use of the perfluorocarbon tracers should be discontinued and development of methods for their collection and analysis should be abandoned. Successful implementation of the tracer scheme would require additional, parallel sampling and analysis equipment and essentially double the logistical and operational effort involved in carrying out a test. This effort would be more valuably directed toward the development of a real-time smoke detection method, as outlined in item (7) above.

LITERATURE CITED

Barad, Morton L., 1958: "Project Prairie Grass, A Field Program in Diffusion," Geophysical Research Papers, No. 59, Vols. 1 and 2, AFCRC-TR-58-235 (I & II),US Air Force Cambridge Research Center, Bedford, MA.

Bendat, Julius S. and Allan G. Piersol, 1971: Random Data: Analysis and Measurement Procedures, (New York, John Wiley and Sons).

Biltoft, Christopher, 1985: "Notes on Atmospheric Stability, Turbulence and its Measurement," DPG-TR-85-204, US Army Dugway Proving Ground, Dugway, UT.

Boughton, B. A., 1983: "Turbulent Atmospheric Transport and Deposition of Particles with Evaporation and Settling," Ph.D. Thesis, University of Illinois at Urbana-Champaign, Urbana, IL.

Businger, J. A., Wyngaard, J. C., Izumi, I. and E. F. Bradley, 1971: "Flux-Profile Relationships in the Atmospheric Surface Layer," J. Atmos. Sci., **28**, 181-189.

Chatwin, P. C., and C. M. Allen, 1985: "A Note on Time Averages in Turbulence with Reference to Geophysical Applications," Tellus, **37B**, 46-49.

Clough, W. S., 1973: "Transport of Particles to Surfaces," Aerosol Sci., **4**, 227-234.

Dasch, J. M., 1982: "A Comparison of Surrogate Surfaces for Dry Deposition Collection," in Precipitation Scavenging, Dry Deposition, and Resuspension, Volume 2, H. R. Pruppacher, R. G. Semonin and W. G. N. Slinn, (eds.), pp. 883-911.

DeVaull, G. E., W. E. Dunn, J. C. Liljegren and A. J. Policastro, 1988: "Development and Evaluation of a Sampling and Analysis Method for Fog-Oil Smoke," AD _____, University of Illinois, Urbana, IL 84PP4822.

Dietz, R. N. and W. F. Dabberdt, 1983: "Gaseous Tracer Technology and Applications," BNL-33585, Brookhaven National Laboratory, Long Island, NY.

Draxler, R. R., 1976: "Determination of Atmospheric Diffusion Parameters," Atmos. Envir., **10**, 99-105.

Durham, M. D. and D. A. Lundgren, 1980: "Evaluation of Aerosol Aspiration Efficiency as a Function of Stokes Number, Velocity Ratio and Nozzle Angle," J. Aerosol Sci., **11**, 179-188.

Dyer, A. J., and B. B. Hicks, 1970: "Flux-Gradient Relationships in the Constant Flux Layer," Quart. J. Roy. Meteor. Soc., **93**, 501-508.

Ferber, G. J., K. Telegadas, J. L. Heffter, C. R. Dickson, R. N. Dietz and P. W. Krey, 1981: "Demonstration of a Long Range Tracer System Using Perfluorocarbons," NOAA Technical Memorandum ERL ARL-101, Air Resources Laboratories, Silver Spring, MD.

Ferber, G. J. and J. L. Heffter, 1983: "Cross Appalachian Tracer Experiments -- Revised Plan," NOAA Air Resources Laboratory, Rockville, MD.

Garland, J. A., 1982: "Dry Deposition of Small Particles to Grass in Field Conditions," in Precipitation Scavenging, Dry Deposition, and Resuspension, Volume 2, H. R. Pruppacher, R. G. Semonin and W. G. N. Slinn, (eds.), pp. 849-857.

Hanna, Steven R., 1981: "Lagrangian and Eulerian Time-Scale Relations in the Daytime Boundary Layer," J. Appl. Meteor., **29**, 242-249.

Hansen, Frank V., 1980: "Flux-Profile Relationships for Development of Standards of Comparison," ASL Internal Report, US Army Atmospheric Sciences Laboratory, White Sands Missile Range, NM.

Hicks, B. B., M. L. Wesely and J. L. Durham, 1980: "Critique of Methods to Measure Dry Deposition," EPA-600/9-80-050.

Hinds, William C., 1982: Aerosol Technology: Properties, Behavior and Measurement of Airborne Particles, (New York, John Wiley and Sons).

Højstrup, Jørgen, 1982: "Velocity Spectra in the Unstable Planetary Boundary Layer," J. Atmos. Sci., **39**, 2239-2248.

Jenkins, R. A. and R. W. Holmberg, 1981: "Chemical Sampling of VEESS Smoke During Smoke Week III," in Smoke Week III EO Systems Performance in Characterized Obscured Environment at Eglin AFB, Florida, August 1980, DRCPM-SMK-T-004-81.

Jenkins, R. A., D. L. Manning, M. P. Maskarinec, J. H. Moneyhun, W. Dalbey and S. Lock, 1983: "Diesel Fuel Smoke Particulate Dosimetry in Sprague-Dawley Rats," ORNL/TM-9195, Oak Ridge National Laboratory, Oak Ridge,TN.

Kaimal, J. C., J. C. Wyngaard, Y. Izumi and O. R. Cote, 1972: "Spectral Characteristics of Surface Layer Turbulence," Quart. J. Roy. Meteor. Soc., **98**, 653-689.

Kaimal, J. C., D. A. Haugen, O. R. Cote, Y. Izumi, S. J. Caughey and C. J. Readings, 1976: "Turbulence Structure in the Convective Boundary Layer," J. Atmos. Sci., **33**, 2152-2169.

Kaimal, J. C., 1978: "Horizontal Velocity Spectra in an Unstable Surface Layer," J. Atmos. Sci., **35**, 18-23.

Kaimal, J. C., W. L. Eberhard, W. R. Moninger, J. E. Gaynor, S. W. Troxel, T. Uttal, G. A. Briggs and G. E. Start, 1986: "Project CONDORS -- Convective Diffusion Observed by Remote Sensors", Report 7, NOAA/ERL Wave Propagation Laboratory, Boulder, CO.

Katz, Sidney, Alan Snelson, Ronald Butler, Raleigh Farlow, Roger Welker, Stephen Mainer, Narayanan Rajendran, 1980: "Physical Characterization of Military Smokes Part II -- Fog Oils and Oil Fogs, Final Report," AD _____, Illinois Institute of Technology Research Institute, Chicago, IL.

Laktionov, A. G., 1969: "Aspiration of an Aerosol Into a Vertical Tube from a Flow Transverse to it," AD 760947, National Technical Information Service (NTIS).

Lindberg, S. E. and G. M. Lovett, 1982: "Application of Surrogate Surface and Leaf Extraction Methods to Estimation of Dry Deposition to Plant Canopies," in Precipitation Scavenging, Dry Deposition, and Resuspension, Volume 2, H. R. Pruppacher, R. G. Semonin and W. G. N. Slinn, (eds.), pp.837-846.

Lovelock, J. E. and G. J. Ferber, 1982: "Exotic Tracers for Atmospheric Studies," Atmos. Envir., **16**, 1467-1471.

Mason, Conrad J. and Harry Moses, 1984: "Meteorological Instrumentation," Ch. 3 in: Atmospheric Science and Power Production, Randerson, Darryl (ed.), US DOE, 85-103.

Moore, G. E., Mei-Kao Liu, and Lu-Huai Shi, 1985: "Estimates of Integral Time Scales From a 100-M Meteorological Tower at a Plains Site," Bound. Layer Met., **31**, 349-368.

Neumann, J., 1978: "Some Observations on the Simple Exponential Function as a Lagrangian Velocity Correlation Function in Turbulent Diffusion," Atmos. Envir., **12**, 1965-1968.

Nieuwstadt, F., 1977: "The Computation of the Friction Velocity and Temperature Scale from Temperature and Wind Profiles by Least-Squares Methods," Bound. Layer Met., **14**, 235-246.

Nickola, P. W., 1977: "The Hanford 67-Series: A Volume of Atmospheric Diffusion Measurements," Document No. PNL-2433, Pacific Northwest Laboratories, Richland, WA.

Nickola, P. W., J. V. Ramsdell, C. S. Glantz and R. E. Kerns, "Hanford Atmospheric Dispersion Data: 1960 Through June 1967," NUREG/CR-3456, PNL-4814, Pacific Northwest Laboratories, Richland, WA.

Olesen, H. R., S. E. Larsen, and J. Højstrup, 1984: "Modelling Velocity Spectra in the Lower Part of the Planetary Boundary Layer," Bound. Layer Met., **29**, 285-312.

Panofsky, Hans A. and John A. Dutton, 1984: Atmospheric Turbulence, (New York, John Wiley and Sons).

Pasquill, F. and F. B. Smith, 1983: Atmospheric Diffusion, (Chichester, Ellis Horwood Ltd.).

Policastro, A. J. and W. E. Dunn, 1985: "Survey and Evaluation of Field Data Suitable for Smoke Hazard Evaluation," AD A161 880, University of Illinois, Urbana, IL.

Policastro, A. J., M. Wastag and W. E. Dunn, 1986: "Preliminary Evaluation of Atmospheric Dispersion Models for Fog Oil Smoke Dispersion," AD _____, Argonne National Laboratory, Argonne, IL.

Rabiner, L. R., 1979: "Power Spectrum Analysis and Correlation," in: Programs for Digital Signal Processing, (New York, IEEE Press).

Sehmel, G. A., 1967: "Estimation of Airstream Concentrations of Particulates from Subisokinetically Obtained Filter Samples," Am. Ind. Hyg Assoc. J., **28**, 243-253.

Sehmel, G. A., 1973: "Particle Eddy Diffusivities and Deposition Velocities for Isothermal Flow and Smooth Surfaces," Aerosol Sci., **4**, 125-138.

Sickles, J. E., W. D. Bach and L. L. Spiller, 1982: "Comparison of Several Techniques for Determining Dry Deposition Flux," in Precipitation Scavenging, Dry Deposition, and Resuspension, Volume 2, H. R. Pruppacher, R. G. Semonin and W. G. N. Slinn, (eds.), pp. 979-988.

Sundaresan, R. and V. V. Shirvaikar, 1984: "A Routine to Compute Mean and Standard Deviation of Fluctuating Wind Direction," Atmos. Envir., **18**, 473-474.

Tennekes, H. and J. L. Lumley, 1972: A First Course in Turbulence, M. I. T. Press, Cambridge, MA.

Tennekes, H., 1979: "The Exponential Lagrangian Correlation Function and Turbulent Diffusion in the Inertial Subrange," Atmos. Envir., **13**, 1565-1567.

Tennekes, H., 1982: "Similarity Relations, Scaling Laws and Spectral Dynamics," Ch. 2 in Atmospheric Turbulence and Air Pollution Modelling, (Nieuwstadt, F. T. M. and H. van Dop eds.), D. Reidel Publishing, Dordrecht, Holland.

Teunissen, H. W., 1980: "Structure of Mean Winds and Turbulence in the Planetary Boundary Layer Over Rural Terrain," Bound. Layer Met., 19, 187-221.

U. S. Army, Operator's and Organizational Maintenance Manual, M3A3E3 Smoke Generator (DRAFT), TM 3-(1040)-(278)-12.

Waldron, Albert W., 1977: "Turbulent Measurements on a Forty-Eight Meter Tower in Desert Terrain," DPG Document No. M615A, US Army Dugway Proving Ground, Dugway, UT.

Watson, H. H., 1954: "Errors Due to Anisokinetic Sampling of Aerosols," Ind. Hyg. Assoc. Quart., 15, 21-25.

APPENDIX A
THE DYNAMIC RESPONSE OF METEOROLOGICAL INSTRUMENTS

The dynamic response of the wind instruments was based on the analysis of Mason and Moses (1984). The cup anemometer was modeled as a first order system parameterized by the distance constant. The gain is given by

$$\text{Gain} = \frac{1}{\sqrt{1 + (\omega\tau)^2}}, \quad \tau = L/U \tag{A.1}$$

where $\omega = 2\pi n$ is the angular frequency, L is the distance constant and U is the mean wind speed.

The bivanes and direction vanes were modeled as a second order system parameterized by the natural wavelength and the damping coefficient. Their gain is given by

$$\text{Gain} = \frac{1}{\sqrt{4\xi^2 (\omega/\omega_n)^2 + \left(1 - (\omega/\omega_n)^2\right)^2}}, \quad \omega_n = 2\pi U/\lambda_n \tag{A.2}$$

where λ_n is the natural wavelength and ξ is the damping coefficient. The values of these parameters are given in Table A.1.

Table A.1. Instrument Parameters

Parameter	Direction Vane	Bivane	Cup Anemometer
Threshold, m/s	0.33	0.33	0.27
Damping Ratio	0.4	0.55	
Natural Wavelength, m	4.1	4.8	
Distance Constant, m			1.52

In order to assess the impact of the instrument response on the data, one must consider the frequency range over which the data are expected to be valid. The upper bound must be the Nyquist or folding frequency, defined as $n_N = 1/(2\Delta t)$ where Δt is the sampling interval in seconds. Data collected from the tower on West Vertical Grid was sampled at 1-second intervals giving it a Nyquist frequency of 0.5 Hz. The data collected from the tower on Horizontal Grid were sampled at 5-second intervals making its Nyquist frequency 0.1 Hz. The lower bound is determined by the duration of the sampling period, normally about one hour. Thus the lowest frequency is about 3×10^{-4} Hz.

Figure A.1 illustrates the behavior of the gain function for the cup anemometers over the frequency range of interest for mean wind speeds of 2, 4 and 8 m/s. It is apparent that at low wind speeds the high frequency response of the cups is quite poor. This would lead to a low estimate of the power spectra at higher frequencies, especially in the data from the West Vertical Grid tower which had a Nyquist frequency of 0.5 Hz versus 0.1 Hz for the data from the Horizontal Grid tower. This effect is demonstrated in Figure A.2 where the wind speed spectra for a low wind speed test conducted on April 10 reveals a marked deviation from the expected -2/3 slope at a frequency of 0.1 Hz. However, as Figure A.3 indicates, this problem only occurs for extremely low wind speeds: spectra from the test on April 2, which had slightly higher wind speeds, showed no deviation from the inertial subrange behavior. Therefore, since this attenuation occurs only at high frequencies having relatively little energy and only for low wind speed conditions, only those spectra used for comparison with the Højstrup model spectra were corrected. No general correction was applied to the wind speed data.

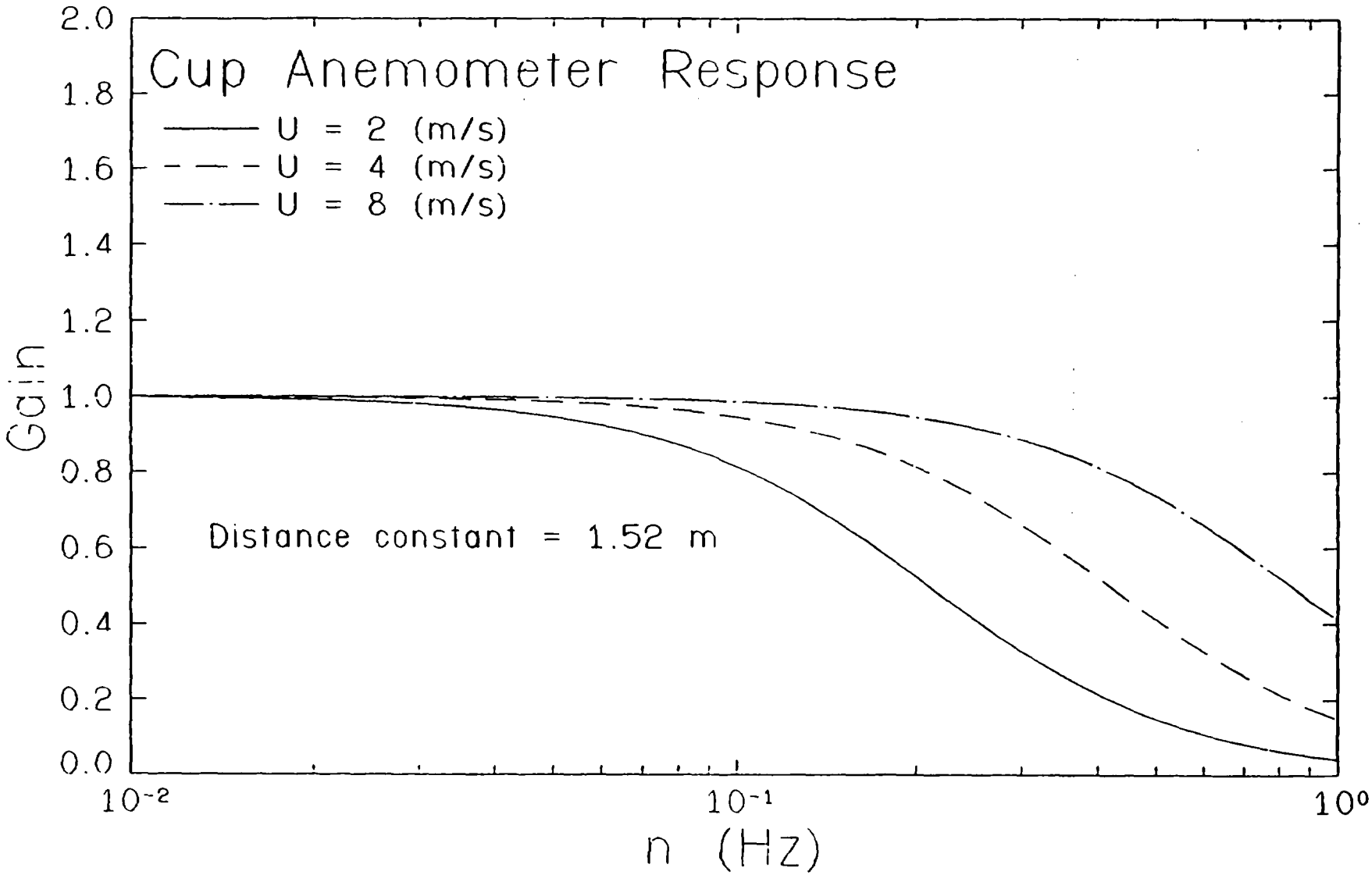

Figure A-1. Response of the Climet 014-102 cup anemometers to a sinusoidal forcing function calculated with equation (A.1).

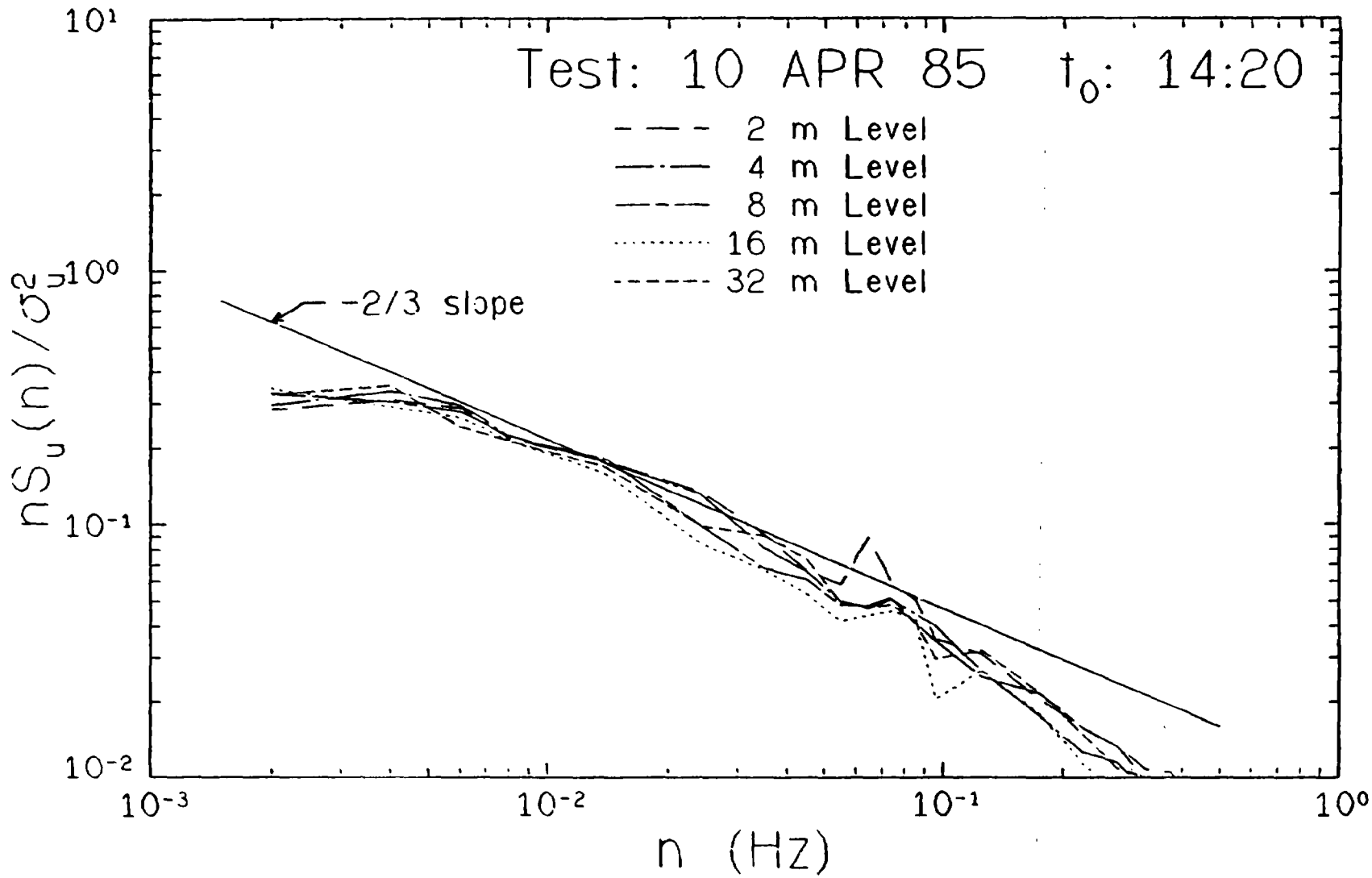

Figure A-2. Uncorrected power spectrum for T0010, mean wind speed ≈ 2 m/s.

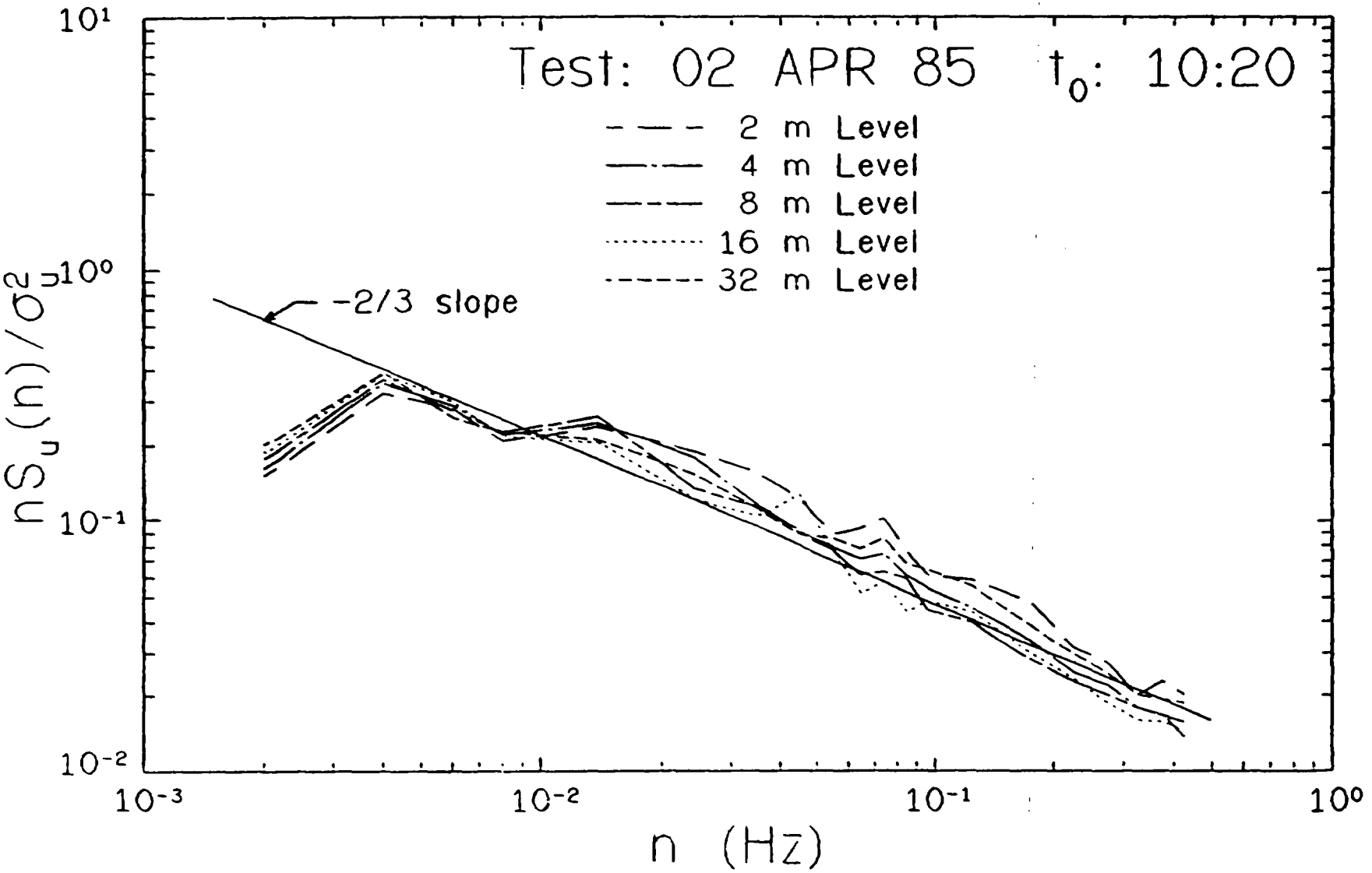

Figure A-3. Uncorrected power spectrum for T0002, mean wind speed = 3.5 m/s.

As Figure A.4 indicates, the response of the bivanes is essentially flat until beyond the Nyquist frequencies of both sets of data. The response of the direction vanes, shown in Figure A.5, is not quite as good as the bivanes, having a hump at high frequency. However, as it is almost beyond the Nyquist frequencies for even low wind conditions, no correction was applied.

In order to assess the effects of the response of the various instruments on the estimates of the variances of the three components of velocity, the measured spectra for tests T0005 and T0010 were corrected for the instrument gain and integrated to yield the variance. In no case did the corrected variances differ from the raw variances by more than 1%.

The response time of the temperature instruments is not as critical as that of the wind sensors since the temperature measurements have only been used to compute u_*, L, θ_o and θ_* over ten-minute averages. For completeness however, it should be noted that the time constant of the thermocouples (24-gauge wire) is less than 1 s while the thermistors have a time constant of about 10 s and the stem-sensitive RTD's time constant is about 1 min.

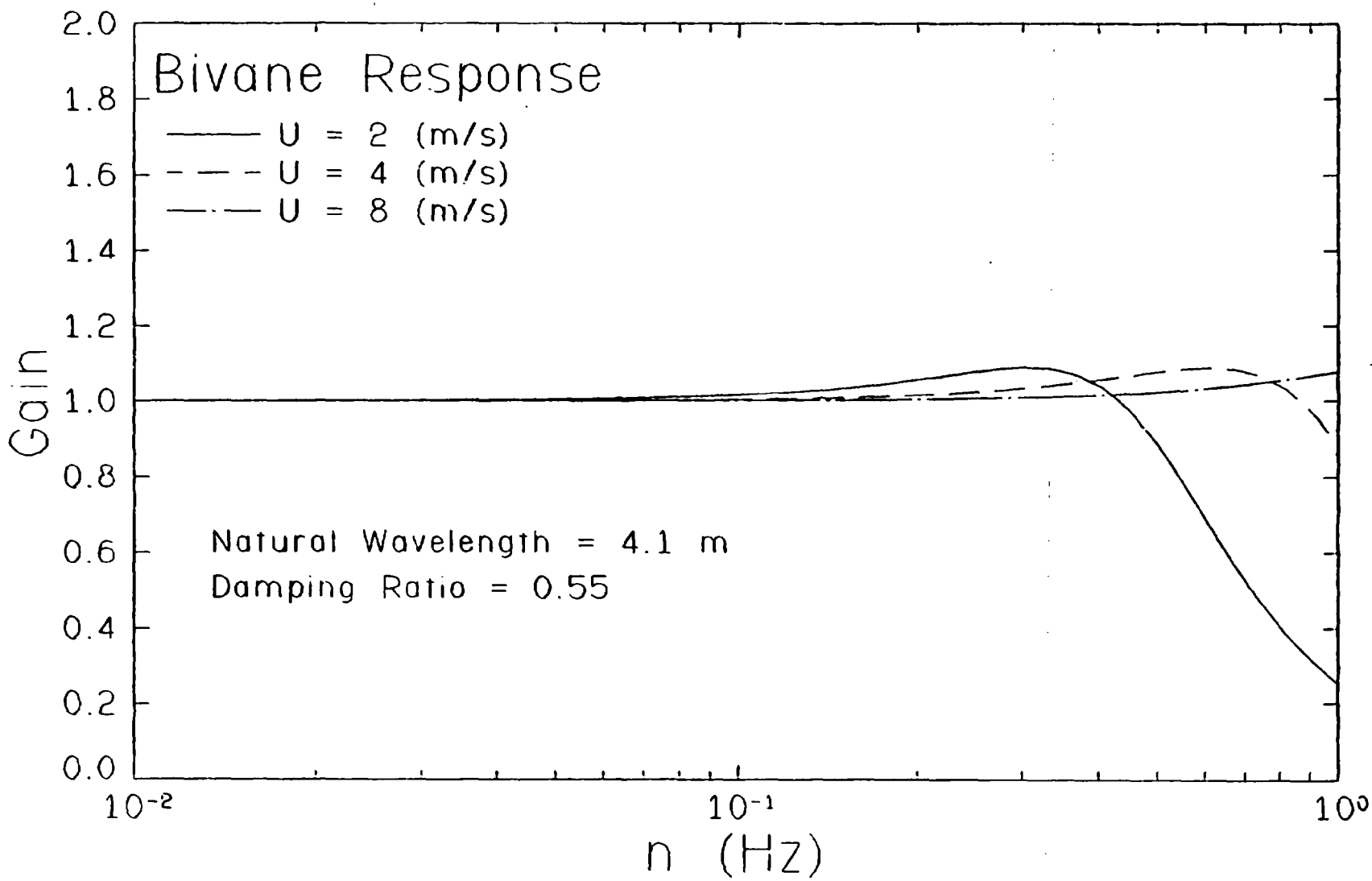

Figure A-4. Response of the Climet 014-47/48 bivanes to a sinusoidal forcing function calculated with equation (A.2).

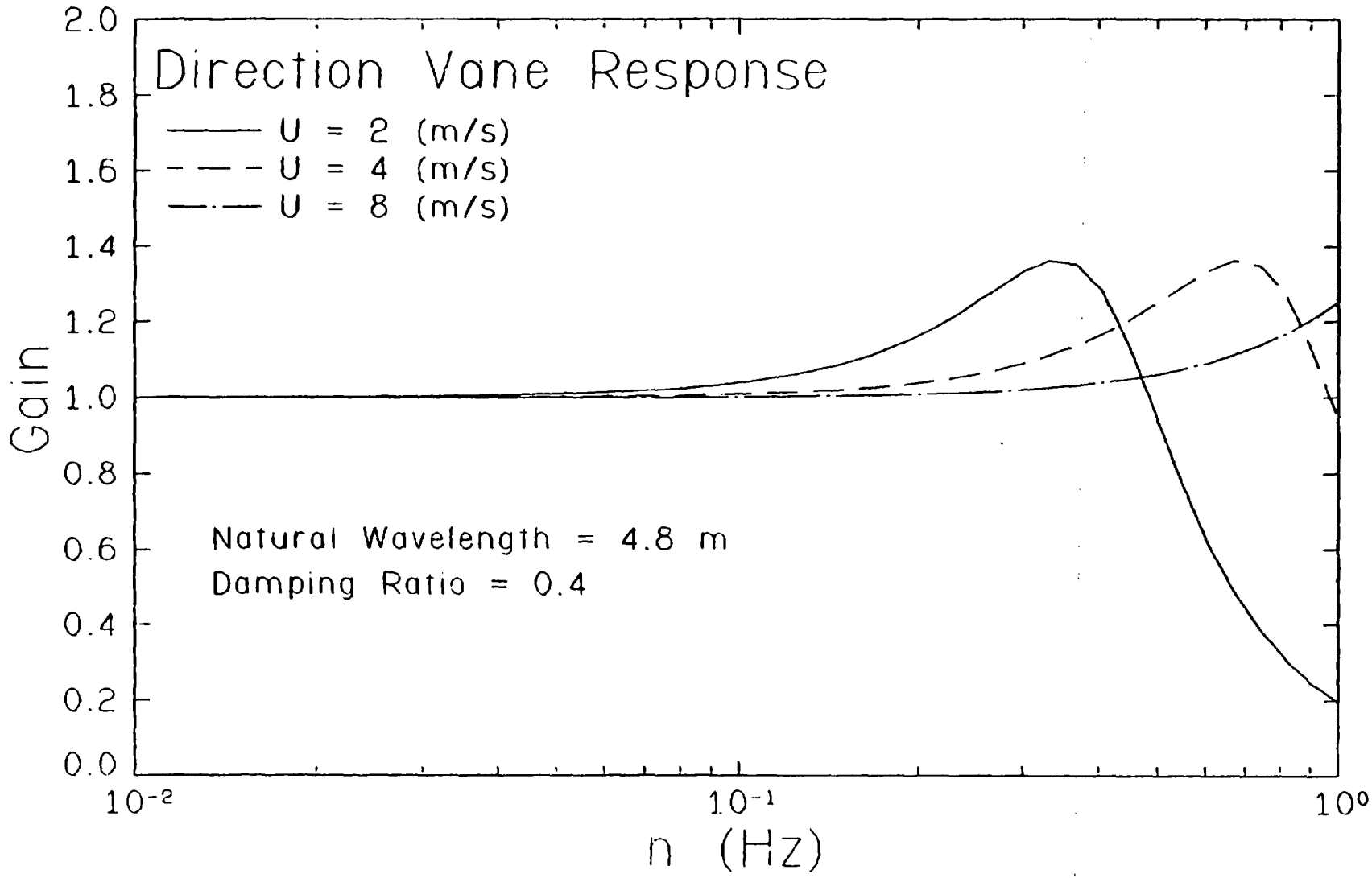

Figure A-5. Response of the Climet 014-6 direction vanes to a sinusoidal forcing function calculated with equation (A.2).

APPENDIX B.
ERRORS IN POWER SPECTRAL DENSITY ESTIMATES

Since the estimates of meteorological quantities such as variances, correlations, integral scales, peak wavelengths and others are directly or indirectly related to estimates of the power spectral density (PSD), it is appropriate to consider the nature and magnitude of the errors arising in the PSD estimation process. We begin with an expression for the normalized mean square error ε^2 of a PSD estimate $S_x(n)$ given by Bendat and Piersol (1977)

$$\varepsilon^2 \equiv \frac{E\left[\left(\hat{S}_x(n) - S_x(n)\right)^2\right]}{S_x^2(n)} \approx \frac{1}{B_e T} + \frac{B_e^4}{576}\left(\frac{S_x''(n)}{S_x(n)}\right)^2 \qquad (B.1)$$

where $E[f(x)]$ represents the expected value of $f(x)$, $B_e = \Delta n$, the "resolution bandwidth" of the estimate, T is the length of the data record and S_x'' refers to the second derivative of S_x with respect to n. For N samples of the signal x(t) at intervals Δt, $T = N\Delta t$.

The mean square error is the sum of two terms: the random or standard error which is a measure of the precision of the estimate, and the bias error which indicates the accuracy of the estimate. The first term in (B.1) represents the random error

$$\varepsilon_R^2 \equiv \frac{Var\left[\hat{S}_x(n)\right]}{S_x^2(n)} \approx \frac{1}{B_e T} \qquad (B.2)$$

If the PSD estimate is determined with the Fast Fourier Transform (FFT) over the entire data record length T then $B_e = 1/T$, in which case

$$\varepsilon_R^2 = \frac{T}{T} = 1 \qquad (B.3)$$

Not only is the random error of the same magnitude as the signal, but it is independent of the length of the data record. Thus, this precedure yields an estimate of the PSD which is not *consistent*. A consistent estimate is one for which the true value is approached in the limit of an infinite record length:

$$\lim_{T \to \infty} \hat{S}_x(n) = S_x(n) \qquad (B.4)$$

If, however, the data record is subdivided into segments of length T_e and the spectral density estimates computed over each segment are ensemble averaged, then $B_e = 1/T_e$ and

$$\varepsilon_R^2 = \frac{T_e}{T} = \frac{1}{N_{seg}} \qquad (B.5)$$

where $N_{seg} = T/T_e$ is the number of data segments. This expression demonstrates that the random error decreases as $(N_{seg})^{1/2}$. Clearly, ensemble averaging is essential in order to obtain a consistent estimate of the PSD.

The second term in (B.1), derived from a Taylor series expansion, provides an approximate estimate for the bias error

$$\varepsilon_B^2 \equiv \frac{E\left[\left(E[\hat{S}_x(n)] - S_x(n)\right)^2\right]}{S_x^2(n)} \approx \frac{B_e^4}{576}\left(\frac{S_x''(n)}{S_x(n)}\right)^2 = \frac{1}{576\,T_e^4}\left(\frac{S_x''(n)}{S_x(n)}\right)^2 \qquad (B.6)$$

where the last term results from the substitution of $1/T_e$ for B_e. Here we see that the bias error is dependent on the shape of the spectrum as well as on the length of the data segments. Estimates of spectra that contain sharp peaks will exhibit a large bias in the neighborhood of the peaks. "Smooth" portions of the spectrum, for which the second derivative is small, will exhibit much less bias. In order to demonstrate this shape dependence, we assume that the auto- correlation has an exponential form

$$R_x(t) = e^{-|t|/\tau} \qquad (B.7)$$

where τ is the integral scale. The single-sided power spectrum is then given by

$$S_x(n) = 2\int_{-\infty}^{\infty} R_x(t)\, e^{-j2\pi nt}dt = 2\int_{-\infty}^{\infty} e^{-|t|\,(1/\tau + j2\pi n)}dt$$

$$= \frac{4\tau}{1 + j2\pi n\tau} = \frac{4\tau}{1 + (2\pi n\tau)^2} \qquad (B.8)$$

and differentiating gives

$$S_x''(n) = \frac{d^2 S_x(n)}{dn^2} = 2\int_{-\infty}^{\infty} (j2\pi t)^2\, R_x(t)\, e^{-j2\pi t}\, dt = \frac{-32\,\pi^2\tau^2}{\left(1 + j2\pi n\tau\right)^3} \qquad (B.9)$$

Thus

$$\frac{S_x''(n)}{S_x(n)} = \frac{-8\,\pi^2\tau^2\left(1 - (2\pi n\tau)^2\right)}{\left(1 + (2\pi n\tau)^2\right)^2} = -8\,\pi^2\tau^2\,\sqrt{H(z)} \qquad (B.10)$$

where

$$H(z) = \left(\frac{1 - z^2}{\left(1 + z^2\right)^2}\right)^2 \qquad (B.11)$$

and $z = 2\pi n\tau = \omega\tau$. Substituting these results back into (B.1), the expression for the mean square error becomes

$$\varepsilon^2 \approx \frac{T_e}{T} + \frac{64\,\pi^4}{576} H(z) \left(\frac{\tau}{T_e}\right)^4 \qquad \text{(B.12)}$$

Note the conflicting constraints on the segment length: $T_e \ll T$ is desirable to reduce the random error but $T_e \gg \tau$ is needed to reduce the bias of the estimate. In other words, the precision of the estimate is improved by increasing the number of trials in the ensemble whereas the accuracy is improved by ensuring that the longest wavelengths in the signal are not excluded from the estimate. To be more specific about these requirements we need to consider the function H(z) more carefully.

H(z) takes on a maximum value of unity at $z = 0$ and then rapidly falls to a minimum value of zero at $z = 1$. As Figure B-1 shows, H(z) does not exceed a value of 0.02 for $z > 1$. Thus for $0.8 \le z \le \infty$, ε^2 may be conservatively estimated by assuming $H(z) = 0.02$:

$$\varepsilon^2 \approx \frac{T_e}{T} + 0.22 \left(\frac{\tau}{T_e}\right)^4 \qquad \text{(B.13)}$$

If the length T of the data record is fixed, one may overlap the data segments in order to increase N_{seg} without decreasing T_e. If the data segments overlap each other by a half, then the number of segments is given by

$$N_{seg} = \text{Integer part of} \left[\frac{T - T_e/2}{T_e/2}\right] \qquad \text{(B.14)}$$

However, this still leads to an increase in the bias error since the "additional" data are not independent. This can be seen by substituting T/N_{seg} for T_e in (B.13)

$$\varepsilon^2 \approx \frac{1}{N_{seg}} + 0.22 \frac{\left(N_{seg}\,\tau\right)^4}{T^4} \qquad \text{(B.15)}$$

Overlapping data segments is analogous to smoothing in the frequency domain in that it serves to reduce the random error at the expense of increasing the bias error.

The effect of varying the segment length T_e on the random and bias errors is illustrated in Figure B-2 for a signal with $T = 5000$ and $\tau = 32$. Clearly, the bias error decreases as T_e increases while the random error grows in magnitude. Figure B-2 also compares the errors for contiguous and overlapped data segments. The trade-off of increased bias for decreased random error is plainly evident. Thus, in order to minimize the mean square error, the following two requirements must be satisfied simultaneously:

$$\begin{aligned} &N_{seg} \gg 1, \text{ to minimize } \varepsilon_R, \\ &(N_{seg}\,\tau)^4 \ll T^4, \text{ to minimize } \varepsilon_B. \end{aligned} \qquad \text{(B.16)}$$

The effect of these requirements is to place a severe restriction on the maximum allowable integral time which the signal may possess if it is to be analyzed within a given rms error and with a fixed record length. They also imply that given a fixed record length T, PSD estimates for signal with greater values of τ are subject to

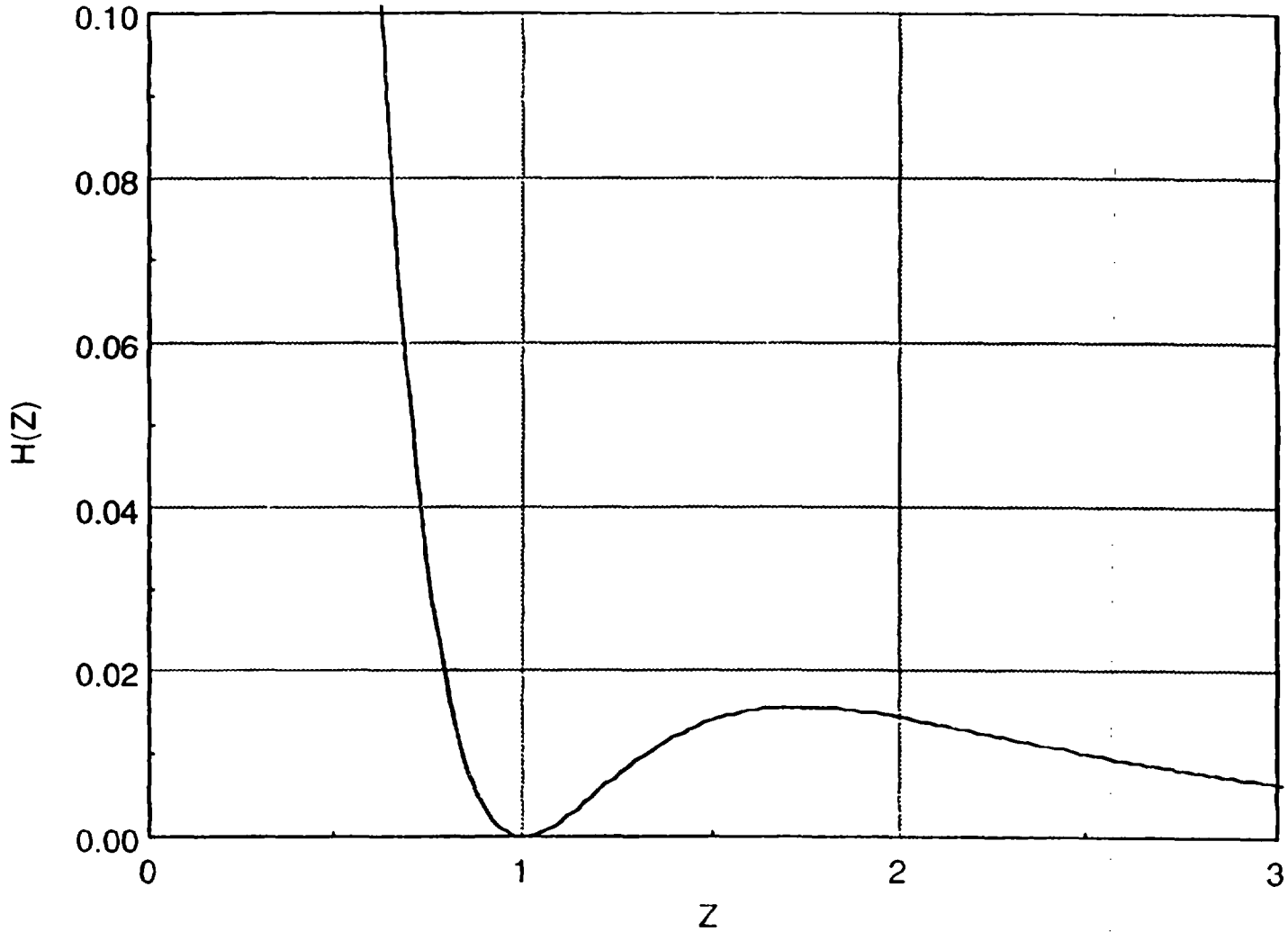

Figure B-1. The behavior of the bias error function H. H is based on the assumed exponential form for the auto-correlation.

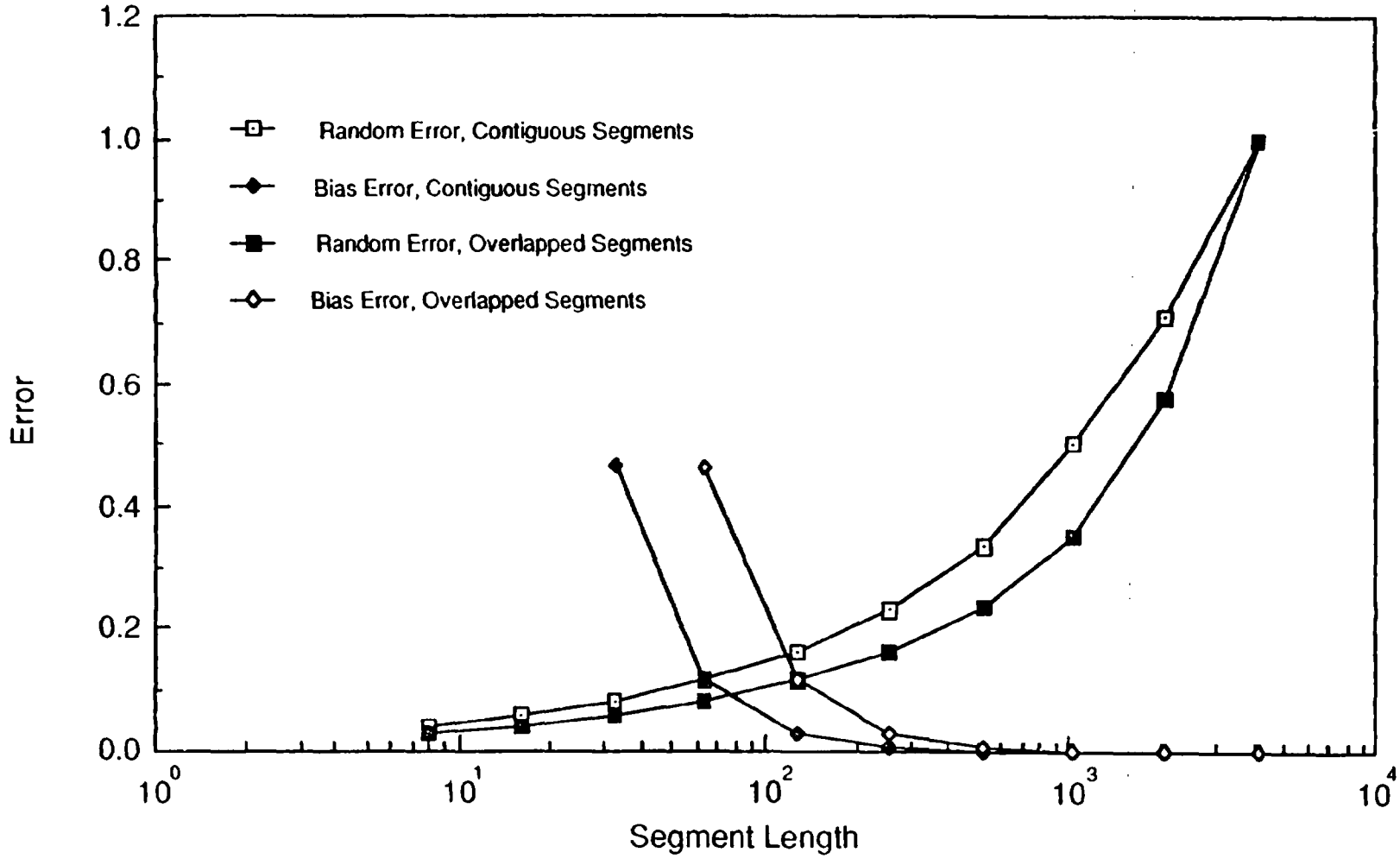

Figure B-2. The variation of the random error and bias error with segment length for contiguous and overlapped segments.

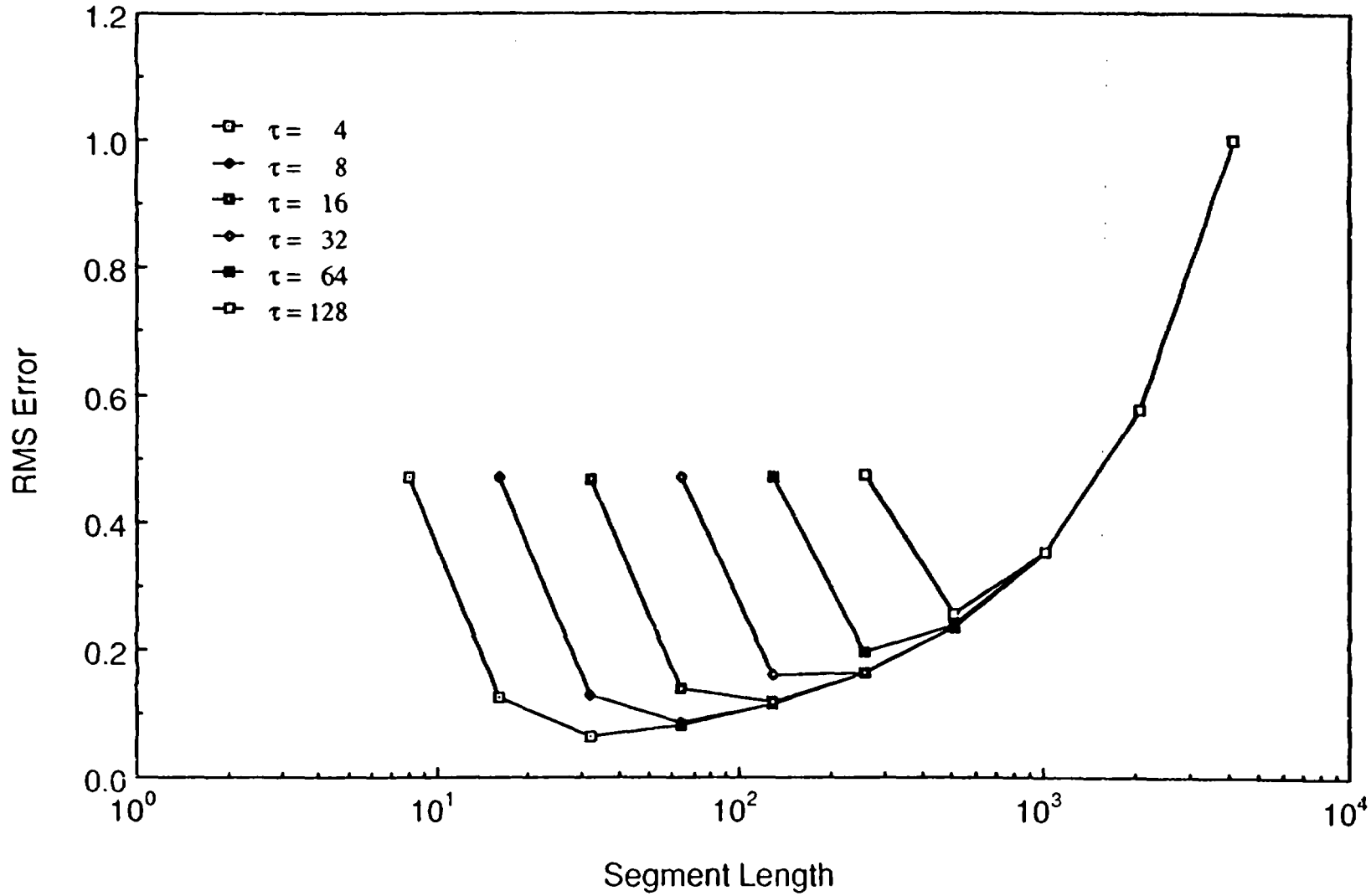

Figure B-3. The variation in rms error with segment length for several values of the signal integral scale. Segments are overlapped.

increasing error. This is illustrated for several values of τ and for T = 5000 in Figure B-3. Here we see that the minimum rms error increases from about 5% for τ = 4 at T_e = 32 to 25% for τ = 128 and T_e = 512.

Figures B-4, B-5 and B-6 present estimates of the power spectrum and auto-correlation for τ = 4, 16 and 64 respectively. These estimates have been computed for 5000 values of a signal x using various window lengths L (L = T_e). (The term window length is encountered in the electrical engineering literature.) The signal x was generated using

$$x_i = \rho\, x_{i-1} + \sqrt{1 - \rho^2}\; r_i \qquad \text{(B.17)}$$

where $\rho = e^{-\Delta t/\tau}$, $\Delta t = 1$ and r_i is a gaussian random variable with $E[r_i] = 0$ and $E[r_i^2] = 1$. The auto-correlation was also computed directly from the data with

$$R_j = \frac{1}{N} \sum_{i=1}^{N-j} x_i\, x_{i+j}\;;\; (j = 0, 1, 2, \ldots, m) \qquad \text{(B.18)}$$

where m is the maximum lag.

Figure B-4a compares two estimates of the power spectrum with the analytical solution given by (B.8) for τ = 4. Both estimates appear to be close to the analytical result, but the estimate for L = 2048 has a much larger random error. This is in keeping with the results presented in Figure B-3: for τ = 4, the bias error is small for L > 16 but the random error for L = 2048 is almost 60% whereas for L = 64 it is only about 5%. Integral scales derived from the peak wavelength should be reasonably accurate since the peak of the estimate is close to the true peak. Figure B-4b presents the auto-correlations computed by taking the inverse FFT of the two spectral estimates in Figure B-4a as well as the auto-correlation computed directly from the data. The analytical solution, the exponential function, is also presented for the purpose of comparison. For short lag times the estimates are reasonably close to exponential in form although for longer times none are satisfactory. This implies that integral scales computed by a direct integration of the auto-correlation will probably not be as accurate as values chosen as the lag for which the correlation falls to e^{-1}.

Figure B-5a shows spectra computed for L = 64, 256 and 2048 along with the analytical solution for τ = 16. A decrease in bias error associated with an increase in window length is accompanied by an increase in random error. It would be difficult to accurately estimate the peak wavelength with any of these PSD estimates. As the window length decreases, the longest wavelength which may be resolved also decreases. This is reflected in the auto-correlations presented in Figure B-5b; it is evident that as the window length decreases, the auto-correlation falls to zero more rapidly than the exponential. As the window length increases, the correlation estimate is derived from an increasingly noisly spectrum and hence is also noisier. The result of the direct computation is shown to perform very poorly, especially at large lags. This is because as the lag interval increases, the estimate is based on fewer realizations since the length of the data record is fixed. As a result, it is not surprising that directly integrating any of these yields a poor estimate of the integral scale. Neither is the method of looking at where the correlation falls to e^{-1} expected to perform well for the shorter window lengths.

Figures B-6a and B-6b present spectra and correlations for L = 64, 256 and 2048 for a signal with τ = 64. The complementary relationship of bias error and random error with window length discussed above are seen to be more pronounced. The high-pass filtering effect of window length is demonstrated by the correlations. The problem becomes more severe as the window length is decreased. Computation of integral scales from these estimates is impossible.

Table B-1 summarizes the results of four methods of computing integral time scales from power spectra and correlation estimates. These methods include

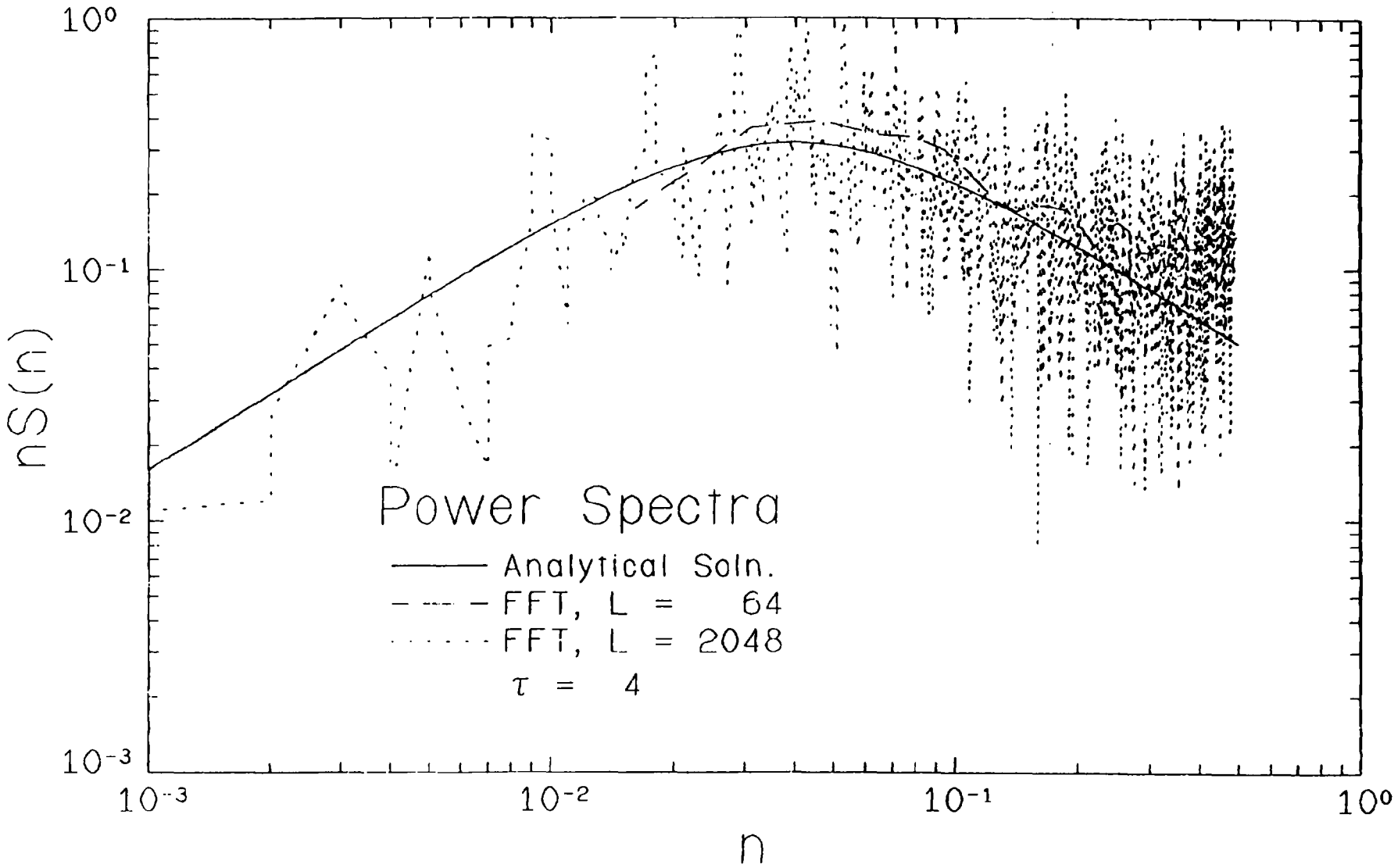

Figure B-4a. Power spectra of a signal with τ = 4 for different window lengths.

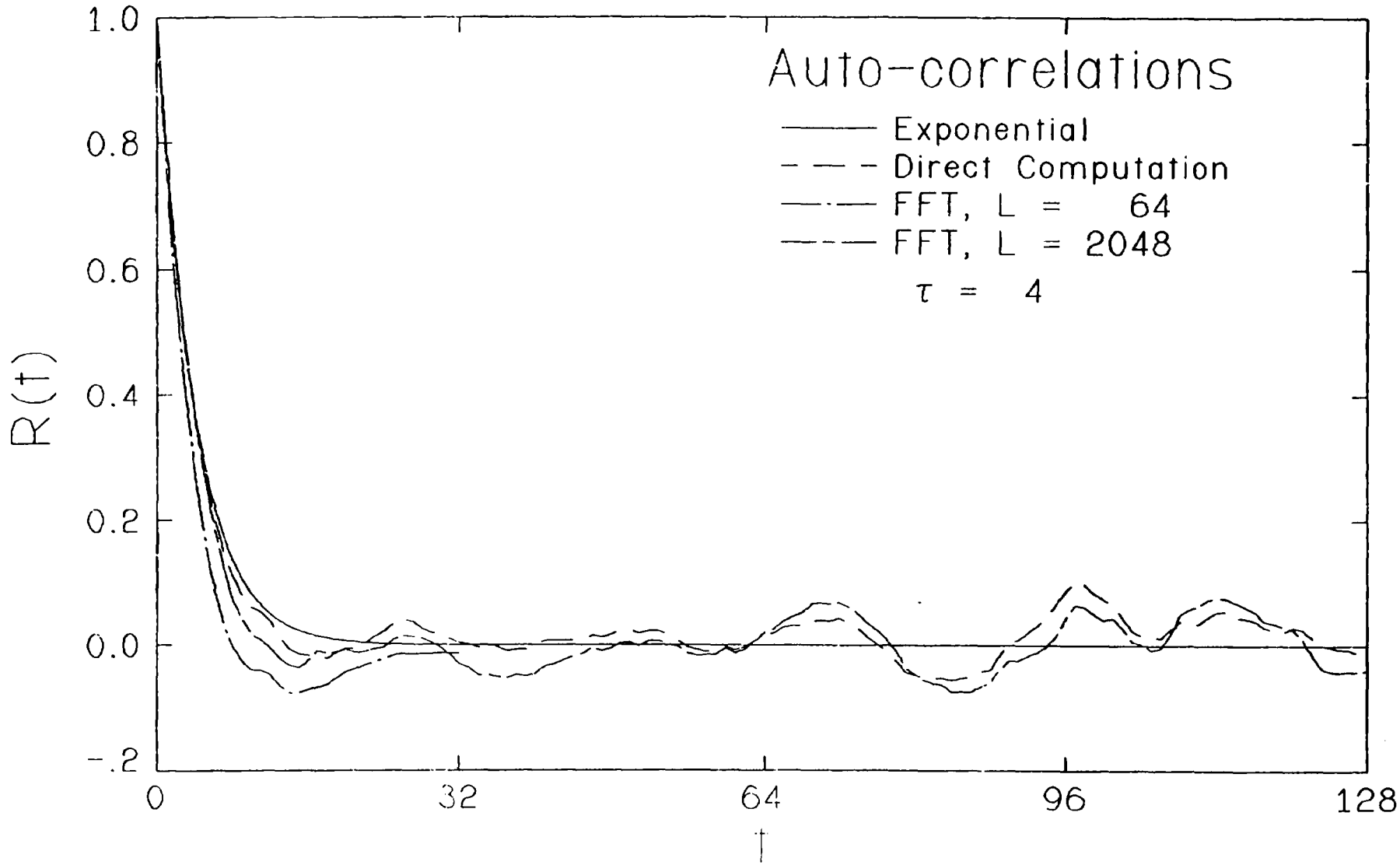

Figure B-4b. Auto-correlations of a signal with $\tau = 4$ for different window lengths.

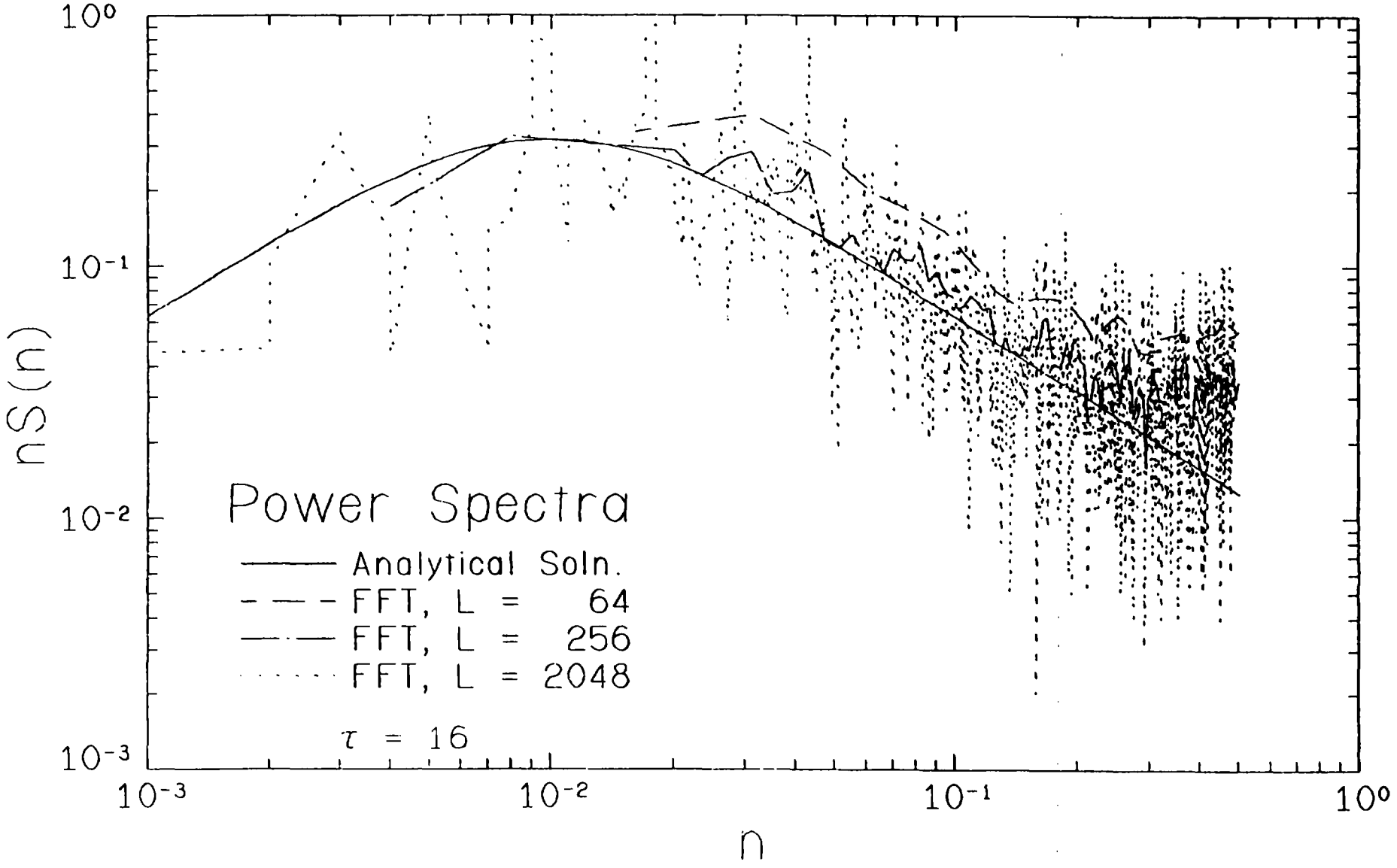

Figure B-5a. Power spectra for a signal with τ = 16 for different window lengths.

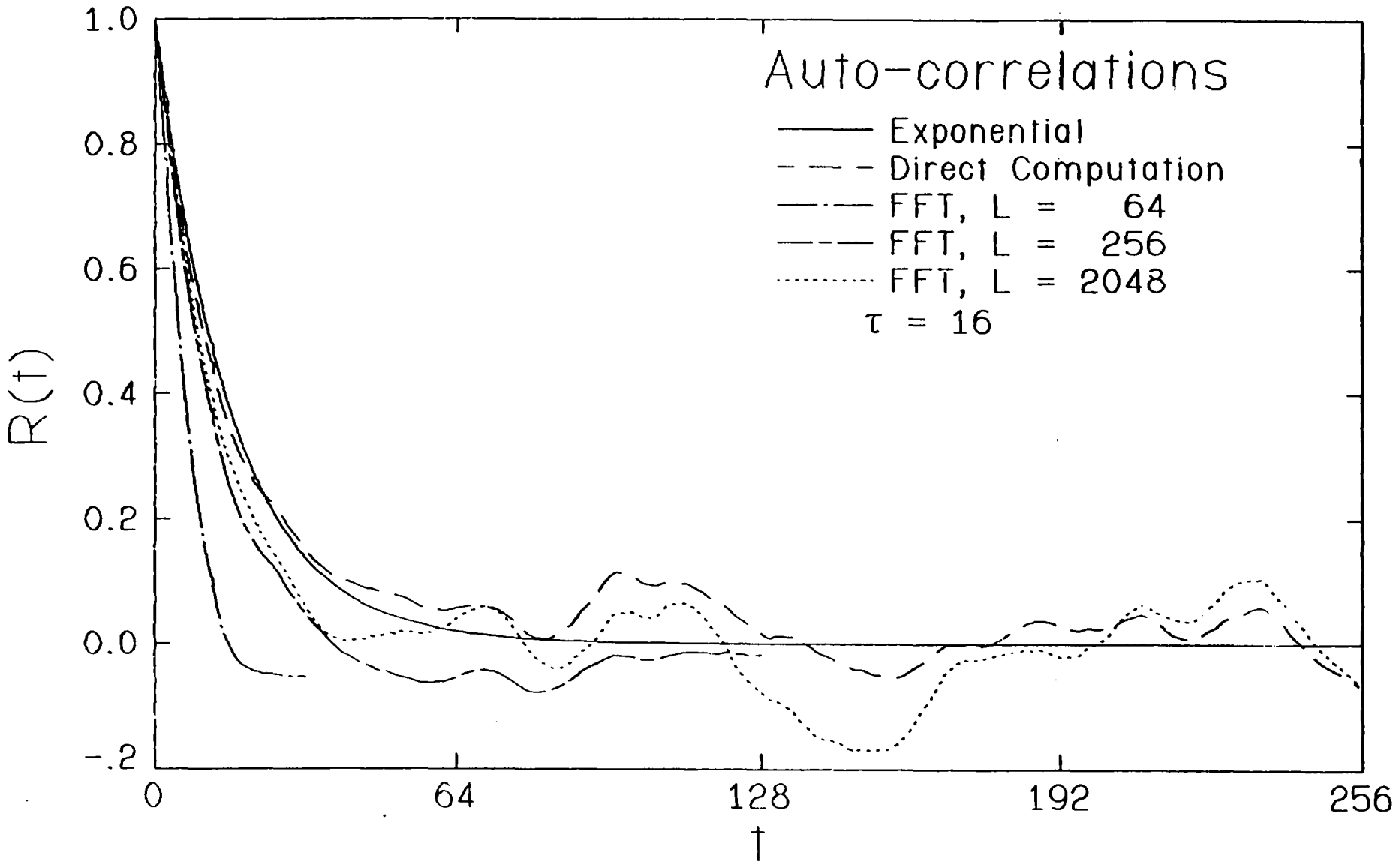

Figure B-5b. Auto-correlations for a signal with τ = 16 for different window lengths.

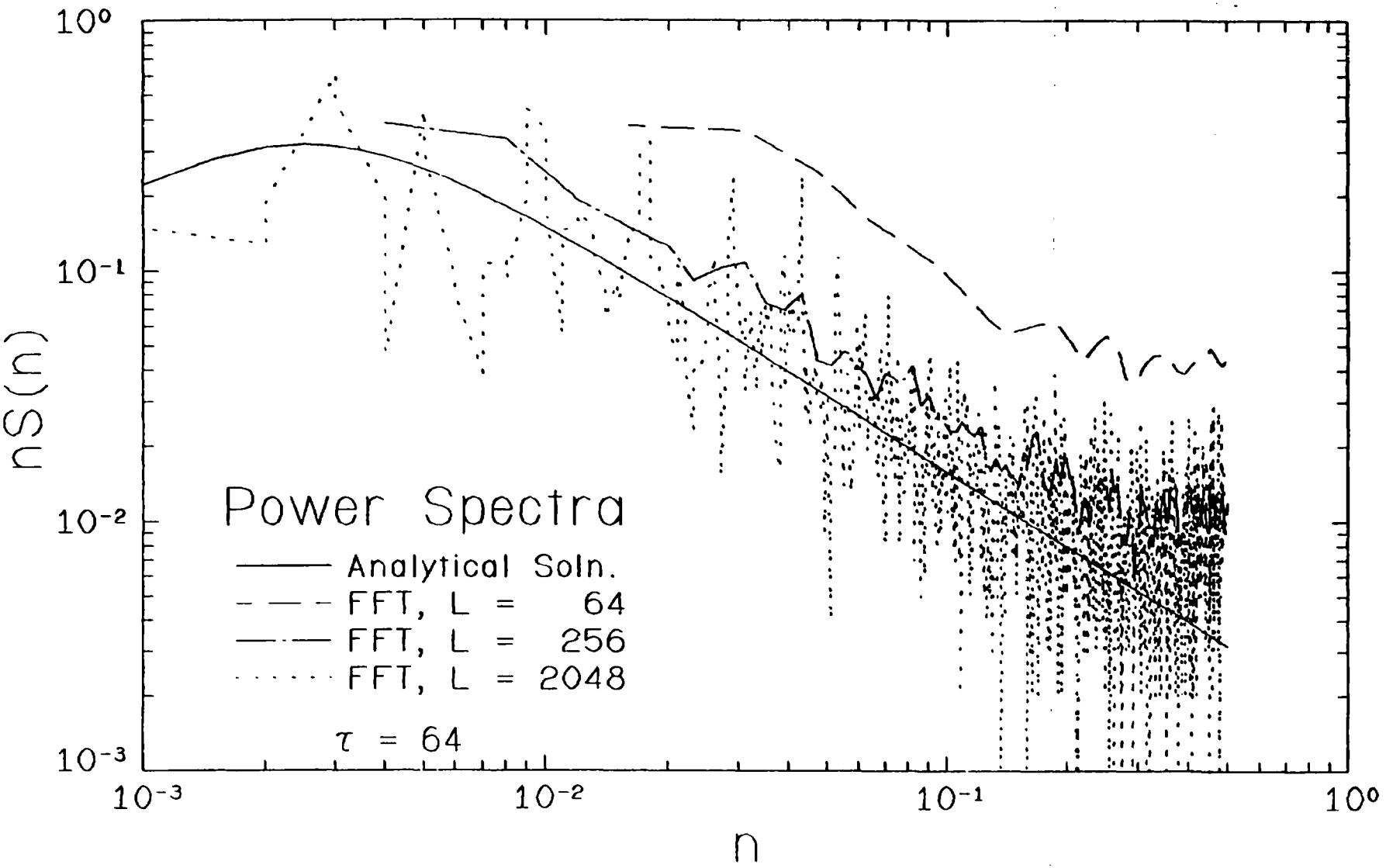

Figure B-6a. Power spectra for a signal with τ = 64 for different window lengths.

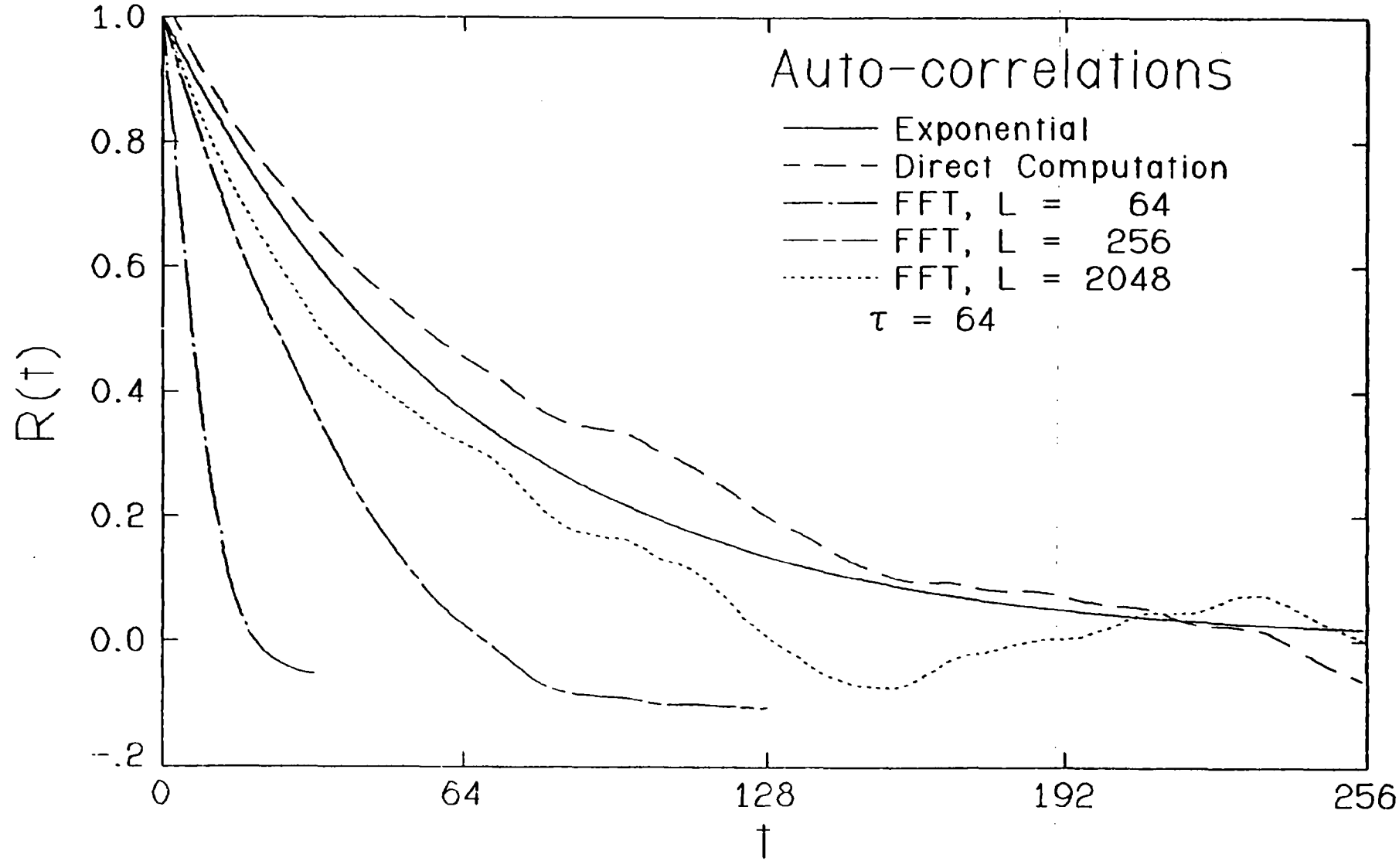

Figure B-6b. Auto-correlations for a signal with τ = 64 for different window lengths.

1. *Direct integration of the auto-correlation estimate.* The auto-correlation estimate may be computed directly from the data or by an inverse FFT of the power spectrum. The data in Table B-1 were computed from an estimate of the auto-correlation determined by the latter method.

2. *Peak of the frequency-weighted spectrum.* If the auto-correlation is assumed to have an exponential form, then the integral scale may be computed via the expression $\tau = 1/(2\pi n_{max})$ where n_{max} is the peak of the frequency-weighted spectra $nS_x(n)$ given in Figures 4a, 5a and 6a.

3. *The lag for which the correlation falls to e^{-1}.* The integral scale is arbitrarily chosen to equal the lag time for which the auto-correlation falls to e^{-1} of its initial value. Implicit in this method is the assumption of an exponential form for the auto-correlation.

4. *Integration of the non-linear least-squares fit to the correlation.* An exponential function is fit to the correlation estimate and this estimate is integrated to compute the integral scale. This method can be used to treat noisy or marginally-exponential correlations. Here it has been applied to correlation estimated computed directly from the signal via (B.18).

These results underscore the severity of the requirements set forth in (B.16). When τ is small and N_{seg} large, as for the case when $\tau = 4$, all four methods perform fairly well. As τ grows in magnitude or N_{seg} decreases, the results are increasingly in error. When the conditions in (B.16) are violated, none of these methods provide reliable estimates of the integral scale because the PSD estimates upon which they are ultimately are substantially in error. This demonstrates that the determination of power spectral density estimates must be performed with great care if they, and results derived from them, are to be valid.

Table B-1. Integral Time Scales Computed by Various Methods for Several Window Lengths.

Window Length (s)	Integration of R(t)	$\tau = 1/(2\pi n_{max})$	τ = t for which $R(t) = e^{-1}$	Integration of fit to R(t)
τ = 4 sec				
64	3.73	3.40	3.94	3.13
128	3.36	4.07	4.26	3.34
256	3.66	3.70	4.42	3.54
512	7.17	3.70	4.83	3.84
1024	3.52	3.70	4.42	3.71
2048	1.79	3.70	4.98	3.80
τ = 8 sec				
64	6.55	5.09	4.94	4.82
128	6.77	5.09	6.00	5.64
256	7.56	5.09	6.76	6.39
512	14.49	3.70	7.89	7.60
1024	7.34	3.70	6.97	7.13
2048	3.79	3.70	7.72	6.71
τ = 16 sec				
64	9.93	5.09	4.87	6.56
128	12.75	10.19	7.90	9.02
256	14.98	20.37	10.41	11.70
512	28.60	16.30	14.08	15.00
1024	15.49	16.30	12.02	15.40
2048	8.28	9.05	12.61	14.33
τ = 32 sec				
64	12.23	10.19	2.15	7.63
128	20.64	20.37	9.00	13.55
256	26.97	20.37	15.12	20.33
512	52.15	16.30	26.05	29.52
1024	31.69	16.30	22.94	32.70
2048	17.55	17.16	21.88	26.59
τ = 64 sec				
64	12.71	10.19	0.	7.81
128	26.06	20.37	6.04	17.04
256	42.84	40.74	20.11	30.89
512	83.21	81.49	37.69	48.64
1024	62.43	54.32	43.43	61.38
2048	32.68	54.32	36.37	51.59
τ = 128 sec				
64	12.28	10.19	0.	7.66
128	26.55	20.37	0.	17.85
256	52.77	40.74	17.06	37.77
512	108.68	81.49	37.09	66.20
1024	120.50	162.97	79.82	101.90
2048	41.02	162.97	72.24	100.68

APPENDIX C.
ESTIMATION OF INTEGRAL SCALE FROM PEAK OF POWER SPECTRUM

One method of estimating the integral time scale of a signal is to relate it to the peak of the estimated power spectrum. If one assumes that the correlation function is adequately described by an exponential

$$R_x(t) = \exp(-t/\tau) \tag{C.1}$$

then the corresponding single-sided power spectrum is given by

$$S_x(n) = 2\int_{-\infty}^{\infty} R_x(t)\, e^{-j2\pi nt} dt = 2\int_{-\infty}^{\infty} e^{-|t|\,(1/\tau + j2\pi n)} dt$$

$$= \frac{4\tau}{1 + j2\pi n\tau} = \frac{4\tau}{1 + (2\pi n\tau)^2} \tag{C.2}$$

The frequency-weighted power spectrum $nS_x(n)$ is then

$$n\,S_x(n) = \frac{4\tau n}{1 + j2\pi n\tau} = \frac{4\tau n}{1 + (2\pi n\tau)^2} \tag{C.3}$$

Differentiate this to find the maximum

$$\frac{\partial\left(nS_x(n)\right)}{\partial n} = \frac{4\tau}{1 + (2\pi n\tau)^2} + \frac{-8n\tau\,(2\pi n\tau)^2}{\left(1 + (2\pi n\tau)^2\right)^2} = 0 \tag{C.4}$$

Solving for the frequency n_{max} at which $nS_x(n)$ is a maximum gives

$$n_{max} = \frac{1}{2\pi\tau} \tag{C.5}$$

The integral scale is thus given by

$$\tau = \frac{1}{2\pi n_{max}} \tag{C.6}$$

APPENDIX D
Summaries of Test Day Data

The tables in this appendix summarize the data collected during the three successful dispersion trials: T0009, T0010 and T0011. Data characterizing the meteorology and source are listed first, followed by concentration calibration data and finally the concentration data itself.

The mean wind speed (m/s), mean wind direction (degrees east of north), and standard deviations of the wind direction and inclination (both in degrees) are listed for each location of the smoke generator. The source parameters include the coordinate locations of the generator (refer to figures 2.2 and 2.3 for grid description), the start and stop times, and the duration (in minutes) and rate (g/s) of the release.

The calibration information includes the average background level for a "blank" or unexposed sample tube (in arbitrary units of the gas chromatograph, "GC counts") and the 1.0 microliter calibration value (in GC counts). The background contamination is determined by dividing the background amount by the calibration; it represents the equivalent amount of oil necessary to produce the observed background level. The effective detection threshold is the average concentration of fog oil which would have been required during the test to equal the background level. It is computed by dividing the backgound contamination level by the product of the average aspiration rate and the test duration (i.e., the average volume of air sampled). Average concentrations less than about half of this value for a given test should be considered of dubious validity.

The concentration data include the location designation and grid coordinates, the raw output of the gas chromatograph (in arbitrary units of the gas chromatograph), the amount of oil in the sample (μl), after subtracting the background, the measured aspiration rate of that sample (liters per minute, Lpm) and the computed average concentration (mg/m^3). A listing of zero GC counts indicates that the data from that sample is missing. This almost always occurred through a failure of the software supplied by Perkin-Elmer to control the gas chromatograph. Negative concentration values result from samples which are less that the average background level. Such samples were considered not statistically valid and accordingly excluded from the discussion of the data presented in section 2.

Table D-1. Average Concentrations for T0009

Test: 0409851
Smoke: Fog Oil

Wind Speed	Direction	Sigma Theta	Sigma Phi
5.2	11.0	18.7	8.8

Xsrc	Ysrc	Start	Stop	Duration	Rate (g/s)
-3.7	30.0	13:38	14:53	69	43.2

Average blank DPG tube (GC counts)	41,736,391
Average 1.0 ul calibration (GC counts)	113,459,616
Background contamination (ul)	0.37
Effective Detection Threshold (mg/m3)	3.44

Location	X (m)	Y(m)	GC Counts	Oil (ul)	Flow (Lpm)	Conc (mg/m3)
J-25-1	25	-25	103885933	0.55	1.18	6.12
J-25-2	25	-20	328013153	2.52	1.27	26.20
J-25-3	25	-15	400218997	3.16	1.23	33.88
J-25-4	25	-10	772654343	6.44	1.51	56.27
J-25-5	25	-5	1253401945	10.68	1.75	80.48
J-25-6	25	0	1175305883	9.99	1.42	92.79
J-25-7	25	5	1420150140	12.15	1.37	116.95
J-25-8	25	10	0	-0.37	1.46	-3.32
J-25-9	25	15	766059412	6.38	1.37	61.46
J-25-10	25	20	477035774	3.84	1.46	34.66
J-25-11	25	25	329376061	2.54	1.65	20.26
J-50-1	50	-50	108183539	0.59	1.18	6.55
J-50-2	50	-40	21286547	-0.18	1.51	-1.57
J-50-3	50	-30	125948517	0.74	1.60	6.12
J-50-4	50	-20	404984299	3.20	1.42	29.73
J-50-5	50	-10	234424237	1.70	1.32	16.97
J-50-6	50	0	169012555	1.12	1.09	13.57
J-50-7	50	10	26953472	-0.13	1.32	-1.30
J-50-8	50	20	119821550	0.69	1.60	5.67
J-50-9	50	30	21066162	-0.18	1.42	-1.69
J-50-10	50	40	53769502	0.11	1.42	0.99
J-50-11	50	50	19387999	-0.20	1.51	-1.72
J-100-1	100	-100	7363951	-0.30	1.46	-2.74
J-100-2	100	-75	122439328	0.71	1.42	6.61
J-100-3	100	-50	83540036	0.37	1.42	3.42
J-100-4	100	-25	71921423	0.27	1.42	2.47
J-100-5	100	0	83841768	0.37	1.42	3.45
J-100-6	100	25	10129747	-0.28	1.42	-2.59
J-100-7	100	50	50724496	0.08	1.32	0.79
J-100-8	100	75	37818539	-0.03	0.94	-0.48
J-100-9	100	100	7970892	-0.30	1.51	-2.60
J-200-1	200	-200	51352757	0.08	1.46	0.77
J-200-2	200	-150	57611244	0.14	1.23	1.50
J-200-3	200	-100	42327338	0.01	1.37	0.05
J-200-4	200	-50	47143498	0.05	1.37	0.46
J-200-5	200	0	58460953	0.15	1.42	1.37
J-200-6	200	50	5288399	-0.32	1.46	-2.90
J-200-7	200	100	32859197	-0.08	1.51	-0.68
J-200-8	200	150	25962479	-0.14	1.51	-1.21
J-200-9	200	200	35097692	-0.06	1.13	-0.68

Table D-1. Average Concentrations for T0009

N-2	400	-200	0	-0.37	1.37	-3.54
N-2.5	400	-150	25731703	-0.14	1.46	-1.27
N-3	400	-100	31186857	-0.09	1.42	-0.86
N-3.5	400	-50	15070175	-0.24	1.42	-2.18
N-4	400	0	38299468	-0.03	1.46	-0.27
N-4.5	400	50	24801013	-0.15	1.42	-1.39
N-5	400	100	14866255	-0.24	1.60	-1.95
N-5.5	400	150	25931781	-0.14	1.46	-1.26
N-6	400	200	25099386	-0.15	1.60	-1.21

Table D-2. Average Concentrations for T0010

Test: 0410851
Smoke: Fog Oil

Wind Speed	*Direction*	*Sigma Theta*	*Sigma Phi*
2.6	201.0	43.9	15.7

Xsrc	*Ysrc*	*Start*	*Stop*	*Duration*	*Rate (g/s)*
400.0	0.0	14:20	15:38	62	41.7

Average blank DPG tube (GC counts)	41,736,391
Average 1.0 ul calibration (GC counts)	113,459,616
Background contamination (ul)	0.37
Effective Detection Theshold (mg/m3)	3.69

Location	*X (m)*	*Y(m)*	*GC Counts*	*Oil (ul)*	*Flow (Lpm)*	*Conc (mg/m3)*
N-25-1	375	-25	92957132	0.45	1.51	4.39
N-25-2	375	-20	62310250	0.18	1.42	1.87
N-25-3	375	-15	20530984	-0.19	1.65	-1.66
N-25-4	375	-10	128513968	0.76	1.51	7.43
N-25-5	375	-5	212514764	1.51	1.65	13.39
N-25-6	375	0	178904109	1.21	1.42	12.50
N-25-7	375	5	483938712	3.90	1.75	32.69
N-25-8	375	10	284381435	2.14	1.65	19.02
N-25-9	375	15	61487904	0.17	1.56	1.64
N-25-10	375	20	225234840	1.62	1.37	17.33
N-25-11	375	25	163969238	1.08	1.18	13.40
N-50-1	350	-50	49188892	0.07	1.42	0.68
N-50-2	350	-40	52745234	0.10	1.70	0.84
N-50-3	350	-30	53249540	0.10	1.70	0.88
N-50-4	350	-20	67253271	0.22	1.60	2.06
N-50-5	350	-10	108623005	0.59	1.51	5.73
N-50-6	350	0	165677339	1.09	1.70	9.43
N-50-7	350	10	0	-0.37	0.99	-5.45
N-50-8	350	20	0	-0.37	1.51	-3.58
N-50-9	350	30	90806122	0.43	1.46	4.35
N-50-10	350	40	68217305	0.23	1.37	2.50
N-50-11	350	50	100324024	0.52	1.75	4.33
N-100-1	300	-100	39484719	-0.02	1.56	-0.19
N-100-2	300	-75	41718123	0.00	1.18	0.00
N-100-3	300	-50	16357551	-0.22	1.65	-1.99
N-100-4	300	-25	43525225	0.02	1.60	0.14
N-100-5	300	0	11760968	-0.26	1.46	-2.66
N-100-6	300	25	0	-0.37	1.70	-3.18
N-100-7	300	50	0	-0.37	1.46	-3.70
N-100-8	300	75	48097616	0.06	1.75	0.47
N-100-9	300	100	48814875	0.06	1.42	0.64
N-200-1	200	-200	0	-0.37	1.42	-3.80
N-200-2	200	-150	44835146	0.03	1.18	0.34
N-200-3	200	-100	0	-0.37	1.25	-4.32
N-200-4	200	-50	0	-0.37	1.37	-3.94
N-200-5	200	0	0	-0.37	1.04	-5.19
N-200-6	200	50	0	-0.37	1.42	-3.80
N-200-7	200	100	0	-0.37	1.27	-4.25
N-200-8	200	150	0	-0.37	1.51	-3.58
N-200-9	200	200	86125163	0.39	1.60	3.59

Table D-2. Average Concentrations for T0010

N-2	400	-200	0	-0.37	1.42	-3.80
N-2.5	400	-150	0	-0.37	1.42	-3.80
N-3	400	-100	41614862	0.00	1.04	-0.02
N-3.5	400	-50	36700575	-0.04	1.51	-0.43
N-4	400	0	46893735	0.05	1.46	0.46
N-4.5	400	50	0	-0.37	1.32	-4.09
N-5	400	100	43873773	0.02	1.18	0.23
N-5.5	400	150	44663171	0.03	1.46	0.26
N-6	400	200	0	-0.37	1.70	-3.18
J-4	0	0	59253095	0.15	1.42	1.60

Table D-3. Average Concentrations for T0011

Test: 0411851
Smoke: Fog Oil

Wind Speed	*Direction*	*Sigma Theta*	*Sigma Phi*
7.2	338.0	11.0	4.8
6.3	5.0	14.7	7.1

Xsrc	*Ysrc*	*Start*	*Stop*	*Duration*	*Rate (g/s)*
-4.0	0.0	9:38	9:45	7	38.1
-4.0	24.0	10:30	11:55	85	37.6

Average blank DPG tube (GC counts)	41,736,391
Average 1.0 ul calibration (GC counts)	113,459,616
Background contamination (ul)	0.37
Effective Detection Threshold (mg/m3)	2.63

Location	*X (m)*	*Y(m)*	*GC Counts*	*Oil (ul)*	*Flow (Lpm)*	*Conc (mg/m3)*
J-25-1	25	-25	151038065	0.96	1.27	7.48
J-25-2	25	-20	205991136	1.45	1.42	10.11
J-25-3	25	-15	351741454	2.73	1.56	17.35
J-25-4	25	-10	583914898	4.78	1.60	29.45
J-25-5	25	-5	419257954	3.33	1.37	24.04
J-25-6	25	0	333756708	2.57	0.61	41.49
J-25-7	25	5	816618129	6.83	1.46	46.17
J-25-8	25	10	1896990764	16.35	1.46	110.54
J-25-9	25	15	712620120	5.91	1.18	49.57
J-25-10	25	20	566232212	4.62	1.42	32.29
J-25-11	25	25	160301242	1.04	1.42	7.30
J-50-1	50	-50	95103487	0.47	1.27	3.65
J-50-2	50	-40	178397764	1.20	1.42	8.41
J-50-3	50	-30	136301775	0.83	1.42	5.82
J-50-4	50	-20	300433753	2.28	1.42	15.93
J-50-5	50	-10	395751474	3.12	1.18	26.15
J-50-6	50	0	205540025	1.44	0.85	16.81
J-50-7	50	10	247391853	1.81	1.46	12.25
J-50-8	50	20	103482866	0.54	1.32	4.07
J-50-9	50	30	121564496	0.70	1.42	4.91
J-50-10	50	40	37191286	-0.04	1.42	-0.28
J-50-11	50	50	99916279	0.51	1.23	4.13
J-100-1	100	-100	52932426	0.10	1.60	0.61
J-100-2	100	-75	87199240	0.40	1.51	2.62
J-100-3	100	-50	106426864	0.57	1.42	3.98
J-100-4	100	-25	127508219	0.76	1.51	4.95
J-100-5	100	0	166595403	1.10	1.42	7.69
J-100-6	100	25	68095868	0.23	1.37	1.68
J-100-7	100	50	0	-0.37	1.32	-2.75
J-100-8	100	75	50453595	0.08	0.99	0.77
J-100-9	100	100	48496311	0.06	1.37	0.43
J-200-1	200	-200	80943779	0.35	1.42	2.41
J-200-2	200	-150	0	-0.37	1.27	-2.86
J-200-3	200	-100	96621133	0.48	1.42	3.38
J-200-4	200	-50	53771582	0.11	1.42	0.74
J-200-5	200	0	66104094	0.21	1.70	1.25
J-200-6	200	50	33729958	-0.07	1.18	-0.59
J-200-7	200	100	0	-0.37	1.42	-2.57
J-200-8	200	150	36924968	-0.04	1.70	-0.25
J-200-9	200	200	20134368	-0.19	1.60	-1.17

Table D-3. Average Concentrations for T0011

N-2	400	-200	62008018	0.18	1.56	1.13
N-2.5	400	-150	50869294	0.08	1.65	0.48
N-3	400	-100	41847336	0.00	1.23	0.01
N-3.5	400	-50	72663812	0.27	1.42	1.90
N-4	400	0	35514361	-0.05	1.65	-0.33
N-4.5	400	50	54672546	0.11	1.37	0.82
N-5	400	100	50437632	0.08	1.09	0.70
N-5.5	400	150	87541155	0.40	1.51	2.64
N-6	400	200	46626717	0.04	1.42	0.30

DISTRIBUTION LIST

No. of Copies	
25	Commander U.S. Army Biomedical Research and Development Laboratory ATTN: SGRD-UBZ-C Fort Detrick Frederick, MD 21701-5010
2	Commander U.S. Army Medical Research and Development Command ATTN: SGRD-RMI-S Fort Detrick Frederick, MD 21701-5012